A NARR DERIVED LOW-LEVEL JET CLIMATOLOGY OVER NORTH AMERICA

By

Dana L Doubler

A THESIS

Submitted to
Michigan State University
in partial fulfillment of the requirements
for the degree of

Geography – Master of Science

2013

ABSTRACT

A NARR-DERIVED LOW-LEVEL JET CLIMATOLOGY OVER NORTH AMERICA

By

Dana L Doubler

Previous climatological studies of low-level jets (LLJs) have been restricted to individual geographic regions. In this study, an expanded climatology of the characteristics of northerly low-level jets (N-LLJs) and southerly low-level jets (S-LLJs) is provided for North America and nearby coastal areas to better document the spatial variations of these important mesoscale circulation features. In addition, time of initiation and persistence of S-LLJ events in central North America and over the Gulf of Mexico are analyzed. The North American Regional Reanalysis (NARR), with a 32-km horizontal resolution and a 3-hourly temporal resolution, was used to analyze (by time of day, month, season and year) the frequency, height above ground level, and wind speed of LLJs, and, for S-LLJs in central North America only, diurnal and seasonal variations in the time of initiation and duration jet events. The spatial analyses highlight well-known wind maxima but also point to previously-unknown locations that experience frequent jet-like wind maxima. The analyses also suggest that boundary-layer forcing is important for S-LLJ occurrence, including S-LLJs that form at high latitudes in summer and those that form in the central and southern plains in winter. The NARR-derived analyses supplement and enhance the understanding of the climatological characteristics of low-level wind maxima across North America and coastal environs. The findings also highlight that many aspects of low-level wind maxima remain incompletely understood and point to the need for considerable further research on the processes contributing to jet formation.

.

For my Dad, my Mom, and Sid

ACKNOWLEDGEMENTS

I would like to thank my advisor, Dr. Julie Winkler, for her extraordinary guidance and patience throughout my master's level experience. I would also like to thank my committee members, Dr. Claudia Walters, Dr. Sharon Zhong, and Dr. Lifeng Luo for their help and input. Other individuals at Michigan State University I would like to acknowledge are Xindi Bian for his help with analyzing the NARR dataset, Jovanka Nikolic for her assistance with the analyses, and all of the other graduate students I have gotten to know. All of you helped me greatly throughout this process.

I wish to acknowledge and dedicate this thesis to my family: Chuck, Carol, and Katie Doubler. I am amazed by the physical and mental strength they have displayed during the past year and a half, and I am extremely thankful for their encouragement. I love you all and could not have completed this degree without you.

TABLE OF CONTENTS

LIST OF TABLES

LIST OF FIGURES

KEY TO ABBREVIATIONS

° - degrees

> - greater than

< - less than

≥ - greater than or equal to

≤ - less than or equal to

% - percent

AGL - above ground level

DOE - Department of Energy

e.g. - exempli gratia (for example)

GrADS - Gridded Analysis and Display Systems

hPa – hectopascal(s)

i.e. - id est (that is)

LLJ - low-level jet

km - kilometer(s)

m - meter(s)

ms^{-1} - meters per second

MSL - mean sea level

N - north

N-LLJ - northerly low-level jet

NARR - North American regional reanalysis

NCEP - National Centers for Environmental Prediction

NOAA - National Oceanic and Atmospheric Administration

S - south

S-LLJ - southerly low-level jet

U.S. - United States

UTC - Coordinated Universal Time

W - west

CHAPTER 1. INTRODUCTION, BACKGROUND, AND OBJECTIVES

1. Introduction

A low level jet (LLJ) is a maximum in the vertical profile of horizontal wind speeds in the lower troposphere (Walters et al. 2008). LLJs can originate from any direction, but often are characterized as being southerly or northerly. In previous literature, the most commonly studied location of LLJs is in the Great Plains of the United States, where Southerly-LLJs (S-LLJs) are more frequently observed than Northerly-LLJs (N-LLJs). Whiteman et al. (1997) made the distinction between S-LLJs and N-LLJs in north-central Oklahoma, which differ in frequency and climate characteristics. N-LLJs are less frequent but occur commonly year round, whereas S-LLJs are most common during the summer at night (Whiteman et al. 1997). Numerous previous studies have highlighted the climatology of S-LLJs in different locations across the U.S. (e.g., Arritt et al. 1997; Banta et al. 2002; Bonner 1968; Higgins 1997; Whiteman et al. 1997). In comparison, the climatology of N-LLJs has infrequently been studied (e.g. Kapela et al. 1995; Walters et al. 2008).

LLJs influence temperature and moisture advection and contribute to atmospheric lifting and convection (Bonner 1968; Stensrud 1996; Walters et al. 2008). LLJs also have been noted to influence the migration of birds and insects, which in turn may influence the agricultural industry (Stensrud 1996). Studies on LLJ occurrences have concluded that LLJs may be a factor in the development of major weather phenomena. S-LLJs are identified as a contributing element to precipitation, thunderstorms, tornadoes, the spread of wildfires, and flooding, while N-LLJs contribute to winter storms (e.g., Arritt et al. 1997; Bonner 1968; Higgins 1997; Sjostedt et al. 1990; Walters et al. 2008; Zhong et al. 1996). LLJs contribute to severe weather events by enhancing convection due to shear instability (Wu and Raman 1998). Operations, including nighttime aircraft flying, military operations, and pollution dispersion, are also affected by LLJs (Sjostedt et al. 1990).

As previously stated, S-LLJs are the most frequently observed LLJ type in the U.S. (i.e., Bonner 1968; Rife et al. 2010; Whiteman et al. 1997). S-LLJs occur commonly in the Great Plains region to the east of the Rocky Mountains and northwest of the Gulf of Mexico (Bonner 1968). Previous studies have noted that areas located either east of a mountain range or near land-sea moisture gradients frequently experience LLJs (Stensrud 1996), making the Great Plains an ideal location for LLJ development. S-LLJs enhance severe weather in the Great Plains by transporting moisture from the Gulf of Mexico (Wu and Raman 1998). S-LLJs most often occur nocturnally and during the summer months (Bonner 1968; Stensrud 1996). S-LLJs transport warm, moist air to the interior of the U.S. (Pitchford and London 1962, Walters and Winkler 2001) and contribute to clouds and precipitation during the summer months (Stensrud 1996, Higgins et al. 1997).

The relative contribution of different forcing mechanisms to S-LLJ formation has been debated. Several authors have distinguished between boundary-layer forced and synoptically-forced jets (e.g. Stensrud 1996; Uccellini 1980; Wu and Raman 1998). In particular, Stensrud (1996) declared that a distinction should be made between these two types of LLJs due to the spatial, temporal, and forcing mechanism differences between boundary and synoptic LLJs. However, the climatological differences between boundary-layer and synoptic LLJs have been mostly overlooked in the literature, even though several articles note the differences in the mechanisms contributing to boundary-layer and synoptic jets (e.g. Wu and Raman 1998; Uccellini 1980). Boundary-layer LLJs are typically nocturnal and are seen in the lowest part of the atmosphere (Zhong et al. 1996). Boundary-layer jets also do not vary much in elevation and are short lived (Blackadar 1957; Wexler 1961). The diurnal changes in solar radiation seen in the planetary boundary-layer contribute to this type of LLJ, due to the observed daily patterns of boundary-layer jets (Rife et al. 2010). Mechanisms of synoptic LLJs vary greatly from those responsible for boundary-layer LLJs, and synoptic LLJs do not have strong diurnal patterns. Jets which are seen in conjunction with synoptic flows appear at higher altitudes with stronger wind speeds compared to boundary-layer jets (Wu and Raman 1998). Synoptic jets often occur underneath the exit region of an upper tropospheric jet and extend beyond the boundary-layer (Sjostedt et al. 1990). Wu and Raman (1998) noted that jets that are embedded within mid-latitude cyclones in the Great Plains region create strong moisture and temperature advection, thus enhancing the severity of storms in the region. The differing effects which boundary-layer and synoptic-layer LLJs have on the regional weather and climate indicate that further study of these mechanisms should be made.

Only a few articles have analyzed N-LLJs (e.g., Kapela et al. 1995; Walters et al. 2008) despite their year-round persistence. Although N-LLJs are less frequent and usually weaker than S-LLJs, they impact the climate of a region with cold air advection and are particularly linked to the occurrence of blizzards in the U.S. (e.g. Bonner 1968, Kapela et al. 1995; Walters et al. 2008). Further study of N-LLJs is essential for understanding the impact of LLJs on the climatology of North America, since few previous studies have investigated their influence on the regional climate. Walters et al. (2008) mention that N-LLJs are more frequent across a broader area than previously thought, and that a N-LLJ climatology for North America should be prepared in order to understand climate impacts across North America.

The overall goals of this study are to develop an expanded climatology and an electronic atlas of LLJs that illuminate the spatial variations of S-LLJ and N-LLJ characteristics across

North America and provide insights on the mechanisms responsible for jet formation, particularly the mechanisms responsible for the relative frequency of boundary-layer versus synoptic S-LLJs.

2. Background

a) Identification of Low-Level Jets

The specific definition of a LLJ is influenced by the location and climate of an area. The most common definitions originate from Bonner (1968) and Andreas (2000). Bonner (1968) defined a LLJ as when a maximum wind speed in the vertical profile is twice the magnitude of the wind speed at the next higher minimum above the maximum. In contrast, Andreas (2000) defined a LLJ as when the wind speed profile shows a maximum in wind speed that is 2 ms^{-1} faster than speeds above and below the maximum. Bonner's (1968) definition also includes a classification system for LLJ strength based on the magnitude of the maximum wind speed at the jet nose. LLJs have minimum speeds of 12 ms^{-1} and above, but wind maxima as low as 3 to 4 m/s have also been used in studies (e.g., Andreas 2000).

Previous studies have used rawinsonde and wind profiler data to study LLJs, but these data sources have limitations. Several studies have used rawinsonde observations specifically collected for the analysis. These studies are restricted to studying LLJs for short time spans and a small area. For example, Wu and Raman (1980) used rawinsonde observations from six locations to analyze LLJs in Kansas and Oklahoma for a period of only nine days. Routinely-collected rawinsonde data have also been used in LLJ climatological studies. Many of these studies focused on relatively short time periods of a few weeks or months (e.g., Andreas et al. 2000) or only a couple of years (e.g. Bonner 1968), although long-term (e.g., 40 years) climatologies are also available (e.g., Walters et al. 2008). Although rawinsondes provide data with high vertical resolutions and make observations twice per day, using rawinsonde observations to develop a LLJ climatology for larger regions over multiple years is complicated by changes in time in observation and data collection methods and by the coarse spatial resolution of the rawinsonde network over North America (Mitchell et al. 1995). Wind profiler observations are available for a shorter period than rawinsonde observations and are also restricted to smaller regions. Profiler observations are often contaminated by migratory birds in the Great Plains region, and a velocity variance threshold must be used to reject inaccurate data (Arritt et al. 1997). For a North American LLJ climatology, wind profilers would not be sufficient since stations are only found in the southern and central U.S. (Arritt et al. 1997; Zhong et al. 1996).

b) Mechanisms

The debate of what causes a LLJ to form goes back several decades. The mechanisms for S-LLJs have been the subject of the majority of the past research. The topic first emerged when Wagner (1939) stated that gradients in pressure and temperature fields can cause a jet to form near the surface. Blackadar (1957) argued that inertial oscillations near the friction layer cause variations in wind speed and direction, resulting in a vertical wind maximum. This diurnal oscillation of the wind over a broad area can give rise to S-LLJs. Wu and Raman's (1998) S-LLJ study in the Great Plains indicated that inertial oscillations are a major mechanism for jet formation and supported the findings of Blackadar (1957). Wexler's (1961) explanation is more physical, with the elevated topography of the Rocky Mountains displacing the wind originating from the Gulf of Mexico, and Holton (1967) explains that temperature variation and the horizontal pressure gradient along the slopes of the Rocky Mountains cause wind fluctuations. Uccellini and Johnson (1979) stated that the LLJ could be formed by coupling with an upper-level jet streak. All of these differing explanations could cause a wind maximum to form, and may all contribute to the formation of a LLJ.

c) Climatology

In the United States, LLJs are most frequent in the southern Great Plains (Arritt et al. 1997; Bonner 1968; Walters et al. 2008), and Bonner (1968) identified that LLJs are most frequent along the Oklahoma and Kansas border. As stated previously, common LLJ characteristics in this area are that they are mainly S-LLJs and occur most frequently during the night and in the mid to late summer months (Arritt et al. 1997; Banta et al. 2002; Bonner 1968; Higgins 1997; Walters et al. 2008). Several studies conclude that the advection of moisture from the Gulf of Mexico and advection of cool air from the Rocky Mountains are associated with the high frequency of LLJs in this region (e.g., Arritt et al. 1997; Bonner 1968; Higgins 1997; Walters et al. 2008). These LLJs can be associated with severe weather occurrences in the Great Plains, and an increased number of extreme weather events is associated with an increase in LLJ frequency and strength. Strong and frequent LLJs occurred during the 1993 flood in the Great Plains, when LLJ velocities reached over 20 ms^{-1} (Arritt et al. 1997). LLJs are connected to thunderstorm development in this region as well (Bonner 1966). Several different methods have been used to study LLJs in the Great Plains, including rawinsonde data (e.g., Andreas et al. 2000; Wu and Raman 1980), wind profiler observations (e.g., Arritt et al. 1997), and reanalysis datasets (e.g., Rife et al. 2010).

The climatology of the Carolina LLJ differs greatly from the Great Plains LLJ climatology. Based on rawinsonde data, the Carolina LLJ was found to occur in any season, and only 5% occur in the early morning hours (Sjostedt et al. 1990). Most LLJ cases in this region coincide with a 300-mb upper level jet streak, and occur on the anticyclonic shear side (Sjostedt et al. 1990). Jets in this region are strongly synoptic, and do not show strong diurnal patterns.

The Pacific coast N-LLJ is most frequent in the late afternoon/early evening, unlike the Great Plains and Carolina LLJ (Burk and Thompson 1996; Davis et al. 2000). During the summer, N-LLJs dominate in the northeastern Pacific region due to the strong North Pacific High to the west and thermal low to the east (Burk and Thompson 1996; Davis et al. 2000). Land-ocean temperature differences, especially in the summer, also greatly enhance the Pacific coast N-LLJ (Burk and Thompson 1996). Although the frequency in winter is much less than summer, extratropical cyclones during the winter generate a moderate frequency of N-LLJs in this region (Ralph et al. 2005). El Niño- Southern Oscillation greatly affects the interannual climate patterns of the Pacific coast N-LLJ, and during El Niño years, jet strength increases (Ralph et al. 2005). N-LLJ strength varies diurnally, similar to the Great Plains LLJ, but the role of mountains and sea breeze is not well understood (Davis et al. 2000).

Based on field experiments and reanalysis data, the Bermuda High in the Atlantic Ocean generates easterly and southerly flowing LLJs throughout the Intra-American Sea (Munoz et al. 2008). A strong core of easterly LLJs exist in the western Caribbean Sea, and when these LLJs flow towards land, they are directed northward and become southerly (Amador 2008; Munoz et al. 2008). The Yucatan Peninsula, western Gulf of Mexico, and southern Texas experience S-LLJs due to these wind patterns (Munoz et al. 2008). The S-LLJs are strongest in February and in July (Amador 2008; Munoz et al. 2008). The Intra-American Sea is also believed to be heavily affected by the El Niño- Southern Oscillation phases, and S-LLJs also become stronger during the warm phases (Amador 2008). The characteristics of LLJs in the Intra-American Sea are not well understood due to a lack of observational data in this region (Amador 2008).

The difference in mechanisms and climatology of LLJs across these four areas of North America indicate that LLJ type varies from location to location. A better understanding of S-LLJs and N-LLJs climatologies and forcing mechanisms is necessary to develop a North American LLJ climatology.

d) Impacts of Low-Level Jets

Most studies on LLJs examine the location and frequency of LLJs, but few have examined the climate impacts LLJs have on a region. Several studies have noted correlations of weather phenomena with LLJs (e.g., Arritt et al. 1997; Bonner 1966; Bonner 1968; Higgins 1997; Walters et al. 2008; Wu and Raman 1998). Amount of precipitation in relation to appearance and strength of LLJs in the Great Plains was noted by Higgins et al. (1997), who found that an increase in precipitation in the Central Great Plains at night during the summer months correlated to the presence of LLJs in the area. The Intra-Americas LLJ is thought to contribute to precipitation as well, and precipitation in Central America has been shown to correlate with stronger LLJs in this region (Amador 2008). LLJs are also important to convective systems and help sustain deep convection (Chen 1986; Pitchford and London 1962). The flooding episode during 1993 in the Great Plains also coincided with an increase of LLJs (Arritt et al. 1997). During this 1993 flooding episode, many strong LLJs were observed, reaching over 20 ms^{-1} (Arritt et al. 1997). Thunderstorm occurrences with LLJs have been frequently examined (e.g., Bonner 1968; Chen 1986; Pitchford and London 1962; Wu and Raman 1998). Bonner

(1968) mentions that the existence of a LLJ may impact atmospheric convection and thunderstorm development. The study of LLJs occurring during severe storm events indicates that LLJs contribute to the moisture and temperature advections in storm systems (Wu and Raman 1998). Bonner (1968) also correlated tornado probabilities with LLJ frequency, and noted that the highest probability of tornadoes in the Great Plains is located in central Oklahoma (Bonner 1966). Arritt et al. (1997) noted that strong LLJs were most often associated with warm advection, and this advection may have strengthened the LLJs. The persistence and spread of forest fires has also been mentioned in relation to LLJs (Bonner 1968; Charney et al. 2003), along with the strength of blizzards and winter storms (e.g. Kapela et al. 1995; Walters et al. 2008).

3. Research Needs

The study of LLJs across all of North America is severely underdeveloped. Climatological studies have investigated S-LLJs using rawinsonde observations, Doppler radar, minisondes, and wind profiles in mainly the Great Plains region, but the climatology of LLJs outside of the Great Plains is not well understood. Additionally, only a few studies have analyzed N-LLJs (e.g., Walters et al. 2008). Also, many investigators utilized only a few years of wind data to analyze LLJs (e.g., Bonner 1968, Whiteman et al. 1997); few studies have analyzed LLJs over an extended period.

Limitations of the measurements typically used to identify LLJs have also lead to an incomplete understanding of the spatial and temporal variations of LLJs. The rawinsonde network has a coarse spatial resolution, and observations are routinely taken only twice per day (00 UTC and 12 UTC). The wind profiler network is incomplete, and primarily covers the south central portion of the U.S. New datasets provide exciting opportunities for a greater spatial and temporal coverage. In particular, reanalysis datasets, which are a blend of observational data and output from weather forecast models, provide uniform coverage at a fine (around 30-50 km) resolution over all of North America with wind data multiple times per day.

The limitations of the datasets used for climatological analyses have also hampered our understanding of the frequency of diurnally-forced LLJs compared to jets that are primarily forced by synoptic-scale mechanisms. In particular, the rawinsonde observations do not allow for the timing of jet formation and persistence to be accurately assessed. Additionally, the sparse spatial resolution of the rawinsonde network, especially at high latitudes, has limited our understanding of the climatology of LLJs at higher latitudes. Also, the lack of observation stations over water bodies limits the study of LLJs over nearby coastal regions. Furthermore, the discontinuities in rawinsonde time series limit any investigation of the interannual variability of LLJs.

The use of reanalysis datasets provides an exciting opportunity to investigate these important aspects of LLJs. The newly-available reanalysis datasets permit expanded climatological study of LLJs across North America.

An additional need is an online resource. Because of the significance and multiple impacts of LLJs, it would be useful to weather forecasters and other stakeholders to have an online web tool to help them understand the LLJ climatology. By providing such a tool, users may identify LLJs characteristics for a variety of applications.

4. Objectives

As stated earlier, the overall goals of this research are to develop an expanded climatology of LLJs focusing on spatial variations in LLJ characteristics across North America and to provide insights on the relative contribution of diurnal versus synoptic mechanisms for jet formation using a fine resolution reanalysis dataset. The dataset that has been utilized in this study is the North American Regional Reanalysis (NARR) (Mesinger et al. 2006).

The specific objectives were to:

1) Prepare a detailed LLJ climatology for North America using 8 times daily NARR reanalysis for the period of 1979-2009. The climatology focuses on the spatial and temporal patterns in the frequency of LLJs from both southerly and northerly directions.

2) Characterize the timing and persistence of S-LLJs, including the spatial variations in these characteristics, as a preliminary assessment of the relative contribution of boundary-layer versus synoptic forcing to jet formation and persistence.

3) Investigate the interannual variation of LLJ frequencies during the 31-year (1979-2009) study period for selected NARR gridpoints where N-LLJs and S-LLJs are frequent.

4) Incorporate the spatial patters of LLJ frequency and characteristics identified from the above objectives into an electronic atlas that is easily searchable and can be made available via the internet.

CHAPTER 2. METHODS

1. Introduction

The study area includes a selection of the NARR domain which covers the continental United States, southern Canada, Mexico, and the Intra-Americas. Use of this domain provides insight into LLJs in Canada and Mexico, which have not been well studied, and can give further insight into LLJs over the Gulf of Mexico and the Carolinas. Below the criteria for a LLJ occurrence are given, along with an overview of the benefits of using the NARR dataset compared to traditional wind observations. The variables that were extracted from the NARR dataset and evaluated for this study are also given, along with a brief discussion of the importance of the variables selected for the analysis.

2. Low-Level Jet Definition

The definition of a LLJ for this study is a wind maximum of ≥12 ms^{-1} with a velocity decrease of half the maximum above and below the jet, with a minimum wind shear of 6 ms^{-1} regardless of wind maximum. Recent studies have used similar definitions, stemming from the Bonner's (1968) early jet definition (e.g. Walters 2008). The results from these studies have shown that this LLJ definition can identify LLJs that impact convective systems (Walters et al. 2008). Bonner (1968) examined LLJs with a wind maximum at or below 1500 m above ground level. For this study, the wind maxima must occur at or below 3000 m above ground level (AGL), with the required wind speed decrease to occur below 5000 m AGL. The use of meters AGL is needed to identify LLJs across the varied North American terrain, and the relatively thick vertical layer is used to identify both boundary-layer jets, which are often found close to the ground, and synoptically-forced jets, which often have a slant-wise flow. The LLJ definition used here is similar to Bonner's (1968) LLJ definition, except a decrease in wind speed is required below the jet, as well as above, following Walters et al. (2008).

3. The NARR Dataset

The NARR dataset is a high-resolution reanalysis dataset whose domain includes all of North America (Figure 1). A reanalysis dataset can be considered a "blend" of observations and model output (Winkler et al. 2011). The NARR project used several weather forecast models, including the NCEP-DOE Global Reanalysis and NCEP Eta Model (Mesinger et al. 2006). These models are assimilated with observational data to provide a more accurate (climate) reanalysis at a fine horizontal resolution (Mesinger et al. 2006). Improvements in the NARR compared to earlier reanalyses resulted from more assimilated observations, improved assimilation schemes, higher resolution, and improved modeling methods (Mesinger et al. 2006). The original dataset includes a 32-km horizontal resolution and 45 vertical levels, with data available at 3 hour intervals, starting at 00 UTC for a total of 8 wind data per day (Mesinger et al. 2006). The archived data contains 25 vertical levels at a 25 hPa vertical resolution below the 700 hPa layer and 50 hPa vertical resolution above the 700 hPa layer, with vertical resolution returning to 25 hPa in the upper troposphere. The data extends from 1979 to present (Mesinger et al. 2006).

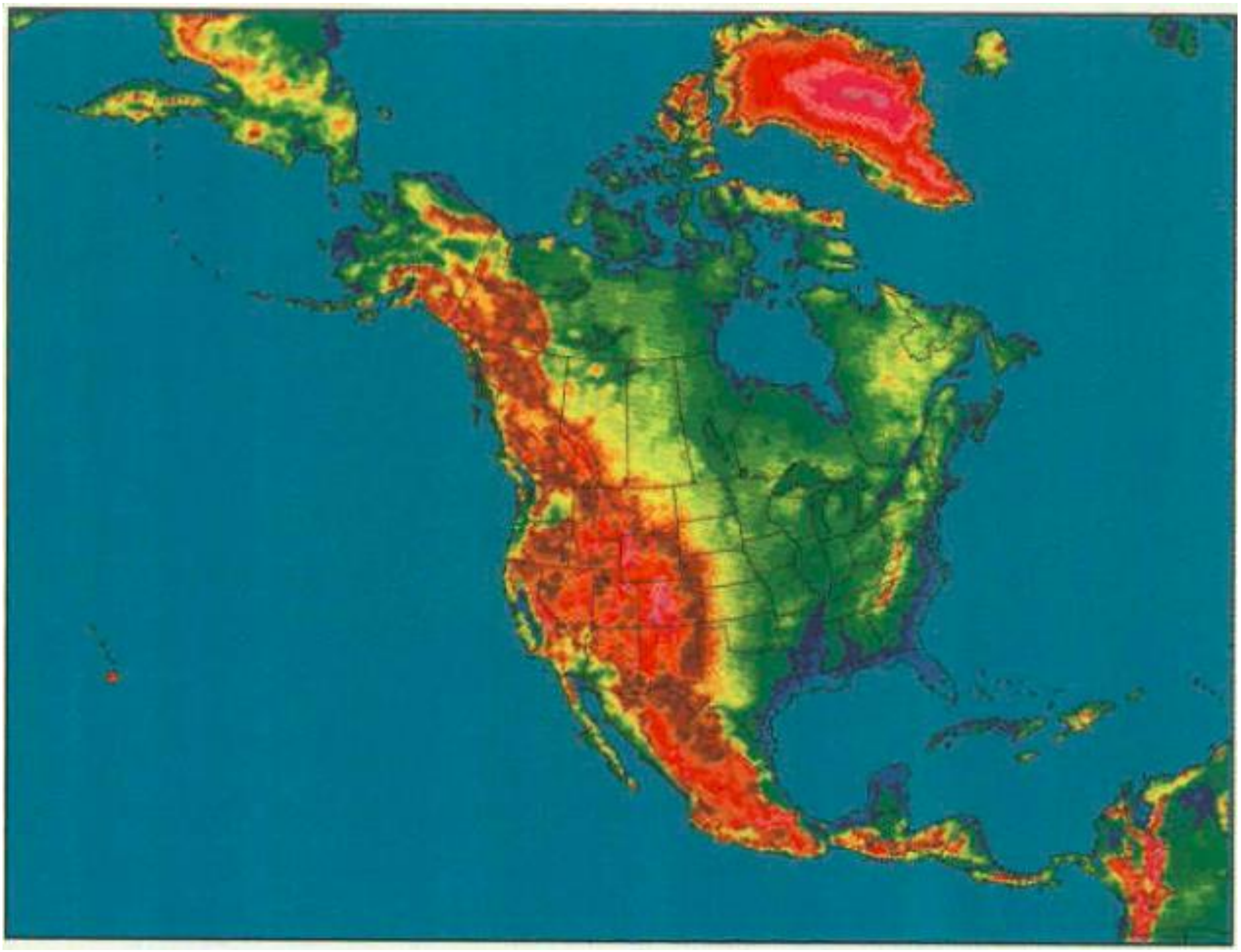

Figure 1. The NARR domain (Mesinger et al. 2006). [For interpretation of the references to color in this and all other figures, the reader is referred to the electronic version of this thesis.]

4. Climatological Analysis of Low-Level Jets

LLJs were extracted using the definitions above for each 3-hourly time step in the NARR dataset (and output to separate files labeled by the year, month, day, and hour). Each file only includes those gridpoints where a LLJ was identified. The variables that were extracted for each jet profile signature (i.e. the LLJ vertical profile of wind speed) are shown in Table 1.

Variable	*Elevation*	*Unit*	*Application*
i and j	Gridpoint where LLJ was identified	-	Location of LLJ vertical signature
u and v wind component	Jet nose level	ms^{-1}	Used to calculate direction and speed of maxima along with vertical shear
u and v wind component	Minimum wind speed above the jet maximum	ms^{-1}	Used to calculate direction and speed of minima along with vertical shear
u and v wind component	Minimum wind speed below the jet maximum	ms^{-1}	Used to calculate direction and speed of minima along with vertical shear
Elevation	Jet nose level	meters AGL	Meet LLJ height requirements
Elevation	Minimum above jet nose	meters AGL	Meet LLJ height requirements
Elevation	Minimum below jet nose	meters AGL	Meet LLJ height requirements
Elevation	Surface	meters MSL	Meet LLJ height requirements

Table 1. Variables extracted from the NARR dataset.

5. Methods

a) Methods for Objective 1 – Frequency, Speed, and Elevation of LLJs

To address Objective 1, software was developed to read the 3-hourly files and compile the jet frequency at each gridpoint. Jet frequency was calculated by summing all NARR time steps in which a LLJ was present at a gridpoint during an aggregation level, and dividing by all times steps possible for the same aggregation level. The jet frequencies for each 3-hourly time step were aggregated by 1) month, 2) season, and 3) year. The jet frequencies also were separated by 1) northerly, defined as originating from 293°-67°, and 2) southerly, defined as originating from 113°-247° (Walters et al. 2008). Grid Analysis and Display System (GrADS) software was used to map the spatial variations of the N-LLJs and S-LLJs by time of day and aggregation period (i.e., month, season, and year). The locations of frequent N-LLJ and S-LLJ occurrences were identified from the resulting climatological maps for the North American continent.

b) Methods for Objective 2 – Timing and Persistence of S-LLJs

The spatial patterns in the time of initiation and duration provide an indication of the relative contribution of boundary-layer forcing to the S-LLJ climatology under the assumption that diurnally-forced S-LLJs are most likely to form during the nighttime and early morning hours, persist for only a relatively short period, and are located at relatively low elevations. To determine the timing and persistence of individual jet events, successive time steps at individual NARR gridpoints were queried for the existence of a S-LLJ (113°-247°) jet profile signature. The starting time and the duration of a jet signature were then recorded. For each 3-hourly archive time, the following maps were compiled based on the accumulated data by gridpoint: the percent of jets that originated at this time step, and the percent of jets that originated at this time step and that persisted <3 hours, <6 hours, <9 hours, etc. Several select NARR gridpoints were also analyzed throughout the study domain to further determine the persistence patterns of S-LLJs. These gridpoints were selected based on their frequent occurrence of LLJs, as evident in the maps produced for Objective 1. All jet events which occurred in the 31-year period from 1979-2009 were recorded along with the duration of each jet event. The proportion of the jet events that were first identified at each of the NARR 3-hourly time steps was calculated and mapped. In addition, the average duration was calculated for the jet events that began at each of the 3-hourly time steps.

c) Methods for Objective 3 – Interannual Variation

Trend and variability analyses were conducted for selected gridpoints across North America where the climatological analyses indicated that N-LLJs and/or S-LLJs are highly frequent and/or are located in areas where previously-studied LLJs occur. These analyses were conducted annually and seasonally, and focused on the temporal trends and interannual variability of jet frequency. The analysis of temporal trends focused on linear trends. Interannual variability was expressed as a detrended, standardized frequency calculated as:

$$(\omega_{(y-1)} - \omega_{(y)}) / \omega_{(1979\text{-}2009)})$$

where ω is the frequency, and y is the year for which the calculation is being performed. A map of the selected gridpoints is shown below:

NARR Gridpoint Locations for Time Series Analysis

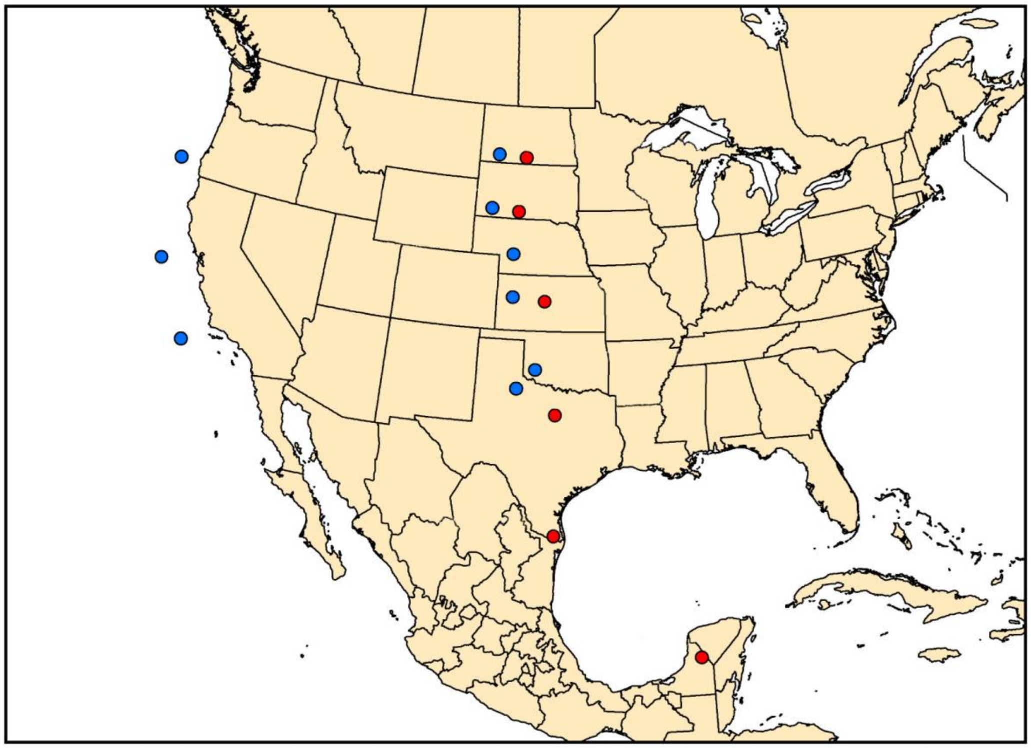

S-LLJ gridpoints are shown in red and N-LLJ gridpoints are shown in blue.

Figure 2. Gridpoints for which the long-term trends and interannual variability of N-LLJs and S-LLJs were analyzed. Locations were determined based on the climatological analysis.

d) Methods for Objective 4 – Electronic Atlas

Given the vast amount of N-LLJ and S-LLJ characteristics being analyzed, a climatological LLJ atlas helps to provide clarity and cohesion to the study findings. The atlas is available online for users to explore. Users may choose which LLJ characteristics to view from several drop down menus. Table 2 lists the maps that are provided as part of the electronic atlas. The software used to create the maps was GrADS which allowed easy management of the numerous LLJ climatological maps.

	S-LLJ frequency	N-LLJ frequency	S-LLJ speed	N-LLJ speed	S-LLJ nose elevation	N-LLJ nose elevation	S-LLJ persistence
Annual	1 Map	1 Map	1 Map	1 Map	1 Map	1 Map	16 Maps
Seasonal	4 Maps	4 Maps	4 Maps	4 Maps	4 Maps	4 Maps	16 Maps
Monthly	12 Maps	12 Maps	12 Maps	12 Maps	12 Maps	12 Maps	
Hourly	129 Maps	129 Maps	129 Maps	129 Maps	129 Maps	129 Maps	

Table 2. Maps for electronic atlas.

CHAPTER 3. A NARR-DERIVED CLIMATOLOGY OF NORTHERLY AND SOUTHERLY LOW-LEVEL JETS IN NORTH AMERICA

In collaboration with

Julie A. Winkler, Xindi Bian, Shiyuan Zhong, and Claudia Walters

1. Introduction

Knowledge of the spatial and temporal variations of low-level wind maxima over North America and surrounding coastal areas remains incomplete, in spite of the significant impact of low-level jets (LLJs) on local and regional weather and climate. This is in part due to the limited availability of upper-level wind observations. The majority of previous climatological investigations of LLJs were developed using routine rawinsonde observations (e.g., Bonner 1968; Walters et al. 2008). However, these observations are taken only twice daily (00 and 12 UTC), and the density of the observations is coarse, with rawinsonde locations in North America spaced at a minimum several hundred kilometers apart. Additionally, inhomogeneities in the rawinsonde record (e.g., changes in station locations, sonde types, observational protocols and archiving procedures) complicate the use of these observations in climatological research (Bosart 1990; Schwartz and Doswell 1991; Winkler 2004; Walters et al. 2013). Alternative data sources have been equally problematic. For example, utilization of observations from the NOAA National Profiler Network is hampered by the relatively small areal extent of this network and by an elevated (approximately 500 m) lower range gate that restricts the detection of some LLJs (Mitchell et al. 1995; Arritt et al. 1997).

Reanalysis datasets, with their relatively fine spatial and temporal resolution, provide an alternative resource for climatological analyses of low-level wind maxima. Reanalyses are a dynamically-consistent assimilated product that incorporates first guess model fields with observations from multiple sources, including rawinsondes, dropsondes, pibals, commercial aircraft, satellites, and radar wind profilers (Shafran et al. 2004). Recently, Walters et al. (2013) compared the characteristics of LLJs identified from vertical wind profiles obtained from the North American Regional Reanalysis (NARR; Mesinger et al. 2006) with jet characteristics identified from rawinsonde observations for 12 locations in central North America. They found that the relative differences in jet frequency between locations and between the 00 and 12 UTC observations times were generally consistent for the two datasets, although the absolute frequency of LLJs was smaller for NARR compared to rawinsonde observations at most of the study locations. Furthermore, average LLJ speed and elevation did not differ significantly between the two datasets at the majority of the locations. Walters et al. (2013) also concluded that NARR is the more appropriate of the two datasets for assessing temporal trends in LLJ frequency, as abrupt inhomogeneities that correspond which changes in rawinsonde instrumentation and protocols, particularly the recent introduction of the Radiosonde Replacement System, are mostly absent from the NARR time series.

The overall goal of this research is to develop an expanded, long-term climatology of LLJ frequency, speed, and elevation, focusing on spatial and temporal variations across the majority of North America and coastal environs using a fine resolution reanalysis dataset. NARR, which has a 32 km resolution and a 3-hourly time step, was selected for the analysis, as it has previously successfully been used to estimate the characteristics of southerly wind maxima in the central U.S. (Weaver and Nigam 2008) and as boundary conditions for simulations of LLJ events (e.g., Storm et al. 2009). Also, as discussed above, a recent study (Walters et al. 2013) carefully compared the jet characteristics identified from NARR and rawinsonde observations at selected locations, thus facilitating the interpretation of the NARR-derived climatology presented here.

Long-term (31-year) climatological analyses of jet frequency and mean speed and elevation are presented below for each three-hourly time step by annual, seasonal, and monthly aggregation levels in order to evaluate seasonal, intra-seasonal, and diurnal variations in jet characteristics. The interannual variability and temporal trends in LLJ frequency are also investigated. In addition, the NARR-derived climatological characteristics are compared to the characteristics, as identified from previous climatological analyses and case studies, of several previously-documented and well-known North American wind maxima, including the southerly Great Plains jet (e.g., Bonner 1968), the southerly arm of the Caribbean jet (e.g., Cook and Vizy 2010), the northerly Carolina jet (e.g., Doyle and Warner 1991), and the northerly Pacific coast jet (e.g., Burk and Thompson 1996; Parish 2000; Bielli et al. 2002).

The small number of previous applications of NARR for climatological analyses have focused either on the southerly Great Plains jet (Weaver and Nigam 2008) or the Caribbean jet (Cook and Vizy 2010). The greater spatial extent of the analysis presented here allows for more detailed comparisons of the characteristics and potential linkages of LLJs across North America. The analysis builds on previous long-term, rawinsonde-based LLJ climatologies (e.g., Walters et al. 2008) through its greater spatial and temporal detail.

2. Methods

As noted above, the long-term LLJ climatology is derived from vertical wind fields obtained from the North American Regional Reanalysis (NARR). NARR is generated using the lateral boundaries and data from the NCEP-DOE Global Reanalysis, the NCEP Eta Model and its data assimilation system, a version of the Noah land-surface model, and numerous observational datasets (Mesinger et al. 2006). NARR has a 3-hourly temporal resolution, or a total of 8 time steps per day and a 32 km horizontal resolution. The archived dataset has a 25 hPa vertical resolution below and a 50 hPa resolution above the 700 hPa layer, with vertical resolution returning to 25 hPa in the upper troposphere. The dataset begins in 1979, and the 31-year period from 1979-2009 was used to derive the LLJ climatology presented below.

A subset of the NARR domain, extending from central Canada (approximately 60°N) southward to southern Mexico (approximately 15°S), and from the eastern Pacific (approximately 140°W) to the western Atlantic (approximately 60°W), was used for the investigation. This study area was selected as it captures the locations of several well-known North American LLJs (e,g., the Great Plains jet, the southerly arm of the Caribbean jet, the Carolina jet, and the Pacific coast jet). Also, the study area excludes the periphery of the NARR domain, where observations are less numerous and the climate model fields are less reliable. Nonetheless, cautious interpretation is needed of the climatological analyses presented below, as the vertical wind fields can be influenced by differences in the availability of observations across the study area and by model bias.

The following criteria were used to extract LLJs from the wind profiles at each NARR gridpoint: (1) the jet "nose" (i.e., elevation of maximum wind speed) had to be located at or below 3000 m AGL, (2) wind speeds at the jet nose were ≥ 12 ms^{-1}, (3) the wind speed above the jet nose decreased by ≥ 6 ms^{-1} to the next minimum or to 5000 m AGL (whichever was lower), and (4) a wind speed decrease of ≥ 6 ms^{-1} which must not occur at the surface was found below the jet nose. This criterion was applied in several recent studies (e.g., Walters and Winkler 2001; Walters et al. 2008; Walters et al. 2013). The thresholds for wind speed and the wind shear above the jet nose correspond to those initially employed by Bonner (1968) in his landmark study of

LLJs in the central U.S. The maximum elevation of the jet nose (3000 m AGL) follows that of Walters and Winkler (2001) and Walters et al. (2008). The focus is on meridional (rather than zonal) jets, given their frequency over the study area, with LLJs classified as southerly (S-LLJs) if their direction fell between 113-247°, and as northerly (N-LLJs) if they originated between 293-67°.

At each gridpoint, S-LLJ and N-LLJ frequencies were aggregated annually, seasonally, and monthly across all time steps and separately for each 3-hourly time step. All frequencies are expressed as a percentage of the total number of time steps for a particular accumulation period/time step combination. The Grid Analysis and Display System (GrADS) software was used to map the spatial variations of the N-LLJ and S-LLJ characteristics. Because of space considerations, only selected plots are displayed below; a complete collection of the climatological maps is available online at http://www.geo.msu.edu/~llj/.

Temporal trends in LLJ frequency, along with the interannual variability of jet frequency, were calculated for selected NARR gridpoints where, based on the climatological maps, LLJs frequencies are particularly large. These analyses were conducted both annually and seasonally. Temporal trends and their significance were estimated using simple linear regression. In order to evaluate the interannual variability in jet frequency, the temporal trend at a gridpoint was first removed by simply differencing the current year's frequency from that of the previous year; the detrended frequencies are expressed as a percentage of the mean for the 31-year study period at a gridpoint in order to facilitate spatial comparisons.

3. Results

a) Frequency of Southerly and Northerly Low-Level Jets

The frequency of S-LLJs and N-LLJs in the NARR vertical wind profiles was separately computed for annual, seasonal, and intra-seasonal (i.e., monthly) aggregation levels, and, within each of these periods, for each 3-hourly NARR time step (00, 03, 06, 12, 15, 18, 21 UTC). The frequencies are expressed as a percentage of the total number of NARR time steps for each accumulation period/time step combination.

1) ANNUAL

At the annual aggregation level, elevated (>5%) S-LLJ frequencies extend from the northern Great Plains and central Canada southward to the western Gulf of Mexico and the Yucatan Peninsula (Figure 3). Within this broad area, S-LLJ frequencies exceeding 10% are found from northern Nebraska to the western Gulf of Mexico, with frequencies exceeding 15% in southern Texas and northeastern Mexico. S-LLJ frequencies >5% also occur over coastal British Columbia, and a small portion of the Atlantic Ocean off of the Carolina Coast. When time of day is considered, S-LLJs are least frequent in the NARR wind profiles at 21 UTC, when jet frequencies >10% are limited to the western Gulf of Mexico. After 21 UTC, S-LLJ frequencies >10% expand both northwards from the western Gulf of Mexico into the Great Plains and southwards to the Yucatan Peninsula, with the highest S-LLJ frequencies occurring at 09 UTC. At this time, three separate maxima with frequencies >25% are located in western Kansas/Oklahoma, central Texas, and southern Texas/northeastern Mexico. Jet frequencies remain elevated at 12 UTC, after which they decrease substantially, particularly between 15 and 18 UTC.

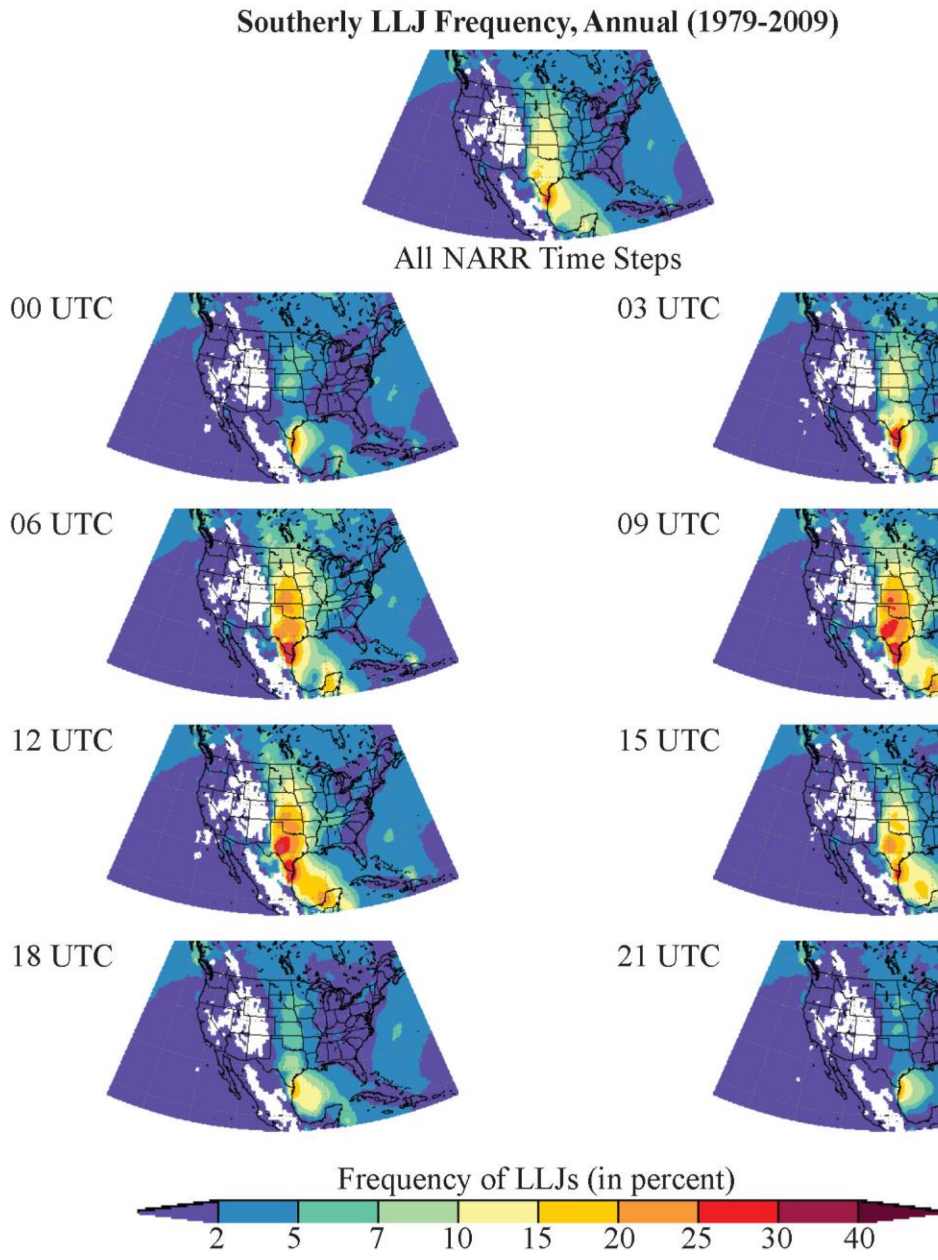

Figure 3. Annual frequency of S-LLJs from 1979 to 2009 expressed as a percentage of the total number of time steps, summed over all NARR time steps (top figure) and individually for each time step (bottom figures). Gridpoints with no jet cases and/or surface elevations >2km MSL are shown in white.

For N-LLJs, the annual frequency plot is dominated by a large maximum along the Pacific coast from central Oregon to central Baja California (Figure 4). N-LLJs are most frequent along the coast of California, particularly northern California, where frequencies in excess of 20%, and in some places >25%, are found. N-LLJs in this area occur at all times of day, although the areal extent of frequencies >25% is largest at 03, 06, and 09 UTC. Smaller, much less prominent maxima with N-LLJ frequencies >5% are found in the Great Plains (South Dakota and Nebraska), southern Hudson Bay, eastern Canada, and the extreme southern Gulf of Mexico. Of these maxima, the one located in the Great Plains displays a marked diurnal variation with a considerably larger area experiencing N-LLJ frequencies >5% at 12 and 15 UTC compared to other times of the day.

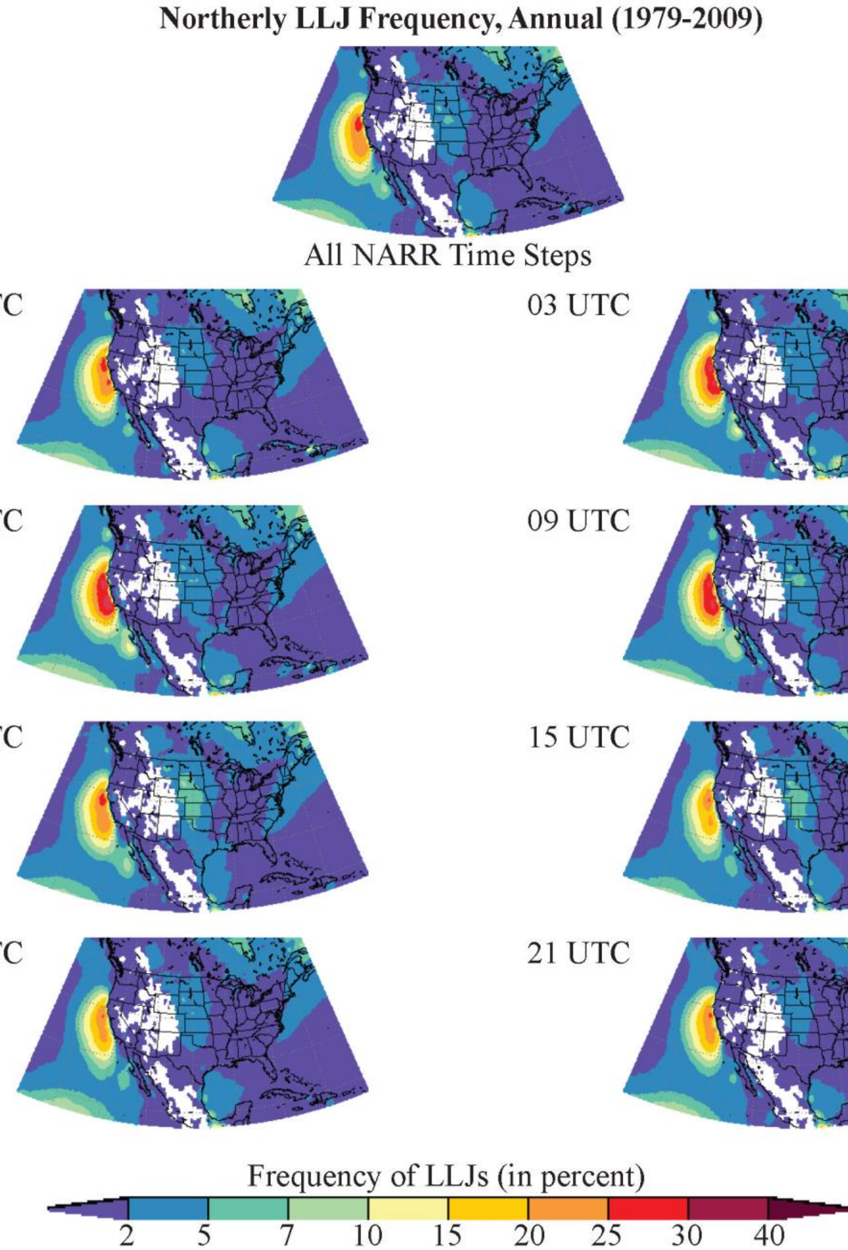

Figure 4. Annual frequency of N-LLJs from 1979 to 2009 expressed as a percentage of the total number of time steps, summed over all NARR time steps (top figure) and individually for each time step (bottom figures). Gridpoints with no jet cases and/or surface elevations >2km MSL are shown in white.

2) WINTER

The primary area of elevated (>5%) S-LLJ frequencies during winter extends from eastern South Dakota and southern Minnesota southward to the western Gulf of Mexico and the Yucatan Peninsula (Figure 5). Within this region, S-LLJ frequencies are largest in central and southern Texas and the western Gulf of Mexico, with values exceeding 25% immediately along the coast of south Texas and northeastern Mexico. Additional areas with S-LLJ frequencies >5% are found along and off the coast of British Columbia, over central Kentucky and Tennessee, and in the western Atlantic off the eastern coast of the U.S. When intra-seasonal variations in S-LLJ frequencies are considered, the most notable feature is the substantial increase in S-LLJ frequency from January to February in the western and central Gulf of Mexico and over the Yucatan Peninsula. Additionally, the area over the Atlantic Ocean with S-LLJ frequencies >5% increases in size from early to late winter. In contrast, the frequency of S-LLJs along the coast of British Columbia decreases as the winter season progresses.

The N-LLJ frequency maximum seen along the Pacific coast on the annual plot is relatively weak in winter (Figure 6). The largest frequencies, which fall between 7-10%, are found at NARR gridpoints off the coast of southern California. N-LLJ frequencies in this area are somewhat larger in December compared to January and February. In contrast, the area of elevated (>5%) N-LLJ frequencies in the Great Plains is more pronounced in winter compared to the maximum seen on the annual plot. The magnitude and areal extent of this maximum is similar for the three winter months. The modest N-LLJ frequency maximum over southern Hudson Bay is stronger in December and January than in February, whereas the frequency maximum over eastern Canada strengthens from December to February. There is little intra-seasonal variation in the N-LLJ frequency maximum located in the southern Gulf of Mexico.

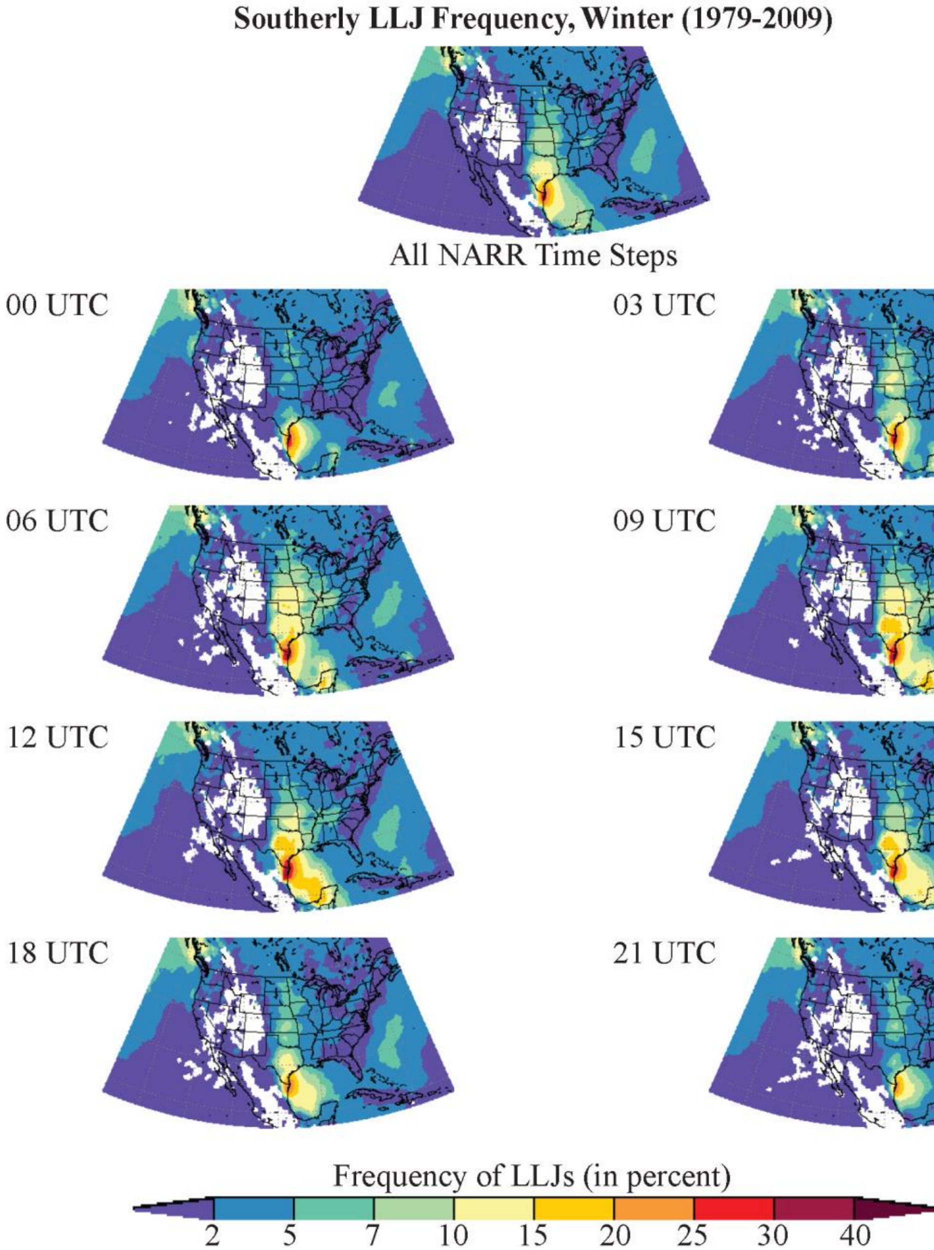

Figure 5. Winter (December-February) frequency (percentage) of S-LLJs from 1979 to 2009 expressed as a percentage of the total number of time steps, summed over all NARR time steps (top figure) and individually for each time step (bottom figures). Gridpoints with no jet cases and/or surface elevations >2km MSL are shown in white.

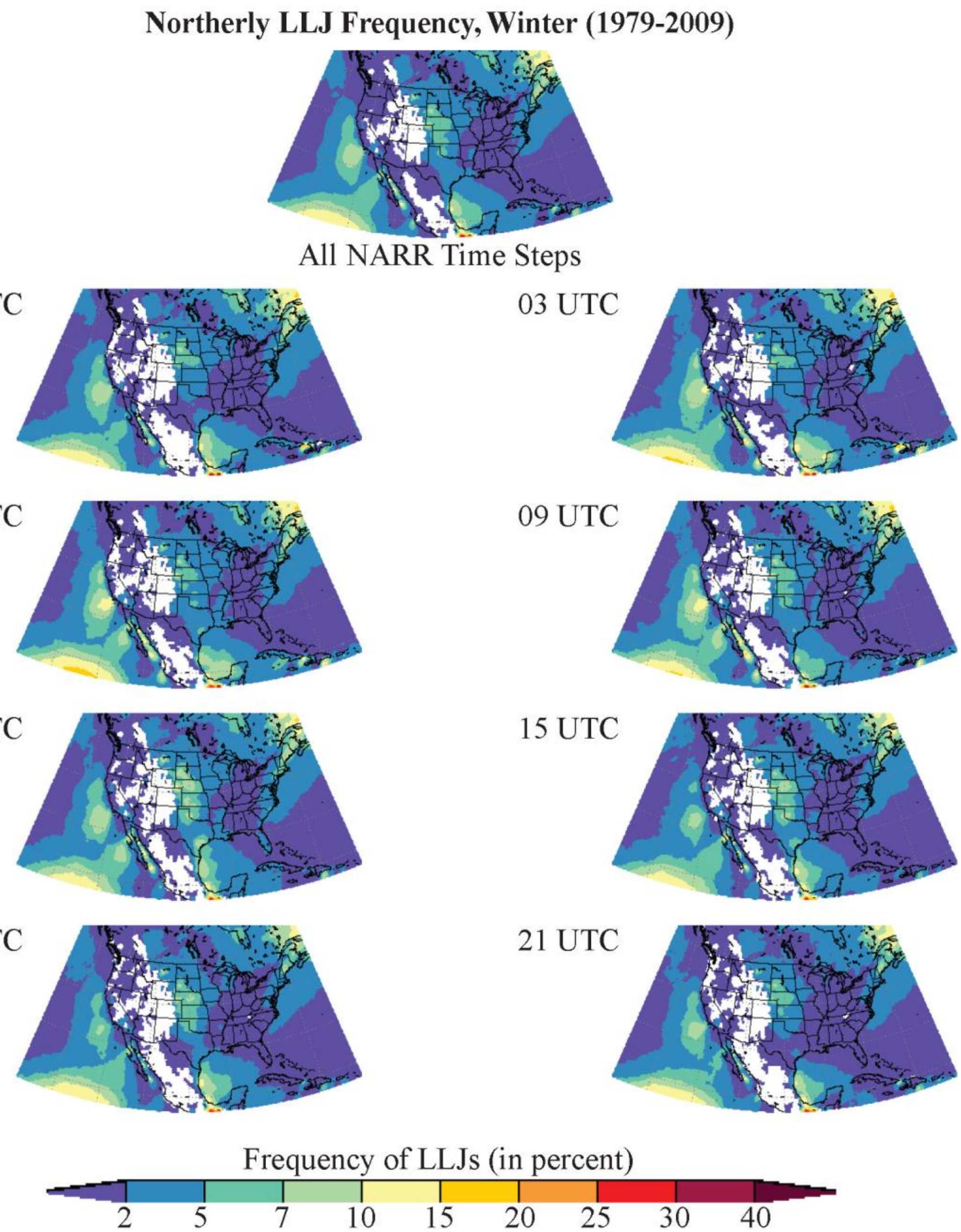

Figure 6. Winter (December-February) frequency (percentage) of N-LLJs from 1979 to 2009 expressed as a percentage of the total number of time steps, summed over all NARR time steps (top figure) and individually for each time step (bottom figures). Gridpoints with no jet cases and/or surface elevations >2km MSL are shown in white.

Substantial diurnal variations in S-LLJ frequency are observed in winter. The diurnal variations appear to be larger for S-LLJs in the Great Plains, compared to the western Gulf of Mexico where jet frequencies are relatively large at all NARR time steps. Wintertime S-LLJs in the Great Plains are less frequent at the 21 and 00 UTC time steps, with a substantial increase in frequency observed from 00 to 03 UTC. Jet frequencies remain large (>10%) through approximately 15 UTC with the highest frequencies seen at 09 and 12 UTC. Diurnal variations in S-LLJ frequency are fairly small over the Atlantic Ocean off the east coast of the U.S. and along and off the coast of British Columbia. The overall strength and timing of the diurnal cycle is similar when the three winter months are considered separately (see Appendix A).

Wintertime N-LLJs along the Pacific coast are slightly more frequent at 03, 06, and 09 UTC and least frequent at 15 and 18 UTC, whereas in the Great Plains N-LLJs in winter are more frequent, and the areal extent of the frequency maximum is larger, from 09-18 UTC. The diurnal cycle for wintertime N-LLJs in the southern Gulf of Mexico is almost opposite that in the Great Plains, with relatively low frequencies and a smaller areal extent at 09 and 12 UTC compared to other times of the day. N-LLJs over southern Hudson Bay are least frequent in at18 and 21 UTC, whereas the diurnal cycle is weak for N-LLJs in eastern Canada. The diurnal patterns are generally similar for all three winter months (see Appendix B).

3) SPRING

The broad area of elevated (>5%) S-LLJ frequencies in central North America seen in winter expands considerably northwards during spring into central Canada (Figure 7). This northward expansion is most evident on the monthly frequency plots for March and April. The largest S-LLJ frequencies during spring are seen from central Texas southeastwards over the Yucatan Peninsula, similar to the spatial pattern for late winter (i.e., February), although the frequencies have increased substantially to over 20% for all NARR 3-hourly time steps, and with frequencies >30% along the coast of south Texas and northeastern Mexico. The frequency maximum over the western Gulf of Mexico is the dominant feature throughout the spring season, although the area of very large (>25%) frequencies expands substantially eastward toward the central Gulf from March to April before contracting somewhat in May. A northward expansion of S-LLJ frequencies >15% from central Texas into southern Kansas is also seen, particularly in May. In contrast, S-LLJ frequencies in the northern portion of the Great Plains (i.e., Nebraska and the Dakotas) remain fairly uniform during the three spring months.

Additional areas of elevated (>5%) S-LLJ frequencies in spring are found along and off the coast of British Columbia, in western Kentucky and Tennessee, and off the east coast of the U.S. Elevated S-LLJ frequencies also occur over western Hudson Bay. During the course of the spring season, the area of elevated S-LLJ frequencies over coastal British Columbia decreases in size and disappears by May. Likewise, the S-LLJ frequency maxima over Kentucky/Tennessee weaken during the spring season and are not evident on the frequency plot for May. In contrast, S-LLJ frequency increases from March to May in the western Hudson Bay region. The temporal evolution of the frequency maximum over the western Atlantic is somewhat more complex. The areal extent and magnitude of the frequency maximum increases from late winter to early spring, but weakens in late spring when it becomes confined to a small area immediately off the coast of North Carolina.

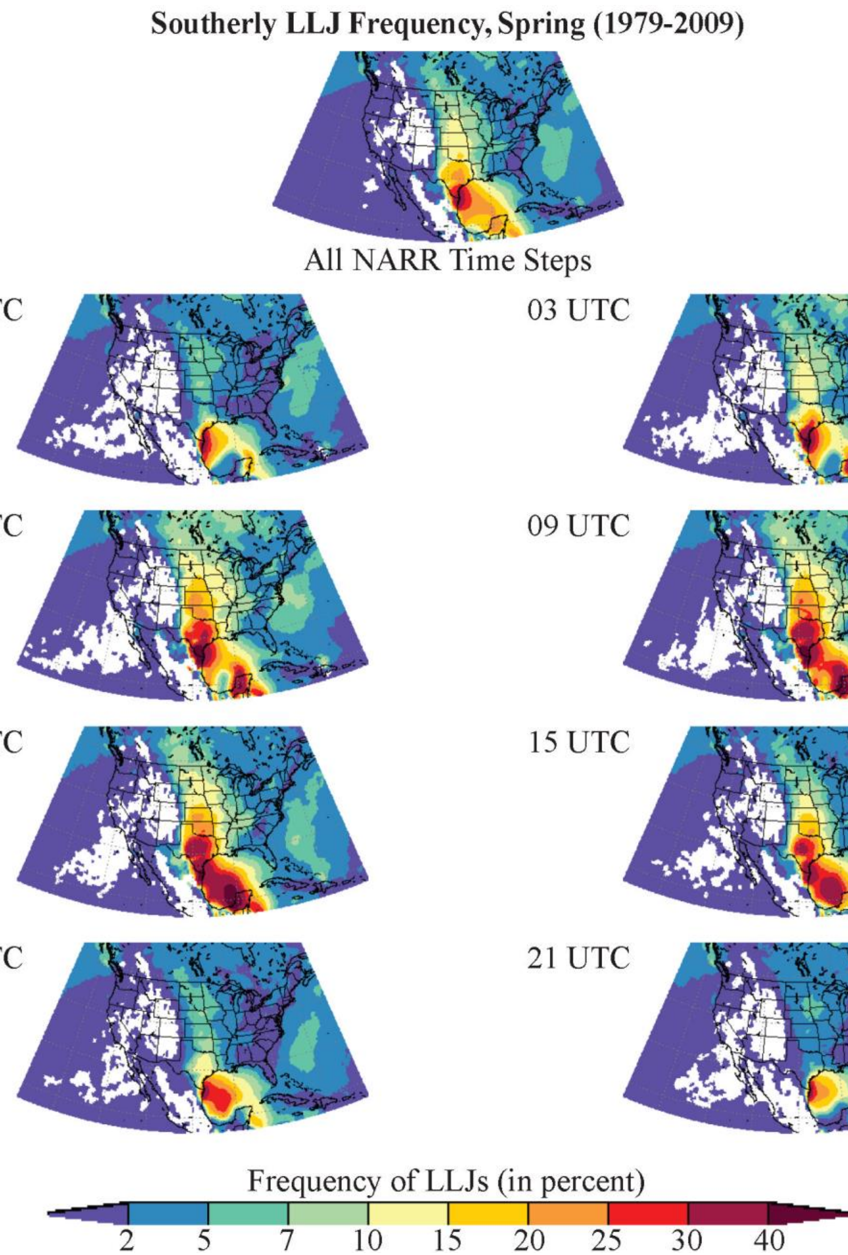

Figure 7. Spring (March-May) frequency (percentage) of S-LLJs from 1979 to 2009 expressed as a percentage of the total number of time steps, summed over all NARR time steps (top figure) and individually for each time step (bottom figures). Gridpoints with no jet cases and/or surface elevations >2km MSL are shown in white.

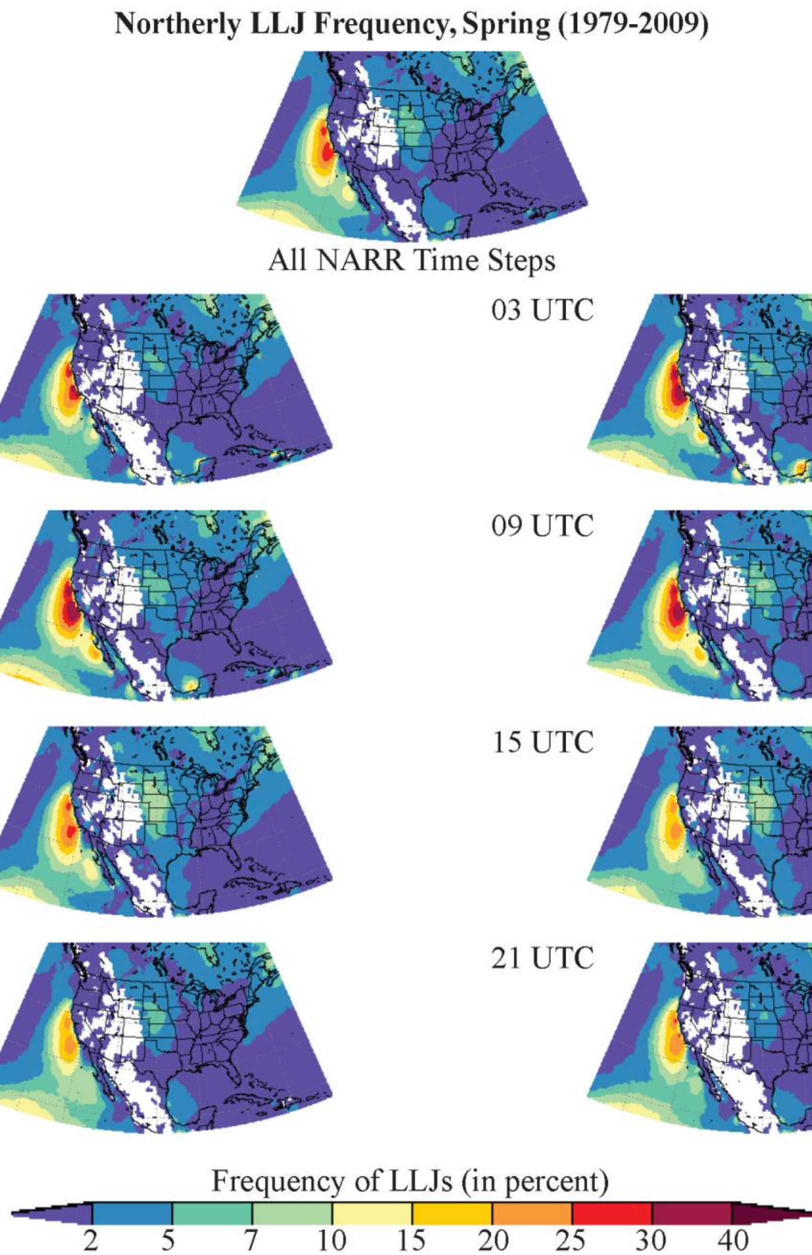

Figure 8. Spring (March-May) frequency (percentage) of N-LLJs from 1979 to 2009 expressed as a percentage of the total number of time steps, summed over all NARR time steps (top figure) and individually for each time step (bottom figures). Gridpoints with no jet cases and/or surface elevations >2km MSL are shown in white.

The frequency of N-LLJs along the Pacific coast increases dramatically from winter to spring (Figure 8). In March, N-LLJ frequencies of 15-20% are found within limited areas off the central and southern California coast, in contrast to a large area of N-LLJ frequencies >30% extending along the entire California coast in May. In addition, the frequency of N-LLJs along the coast of Baja California increases from March to May. Across the rest of the study domain, N-LLJ frequency decreases during the spring season. For example, the N-LLJ maximum in the Great Plains increases in intensity and extent from late winter to early spring (i.e., February to March) but decreases thereafter. The frequency maxima seen in winter in the southern Gulf of Mexico and northeast Canada also weaken and are no longer evident by May, although somewhat elevated jet frequencies are evident throughout the spring season over southern Hudson Bay.

The springtime S-LLJ diurnal pattern is similar to the wintertime diurnal pattern in that the lowest S-LLJ frequencies over North America are seen at 21 UTC, and the highest frequencies at 12 UTC. Diurnal variations are particularly large during spring in central Texas, where S-LLJ frequencies exceed 25% at night and in the morning (06, 09, 12, and 15 UTC) but fall below 5% by 21 UTC. Diurnal fluctuations are also found over the western Gulf of Mexico, although S-LLJ frequencies remain relatively large throughout the day in comparison to the central and southern Great Plains. Diurnal variations are much more modest in the area of elevated S-LLJ frequency off the mid-Atlantic coast. In general, the magnitude of the diurnal variations increases from March to May over central North America and the western Gulf of Mexico and decreases in the area of elevated S-LLJ frequency off the mid-Atlantic coast (see Appendix A). An enhancement of the diurnal cycle as spring progresses is particularly evident in central Texas and northward into Oklahoma and Kansas.

N-LLJs along the Pacific coast are frequent, particularly by late spring, at all NARR time steps, although somewhat larger frequencies occur from the late afternoon to early morning (00, 03, 06 and 09 UTC) on the seasonal and monthly (see Appendix B) plots. Similar to winter, the N-LLJ frequency maximum during early spring in the Great Plains is best defined from early to late morning (09, 12, 15 UTC), whereas the frequency maximum over the southern Gulf of Mexico is best seen at 03 and 06 UTC. N-LLJs over southern Hudson Bay and eastern Canada display little diurnal variation.

4) SUMMER

The area of elevated S-LLJ frequency contracts substantially in summer (Figure 9). The frequency maxima seen during winter and spring in coastal British Columbia, Kentucky/Tennessee, and off the east coast of the U.S. are no longer evident. The primary summertime feature is a north-south oriented frequency maximum extending from North Dakota southward to southern Texas and extreme northeastern Mexico. Multiple centers of larger (>15%) S-LLJ frequencies occur within this broad area, particularly in central Kansas/Oklahoma, southwest Texas, and southern Texas/northeast Mexico. A S-LLJ frequency maximum is also evident over the Yucatan Peninsula, but, in contrast to the previous seasons, the magnitude of the frequency maximum is considerably reduced and it is isolated from the frequency maximum in central North America by an area over the Gulf of Mexico with infrequent (<5%) S-LLJ occurrence. A small S-LLJ frequency maximum is also seen in the vicinity of Hudson Bay, although slightly shifted to the east of the location of a similar maximum in spring.

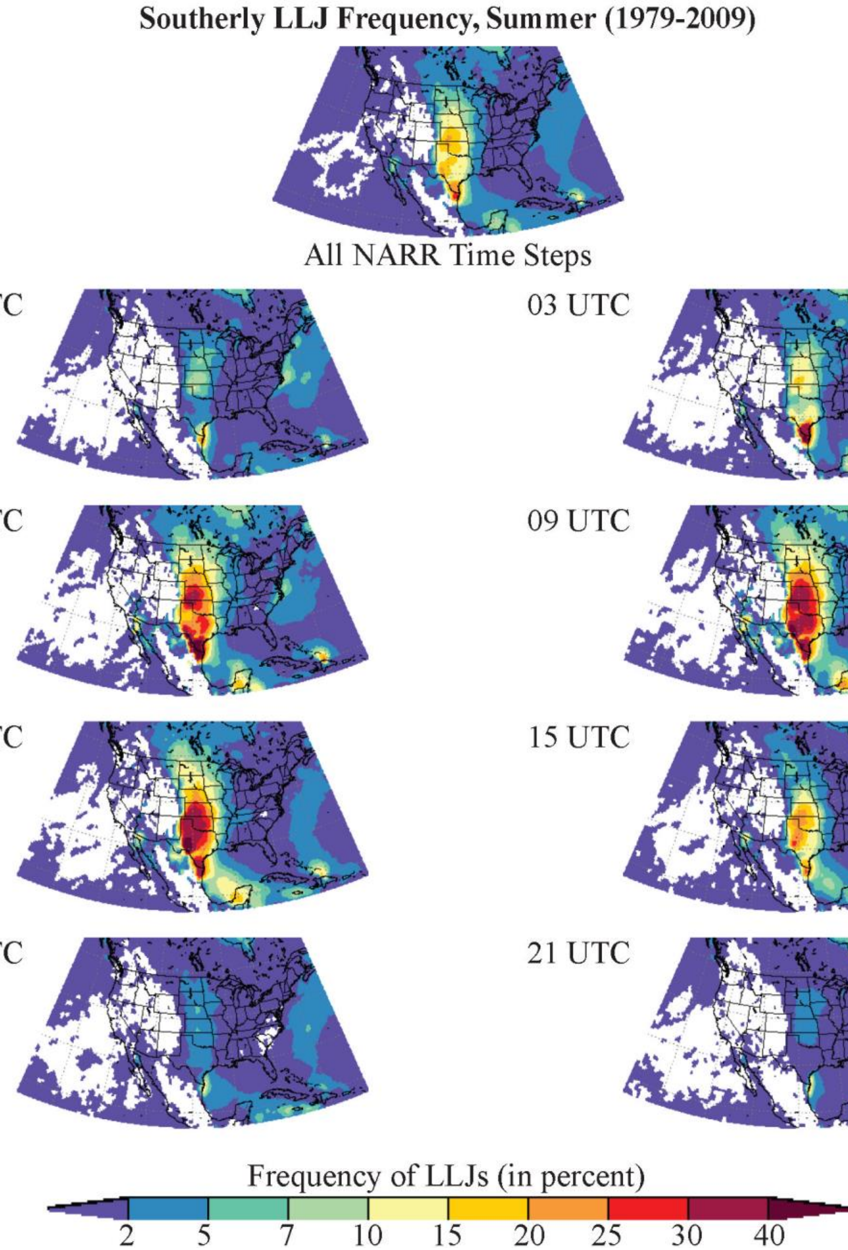

Figure 9. Summer (June-August) frequency (percentage) of S-LLJs from 1979 to 2009 expressed as a percentage of the total number of time steps, summed over all NARR time steps (top figure) and individually for each time step (bottom figures). Gridpoints with no jet cases and/or surface elevations >2km MSL are shown in white.

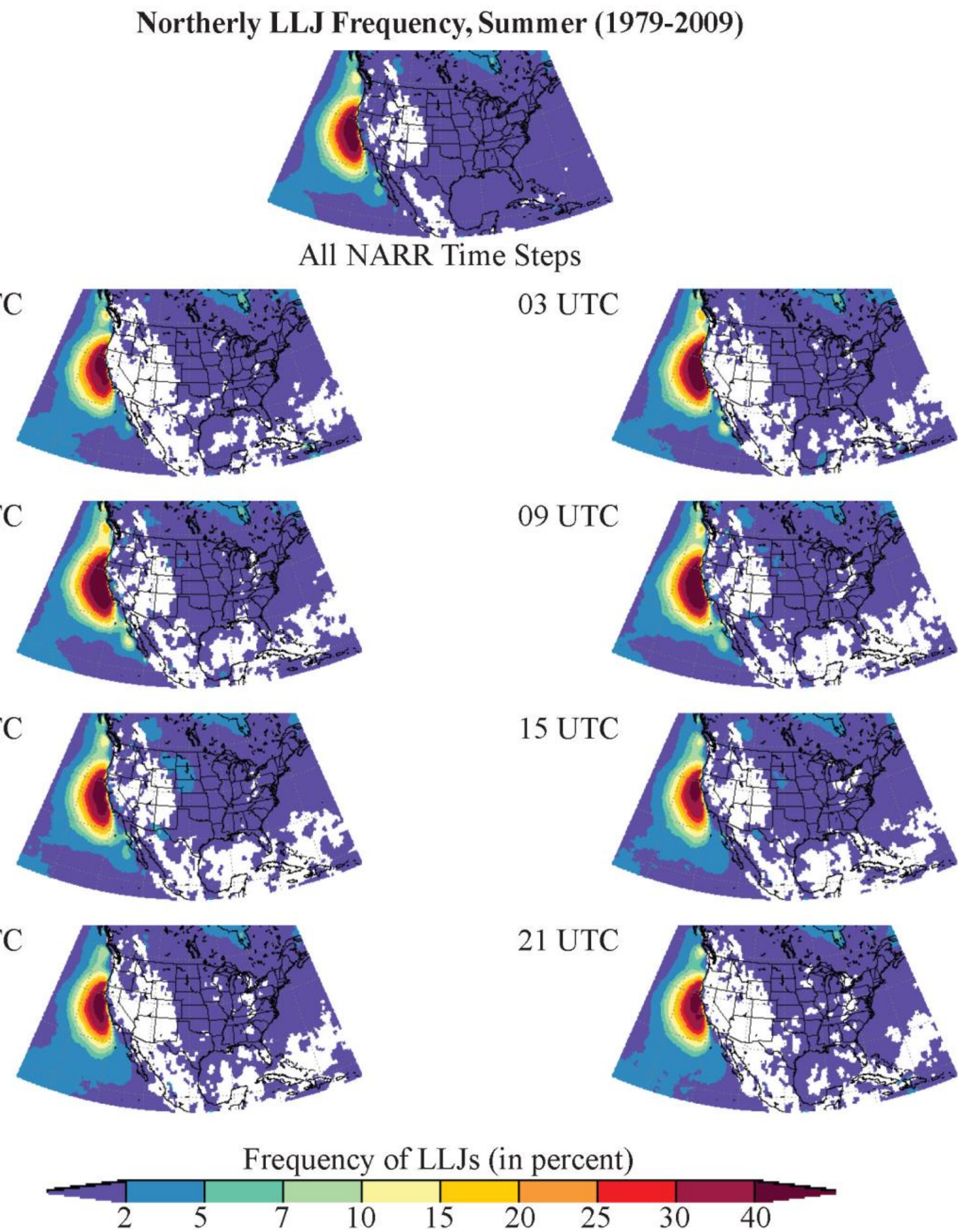

Figure 10. Summer (June-August) frequency (percentage) of N-LLJs from 1979 to 2009 expressed as a percentage of the total number of time steps, summed over all NARR time steps (top figure) and individually for each time step (bottom figures). Gridpoints with no jet cases and/or surface elevations >2km MSL are shown in white.

Intra-seasonal differences of S-LLJ frequency are quite striking during summer. The spatial extent of the S-LLJ frequency maximum over central North America during June is similar to that observed in late spring (i.e., May), but by July this area contracts substantially as S-LLJs become relatively infrequent over the western Gulf of Mexico (see Appendix A). Also, a more distinct frequency maximum is evident in Kansas and Oklahoma in July and August compared to June. The overall frequency of S-LLJs generally decreases in August compared to earlier in the summer, particularly over southern Texas. Also, a frequency maximum is no longer is evident over the Yucatan Peninsula during August, in contrast to earlier in the summer.

N-LLJs during summer primarily occur along the Pacific coast (Figure 10). One exception is a very modest frequency maximum over Hudson Bay, best seen in June and during the evening hours. The Pacific coast frequency maximum is displaced northward compared to winter and spring, extending from British Columbia to northern Baja California. This displacement is greater in July and August than in June.

Large diurnal variations in S-LLJ frequency are observed from southern Nebraska to southern Texas during the summer season. During June and July, S-LLJ frequency is largest in the early morning at 09 and 12 UTC with frequencies exceeding 40% at some NARR gridpoints, in contrast to S-LLJ frequencies of approximately 5% in the early and mid-afternoon (i.e., 18 and 21 UTC) (see Appendix A). Strong diurnal variations are also observed for August (see Appendix A), although, as noted above, the overall frequency of S-LLJs declines in August compared to earlier in the summer. Farther south, diurnal variations in S-LLJ frequency are present over the Yucatan Peninsula, even though S-LLJs are much less frequent in this area in summer compared to winter and spring. As for the central and southern Great Plains, S-LLJs over the Yucatan Peninsula were identified more often in the wind profiles for the nighttime and early morning NARR time steps (i.e., 03, 06, 09, and 12 UTC). Modest diurnal variations in S-LLJ frequency are also evident during summer over Hudson Bay, with S-LLJs more frequent at 06 and 09 UTC. Although a S-LLJ frequency maximum is not evident off the east coast of the U.S. when jet frequencies are accumulated across all NARR time steps, a small (5-10%)

maximum, located immediately along the coast, can be seen for the late afternoon and evening (i.e., 00, 03, and 06 UTC) time steps during June and July but not August.

As noted for spring, N-LLJs along the Pacific coast are frequent at all times of day, although the area of N-LLJ frequencies > 40% has a somewhat larger spatial extent for the evening (03, 06, and 09 UTC) time steps.

5) FALL

Considerable intra-seasonal differences are also seen during the transition season of fall (see Appendix A). On the seasonal and individual monthly plots for October and November, three centers of higher S-LLJ frequencies (Kansas/Oklahoma, central/southwest Texas, and south Texas/northeast Mexico) are found in central North America (Figure 11). In contrast, a broad center, extending from northern Nebraska to northern Texas, is seen in September. The frequency maximum over south Texas/northeastern Mexico is considerably weaker in September and is disconnected from the broader maximum over central North America. However, by November, S-LLJs are most frequent in south Texas/northeastern Mexico. Additionally, the area of >10% S-LLJ frequency contracts southward from northern South Dakota and southern Minnesota in September to northern Kansas by November. In all three months, S-LLJs are infrequent over the Yucatan Peninsula. A frequency maximum over Hudson Bay is evident in September and October but not in November, whereas over British Columbia S-LLJs are infrequent in September but substantially increase in frequency by November.

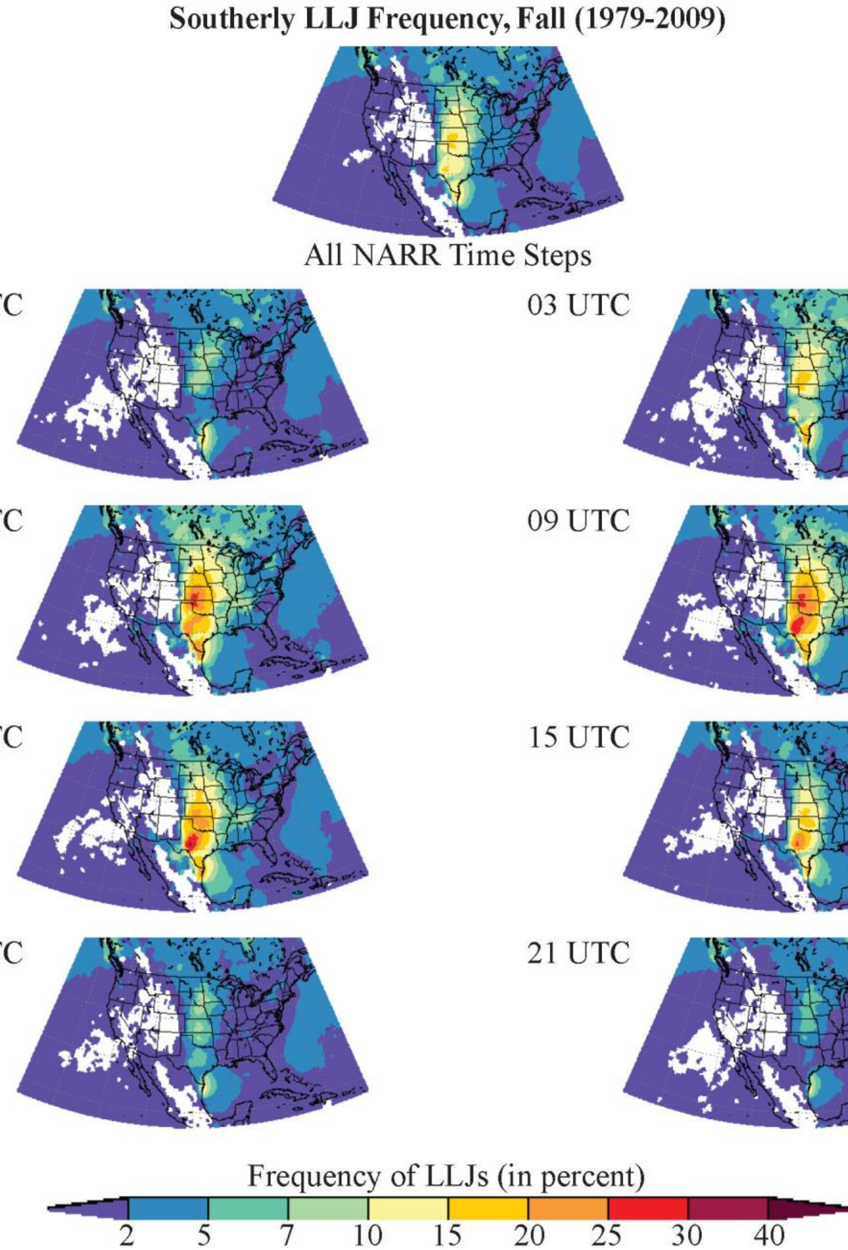

Figure 11. Fall (September-November) frequency (percentage) of S-LLJs from 1979 to 2009 expressed as a percentage of the total number of time steps, summed over all NARR time steps (top figure) and individually for each time step (bottom figures). Gridpoints with no jet cases and/or surface elevations >2km MSL are shown in white.

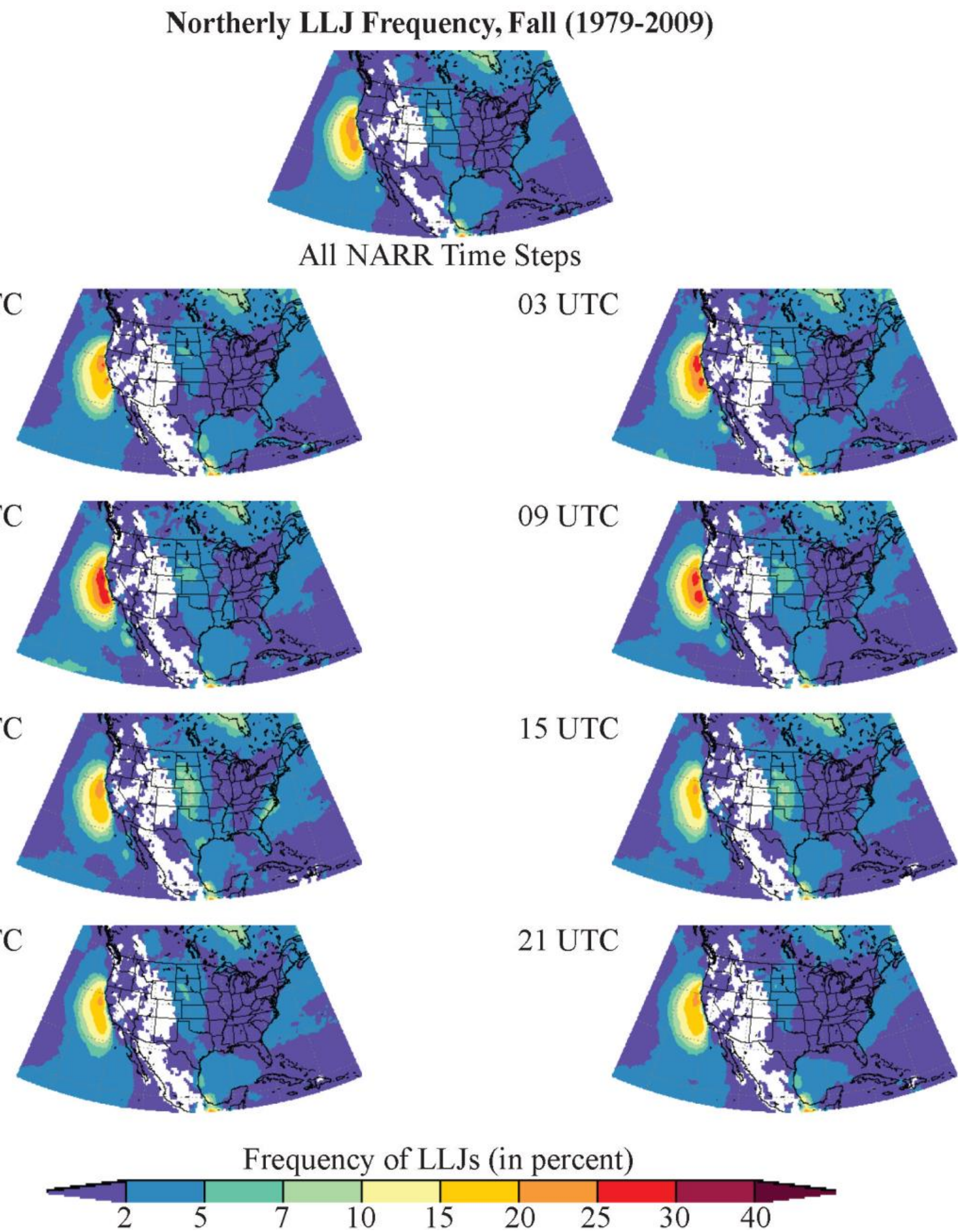

Figure 12. Fall (September-November) frequency (percentage) of S-LLJs from 1979 to 2009 expressed as a percentage of the total number of time steps, summed over all NARR time steps (top figure) and individually for each time step (bottom figures). Gridpoints with no jet cases and/or surface elevations >2km MSL are shown in white.

The N-LLJ frequency pattern for fall reflects the transition from a summer to winter pattern. From September to November, N-LLJ frequencies along the Pacific coast decrease substantially, and the frequency maximum shifts southward. In the Great Plains, an area of elevated (>5%) N-LLJ frequencies is first seen on the October plot and by November extends from southern North Dakota to northern Texas. In October, a N-LLJ frequency maximum is once again found over Hudson Bay, and, by November, maxima are also observed in eastern Canada and the southern Gulf of Mexico, as previously described for the winter season.

During fall, diurnal variations in S-LLJ frequency are small in the western Gulf of Mexico. Although the overall frequency of S-LLJs in this area increases from September through November, the jets are approximately equally frequent for all NARR time steps. On the other hand, the strong diurnal signal seen in summer from central Nebraska to Texas is also present in fall, with more S-LLJs detected in the NARR vertical wind profiles at 06, 09, and 12 UTC compared to the other time steps. In September and October, although not in November, a modest diurnal variation in S-LLJ frequency is evident in central Canada and over Hudson Bay with frequencies of 5-10% at 03, 06, and 09 UTC. Also, S-LLJ frequencies of up to 15% are seen over Kentucky/Tennessee at the evening and early morning time steps (i.e., 06, 09, 12, and 15 UTC), particularly in October and November.

For N-LLJs, the spatial extent of the frequency maximum in the Great Plains is largest in mid-morning (12 and 15 UTC) (Figure 12). In contrast, Pacific coast N-LLJs are more frequent somewhat earlier at 03, 06, and 09 UTC, although this pattern is most evident in September and October, with little diurnal variation observed in November (see Appendix B). Diurnal variations are weak elsewhere (i.e., eastern Canada and southern Gulf of Mexico).

b) Speed and Height of Southerly and Northerly Low-Level Jets

Analysis of the average speed of S-LLJs suggests that, regardless of time of year, the mean speed of S-LLJs in the northern and central Great Plains is larger than that of S-LLJs in southern Texas, western Gulf of Mexico, and the Yucatan Peninsula (Figure 13). In summer, when across the study domain the mean speeds of S-LLJs are weaker than at other times of year, the average speed of S-LLJs in the central Great Plains is, on average, 2-3 ms^{-1} stronger than the average speeds observed farther south over the western Gulf of Mexico and surrounding land areas (Figure 14). Strong (>20 ms^{-1}) average speeds are seen during winter for S-LLJs in the central Great Plains, and for the less frequent S-LLJs over the eastern Pacific, eastern United States, and western Atlantic in all seasons except summer (see Appendix C). The average speeds of N-LLJs in the Great Plains during winter, when they are most frequent, exceed 18 ms^{-1} and in some places 20 ms^{-1} (see Appendix D). Average speeds are also large for cool season N-LLJs over eastern Canada. However, average speeds are weaker (~14-16 ms^{-1}) for N-LLJs over southern Hudson Bay and the extreme southern Gulf of Mexico, compared to the other areas with relatively frequent N-LLJs in winter and the transition seasons of spring and fall (see Appendix D). The average speeds of Pacific coast N-LLJs during summer, when they are most frequent, generally fall between 16-18 ms^{-1} (Figure 15).

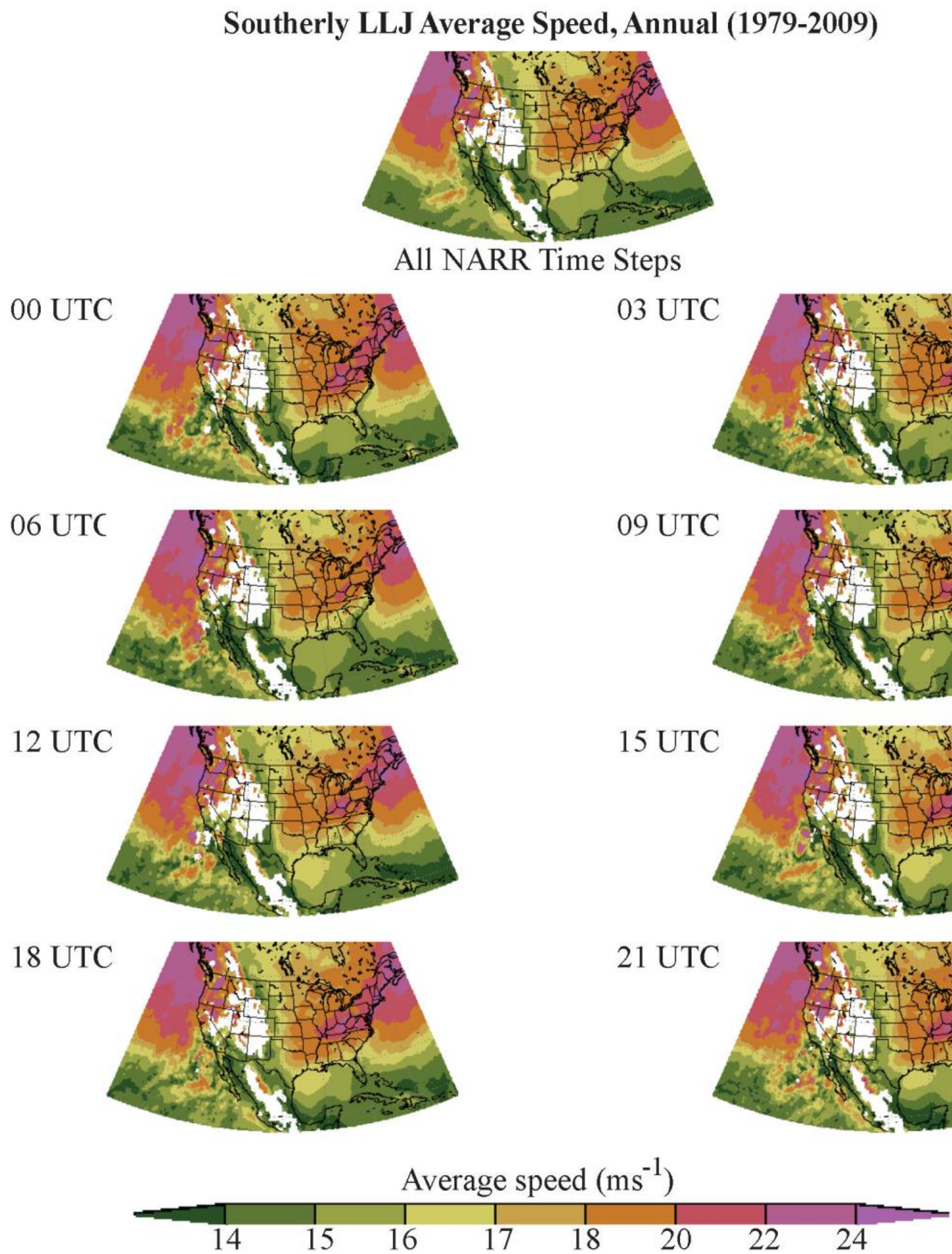

Figure 13. Annual average speed (meters per second) of S-LLJs from 1979 to 2009. Includes annual average speed across all NARR time steps and annual average speed at each individual NARR time step. Gridpoints with no jet cases and/or surface elevations >2km MSL are shown in white.

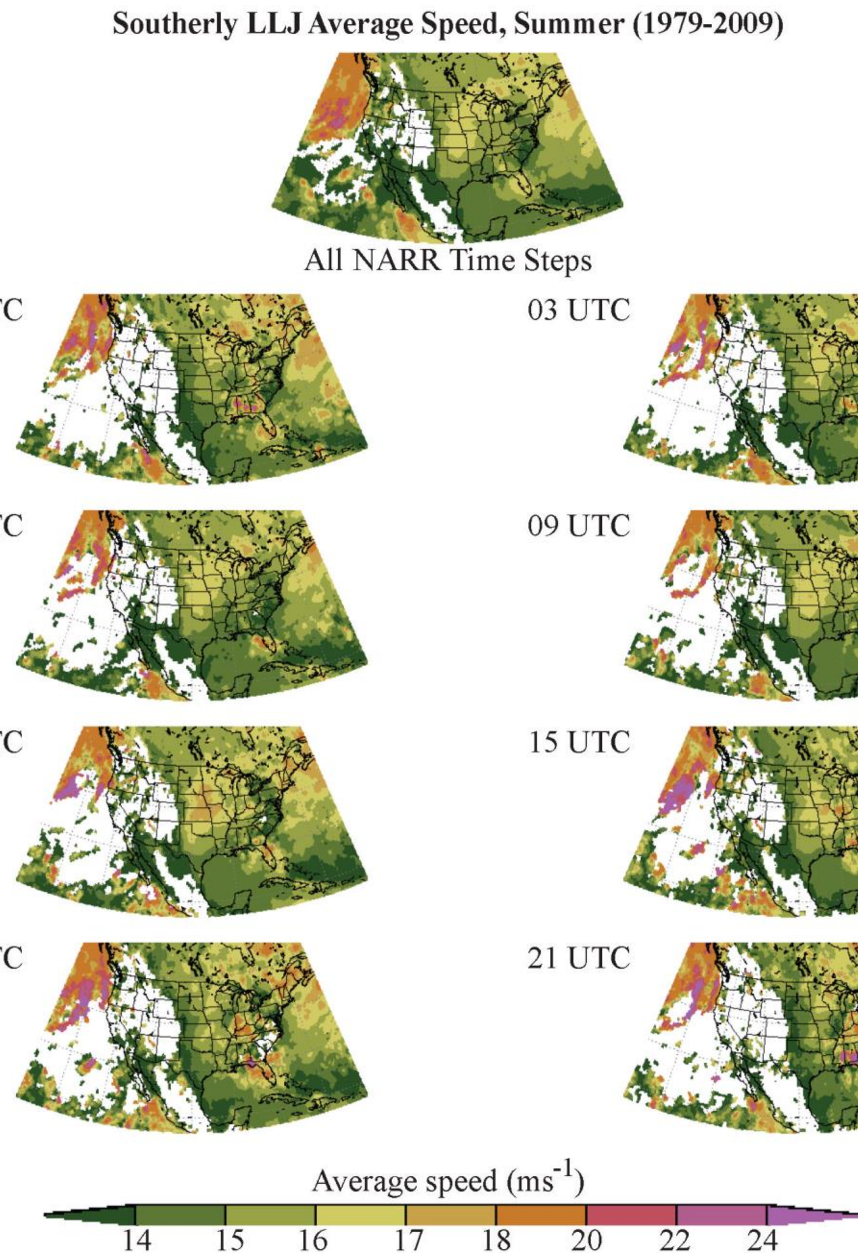

Figure 14. Average speed (meters per second) for S-LLJs that occurred during summer (June-August) from 1979-2009, for all jets (top figure) and for jets at each of the NARR time steps (bottom figures). Gridpoints with no jet cases and/or surface elevations >2km MSL are shown in white.

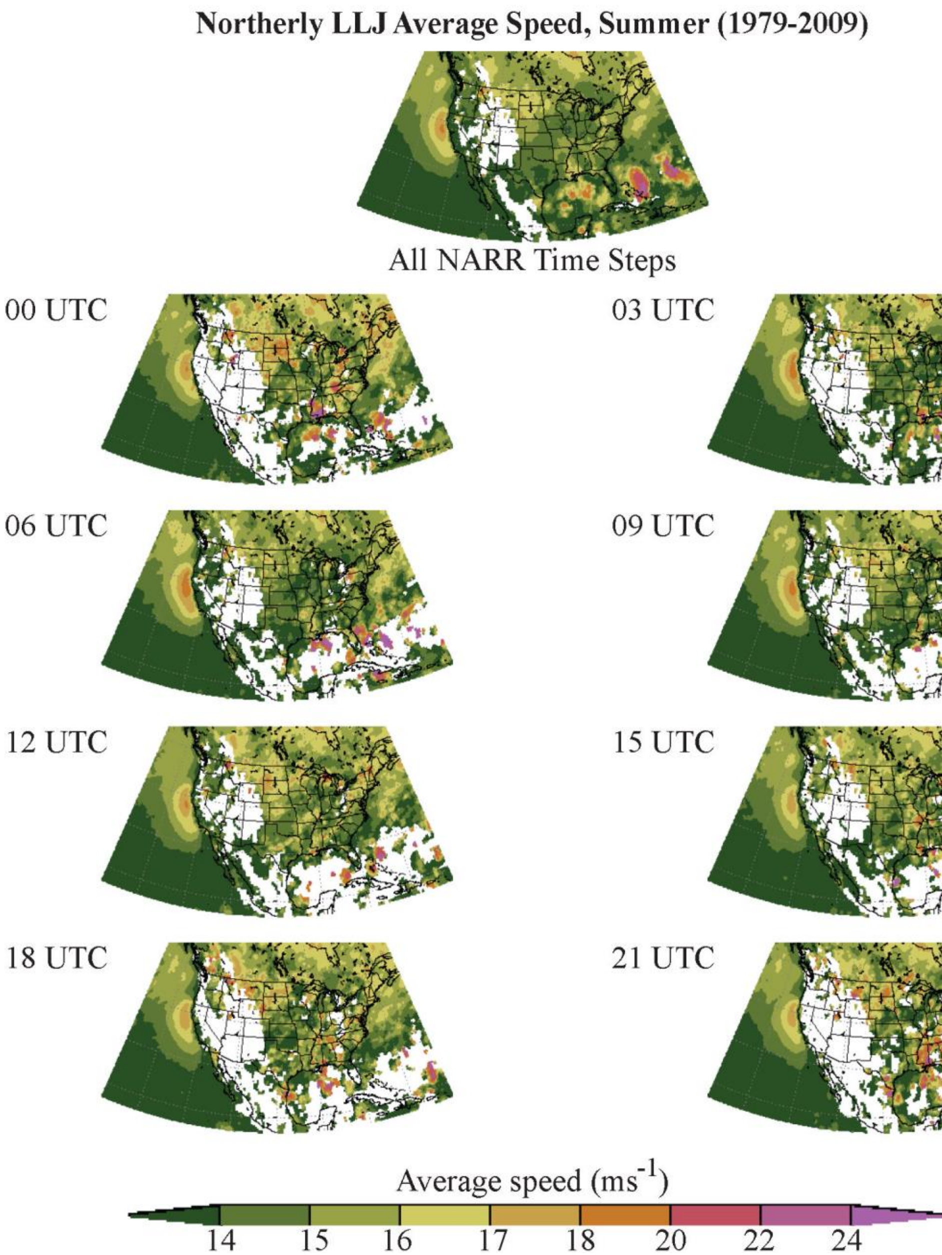

Figure 15. Average speed (meters per second) for N-LLJs that occurred during summer (June-August) from 1979-2009, for all jets (top figure) and for jets at each of the NARR time steps (bottom figures). Gridpoints with no jet cases and/or surface elevations >2km MSL are shown in white.

Diurnal fluctuations in mean speed are modest for both S-LLJs and N-LLJs. For S-LLJs, the largest diurnal fluctuations are seen in spring (see Appendix C) and summer (Figure 14), and primarily for S-LLJs in the central Great Plains. The average speed of summertime S-LLJs in the central plains is largest (>18 ms^{-1}) at 12 UTC and decreases to 14-16 ms^{-1} by 21 UTC. A similar fluctuation is seen in spring. The average speeds of N-LLJs along the Pacific coast during summer are somewhat larger at 03, 06, and 09 UTC compared to other times of the day (Figure 15), whereas little diurnal fluctuation in speed is found for wintertime N-LLJs in the Great Plains (see Appendix D).

Throughout the year, a marked diurnal fluctuation in the average elevation of the "nose" of S-LLJs is evident in central and eastern North America, although not for S-LLJs over the western Gulf of Mexico, the eastern Pacific or the western Atlantic. This fluctuation is most evident in summer (Figure 16), when the average elevation is lower (400-800 m AGL) in the morning hours (06, 09, 12 UTC) and higher (1000 m to over 1400 m AGL) in the afternoon and early evening hours (18, 21, 00 UTC). With the exception of the eastern Gulf of Mexico, S-LLJs over coastal waters tend to be found at relatively low elevations (400-800 m AGL) at all times of day and throughout the year. Seasonal variations in S-LLJ elevation are largest in the southeastern US, eastern Gulf of Mexico, and northern Caribbean. Although relatively infrequent, S-LLJs in this area are found at higher elevations in summer compared to the other seasons (see Appendix E). In general, wintertime N-LLJs in the Great Plains are found at higher elevations (>1000 m AGL) compared to the average elevations (400-600 m AGL) of summertime N-LLJs along the Pacific coast (see Appendix F). Neither display marked diurnal variations in elevation.

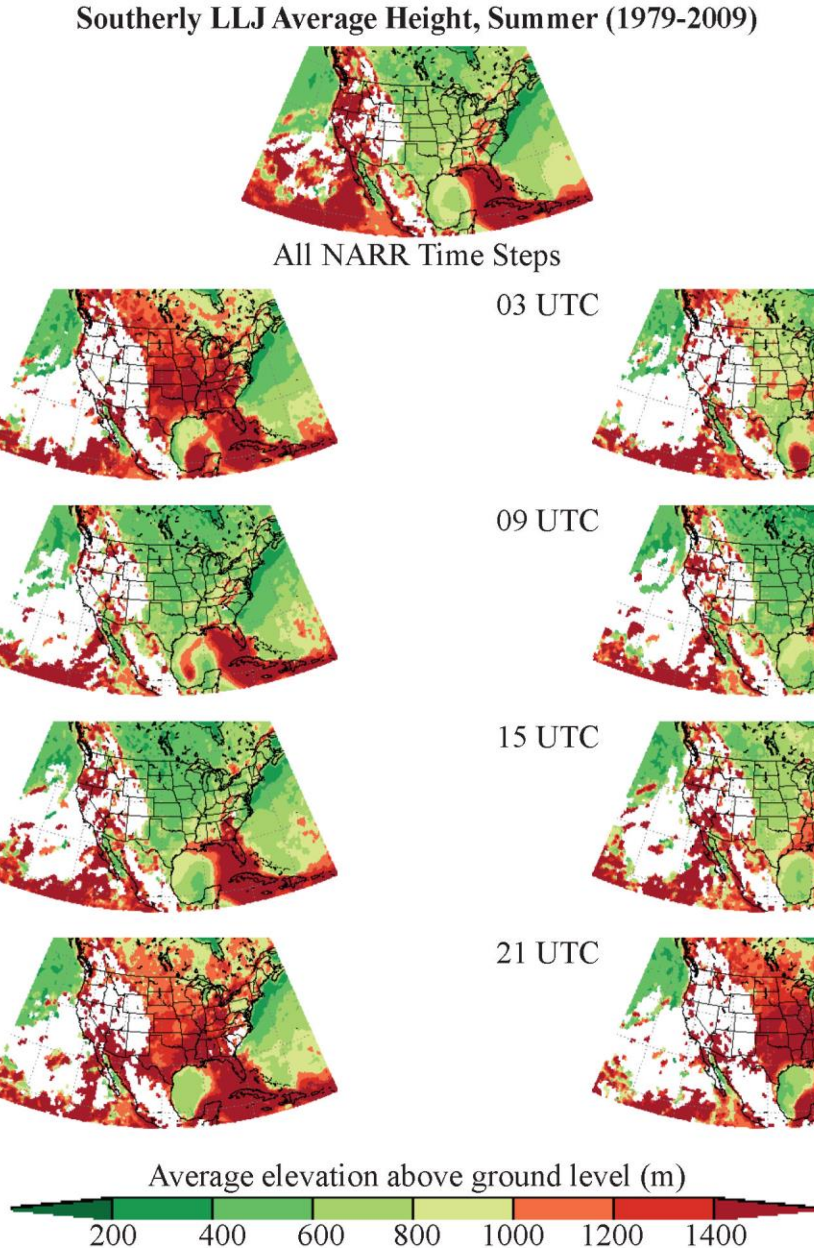

Figure 16. Average elevation (meters of above ground level) for S-LLJs that occurred during summer (June-August) from 1979 to 2009, for all jets (top figure) and for jets at each of the NARR time steps (bottom figures). Gridpoints with no jet cases and/or surface elevations >2km MSL are shown in white.

c) Temporal Trends and Interannual Variability

Analysis of the temporal trends and interannual variability in jet frequency was performed for selected NARR gridpoints in central North America where S-LLJs are particularly frequent and off the Pacific coast and in the Great Plains where N-LLJs are frequent (Figure 2) In terms of temporal trends, significant ($p \leq 0.05$) positive trends in the annual frequency of S-LLJs are seen at all the selected gridpoints in central North America, from south central North Dakota (Figure 17) to the Yucatan Peninsula (Figure 18). S-LLJ frequencies have increased the most (~10% in the 31-year period) at the north central Texas gridpoint. However, seasonal differences exist. In summer, significant trends are observed at four of the six gridpoints, within insignificant trends in central Kansas and the Yucatan Peninsula. In contrast, significant trends during winter are only evident at the north central Texas and Yucatan gridpoints. During fall, the temporal trend in jet frequency is insignificant for the two southernmost gridpoints (southern Texas and the Yucatan) but significant for the more northerly locations. A less clear spatial pattern is seen in spring, with significant trends found at all gridpoints except south central South Dakota and the Yucatan. Interannual variability in S-LLJ frequency is relatively modest, except during fall and winter at the two northernmost gridpoints in the Dakotas (Figure 19), and during summer and fall for the gridpoint in the Yucatan (Figure 20).

Although significant positive ($p \leq 0.05$) trends in annual N-LLJ frequency are observed for the three gridpoints off the Pacific coast, the seasonal analysis indicates that significant trends occur only during fall, and then only for the gridpoints off the coast of Oregon and southern California (Figure 21). Interannual variability in N-LLJ frequency is greatest at these gridpoints in winter, when N-LLJs are less frequent (Figure 22). For N-LLJs in the Great Plains, significant positive trends in jet frequency are observed at the three northernmost gridpoints (southwestern

North Dakota, southwestern South Dakota, central Nebraska) for the annual and winter aggregation levels (Figure 23), but not at the three southernmost gridpoints (western Kansas, southwestern Oklahoma, northern Texas) (Figure 24). The only other significant trend is found at the northern Texas location in spring. Interannual variability is largest in summer (Figure 25 and Figure 26).

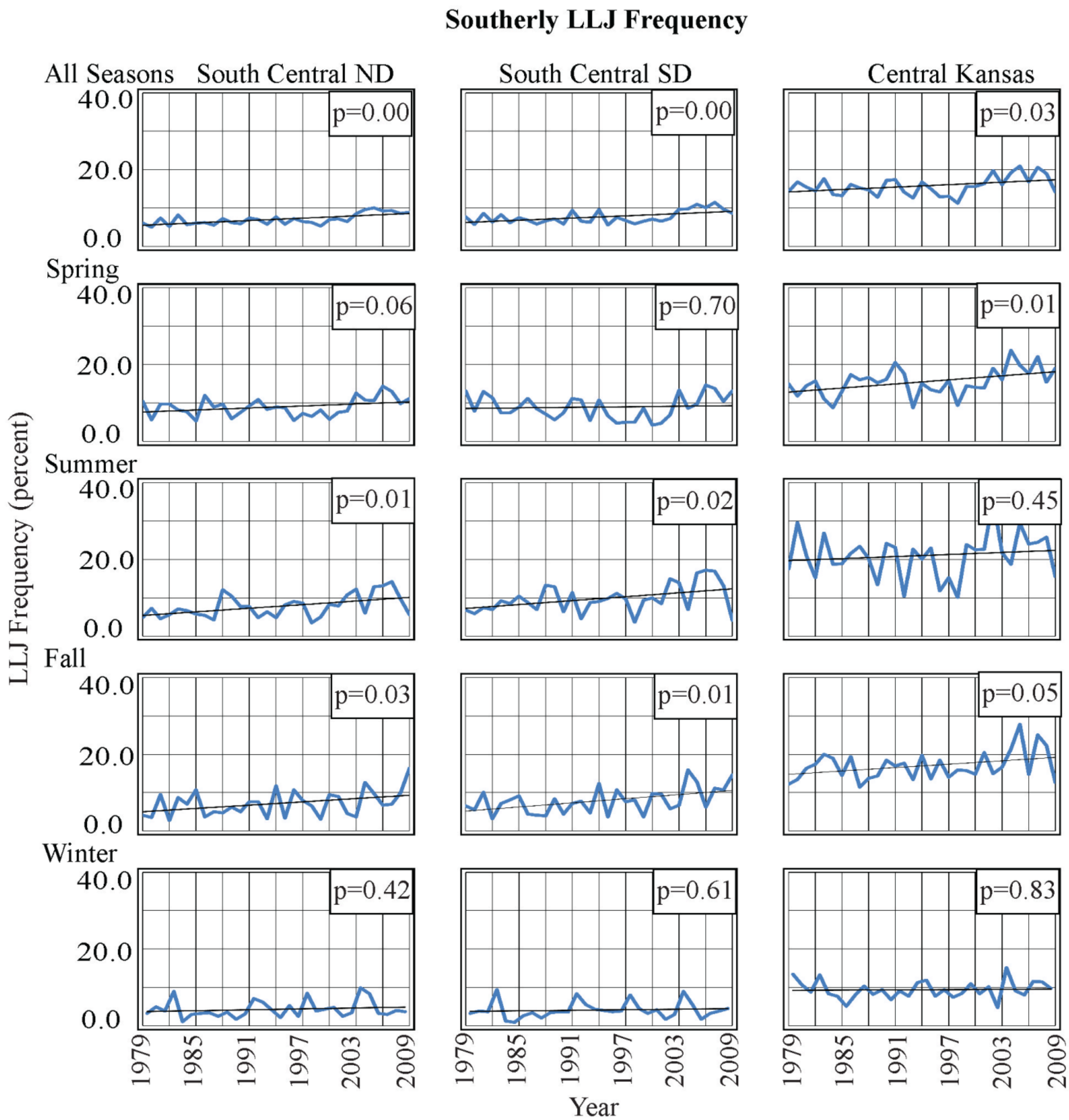

Figure 17. Annual and seasonal frequencies from 1979-2009 of S-LLJs in south central North Dakota (-100.5˚, 46.3˚), south central South Dakota (-100.8˚, 43.4˚), and central Kansas (-98.7˚, 38.6˚). Jet frequencies are expressed as the percentage of all possible NARR time steps per year.

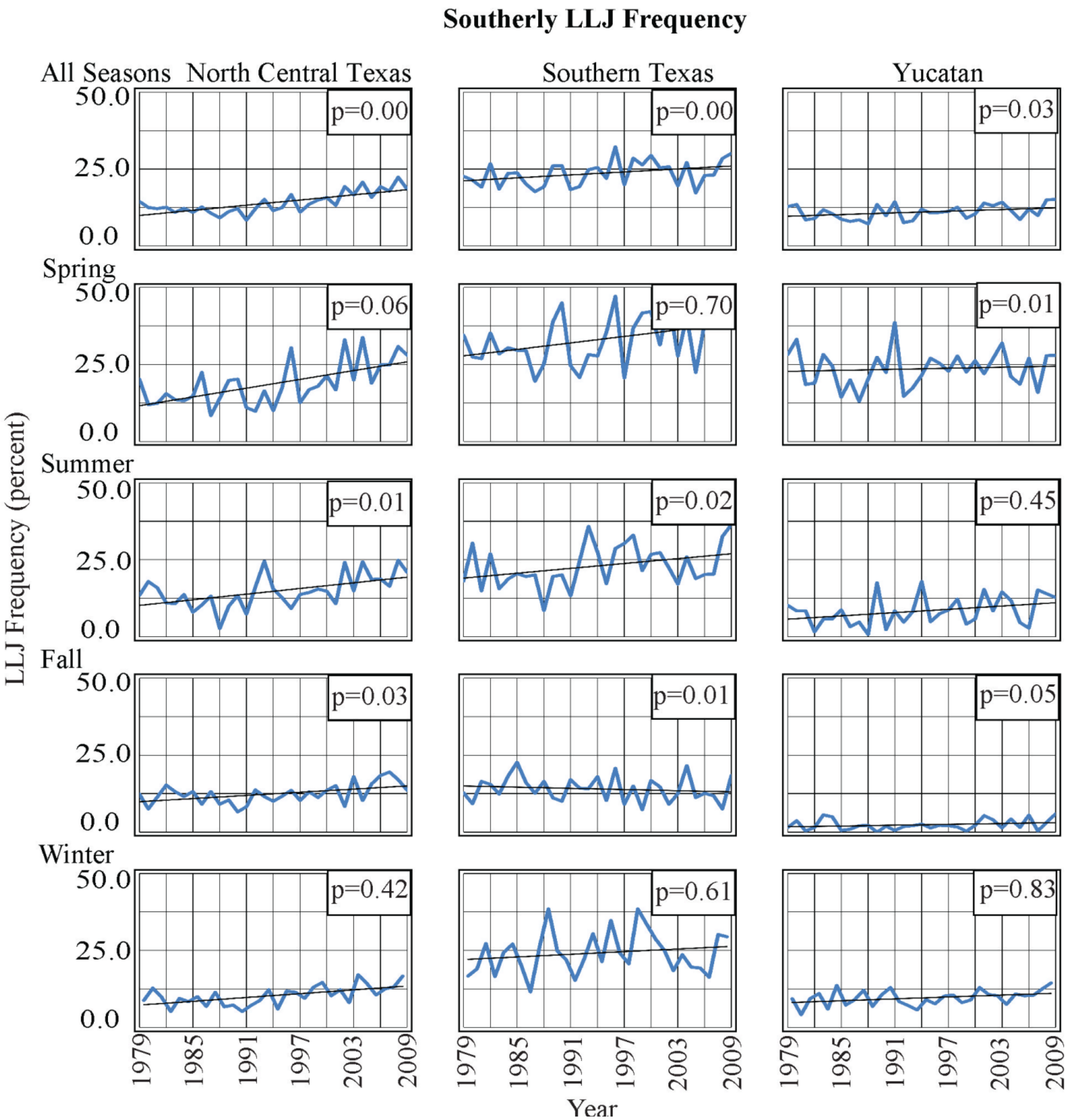

Figure 18. Annual and seasonal frequencies from 1979-2009 of S-LLJs in north central Texas (-97.9˚, 32.5˚), southern Texas (-97.8˚, 26.1˚), and Yucatan (-89.7˚, 19.7˚). Jet frequencies are expressed as the percentage of all possible NARR time steps per year.

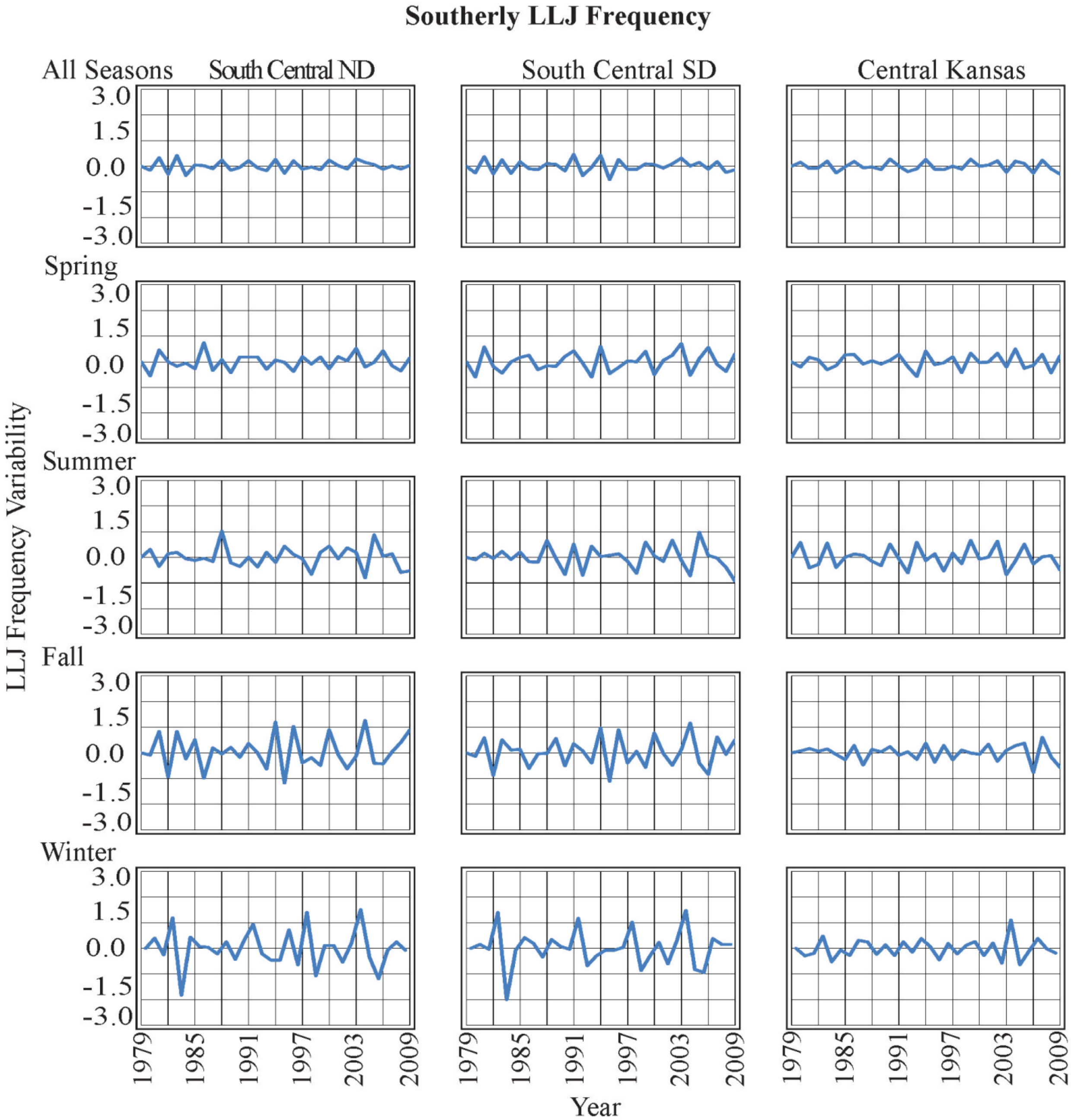

Figure 19. Interannual variability of detrended annual and seasonal frequencies of S-LLJs for the period 1979-2009 at south central North Dakota (-100.5˚, 46.3˚), south central South Dakota (-100.8˚, 43.4˚), and central Kansas (-98.7˚, 38.6˚). (See text for discussion of the detrending procedures.)

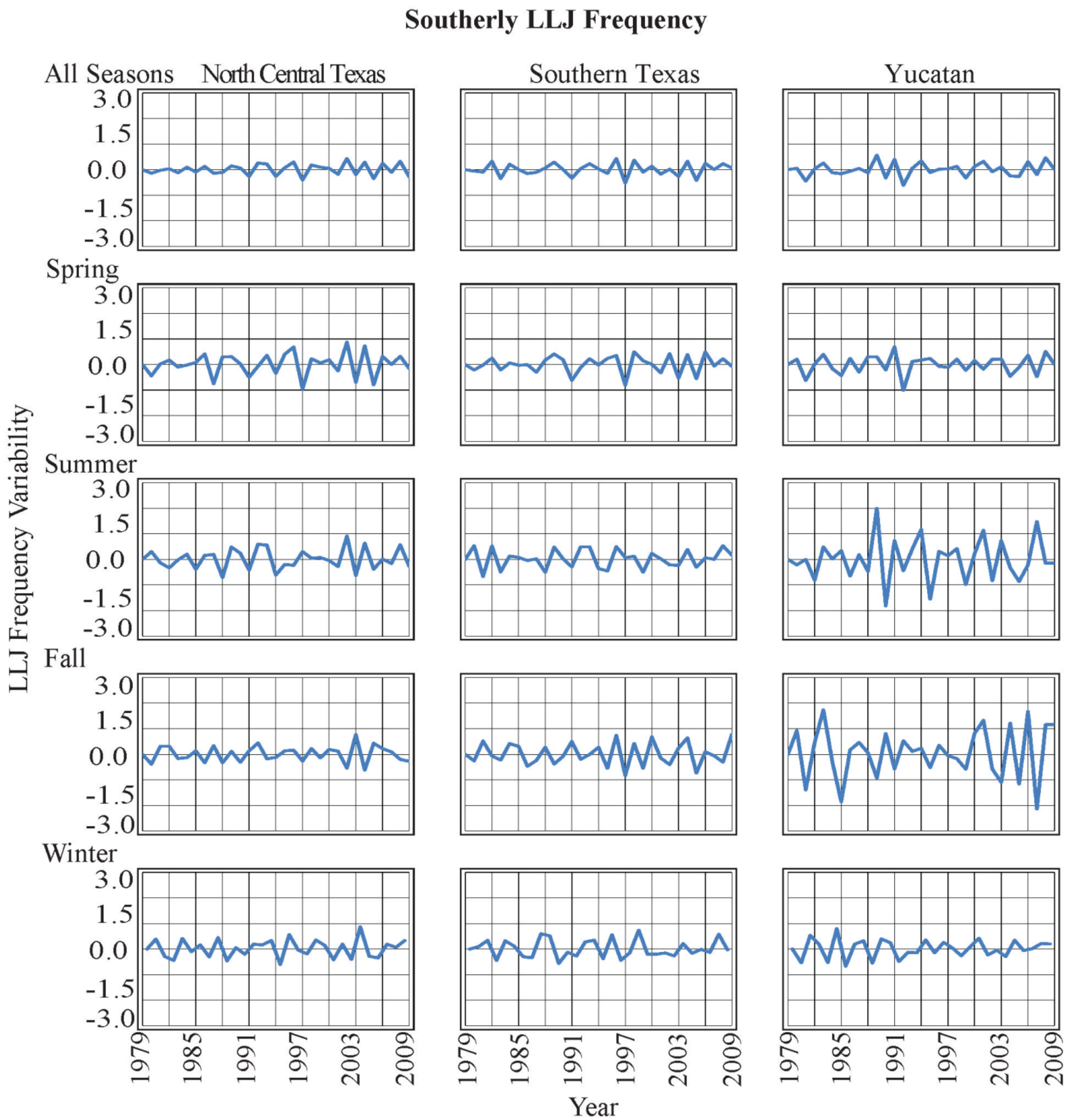

Figure 20. Interannual variability of detrended annual and seasonal frequencies of S-LLJs for the period 1979-2009 at north central Texas (-97.9˚, 32.5˚), southern Texas (-97.8˚, 26.1˚), and Yucatan (-89.7˚, 19.7˚). (See text for discussion of the detrending procedures.)

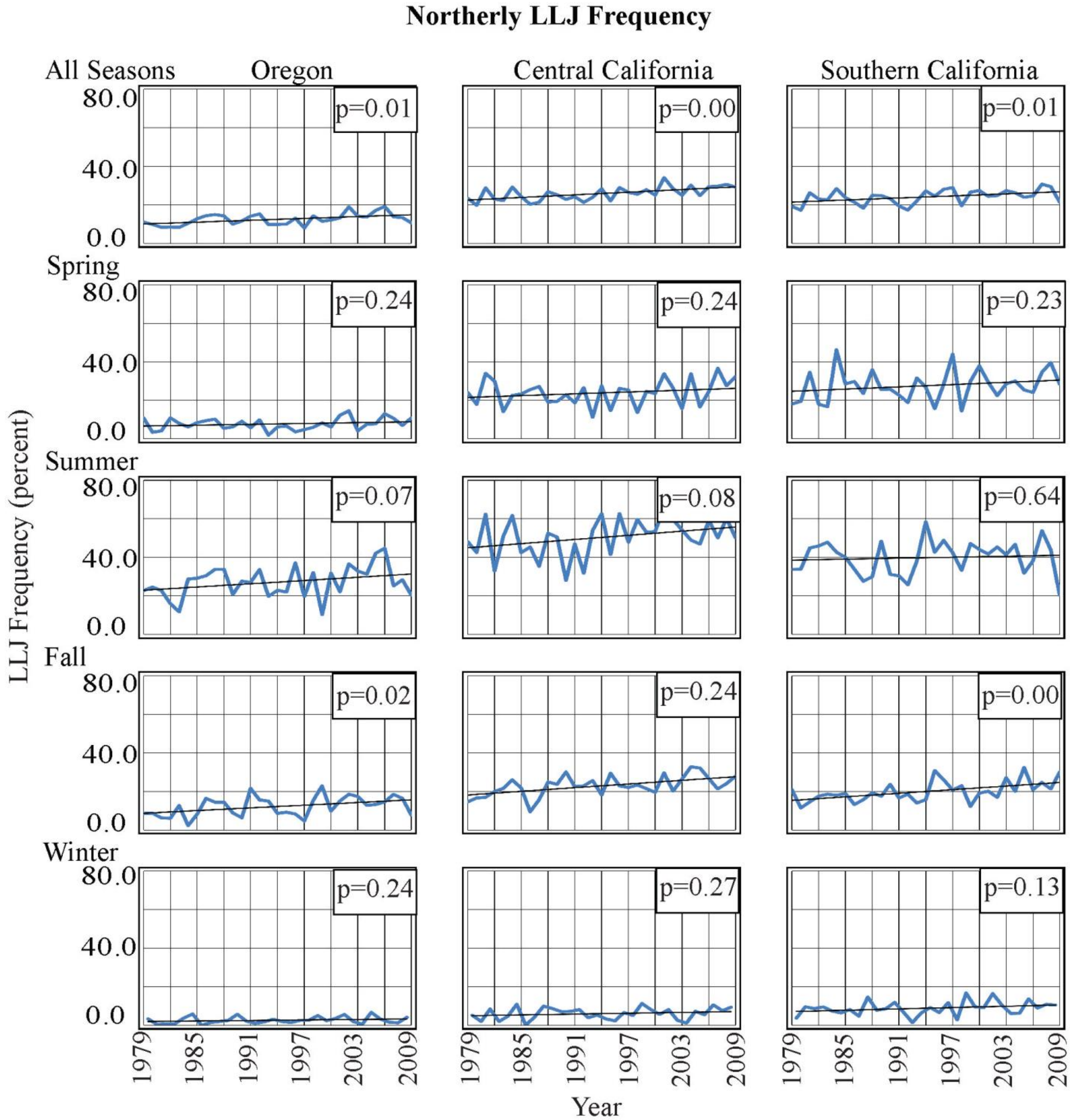

Figure 21. Annual and seasonal frequencies from 1979-2009 of N-LLJs in Oregon (-125.9˚, 42.7˚), central California (-124.9˚, -37.2˚), and southern California (-122.1˚, 33.4˚). Jet frequencies are expressed as the percentage of all possible NARR time steps per year.

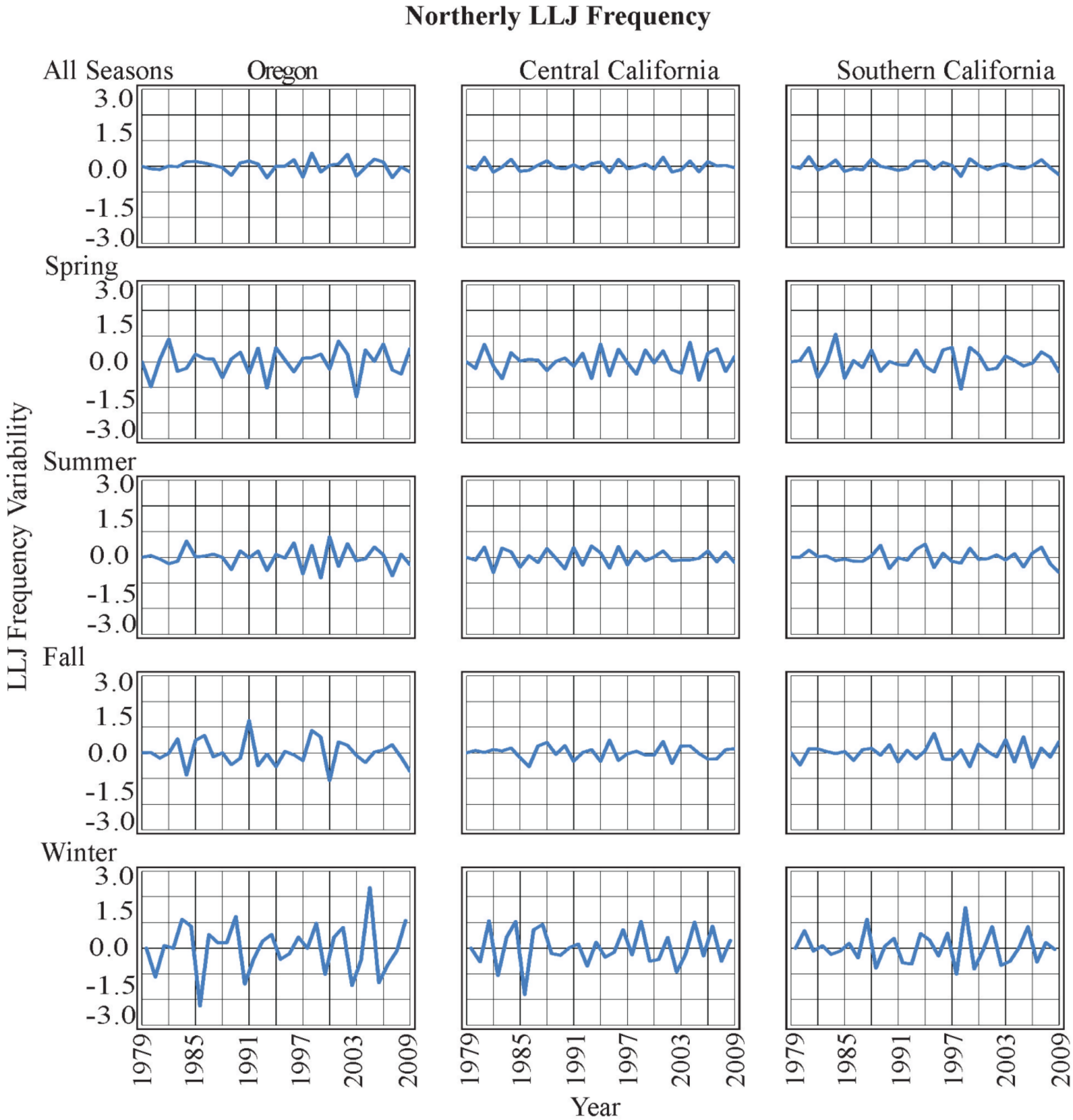

Figure 22. Interannual variability of detrended annual and seasonal frequencies of N-LLJs for the period 1979-2009 at Oregon (-125.9˚, 42.7˚), central California (-124.9˚, -37.2˚), and southern California (-122.1˚, 33.4˚). (See text for discussion of the detrending procedures.)

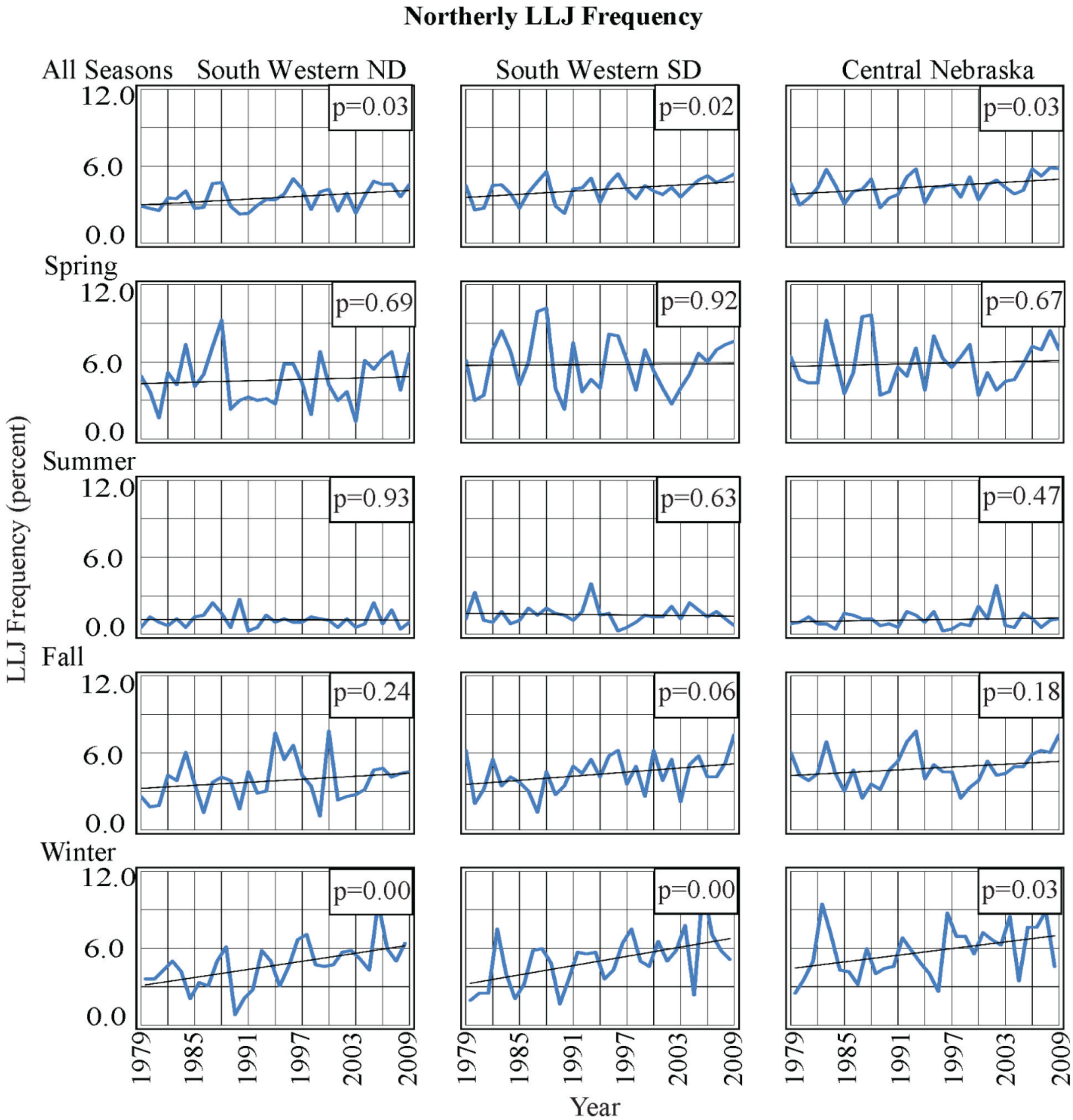

Figure 23. Annual and seasonal frequencies from 1979-2009 of N-LLJs in southwestern North Dakota (-102.6˚, 46.4˚), southwestern South Dakota (-102.8˚, 43.5˚), and central Nebraska (-101.1˚, 41.1˚). Jet frequencies are expressed as the percentage of all possible NARR time steps per year.

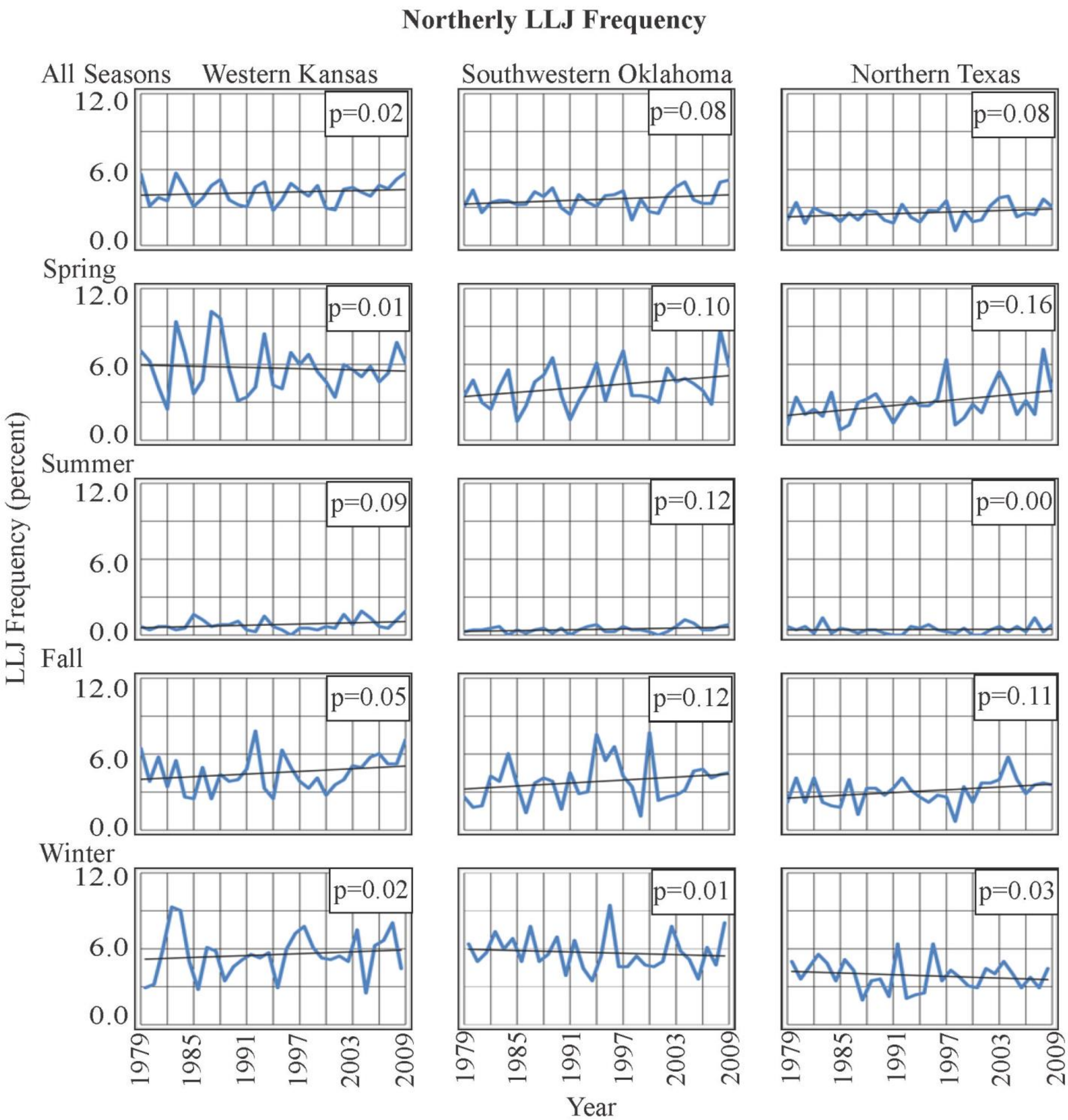

Figure 24. Annual and seasonal frequencies from 1979-2009 of N-LLJs in western Kansas (-100.9˚, 38.8˚), southwestern Oklahoma (-99.2˚, 34.9˚), and northern Texas (-100.4˚, 33.9˚). Jet frequencies are expressed as the percentage of all possible NARR time steps per year.

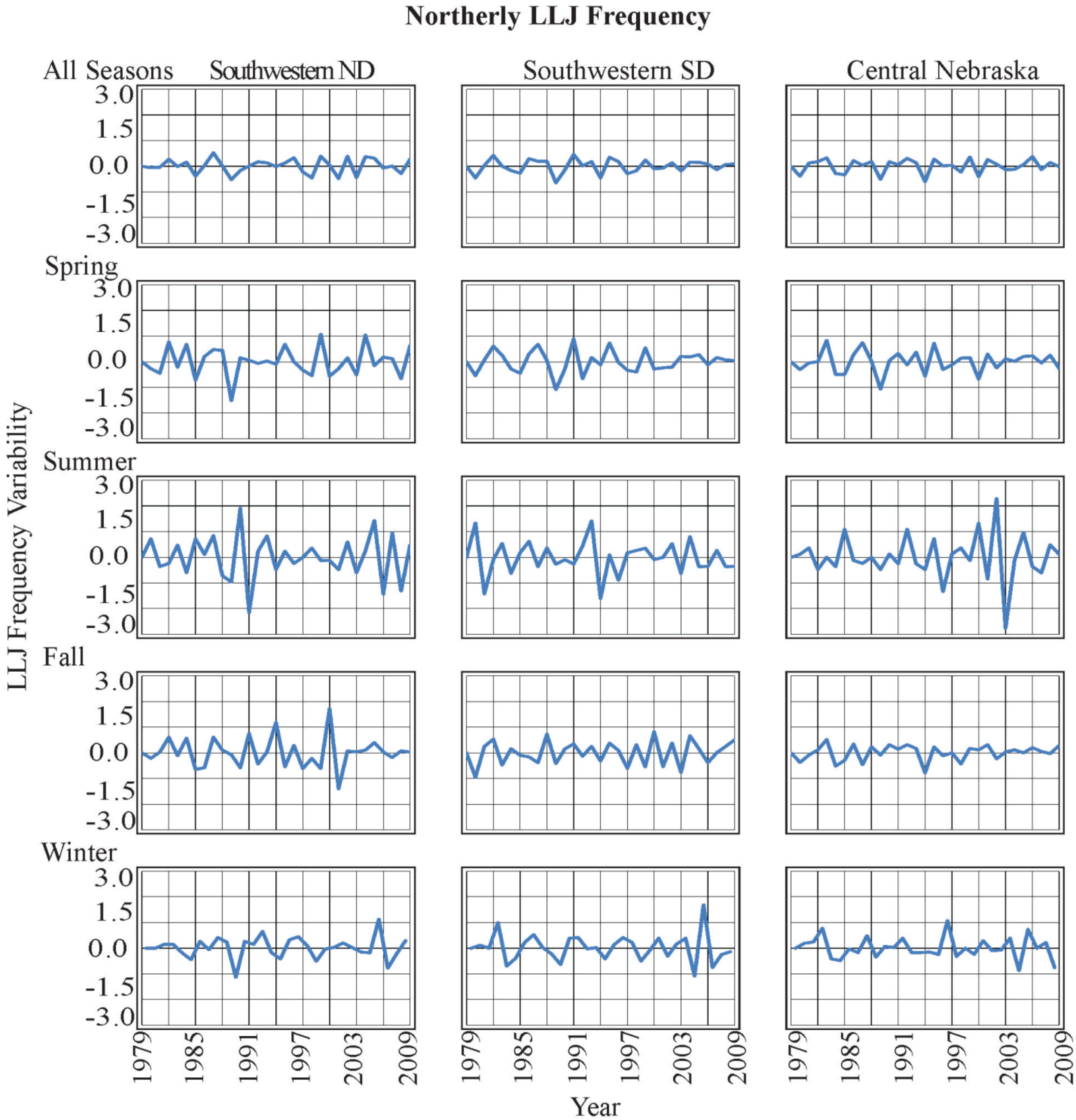

Figure 25. Interannual variability of detrended annual and seasonal frequencies of N-LLJs for the period 1979-2009 at southwestern North Dakota (-102.6˚, 46.4˚), southwestern South Dakota (-102.8˚, 43.5˚), and central Nebraska (-101.1˚, 41.1˚). (See text for discussion of the detrending procedures.)

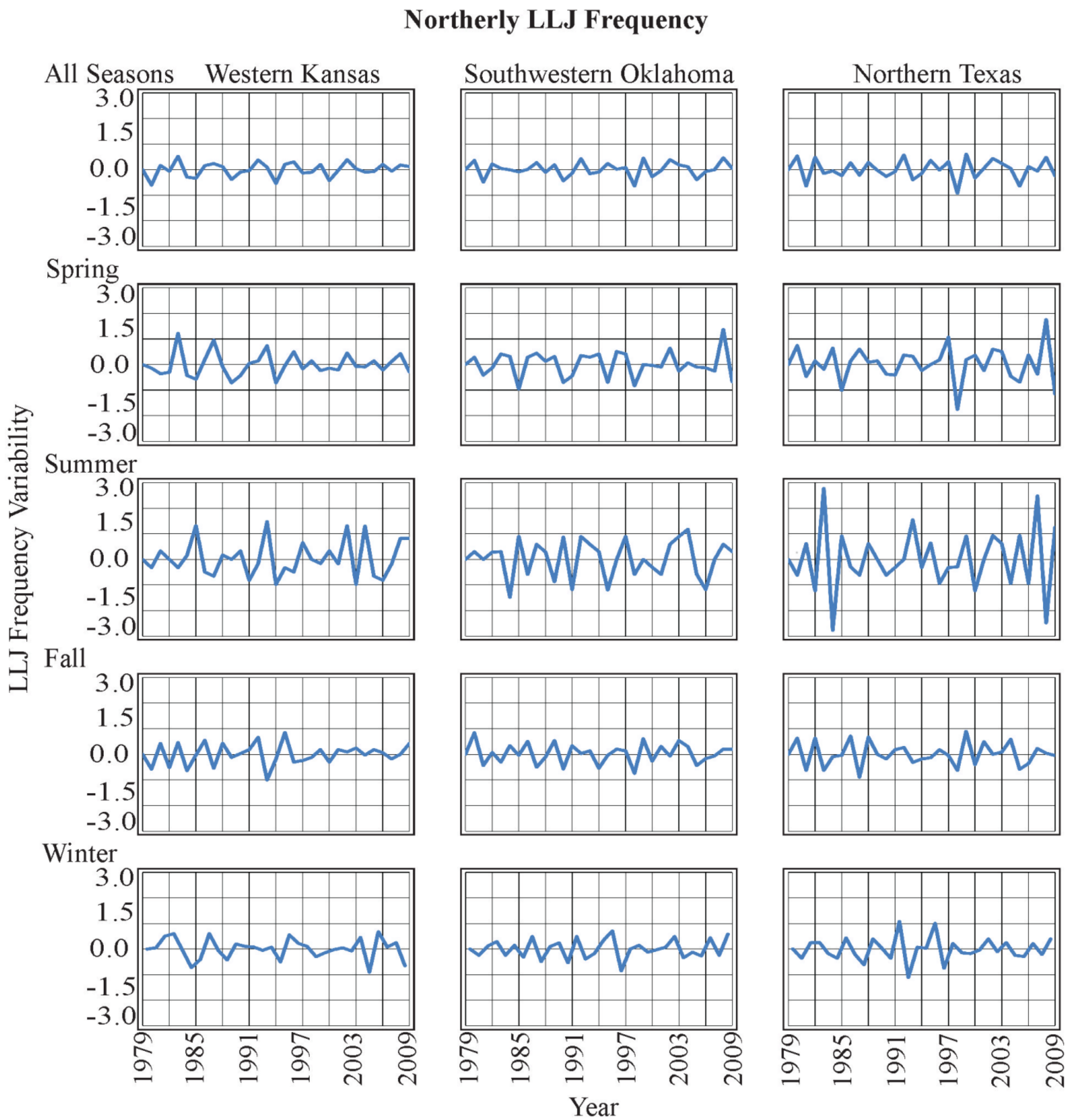

Figure 26. Interannual variability of detrended annual and seasonal frequencies of N-LLJs for the period 1979-2009 at western Kansas (-100.9˚, 38.8˚), southwestern Oklahoma (-99.2˚, 34.9˚), and northern Texas (-100.4˚, 33.9˚). (See text for discussion of the detrending procedures.)

4. Discussion

Below we highlight the insights provided by the NARR-derived climatology that extend our knowledge of the characteristics of LLJs over North America and nearby coastal environs. The discussion is organized by the regions where low-level wind maxima are frequent.

The broad area of elevated S-LLJ frequencies in the central and southern plains is generally referred to in the literature as the "Great Plains" jet. The NARR-derived climatology suggests that this terminology may be masking important differences in jet characteristics within the Great Plains and also very likely differences in forcing mechanisms. The frequency analysis presented here points to three distinct frequency maxima found in Nebraska/Kansas/Oklahoma, northern Texas, and south Texas/northeastern Mexico. Although many of the previous studies (e.g. Bonner 1968) of the Great Plains jet focused on jet occurrences in the northernmost frequency maximum (Nebraska/Kansas/Oklahoma), the NARR-derived climatology indicates that S-LLJs are more frequent in the two southernmost maxima, particularly the maximum over southern Texas. However, average wind speeds, as identified from the NARR wind fields, are weaker for S-LLJs over southern Texas/northeastern Mexico than for jets located farther north. Furthermore, smaller diurnal variations in jet speed are seen for the more southerly S-LLJs. Both of these findings point to differences in forcing between "Great Plains jets" occurring at more southerly versus northerly latitudes. The NARR-derived climatology also illuminates the persistence of jet features into the cool season, including diurnal variations in the frequency of cool-season S-LLJs. While most previous studies (e.g. Arritt et al. 1997; Bonner 1968; Pitchford and London 1962; Walters et al. 2008; Whiteman et al. 1997) focused on S-LLJs during the warm season, additional research is needed to better understand the processes responsible for diurnal variations in the frequency of cool season S-LLJs. Another noteworthy feature obtained from the NARR-derived climatology that merits further investigation is the substantial diurnal variations in the frequency of warm-season S-LLJs at fairly high latitudes in central North America (i.e., Dakota, Manitoba).

Southerly airflow over the western Gulf of Mexico is often referred to as the "southerly arm" of the Caribbean jet (Cook et al. 2008). As the strong easterly Caribbean jet encounters the elevated land surfaces of eastern Mexico and converges with westerly airflow originating from over the Mexican Highlands and Baja Peninsula, it turns anticyclonically over the western Gulf of Mexico (Amador 2008; Munoz and Enfield 2009). Little is known about the climatological characteristics of this jet feature, and the NARR analyses presented here provide important baseline information. Of particular significance are the findings regarding the seasonal variations in jet frequency. During winter and spring, high jet frequencies are seen over the western Gulf of Mexico, suggesting a possible connection with this jet feature and S-LLJs in southern Texas/northeastern Mexico (Cook et al. 2008). However, in late summer and fall, S-LLJs are rarely observed over the western Gulf of Mexico; thus, different mechanisms are needed to help explain the large jet frequencies farther north over southern Texas/northeastern Mexico. The frequent S-LLJ occurrences farther east over the Yucatan Peninsula are more difficult to explain, and more research is needed to understand how these jets form.

The northerly Pacific Coastal jet is a significant circulation feature influencing the western United States, and whose persistence and intensity are attributed to the North Pacific High and land/coast temperature differences (Chao 1985; Burk and Thompson 1996; Holt 1996). In spite of its significance, previous analyses of the Pacific coast jet have been limited to case studies, in part because of the lack of upper-level measurements over coastal waters. Thus, the analyses presented here provide one of the first climatological assessments of this important jet feature. The climatological analyses highlight the prevalence of the Pacific coast jet during much of the year and the latitudinal shifts in jet location with season. The average elevations (400-700 m) and speed (>20 ms^{-1}) of the Pacific coast jet shown here agree well with values obtained from case study analysis (Burk and Thompson 1996; Holt 1996), providing credence to the NARR-derived climatological patterns of these parameters.

The only previous climatological analysis of N-LLJs in the northern plains was performed by Walters et al. (2008) using twice-daily rawinsonde observations. The finer-resolution NARR climatology presented here provides a considerably more detailed understanding of the spatial and temporal features of this primarily cool-season jet feature. In particular, the NARR analysis confirms the existence of diurnal fluctuations in jet frequency. These N-LLJs are more frequently observed in the morning hours, suggesting that boundary-layer forcing such as frictional decoupling influences the development of N-LLJs as well as S-LLJs.

A surprising finding is the lack of a northerly jet feature off the mid-Atlantic Coast, as Sjostedt et al. (1990) previously indicated that a low-level wind maximum with northeasterly airflow is often found off the mid-Atlantic coast. Instead, the NARR-climatology indicated that jet features off the mid-Atlantic coast are more frequent in the cool season and have a southerly wind direction. The analyses also pointed to frequent S-LLJs over Hudson Bay from April to October. To our knowledge, jet features in this area have not previously been described in the literature. The weak diurnal fluctuations in jet frequency suggest that this jet may be primarily forced by synoptic-scale features such as airstreams within migrating mid-latitude cyclones that are frequent in this area during the warm season (Shadbolt et al. 2006; Zishka and Smith 1980). However, this jet feature needs to be treated cautiously given its location in the northern portion of the NARR domain where the density of observations included in the reanalysis is small and model biases are likely larger.

Another unique contribution of this study is the assessment of temporal trends in LLJ frequency. Before the availability of reanalyses, this type of analysis was challenging, if not impossible, because of the many inhomogeneities in the time series of rawinsonde observations. Reanalyses provide an alternative resource, although trends calculated from reanalysis fields should be interpreted cautiously as rawinsonde observations are one of the many inputs to a reanalysis. However, Walters et al. (2013) found that the time series of LLJ frequencies obtained from NARR wind profiles for 12 locations in Great Plains did not display the abrupt discontinuities evident in the time series obtained directly from rawinsonde observations. The trend analyses presented here for representative gridpoints located in areas of greatest LLJ frequency suggest that at most locations the frequency of S-LLJs is increasing. Changes in the frequency of LLJs could be related to changes with time in the boundary-layer features that contribute to the occurrence of these phenomena, such as increasing baroclinity, or with changes in the frequency and/or strength of synoptic-scale circulation features that contribute to LLJ occurrence, such as increased frequency of migratory midlatitude cyclones.

In sum, the NARR-derived analyses presented here supplement and enhance our understanding of the climatological characteristics of meridional low-level wind maxima across North America and coastal environs. The findings also highlight that many aspects of low-level wind maxima remain incompletely understood and point to the need for considerable further research on the processes contributing to jet formation.

5. Conclusion

Previous climatological studies of low-level jets have been restricted to individual geographic regions. In this study, an expanded climatology of northerly (N-LLJ) and southerly (S-LLJ) low-level jets is provided for North America and surrounding coastal areas to better document the spatial and temporal variations of these important mesoscale circulation features. The North American Regional Reanalysis (NARR), with a 32-km horizontal resolution and a 3-hourly temporal resolution, was used to analyze (by time of day, month, season and year) the frequency, height above ground level, and wind speed of LLJs for the 31-year period from 1979-2009.

The spatial analyses highlight the relative frequency and strength of well-known wind maxima. For example, the northerly Pacific coast jet is present in the NARR wind fields on over 30% of the analysis times during summer, and high S-LLJ frequencies are found over the Yucatan Peninsula and western Gulf of Mexico corresponding with the southerly arm of the Caribbean LLJ. The summertime S-LLJ of the Great Plains displays dual maxima with largest frequencies in southern Texas and in Oklahoma/Kansas, and large diurnal variations in jet frequency are present. Other jets described in the literature were not prominent in the NARR climatology, particularly a northerly jet off the eastern coast of the U.S. which is often referred to as the Carolina jet. The analyses also highlight a northerly low-level jet in the Northern Plains that has rarely been discussed in the literature.

In general, the mean speed of S-LLJs in the northern and central Great Plains is larger than that of S-LLJs in southern Texas, western Gulf of Mexico, and the Yucatan Peninsula, whereas cool season N-LLJs in the northern plains have stronger speeds than warm season N-LLJs along the Pacific coast of North America. Diurnal fluctuations in mean speed are stronger for S-LLJs than for N-LLJs. For S-LLJs, the largest diurnal fluctuations are seen in spring and summer and primarily for S-LLJs in the central Great Plains. Diurnal fluctuations in the average elevation of the "nose" of S-LLJs is evident in central and eastern North America, although not for S-LLJs over the western Gulf of Mexico, the eastern Pacific or the western Atlantic. N-LLJs displayed little diurnal variation in elevation.

Significant trends in jet frequency were primarily seen for S-LLJs, whereas trends were generally insignificant for N-LLJs. Inter-annual variability was greatest for those seasons with lower jet frequencies.

CHAPTER 4. A CLIMATOLOGICAL ANALYSIS OF TIME OF INITIATION AND PERSISTENCE OF SOUTHERLY LOW-LEVEL JETS OVER CENTRAL NORTH AMERICA AND THE GULF OF MEXICO

In collaboration with

Julie A. Winkler, Xindi Bian, Shiyuan Zhong, and Claudia Walters

1. Introduction

Southerly low-level jets (S-LLJs) occur frequently in central North America, particularly in the Great Plains and over the Gulf of Mexico (e.g., Arritt et al. 1997; Bonner 1968; Higgins et al. 1997; Walters et al. 2008). These jets have a significant impact on the regional climatology. In particular, S-LLJs influence temperature and moisture advection and contribute to atmospheric lifting and convection (e.g., Bonner 1968; Stensrud 1996; Higgins et al. 1997; Wu and Raman 1998; Walters and Winkler 2001). Multiple mechanisms contribute to the formation of low-level wind maxima. Several authors have distinguished between primarily boundary-layer forced versus synoptic-forced jets (e.g., Uccellini 1980; Chen et al. 1994; Stensrud 1996; Wu and Raman 1998), whereas others have argued that these phenomena are frequently influenced by both types of forcing mechanisms although to varying degrees (e.g., Mitchell et al. 1995; Wu and Raman 1998; Walters 2001).

A number of boundary-layer and synoptic processes have previously been identified as contributing to the formation of S-LLJs in central North America. Boundary-layer mechanisms include differential heating over the sloping terrain of the Great Plains and Rocky Mountains (Holton 1967; Bonner and Paegle 1970; Fast and McCorcle 1990), diurnal changes in eddy viscosity (Blackadar 1957; Buajitti and Blackadar 1957; Bonner and Paegle 1970; Paegle and

Rasch 1973), decoupling of the airflow near the top of the nocturnal boundary layer from surface friction (Hoecker 1965; Hoxit 1975; Parish et al. 1988; Izumi 1964), the latitude-dependent inertial oscillation (Blackadar 1957; Wu and Raman 1998), and variations in soil moisture (Zhong et al. 1996). In terms of synoptic-scale circulation features, S-LLJs in central North America often form as part of the clockwise airflow around the North Atlantic Anticyclone, especially when a strong pressure gradient is located across central North America (Wu and Raman 1998; Walters 2001; Ting and Wang 2006). S-LLJs also can occur below the exit region of an upper tropospheric jet as part of the poleward lower-tropospheric arm of an indirect transverse circulation cell (Uccellini and Johnson 1979; Sjostedt et al. 1990). In addition, S-LLJs are sometimes embedded within mid-latitude cyclones in the Great Plains, often located close to the surface cold frontal boundary (Browning and Pardoe 1973) in an area of strong horizontal temperature gradient.

Strong synoptic forcing is often responsible for the occurrence of S-LLJs over the Gulf of Mexico. Frequently these jets are associated with the Caribbean jet, the east-to-west low-level wind maximum found along the southern edge of the North American anticyclone (Cook et al. 2008). As the Caribbean low-level jet reaches the western edge of the Gulf of Mexico basin, it often turns anticyclonically, and the southerly arm of the Caribbean jet lies over the western Gulf of Mexico. Boundary-layer forcing, particularly low-level temperature gradients, can also contribute to the formation of S-LLJs in this region.

An understanding of the forcing mechanisms for a specific jet event requires detailed analysis, often including numerical simulations. On the other hand, climatological analyses can provide insights on spatial and temporal variations in the relative significance of boundary-layer versus synoptic-scale forcing mechanisms. For example, S-LLJs that are primarily boundary-layer forced are expected to initiate during the nighttime or early morning hours and have relatively short duration, whereas diurnal fluctuations should be weaker, and the duration longer, for synoptic-forced S-LLJs. Thus, a climatological analysis of the time of initiation and persistence of S-LLJs can help distinguish those times of day and/or year, along with locations within central North America and over the Gulf of Mexico, where boundary-layer forcing dominates from those where synoptic-forcing may be more important.

An impediment to such a climatological analysis is the limited availability of upper-level wind measurements. Rawinsonde observations, the primary source of upper-level wind information, are limited by their coarse temporal (twice daily) and spatial (>300 km) resolution. Alternative sources of wind observations are equally problematic. For example, the NOAA National Profiler Network has a relatively small areal extent, and the elevated (approximately 500 m) lower range gate restricts the detection of S-LLJs (Mitchell et al. 1995; Arritt et al. 1997). However, reanalysis datasets with their relatively fine spatial and temporal resolution provide a potential alternative resource for climatological analyses of low-level wind maxima. Reanalyses are a dynamically-consistent assimilated product that incorporates first guess model fields with observations from multiple sources, including rawinsondes, dropsondes, pibals, commercial aircraft, satellites, and radar wind profilers (Shafran et al. 2004). These datasets are becoming increasingly popular in studies of low-level wind maxima. In particular, the North American Regional Reanalysis (NARR; Mesinger et al. 2006), which has an approximately 32 km spatial resolution and a 3-hourly time step, has previously been used as boundary conditions for numerical simulations of specific LLJ events (e.g., Storm et al. 2009), to investigate the variability of S-LLJs in the central U.S. (Weaver and Nigam 2008) and to estimate the climatological values of the frequency and average elevation and speed of both southerly and northerly wind maxima for North America and coastal environs (Chapter 3). In addition, a detailed comparison for multiple locations in the Great Plains of wind maxima observed in rawinsonde observations with those identified from the vertical wind profiles from nearby NARR gridpoints suggested that NARR is able to capture the spatial patterns and diurnal fluctuations in the frequency of low-level wind maxima (Walters et al. 2013).

For the analysis presented here, NARR is used to estimate the climatological patterns of the time of initiation and persistence of S-LLJs in the Great Plains and western Gulf of Mexico for the 31-year period, 1979-2009. Although NARR's 3-hourly time step constraints to some extent the temporal detail that can be detected, the available temporal resolution is nevertheless considerably greater than that of earlier climatological analyses which were handicapped by the twice-daily time step of rawinsonde observations (e.g., Walters et al. 2008). Furthermore, this is the first climatological analysis of which we are aware that specifically focuses on the time of initiation and persistence of low-level wind maxima. This analysis builds on the companion study (Chapter 3) that employed NARR to estimate the spatial and temporal variations in jet characteristics (frequency, speed, and elevation) for North America and coastal environs. The results provide a preliminary assessment of the relative contribution of boundary-layer versus synoptic forcing to S-LLJ formation, based on spatial and temporal variations in the timing and persistence of the wind maxima.

2. Methods

The study area encompasses the area of frequent S-LLJ occurrences in central North America and the Gulf of Mexico, as seen in Chapter 3, and ranges latitudinally from 58°N to 17° N and longitudinally from 105° W to 60°W.

For this analysis, we distinguish between a S-LLJ "profile" and a S-LLJ "event". A S-LLJ profile is defined as a wind maximum at an individual gridpoint of ≥12 ms^{-1} with a velocity decrease of ≥6 ms^{-1} above and below the jet, and a wind direction between 113°-247°. This definition is similar to that used by Bonner (1968) in his early climatological analysis, except that a decrease in wind speed is required below the jet, as well as above, following several recent authors (e.g., Andreas et al. 2000; Banta et al. 2002; Walters and Winkler 2001; Walters et al. 2008). The wind maxima are constrained to elevations at or below 3000 m above ground level (AGL), with the required wind speed decrease reached by 5000 m AGL. Although Bonner (1968) limited low-level wind maxima to elevations of 1.5 km AGL and below, a higher threshold is used here to include both boundary-layer jets, which are typically found at low elevations, and synoptic-forced jets, which often have slant-wise flow with the more northern portions of the jet located considerably above 1.5 km AGL.

The NARR constant pressure wind fields, supplemented with the 10 m wind field, were employed to identify S-LLJ profiles at each NARR gridpoint. NARR is a "blend" of observations and model output and is generated using parameters from the NCEP-DOE Global Reanalysis, the NCEP Eta Model and its data assimilation system, a version of the Noah land-surface model, and numerous observational datasets (Mesinger et al. 2006). The archived data, which have a 32 km spatial resolution, include wind fields at a 25 hPa vertical resolution below the 700 hPa level and a 50 hPa vertical resolution from 700 hPa to 500 hPa. The data extend from 1979 to present and are available at 3 hourly time intervals beginning at 00 UTC (Mesinger et al. 2006).

Successive 3-hourly time steps at the individual NARR gridpoints were queried for the existence of a S-LLJ profile. The detection of a jet profile after one or more time steps without a profile marks the beginning of a S-LLJ "event", and the NARR time step that the jet profile was first detected was recorded along with the number of consecutive time steps with a jet profile. A jet event with the last instance of a jet profile being observed. This information was used to calculate for each gridpoint 1) the percentage of jet events during the 31-year study period that were first observed at each of the 3-hourly time steps (00, 03, 06, 09, 12, 15, 18, 21 UTC), and 2) the average duration of the S-LLJ events, expressed as the average number of consecutive time steps with a jet signature. These analyses are displayed in map form at the seasonal aggregation level. In addition, histograms were prepared for selected NARR gridpoints to help visualize the shape of the distribution of jet event duration for each season. To provide further context for interpreting the initiation and persistence analyses, the seasonal frequencies of S-LLJ profiles at each gridpoint are also displayed. These frequencies are expressed as a percentage of the total number of NARR time steps during a particular season.

Several limitations and assumptions need to be considered when interpreting the findings presented below. Although we refer to the "time of initiation" and "persistence" of S-LLJ events, the 3-hourly resolution of NARR limits the temporal precision of these parameters. Also, we assume that a S-LLJ profile observed at two consecutive time steps persists at that gridpoint throughout the three hours between the time steps. Another caveat is that the analysis is "static", in that it does not consider that some S-LLJs are mobile and, with time, will translate in space. In other words, the persistence analysis is limited to the duration of jet signatures at individual gridpoints. Spatial variations in the density of observations and biases in the numerical models and assimilation methods used to produce the NARR fields may also affect the findings. Although Walters et al. (2013) found that NARR was able to reproduce the relative frequency of jet signatures at 00 and 12 UTC as seen in rawinsonde observations at twelve stations in the

Great Plains, possible spatially- or temporally-specific biases in the NARR fields could limit the extension of the findings of their evaluation to other locations and time steps. In spite of these limitations, the analyses presented below represent a significant initial attempt to better understand the climatological patterns of the initiation and duration of S-LLJ events, along with the inferences for mechanisms responsible for these important atmospheric phenomena.

3. Seasonal Variations in the Time of Initiation and Average Duration of Southerly Low Level Jet Events

The plots of the time of initiation and persistence of S-LLJ events are presented below by season in order to facilitate integration across these parameters. The descriptions for each season begin with a short summary of the spatial variations in the frequency of S-LLJ profiles, so that readers are able to interpret the findings regarding the initiation and duration of S-LLJs events in the context of where S-LLJ profiles are most frequent during a particular season.

a) Winter

In winter, S-LLJ profiles are most frequent, occurring on more than 5% of all time steps, at the NARR gridpoints located within a broad swath from southern South Dakota southward to the Yucatan Peninsula (Figure 27). The largest frequencies (>15%) are located in central and southern Texas and along the western coast of the Gulf of Mexico.

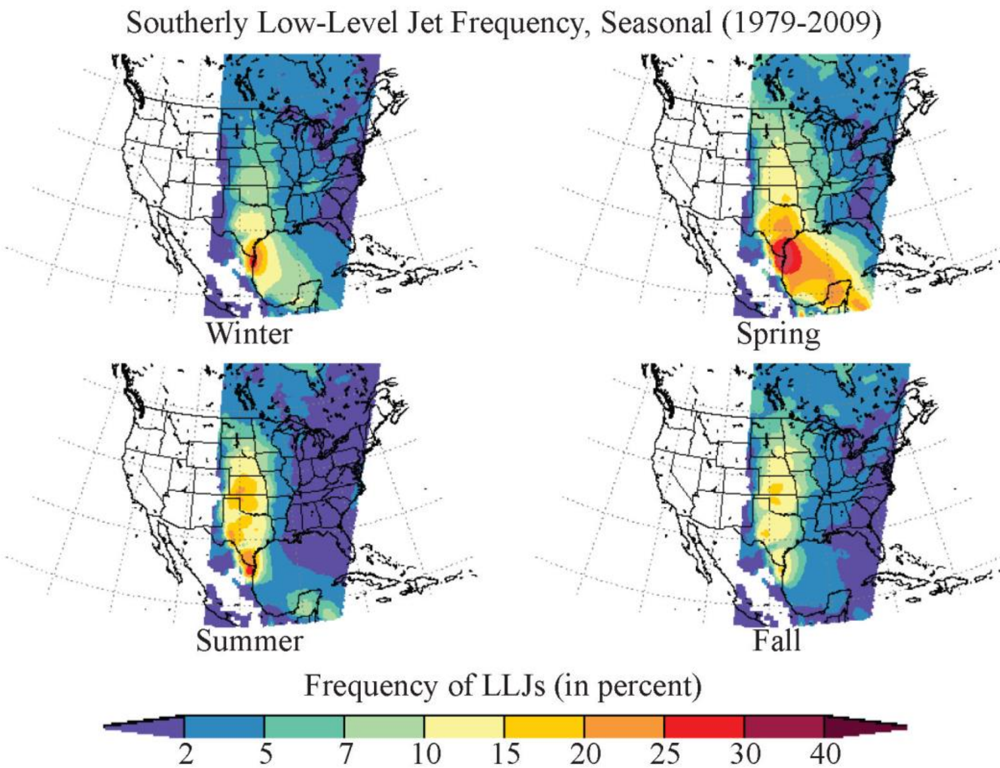

Figure 27. Seasonal frequencies of S-LLJs from 1979 to 2009 expressed as a percentage of the total number of time steps, summed over all NARR time steps. Gridpoints with no jet cases and/or surface elevations >2km MSL are shown in white.

Combining the S-LLJ profiles at each gridpoint into discrete S-LLJ events provides insights on the preferred times when wintertime S-LLJs form. Greater diurnal variations in the time of initiation of S-LLJ events are observed during winter in the central and southern portion of the study domain compared to the northern portion (Figure 28). Wintertime S-LLJ events in the central plains and southern plains are more likely to be first observed at the 03 and 06 UTC time steps, with the percentage of jets initiating at these time steps exceeding 30% for some gridpoints. S-LLJ events in this area are least likely to be initially detected at the 15, 18 and 21 UTC time steps. A similar diurnal pattern is seen for S-LLJ events over the Yucatan Peninsula, whereas jet events over the southern and western Gulf of Mexico form somewhat later around 12 UTC. In contrast, little diurnal preference in the formation of jet events is seen in the northern portion of the study domain, although it should be kept in mind that S-LLJ profiles occur infrequently in this area during winter.

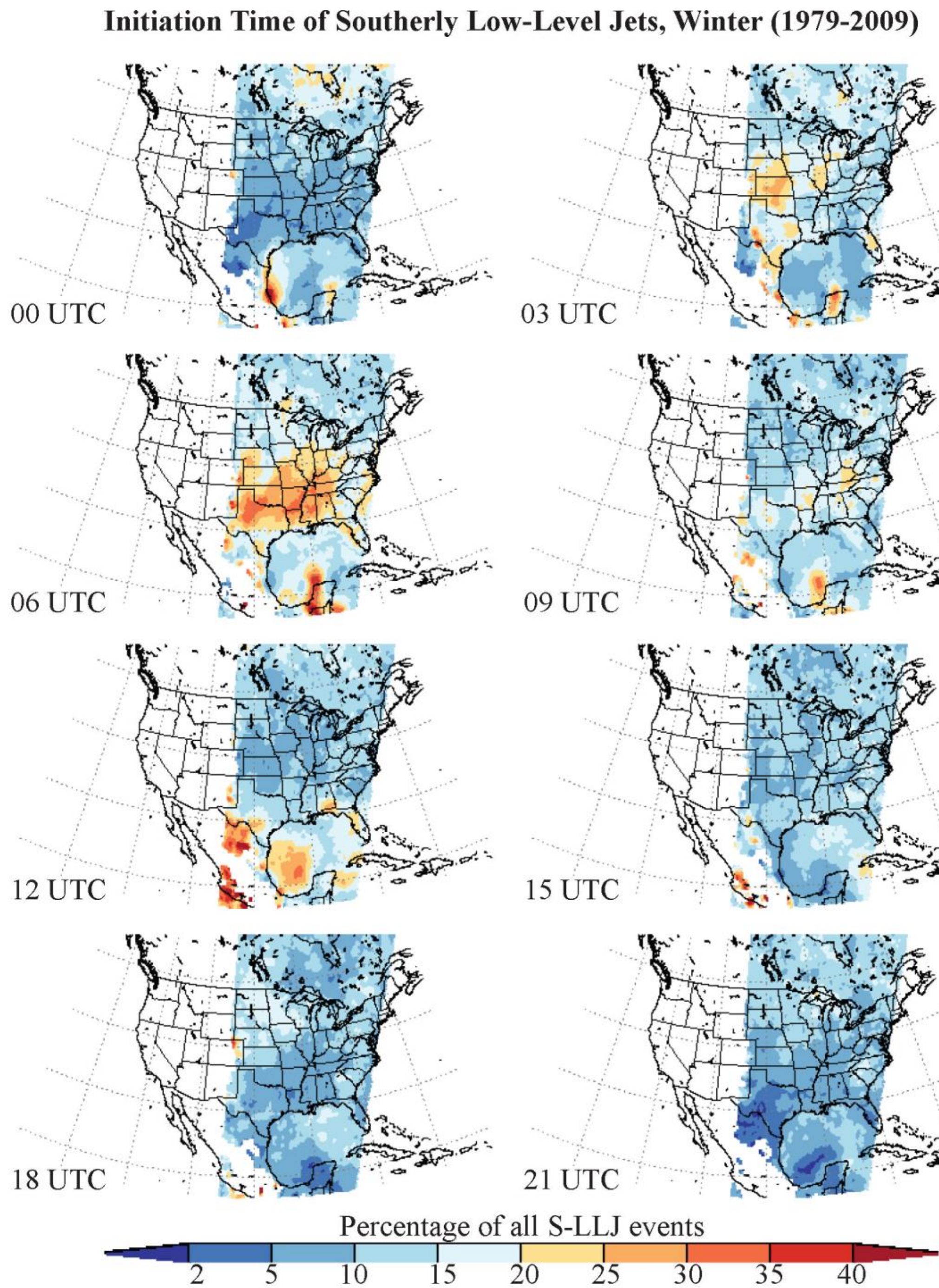

Figure 28. Average persistence of wintertime (December-February) S-LLJ events during 1979-2009, expressed as the number of NARR time steps a jet signature was consecutively detected, and displayed by the NARR time step that the jet event was first identified in the NARR wind profiles. Gridpoints with no jet cases and/or surface elevations >2km MSL are shown in white.

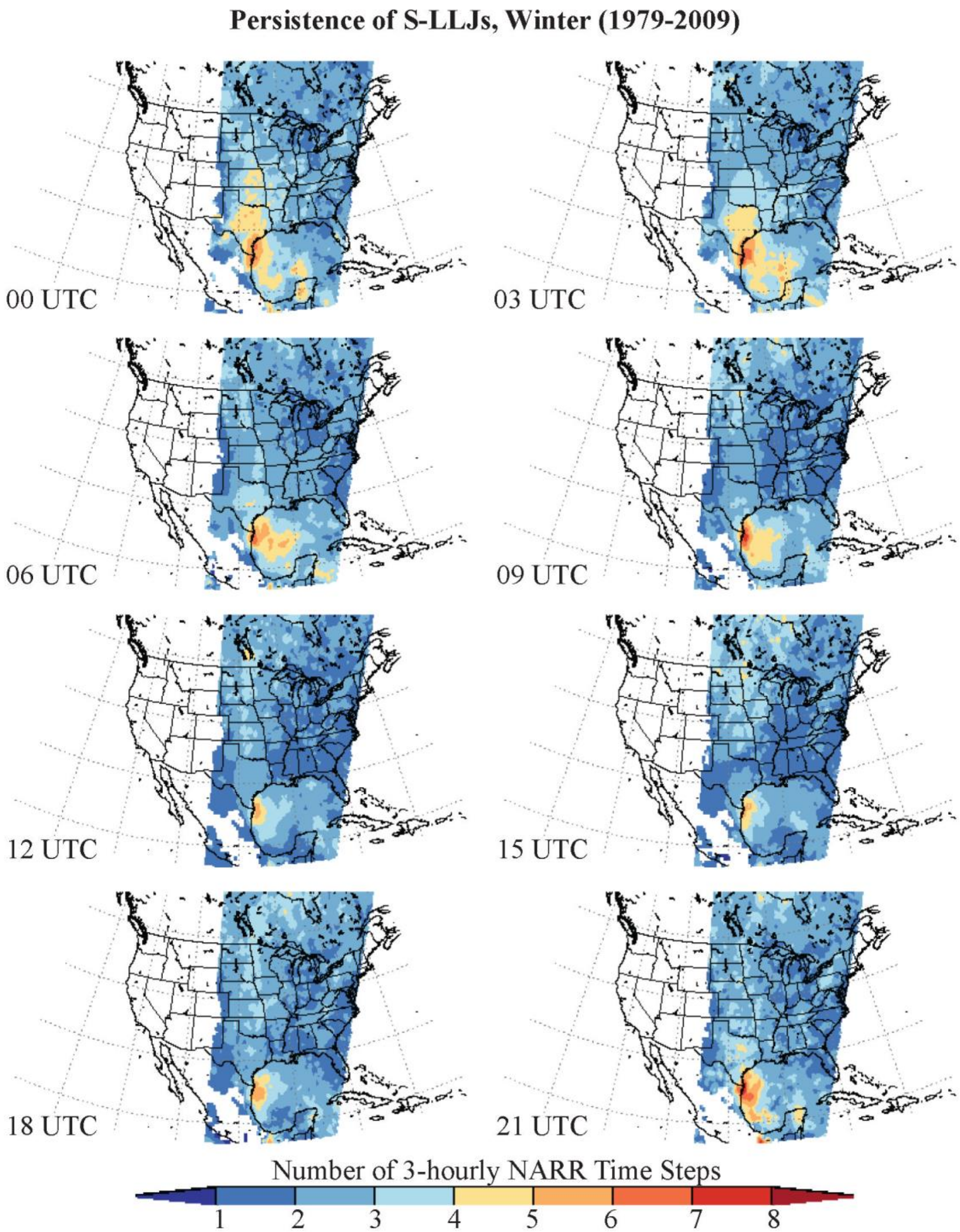

Figure 29. Winter frequency that S-LLJ events during 1979-2009 were first detected at each of the NARR time steps. Gridpoints with no jet cases and/or surface elevations >2km MSL are shown in white.

Wintertime jet events that form in the central and southern plains at 03 and 06 UTC, the most common initiation times, have average durations of less than four NARR time steps (more than 3 hours but fewer than 12 hours) (Figure 29). Longer average durations of 4 or more NARR time steps (≥ 12 hours) are seen for S-LLJ events that form over the Yucatan Peninsula at 21 and 00 UTC, from Kansas to southern Texas at 03 and 06 UTC, and in the western Gulf of Mexico regardless of time of initiation. Elsewhere across the study domain, average durations of less than 3 time steps (<9 hours) are seen.

b) Spring

The frequency of S-LLJ profiles increases from winter to spring across much of the study domain, but particularly over Texas, the western Gulf of Mexico and the Yucatan Peninsula (Figure 27). In this area, S-LLJ profiles are found on more than 20%, and for some locations on more than 30%, of the NARR 3-hourly time steps. Another notable feature during spring is the northward expansion of the area experiencing S-LLJ profiles on >5% of the NARR time steps into southern Manitoba and the eastward expansion of this area into Kentucky and Tennessee. An isolated area of relatively large frequencies of S-LLJ profiles is also seen over Hudson Bay.

Diurnal fluctuations in the time of initiation of S-LLJ events are observed over a broader geographic area during spring than in winter (Figure 30). Springtime S-LLJ events are most often first detected in the NARR wind fields at the 06 UTC time step and least frequently at 15, 18, and 21 UTC across much of the study domain, including the northern Plains and central Canada. Exceptions to this generalization include the extreme western Gulf of Mexico where S-LLJ events are more often (>35%) first identified at the 00 UTC time step; central and southern Texas where over 30% of S-LLJs form at the 03 UTC time step, and Hudson Bay where over 20% of the S-LLJs are first detected at 03 UTC. In addition, S-LLJ events in the southern Gulf of

Mexico are equally likely to form at the 09 and 12 UTC time steps but rarely at other times of day.

Springtime S-LLJ events over the Gulf of Mexico, and to a lesser extent over the Yucatan Peninsula, have longer average durations (>8 NARR time steps) compared to jet events elsewhere in the study domain, particularly those S-LLJ events that form during the afternoon and evening hours (21, 00, 03 and 06 UTC) (Figure 31). The frequent S-LLJ events that form in the central and northern plains at 06 UTC have shorter durations (<4 NARR time steps) than the less frequent S-LLJ events at 21, 00 and 03 UTC. S-LLJ events in this area that form later in the day (12, 15, and 18 UTC) have average durations of only 2-3 NARR time steps. S-LLJ events over Hudson Bay have relatively short durations (<4 NARR time steps) regardless of initiation time.

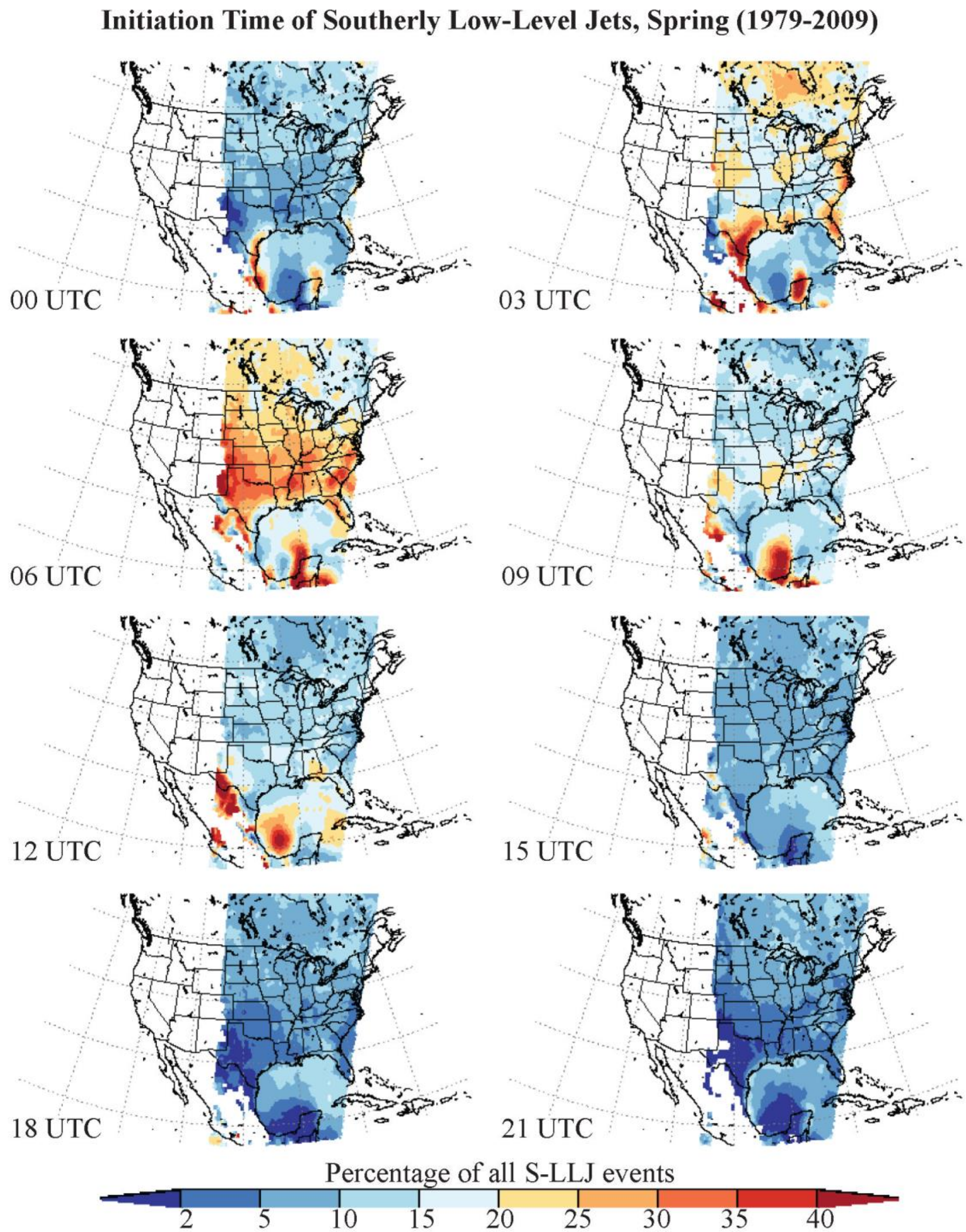

Figure 30. Average persistence of springtime (March-May) S-LLJ events during 1979-2009, expressed as the number of NARR time steps a jet signature was consecutively detected, and displayed by the NARR time step that the jet event was first identified in the NARR wind profiles. Gridpoints with no jet cases and/or surface elevations >2km MSL are shown in white.

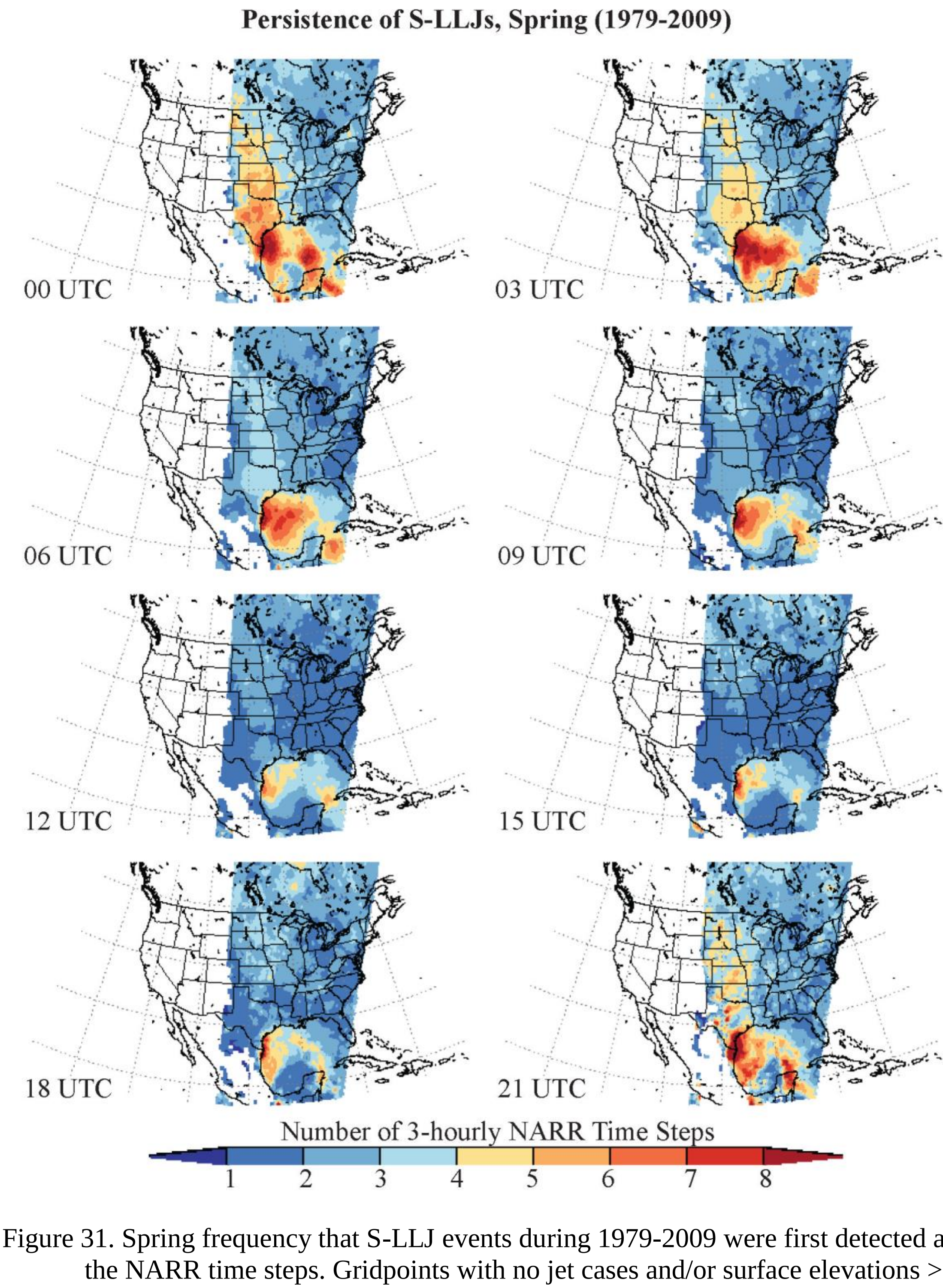

Figure 31. Spring frequency that S-LLJ events during 1979-2009 were first detected at each of the NARR time steps. Gridpoints with no jet cases and/or surface elevations >2km MSL are shown in white.

c) Summer

The elongated, contiguous area of relatively large frequencies of S-LLJ profiles observed during spring contracts during summer, and now extends from North Dakota to southern Texas and extreme northeastern Mexico (Figure 27). Within this area, three centers with frequencies >15% are seen: Kansas/Oklahoma, central Texas, and south Texas/northeast Mexico. Isolated frequency maxima are also found over the Yucatan Peninsula and Hudson Bay. Compared to the other seasons, S-LLJ profiles are infrequent during summer over the western Gulf of Mexico.

S-LLJ events during summer most often form around 06 UTC, including those events at high latitude locations (Figure 32). For many gridpoints, more than 30% of summertime jet events initiated at this time step. Exceptions to this generalization are similar to those found for spring. The frequent S-LLJ events in coastal areas along southeastern Texas form earlier, at 03 rather than 06 UTC, as do the considerably less frequent S-LLJ events north and northeast of the Great Lakes. On the other hand, a later time of initiation (09 or 12 UTC) is observed for S-LLJ events over the western Gulf of Mexico and along the central Gulf Coast, although as noted above S-LLJ profiles are infrequent in these areas during summer.

Regardless of location, summertime jet events that form between 06 and 09 UTC have relatively short durations of 3-4 time steps, with even shorter average durations of less than 2 time steps observed for S-LLJ events that form at 12 and 15 UTC (Figure 33). Although S-LLJ events are less likely to form in the central and southern plains at 21, 00 and 03 UTC compared to other times of the day, the jets that do occur have considerably longer durations (exceeding 6 time steps, or up to 18 hours, at some gridpoints).

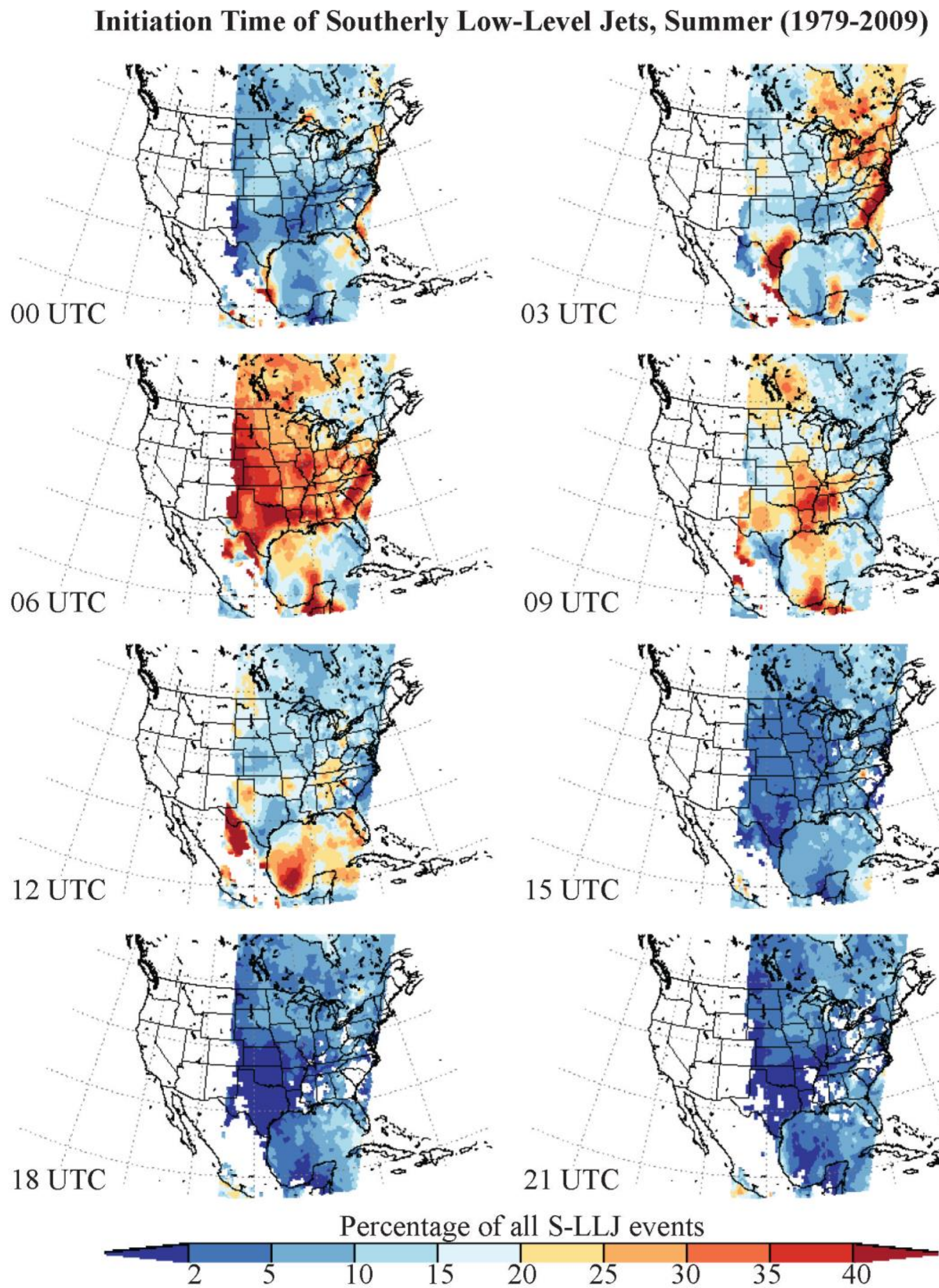

Figure 32. Average persistence of summertime (June-August) S-LLJ events during 1979-2009, expressed as the number of NARR time steps a jet signature was consecutively detected, and displayed by the NARR time step that the jet event was first identified in the NARR wind profiles. Gridpoints with no jet cases and/or surface elevations >2km MSL are shown in white.

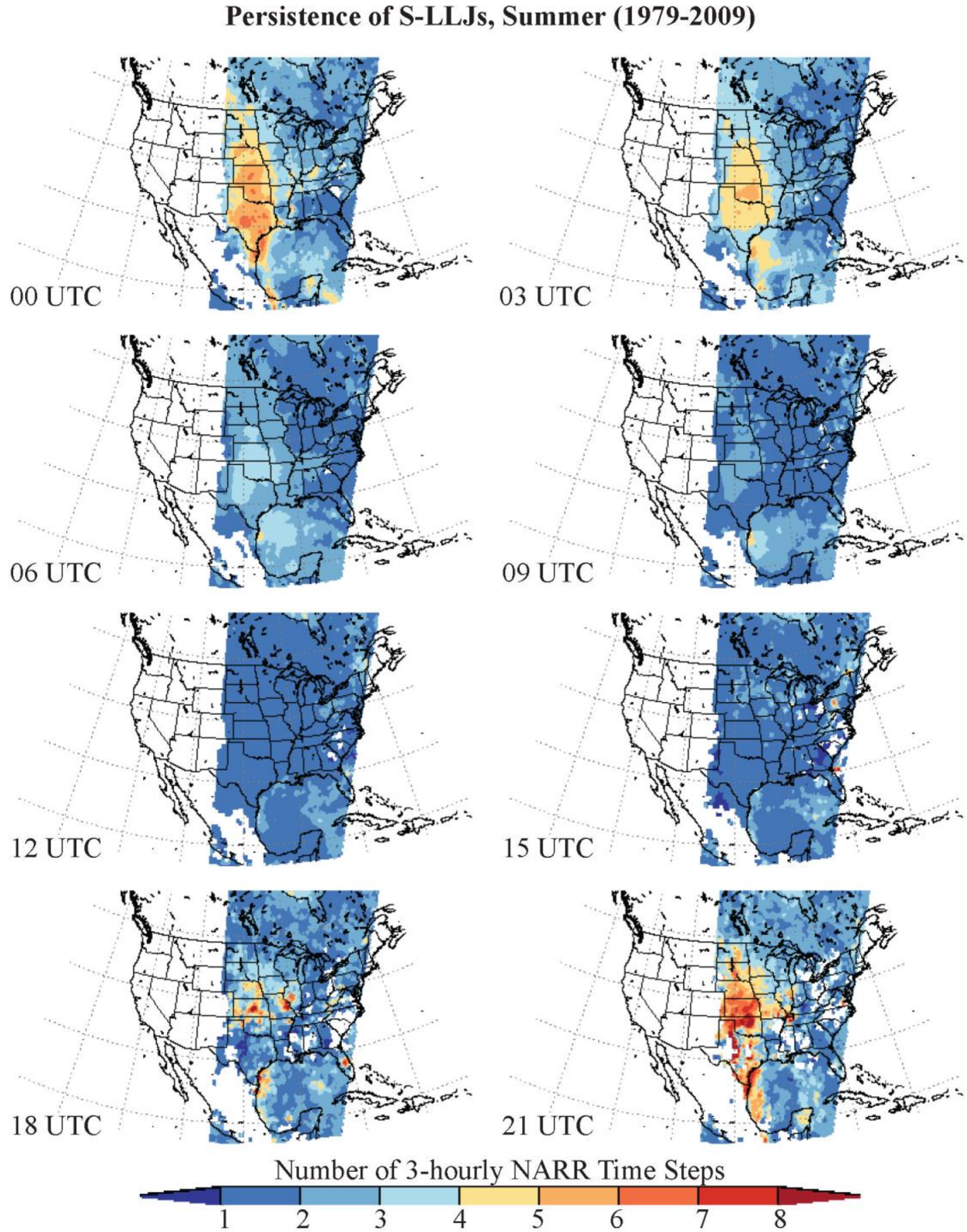

Figure 33. Summer frequency that S-LLJ events during 1979-2009 were first detected at each of the NARR time steps. The white areas on the plots lie outside the study domain. Gridpoints with no jet cases and/or surface elevations >2km MSL are shown in white.

d) Fall

The frequency of S-LLJ profiles decreases substantially from summer to fall, although the spatial extent (North Dakota to northeastern Mexico) of the contiguous area of relatively large frequencies is similar to that seen for summer (Figure 27). S-LLJ profiles remain infrequent during fall over much of the Gulf of Mexico, and, unlike other seasons, S-LLJ profiles are also infrequent over the Yucatan Peninsula.

S-LLJ events during fall in the northern Plains and parts of the central Plains (e.g., western Nebraska and Kansas) form somewhat earlier in the day compared to summertime jet events in this area (03 UTC rather than 06 UTC), although a substantial number of jet events continue to be initially detected at 06 UTC (Figure 34). S-LLJ events over southern Texas continue to form more often at 03 UTC compared to other times of the day, as previously seen for spring and summer. Elsewhere across much of the central and southern plains and over the Yucatan Peninsula, S-LLJ events during fall are more often first identified at the 06 UTC time step. S-LLJ events over the southern Gulf of Mexico continue to initiate most often at 09 and 12 UTC, although, similar to summer, S-LLJ profiles remain relatively infrequent over the Gulf of Mexico during fall. Across the majority of the study domain, very few S-LLJ events initiate at the 15, 18, and 21 UTC time steps.

The spatial distribution of average persistence during fall is also similar to that in summer (Figure 35). Jet events that form in the central and southern plains from approximately midnight to noon local time (06, 09, 12, 15, 18 UTC) have considerably shorter average durations compared to the less frequent jet events that form in the afternoon and evening (21, 00, 03 UTC). Jet events over the extreme western Gulf of Mexico have longer durations (> 4 NARR time steps; up to 16 hours), regardless of initiation time, compared to jet events that from over the central and eastern Gulf.

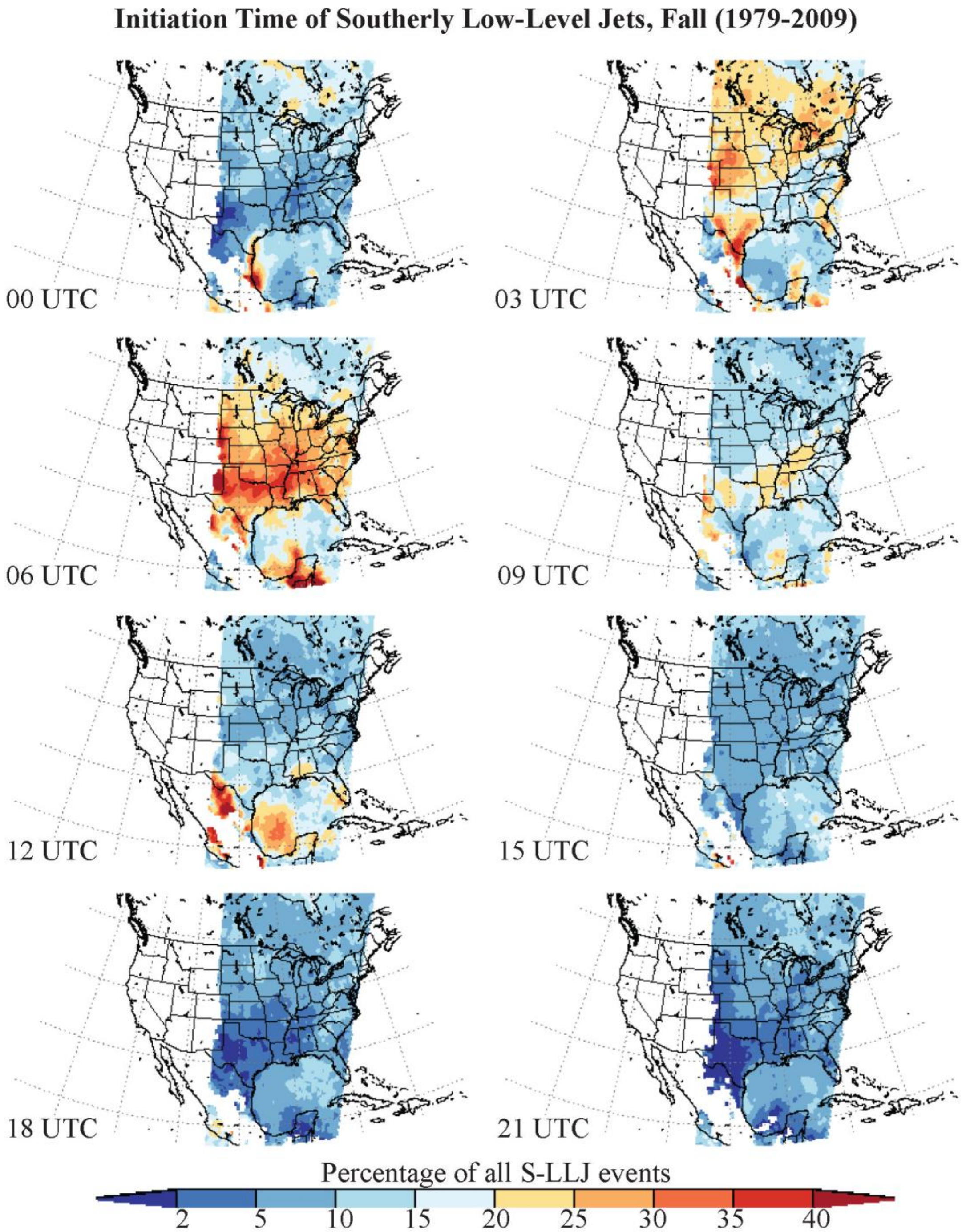

Figure 34. Average persistence of fall time (September-November) S-LLJ events during 1979-2009, expressed as the number of NARR time steps a jet signature was consecutively detected, and displayed by the NARR time step that the jet event was first identified in

the NARR wind profiles. Gridpoints with no jet cases and/or surface elevations >2km MSL are shown in white.

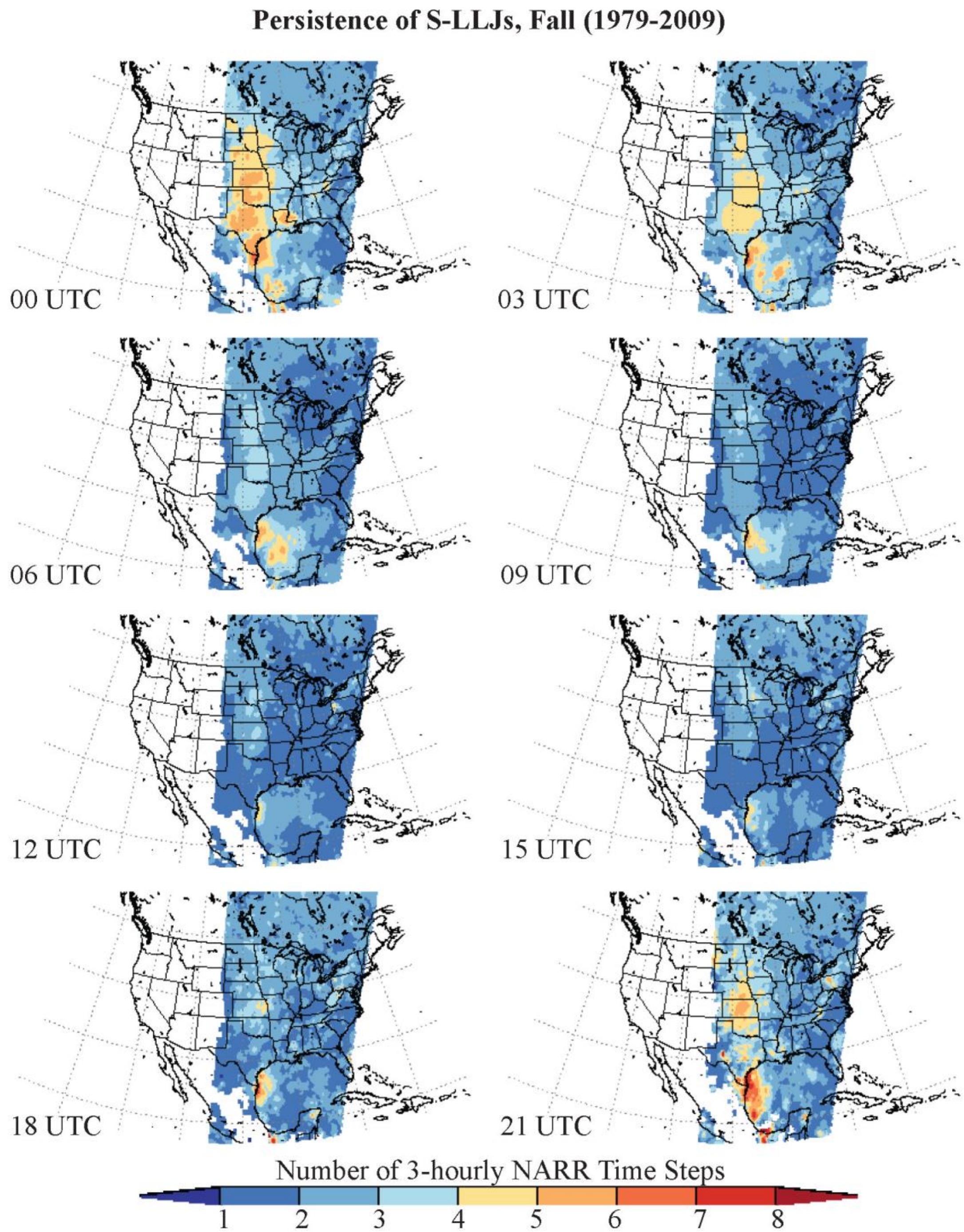

Figure 35. Fall frequency that S-LLJ events during 1979-2009 were first detected at each of the NARR time steps. Gridpoints with no jet cases and/or surface elevations >2km MSL are shown in white.

4. Distribution of the Persistence of Southerly Low-Level Jet Events

The distributions of jet event durations, which are masked by the average values, can also provide insights on the range of forcing mechanisms at different locations. Thus, the analyses presented above of average S-LLJ event duration are supplemented by histograms of jet duration for selected NARR gridpoints located on a roughly north-to-south transect (Figure 36).

S-LLJ Persistence Case Study Locations

Figure 36. Gridpoints for which histograms of the persistence of S-LLJ events were prepared.

Beginning with the northernmost gridpoint located in Manitoba, substantial differences in the distributions of jet durations are seen by season (Figure 37). As shown above, wintertime S-LLJ events at this location are approximately equally likely to form at any time of the day. However, the skewed histograms of jet duration at 21, 00, 03, 06 and 09 UTC suggest that the modal duration for S-LLJ events that form at these time steps is a single NARR time step. In contrast, the durations of S-LLJ events that form in the mid-to-late morning hours (12, 15, and 18 UTC) are fairly equally distributed among the duration classes, ranging from one time step to eight or more time steps. This pattern reverses in spring, when jet events that form at 09, 12, 15, 18, and 21 UTC have skewed duration distributions with a modal duration of only one time step, whereas broader distributions of jet duration are seen for the other time steps, including 03 and 06 UTC, the two NARR time steps when springtime S-LLJ events at this location are most likely to be first detected. Summertime S-LLJ events at this location are more likely to be first detected at the 06 and 09 UTC time steps, and the histograms of jet duration indicate that jets that form at 06 UTC are equally likely to have durations of one, two or three NARR time steps whereas those that form at 09 UTC more often have durations of only one or two time steps. The less frequent jet events that form later in the morning (12 and 15 UTC) during summer have highly skewed duration distributions, with the majority of jets at these times being short-lived. The distributions of jet duration for fall are generally similar to those for summer, with highly skewed distributions seen for jets that form in the late morning and afternoon (12, 15, 18, 21 UTC) compared to other times of the day. Jets that form at 03 UTC, the most frequent time of initiation during fall, are equally likely to have durations of 1 to 4 time steps.

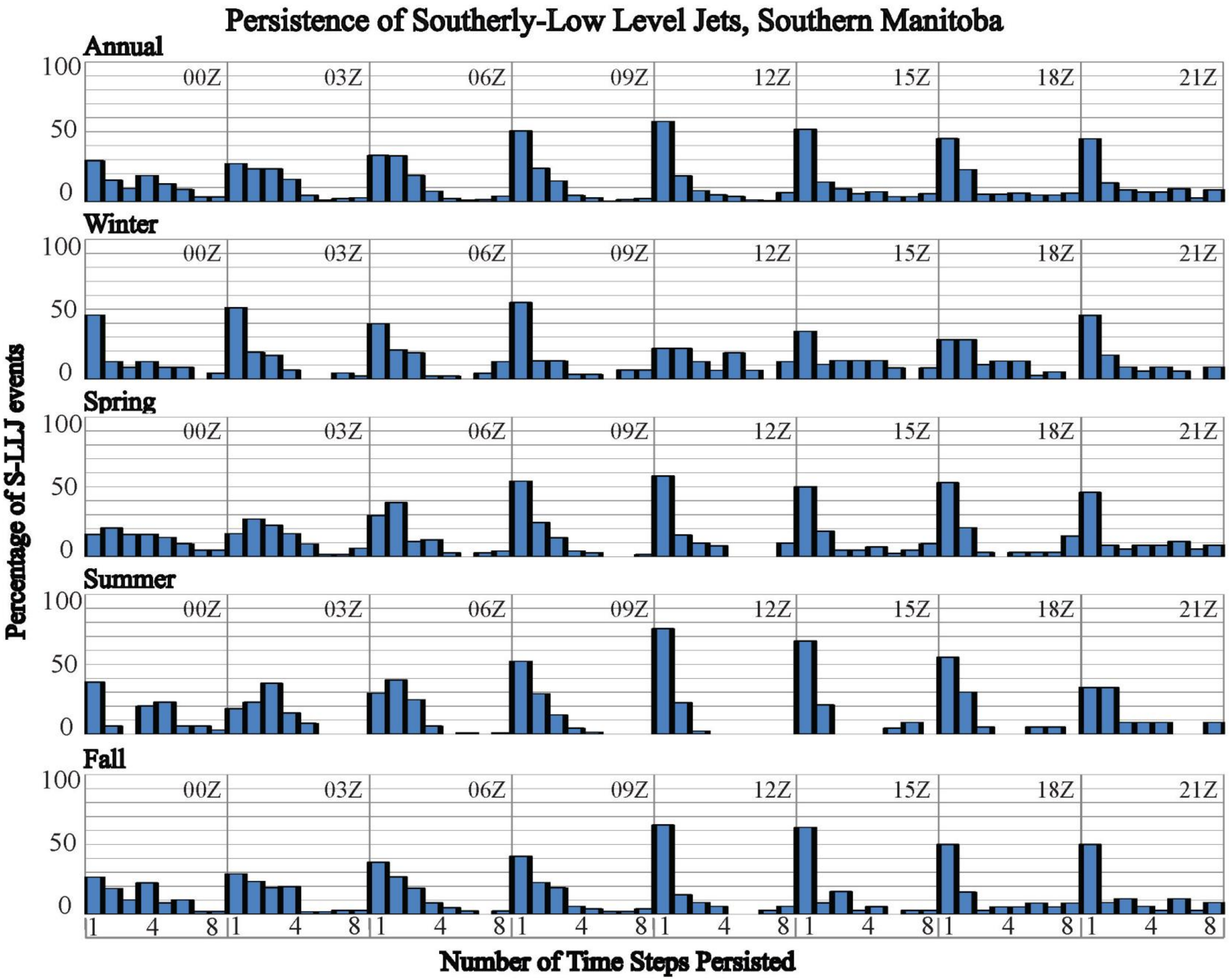

Figure 37. Histograms of the persistence of S-LLJ events, southern Manitoba (-97.6˚, 50.2˚).

Moving southward to the grid location in northeastern South Dakota, the majority of the distributions of jet duration are relatively broad, indicating a range of durations for jets forming at a particular NARR time step (Figure 38). Mid-to-late morning (12, 15, and 18 UTC) S-LLJs during summer, and to a lesser extent spring, are an exception to this generalization. S-LLJs forming at these time steps tend to have shorter durations of only one or two time steps, although there is some indication of a bimodal distribution, especially for 18 UTC, with a small proportion of jets that initiate at these times having exceptionally long durations (≥8 time steps).

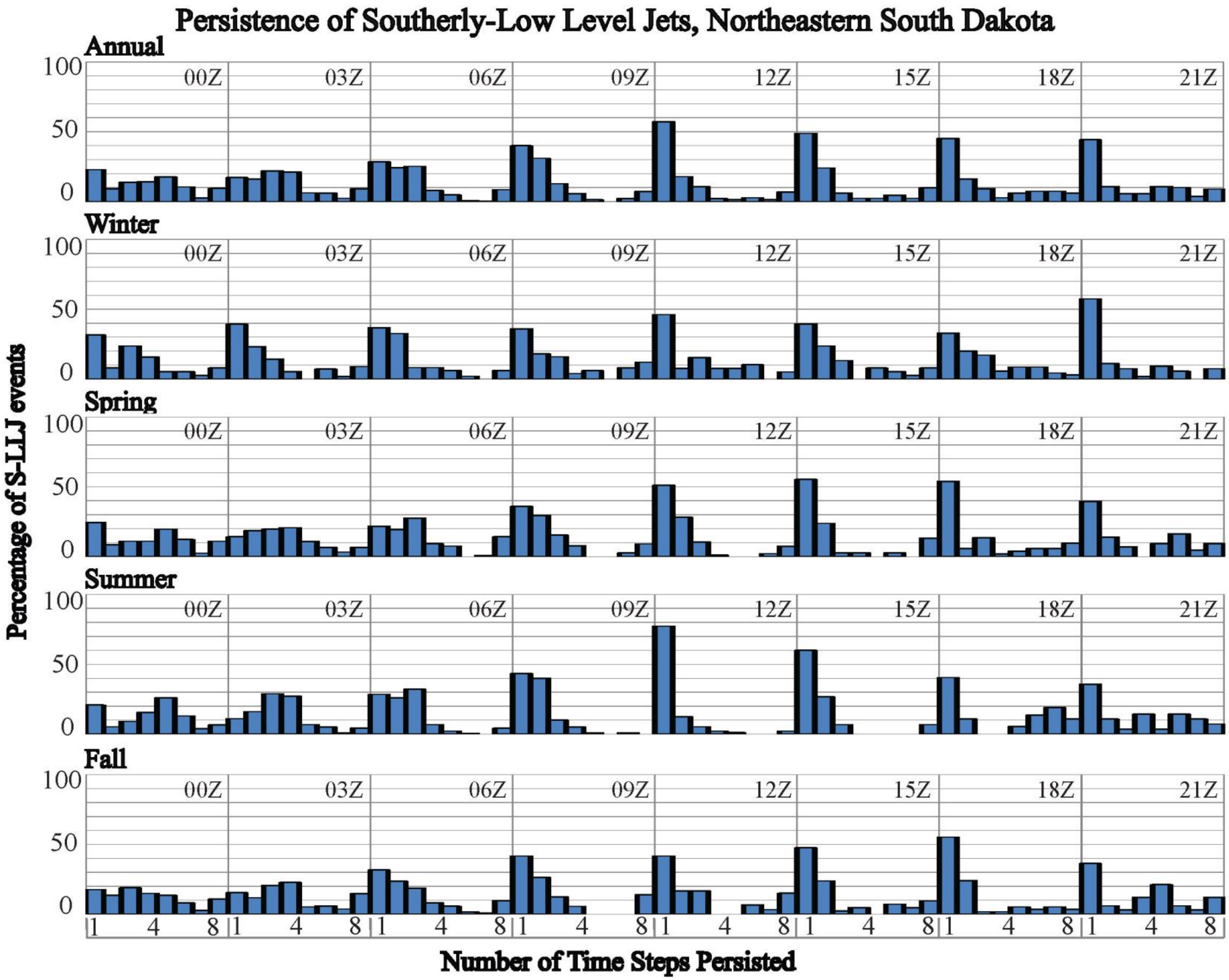

Figure 38. Histograms of the persistence of S-LLJ events, South Dakota (- 97.7˚, 44.9˚).

As described in the previous section, S-LLJ events at the gridpoint located along the Nebraska and Kansas border most often are first detected at 03 and 06 UTC in winter, spring and fall, and at 06 UTC in summer (Figure 39). Regardless of season, the spread of the duration distributions for jets that form at these two time steps is relatively broad, with jet events equally likely to persist anywhere from one to four time steps. On the other hand, S-LLJ events that form at other times of the day, particularly in the late morning (12, 15, 18 UTC), have more skewed distributions with a modal duration of only one time step. To the east, where S-LLJ events often form at 06 and 09 UTC in winter and spring, the duration plots for the representative gridpoint in central Tennessee suggest that, although the modal value is a single time step, jet events with durations of 2-3 time steps are also fairly common (Figure 40). The infrequent jet events that form in the mid-to-late morning (12, 15, 18 UTC) are short lived.

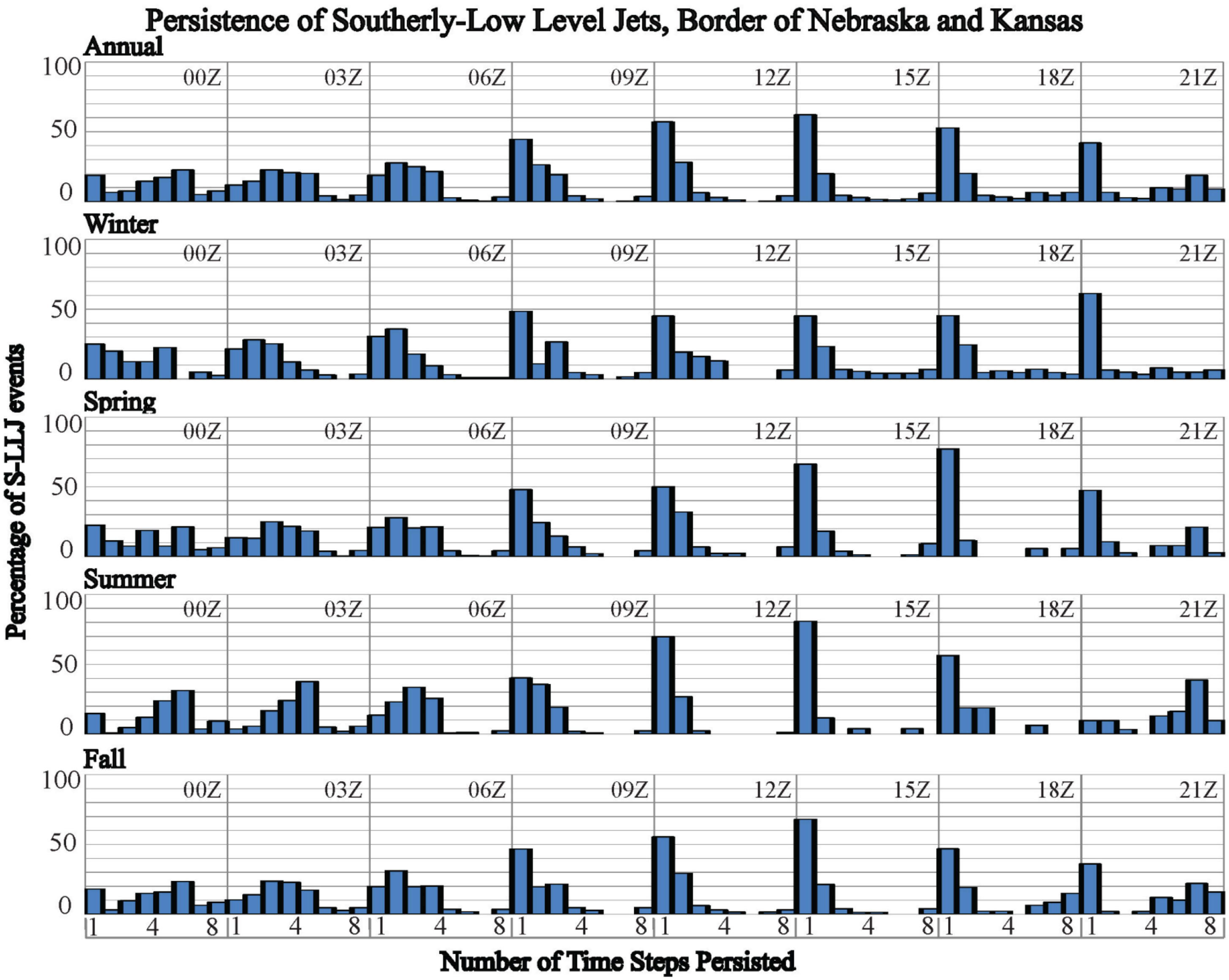

Figure 39. Histograms of the persistence of S-LLJ events, Nebraska/Kansas (-97.4˚, 39.9˚).

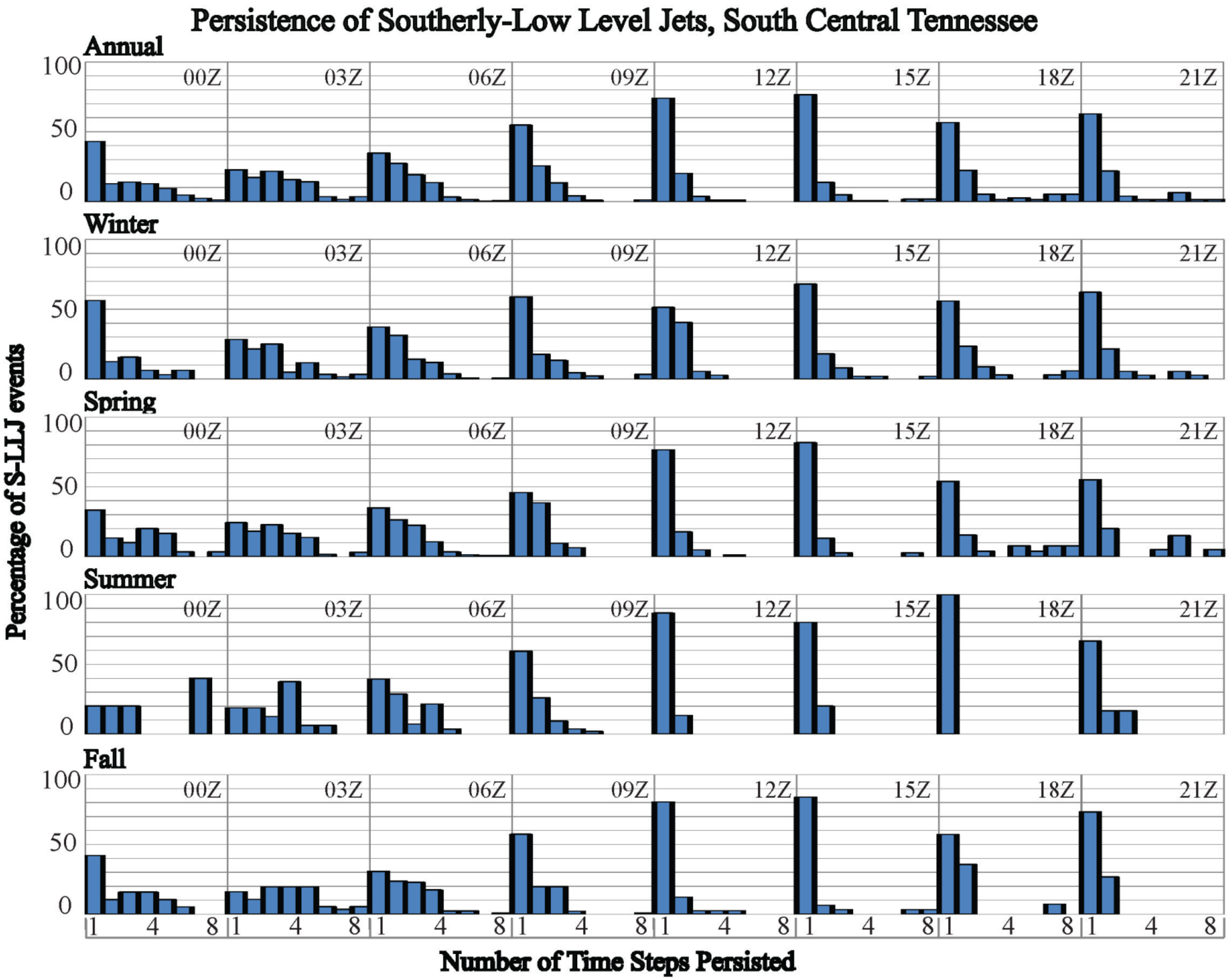

Figure 40. Histograms of the persistence of S-LLJ events, southern Tennessee (-87.6˚, 35.2˚).

Farther south, at the gridpoint in central Oklahoma we see relatively long durations for jet events that form at the preferred initiation time of 06 UTC (Figure 41). The distributions are relatively "bell shaped" and the modal duration is 3 time steps in summer, and 4 time steps in spring and fall, with only a small proportion of jet events forming that this time observed at a single time step. The distribution in winter, when S-LLJ profiles are considerably less frequent, is more skewed with a larger portion of events having shorter durations (1-2 time steps). As for the gridpoints located farther north, highly skewed duration distributions are seen, including in winter, for S-LLJ events that initiate at 12, 15, and 18 UTC, with the majority of these events evident for only one time step.

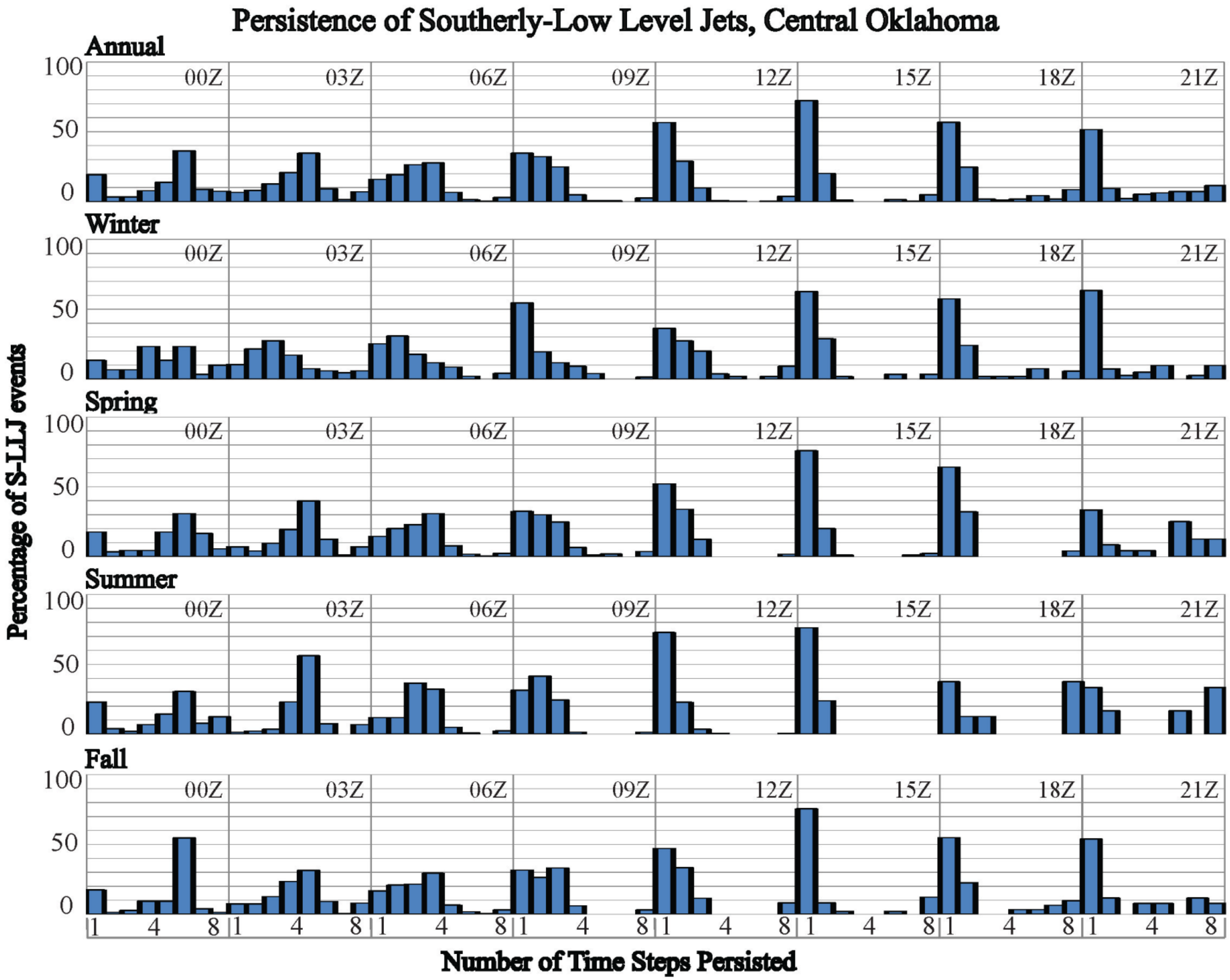

Figure 41. Histograms of the persistence of S-LLJ events, Oklahoma (- 97.5˚, 35.0˚).

S-LLJs are frequent in central Texas throughout the year, and the preferred times of initiation are 03 and 06 UTC, regardless of season. The duration distributions for these two time steps are fairly flat for all seasons, but particularly for fall and winter, indicating that some S-LLJ events that form at these time steps are short-lived whereas others can persist for 4 or more time steps (Figure 42). Jet events that initiate later in the morning (12, 15, and 18 UTC) have much shorter durations, especially in summer, whereas a broader range of durations is observed for jets initiating in the late afternoon and early evening (21 and 00 UTC).

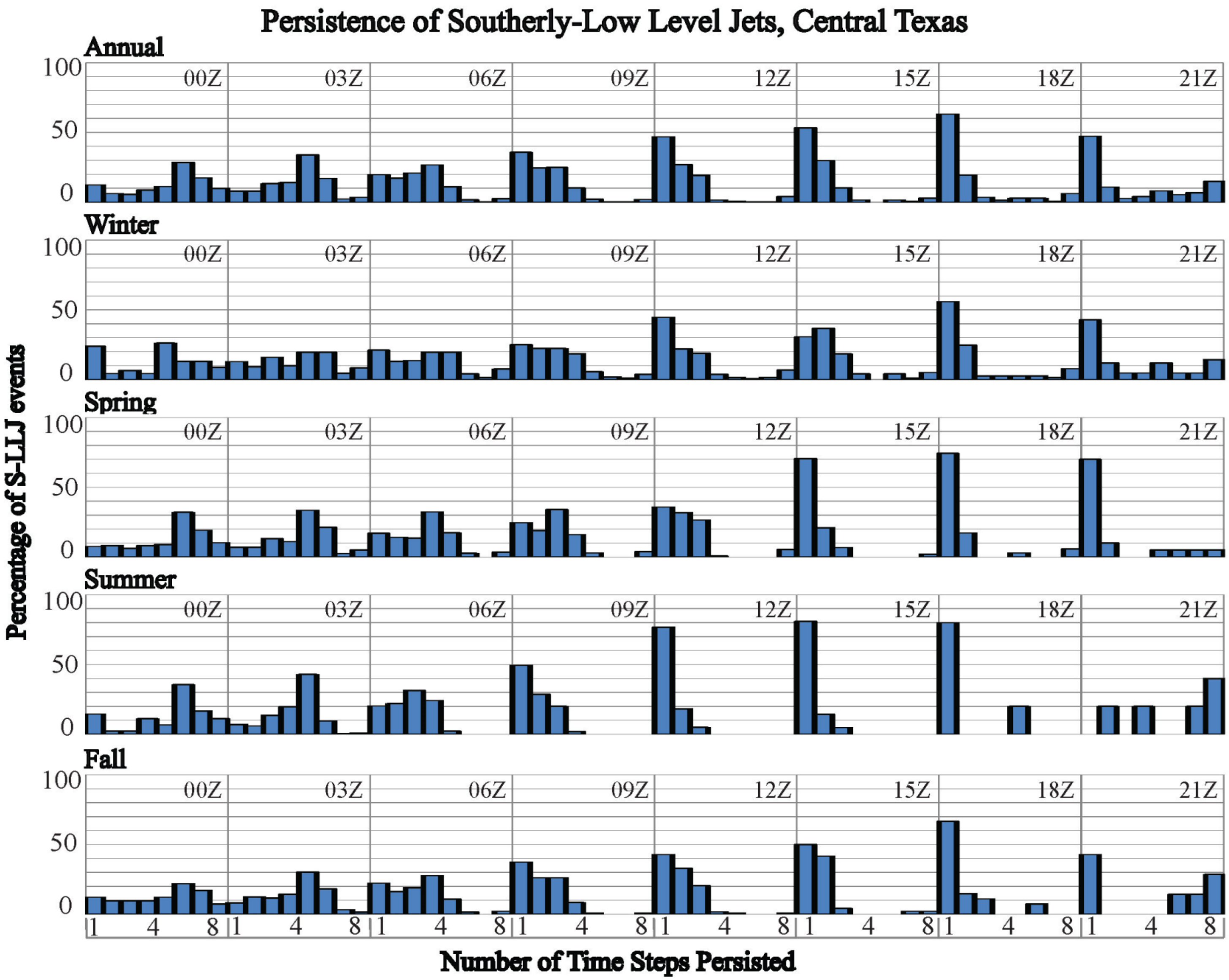

Figure 42. Histograms of the persistence of S-LLJ events, central Texas (- 97.5˚, 30.2˚).

As noted earlier, S-LLJ events in southern Texas and northeastern Mexico, an area of large frequency of S-LLJ profiles, tend to initiate earlier in the evening (00 and 03 UTC) compared to jet events at locations farther north. The distributions of event duration for these time steps are often bimodal, with 30-40% of the jet events persisting for a single time step, and, depending on season, 20-40% of the S-LLJ events persisting for 8 or more time steps (Figure 43). Bimodal distributions are also observed for jet events that form at other times of the day. In general, the bimodal distributions are better defined in winter and the transition seasons of spring and fall and least evident in summer.

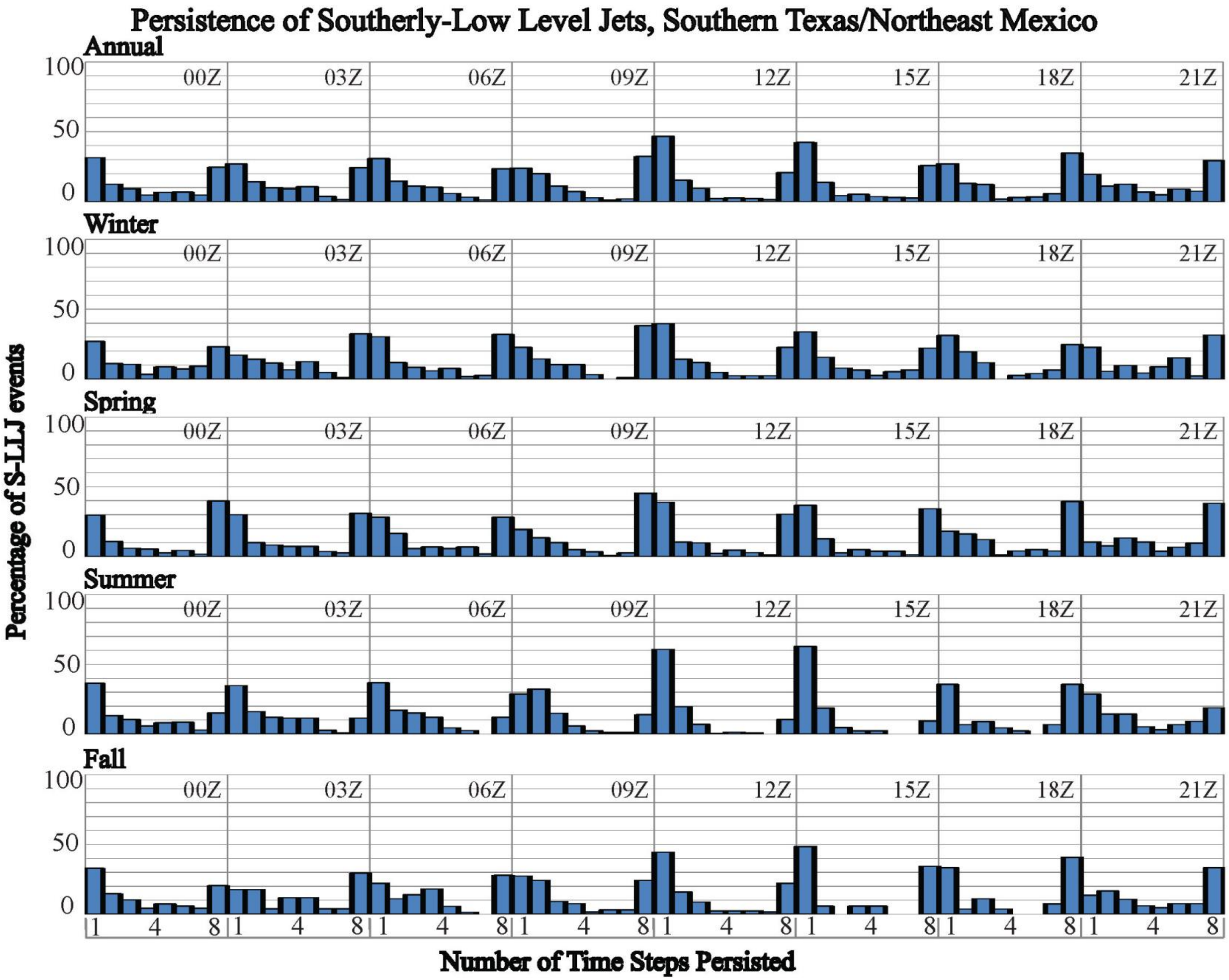

Figure 43. Histograms of the persistence of S-LLJ events,southern tip of Texas(-97.4˚, 25.0˚).

5. Discussion

Below we discuss inferences that can be drawn from the climatological analyses. The discussion is organized around those geographic areas where S-LLJ profiles are particularly frequent.

For most locations and seasons a strong diurnal preference in time of initiation of S-LLJ events is observed. There is, however, an exception to this broad statement. Wintertime S-LLJ events in the northern plains and central Canada, although relatively infrequent, initiated in approximately equal numbers at the eight NARR time steps. This finding indicates that wintertime S-LLJ events are primarily synoptic-driven, most likely occurring within the airstreams of midlatitude cyclones that often form to the west of this area (Whittaker and Horn 1981) or within the indirect circulation associated with strong wintertime upper-level jets (Uccellini and Johnson 1979). The durations of these jet events are shorter than one might expect for a synoptic-driven S-LLJ, but, given the mobility of the synoptic systems with which they are likely linked, limited persistence of jet profiles over an individual gridpoint is not surprising.

A strong diurnal signature in time of initiation of S-LLJ events in the northern Plains and central Canada during summer was found. The majority of summer S-LLJ events in this area formed in the evening and early morning (03, 06, 09, and 12 UTC), with only a very small percentage of jet events initiating in the late morning and afternoon. Thus, boundary conditions, such as frictional decoupling and/or a southerly thermal wind vector at night along the sloping terrain, play an important role in jet formation in this region. Even if the jets form within synoptic-scale southerly airflow, the airflow appears to only take on a jet-like structure during the late evening and early morning hours. The typical summertime jet durations of 1-3 time steps (<9 hours) imply that the jets dissipate in the mid-morning when the nocturnal boundary-layer forcing weakens. An even more unexpected finding was the diurnal fluctuations in jet initiation during the cooler transition seasons of spring and fall. The somewhat earlier time of maximum jet initiation (03, 06 UTC) in spring and fall when day length is shorter compared to summer with longer day length again points to the importance of boundary-layer forcing.

The contribution of boundary-forcing to the formation of S-LLJs in the central plains (Nebraska, Kansas, and Oklahoma) has previously been studied by numerous authors (e.g., Blackadar 1957; Buajitti and Blackadar 1957; Hoecker 1965; Holton 1967; Bonner and Paegle 1970; Hoxit 1975; Fast and McCorcle 1990), although primarily for the warm season, and the strong diurnal fluctuations in the time of initiation and duration of summertime S-LLJ events described above support the findings of these earlier studies. Our analyses indicate that S-LLJ events in this region have a prominent diurnal fluctuation in the cool season as well as the warm season. S-LLJ events in winter, spring, and fall are most likely to initiate in the late evening (03 and 06 UTC), and rarely form in the late morning and afternoon (15, 18, 21 UTC). The average durations and the histograms of the distributions of jet duration are consistent with S-LLJs that dissipate in the late morning when boundary-layer forcing is no longer supportive. Jets during spring and fall very likely often lie within synoptic-scale airflow, such as the airstreams associated with midlatitude cyclones (Carlson 1980; Bierly and Walters 2001).

Although S-LLJs over northern and central Texas are generally considered to be part of the Great Plains jet, the plots shown above of the frequency of S-LLJ profiles indicate that the frequency maximum in this area is relatively disconnected from the somewhat weaker frequency maximum farther north over Nebraska/Kansas/Oklahoma. Also, the analyses of time of initiation suggest that, especially in summer, S-LLJs in this area form over a somewhat broader period (06, 90, 12 UTC) that extends later into the morning hours, although those jets that form in mid-morning have substantially shorter durations than those that form earlier. A possible factor contributing to the broader period over which S-LLJs in north and central Texas form is stronger synoptic-forcing associated with the North American anticyclone that expands westward in summer (Davis et al. 1997). As shown by Cook et al. (2008) using 850 hPa monthly average geopotential height and wind fields obtained from NARR, north and central Texas lies in a region of strong large-scale southerly airflow during the summer months, whereas over the central plains (at ~33°N) the airflow turns eastward and weakens. In addition, numerical simulations conducted by Helfand and Schubert (1995) suggest that the southerly airflow in this region is caused by low-level easterlies along the southern edge of the North American anticyclone converging with low-level westerlies from Baja Californa and the Pacific Ocean and then turning northward. They also argue that because of few synoptic disturbances (e.g., midlatitude cyclones) this airflow is not as disrupted over Texas compared to locations farther north. Nonetheless, boundary-layer forcing is also important, as indicated by the infrequent initiation of S-LLJ events in northern and central Texas in the late morning and afternoon hours.

S-LLJ profiles are also frequent in southern Texas and northeastern Mexico. In all seasons except winter, S-LLJ events in this area initiate earlier in the evening compared to jets at more northern locations. This is particularly evident in summer when over 40% of all jet events in southern Texas and northeastern Mexico were first detected at the 03 UTC time step. The narrow initiation period in summer points to boundary-layer forcing as a major contributor to S-LLJ formation. A possible mechanism is a nocturnal low-level temperature gradient over coastal areas (colder temperatures over land, warmer temperatures over water) and an associated southerly thermal wind vector. Depending on the westward extent of the North American anticyclone during a particular summer, this area may also lie within a weaker pressure gradient and thus experience less synoptic forcing compared to locations farther west and north.

S-LLJ profiles are frequent over the western and southern Gulf of Mexico in winter and spring but not in summer and fall. For both seasons, S-LLJ events in this area primarily form at 09 or 12 UTC. Here again, we speculate that the low-level temperature gradients across the western Gulf contribute to the formation of these jet events. Fewer jet events are observed in summer and fall as the center of North Atlantic anticyclone, with its weak pressure gradient, lies over the region at this time. S-LLJs are also observed over the neighboring Yucatan Peninsula, particularly in spring. Boundary-layer forcing, such as low-level temperature gradients, appears to contribute to these jets given that they are initially detected most often at the 03 and 06 UTC time steps, and rarely form in the late morning and early afternoon.

6. Summary and Conclusions

The study provides one of the first climatological assessments of the time of initiation and persistence of southerly low-level jets (S-LLJs) in central North America and the Gulf of Mexico. Jet profiles identified from wind fields obtained from NARR were combined into jet events, and the NARR 3-hourly time step that a jet event was first detected and the number of consecutive 3-hourly time steps with a S-LLJ profile present were used to estimate the time of initiation and duration of S-LLJ events. The climatological patterns were also used to infer spatial and temporal differences in the boundary-layer and synoptic-scale mechanisms contributing to jet occurrence.

An important finding is the strong diurnal signature evident in the time of initiation of S-LLJ events. Even during winter, when boundary-layer forcing would be expected to be weaker, S-LLJ events were considerably more likely to form in the late evening and early morning for a large portion of the study domain. Also, S-LLJ events at high latitudes displayed pronounced diurnal fluctuations in jet initiation during all seasons except over the northern Plains and central Canada during winter when the jets initiation occurs almost equally over the diurnal cycle. The durations of S-LLJs that formed in the late evening or early morning are consistent with weakening of boundary-layer mechanisms by late morning. Interpretation of the climatological patterns in terms of previous literature on the forcing mechanisms for S-LLJ occurrence allows for a preliminary assessment of the spatial and seasonal variations in the relative contribution of boundary-layer versus synoptic-scale processes to jet formation. However, the constraints of the analysis must be considered when interpreting the climatological patterns, in particular the limited (3-hourly) temporal resolution of the NARR wind fields and potential biases in the NARR wind fields, especially in areas with few wind measurements. In addition, this preliminary analysis is static in character, in that the spatial translation with time of jet events was not considered. Nevertheless, the climatological fields provide some important insights on the processes responsible for jet formation, and point out locations where further mechanistic research is needed to better understand jet formation.

CHAPTER 5. SUMMARY AND CONCLUSIONS

The overall goal of this research was to better understand the climatological characteristics of meridional LLJs over North America and coastal environs. Specific objectives included 1) preparation of a detailed LLJ climatology for North America using 8 times daily NARR reanalysis for the period of 1979-present, focusing on the spatial and temporal patterns in the frequency, speed, and elevation of LLJs from both southerly and northerly directions; 2) characterization of the timing and persistence of S-LLJs as a preliminary assessment of the relative contribution of boundary-layer versus synoptic forcing to jet formation and persistence; 3) investigation of temporal trends and interannual variation of LLJs during the 31-year (1979-2009) study period for selected NARR gridpoints where N-LLJs and S-LLJs are frequent; and 4) incorporation of the spatial patterns of LLJ frequency and characteristics identified from the above objectives into an electronic atlas that is easily searchable and can be made available via the internet. Major findings are highlighted below.

1. Jet Frequency, Speed and Elevation

The spatial analyses highlight the frequency, strength, and elevation of well-known S-LLJs and N-LLJs. One unexpected finding is the high frequency of the Pacific Coastal N-LLJ in the summer, observed on over 30% of all NARR time steps. Also, the Yucatan and western Gulf regions have elevated frequencies of S-LLJs which likely relate to the well-studied Caribbean jet. Findings for the S-LLJ of the Great Plains during the summer are similar to previous research, although the NARR dataset displays three areas of frequency maxima, one along the Oklahoma/Kansas border, another in northern Texas, and the third found in southern Texas/northeastern Mexico where high frequencies of S-LLJs are observed during much of the year. The relatively high N-LLJ frequencies found in the northern plains has not been a focus of previous studies. The well-known Carolina LLJ is almost negligible in the NARR dataset relative to other well studied LLJs.

Both the speed and elevation of the N-LLJs and S-LLJs display little diurnal fluctuation; seasonal and intraseasonal variations of these parameters are also small. Jets observed at locations in the southern portion of the study domain, including the Intra-Americas and northern Mexico, generally have lower mean speeds and higher elevations compared to jets observed elsewhere. The greatest diurnal variations in jet speed are evident during spring and summer for S-LLJs in the Great Plains. Diurnal fluctuations in jet elevation are mostly seen in areas with low jet frequencies, indicating that those diurnal variations must be interpreted cautiously.

2. Time of Initiation and Persistence

The contribution of boundary-layer forcing to the formation of S-LLJs is evident across the study domain. Even during the winter, when boundary-layer forcing would be expected to be weaker, S-LLJ events are considerably more likely to form in the late evening and early morning for a large portion of the study area and persist for only a few NARR time steps. In addition, summertime S-LLJ events at higher latitudes, are short-lived and initiate in the late evening and early morning hours, an indication of boundary-layer forcing. The durations of S-LLJs that formed in the late evening or early morning are consistent with weakening of boundary-layer mechanisms in that they dissipated by late morning.

The climatological findings from this research also point out locations where further mechanistic research is needed to better understand jet development.

3. Temporal Trends and Variability

Significant, positive trends in jet frequency are primarily seen for S-LLJs temporally, whereas trends are generally insignificant for N-LLJs. Inter-annual variability is greatest for those seasons with lower jet frequencies.

4. Further Research

Additional research on LLJ mechanisms is needed in order to further understand the LLJ climatology, including regions of high LLJ frequency (e.g., Hudson Bay) identified in this study that have not been previously described in the literature. The findings also could be advanced by employing reanalysis datasets that have a higher temporal resolution, since the NARR dataset has only a 3-hourly time step. This would further the study of LLJ initiation and persistence, since only an estimate of initiation and dissipation of jet events is possible using NARR. Also, this study assessed jet characteristics including persistence at individual grid points (i.e., an Eulerian approach), and did not consider that LLJs, especially those associated with synoptic-scale circulation features, are mobile and can translate downstream with time. A future analysis that considers the mobility of these features (i.e., a more Lagrangian approach) will provide an improved understanding of jet persistence, especially for synoptic-forced LLJs.

APPENDICES

Appendix A: Southerly Low-Level Jet Frequency Maps

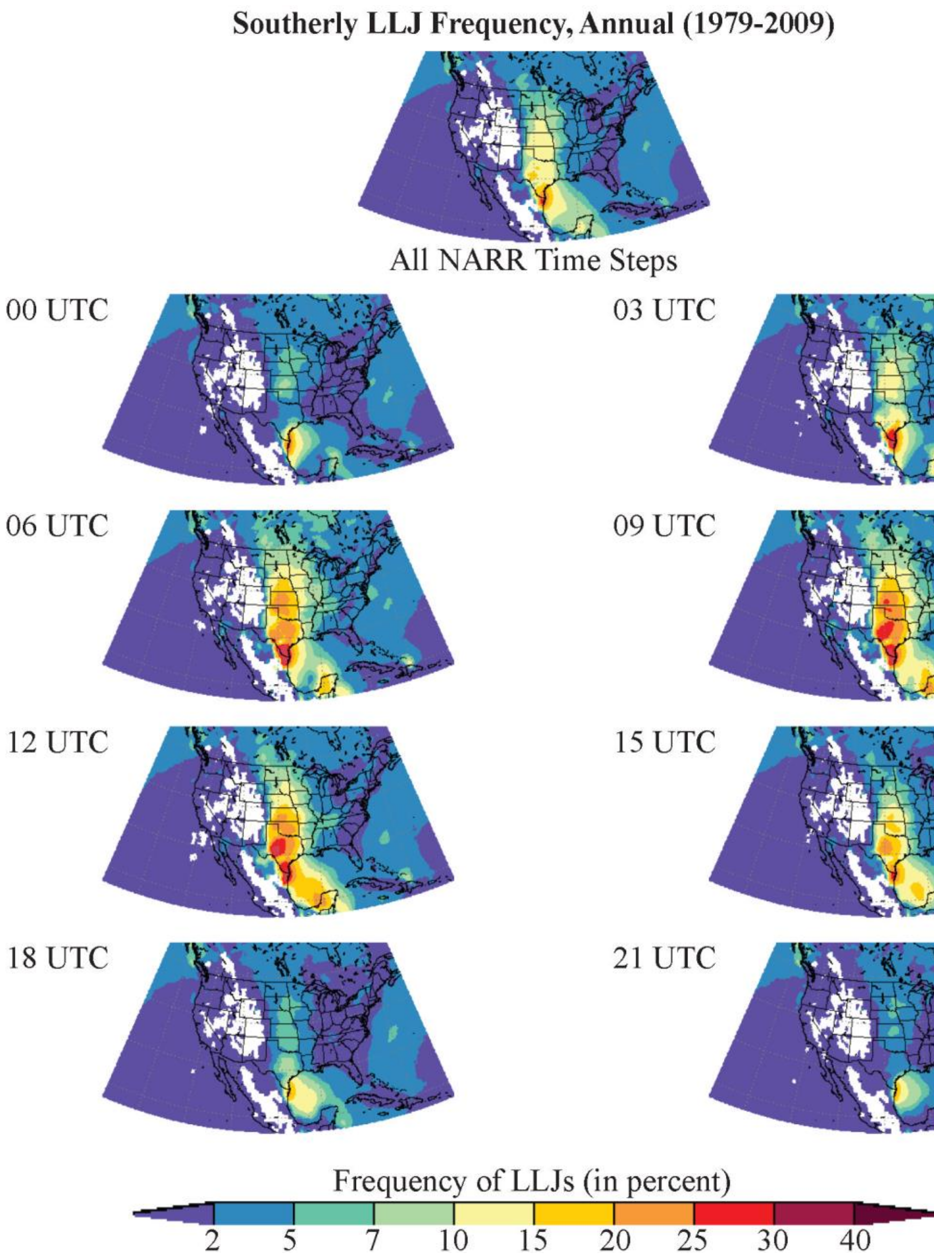

Figure 44. Annual frequency of S-LLJs from 1979 to 2009 expressed as a percentage of the total number of time steps, summed over all NARR time steps (top figure) and individually for each time step (bottom figures). Gridpoints with no jet cases and/or surface elevations >2km MSL are shown in white.

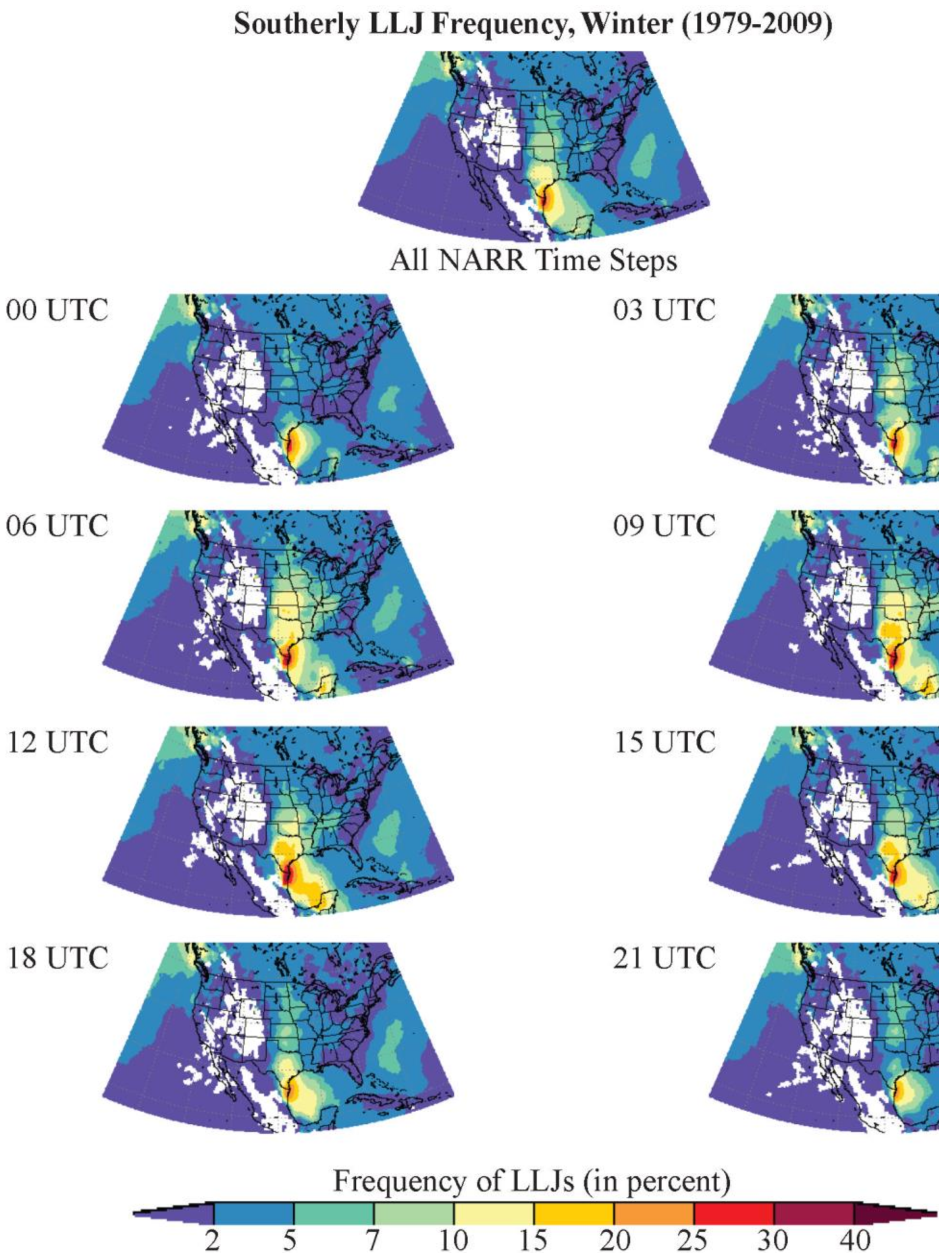

Figure 45. Winter frequency of S-LLJs from 1979 to 2009 expressed as a percentage of the total number of time steps, summed over all NARR time steps (top figure) and individually for each time step (bottom figures). Gridpoints with no jet cases and/or surface elevations >2km MSL are shown in white.

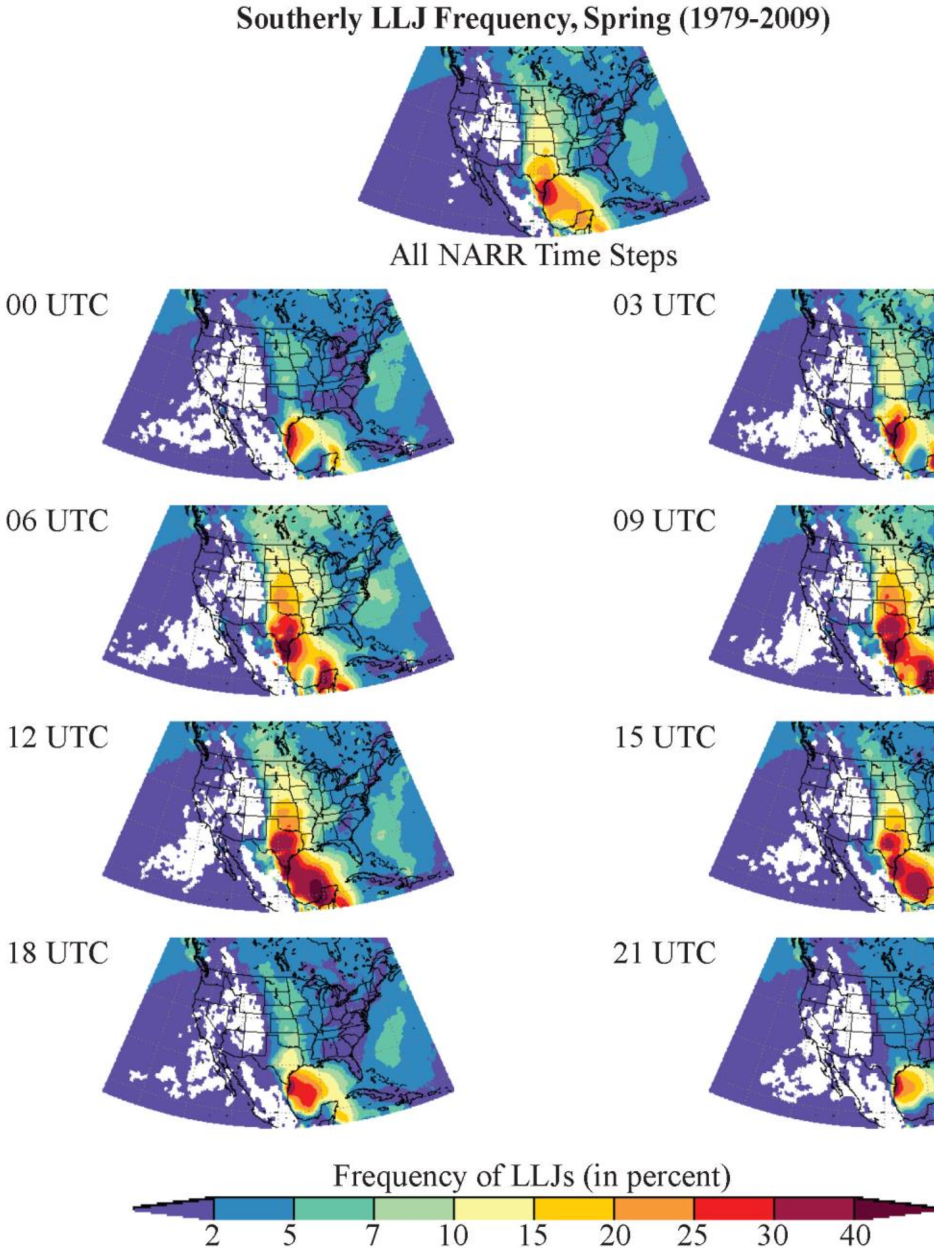

Figure 46. Spring frequency of S-LLJs from 1979 to 2009 expressed as a percentage of the total number of time steps, summed over all NARR time steps (top figure) and individually for each time step (bottom figures). Gridpoints with no jet cases and/or surface elevations >2km MSL are shown in white.

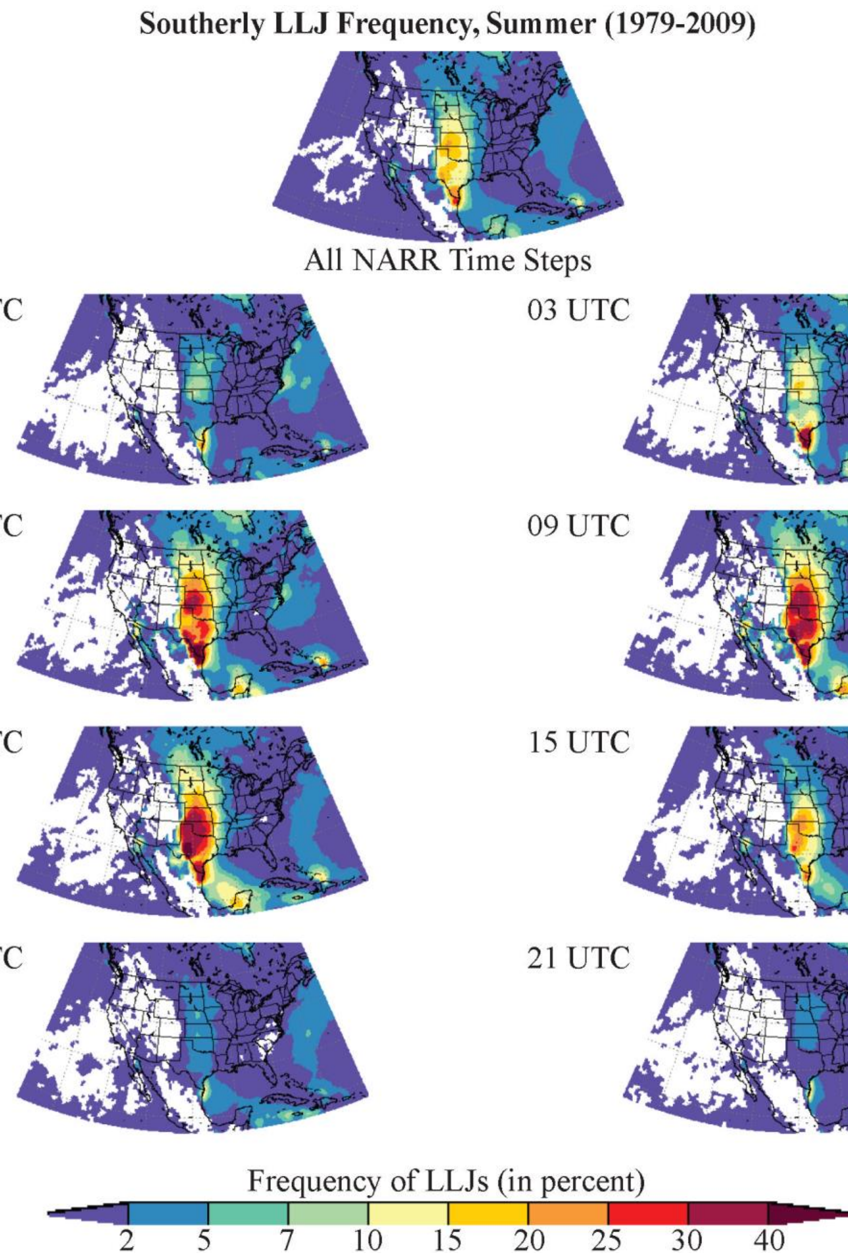

Figure 47. Summer frequency of S-LLJs from 1979 to 2009 expressed as a percentage of the total number of time steps, summed over all NARR time steps (top figure) and individually for each time step (bottom figures). Gridpoints with no jet cases and/or surface elevations >2km MSL are shown in white.

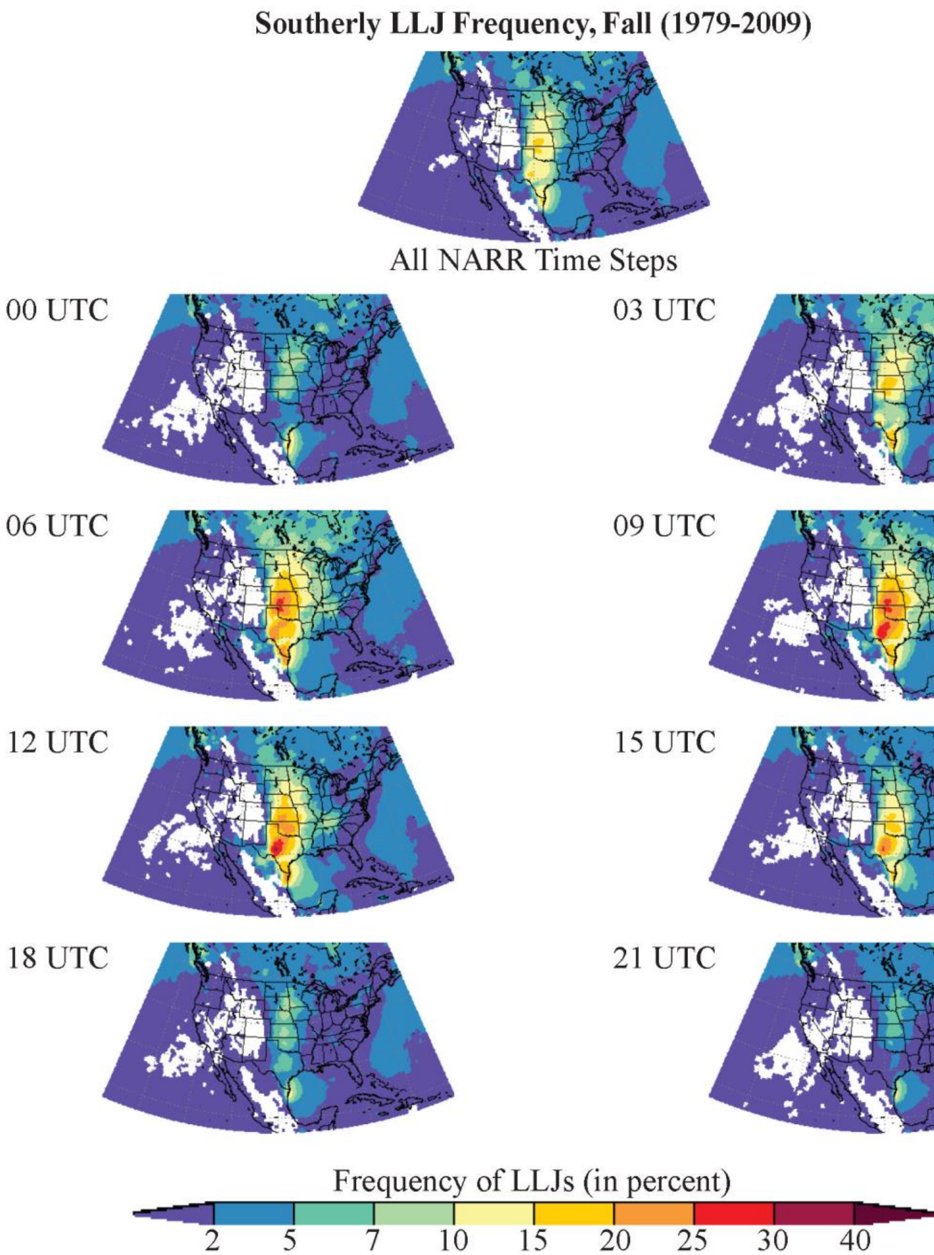

Figure 48. Fall frequency of S-LLJs from 1979 to 2009 expressed as a percentage of the total number of time steps, summed over all NARR time steps (top figure) and individually for each time step (bottom figures). Gridpoints with no jet cases and/or surface elevations >2km MSL are shown in white.

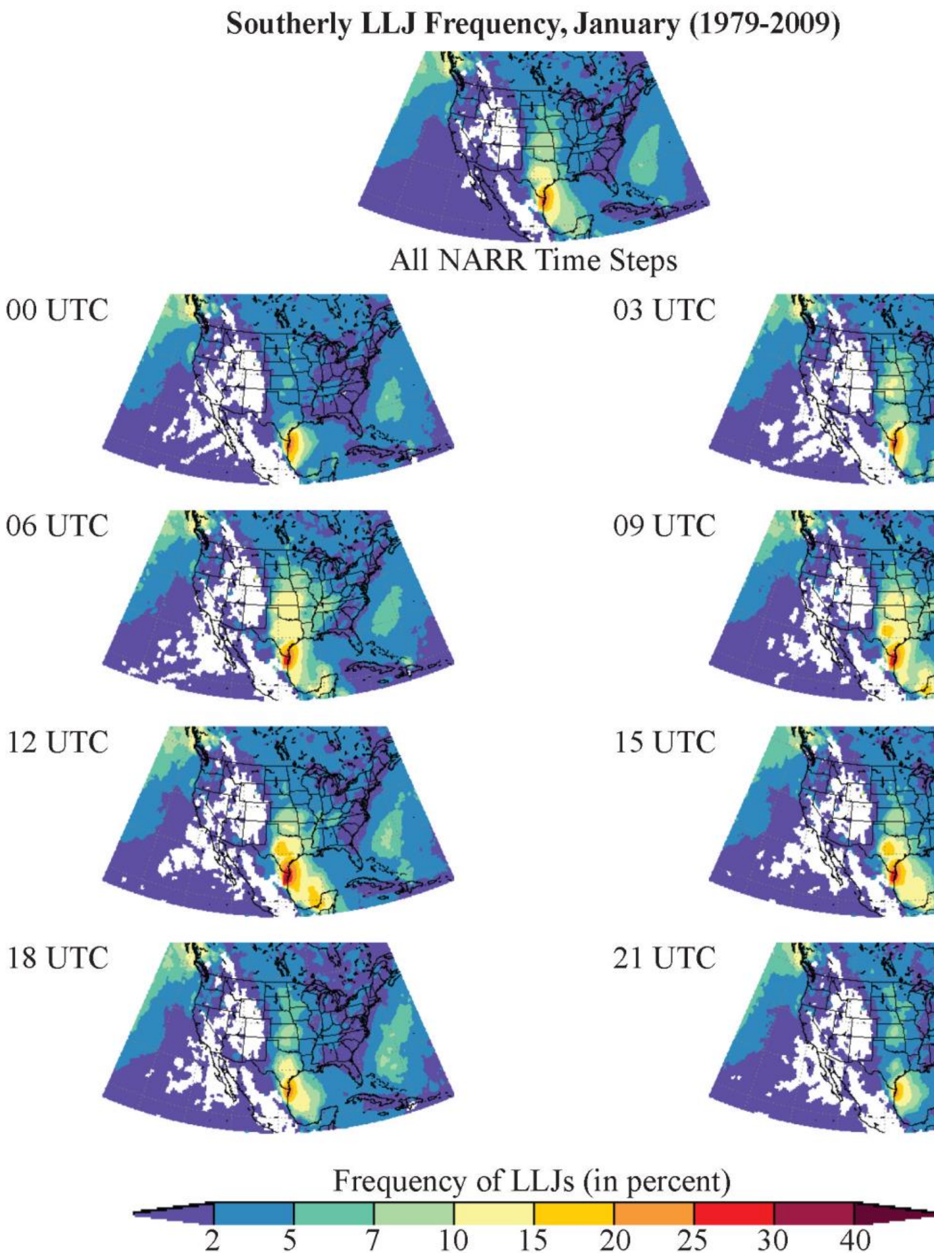

Figure 49. January frequency of S-LLJs from 1979 to 2009 expressed as a percentage of the total number of time steps, summed over all NARR time steps (top figure) and individually for each time step (bottom figures). Gridpoints with no jet cases and/or surface elevations >2km MSL are shown in white.

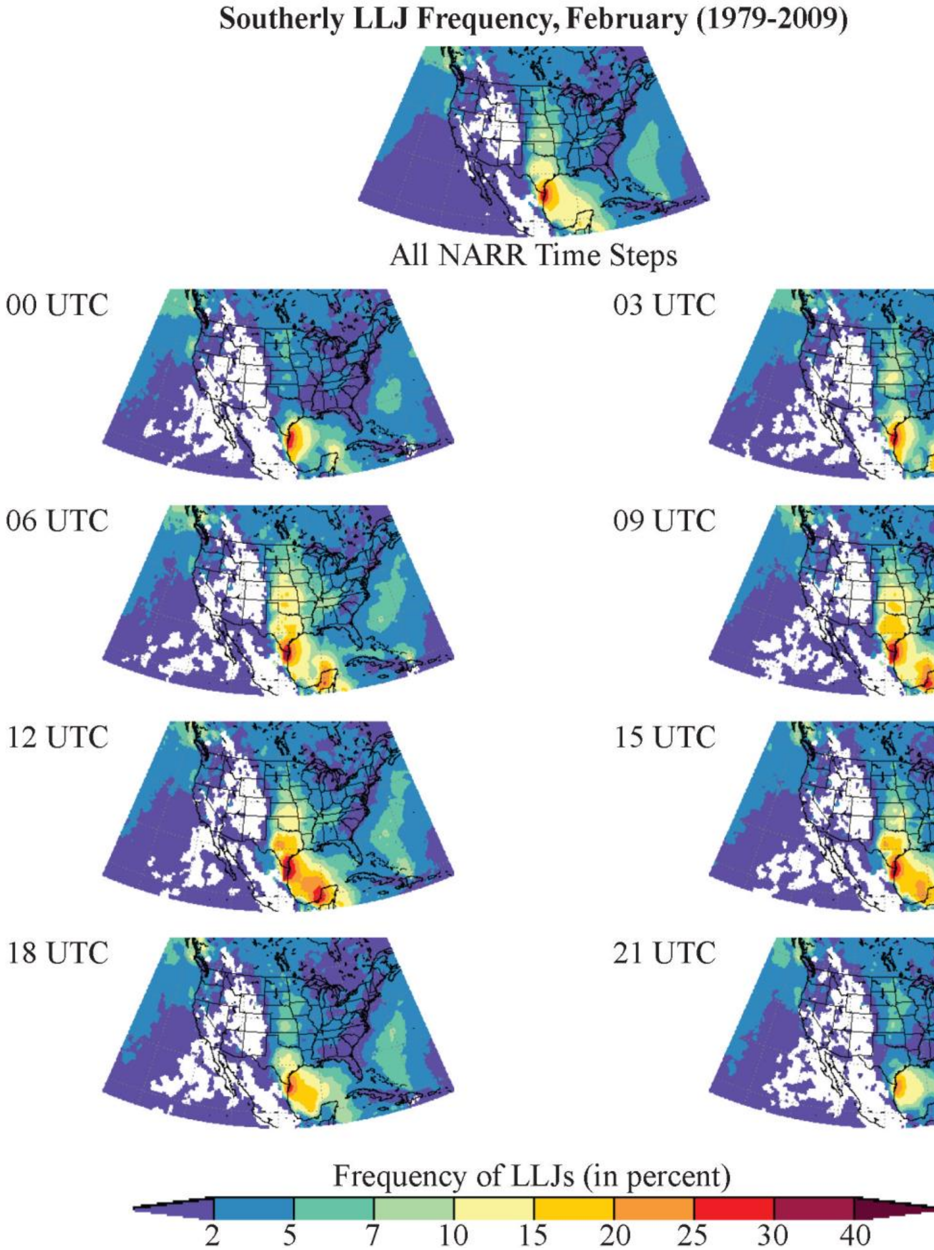

Figure 50. February frequency of S-LLJs from 1979 to 2009 expressed as a percentage of the total number of time steps, summed over all NARR time steps (top figure) and individually for each time step (bottom figures). Gridpoints with no jet cases and/or surface elevations >2km MSL are shown in white.

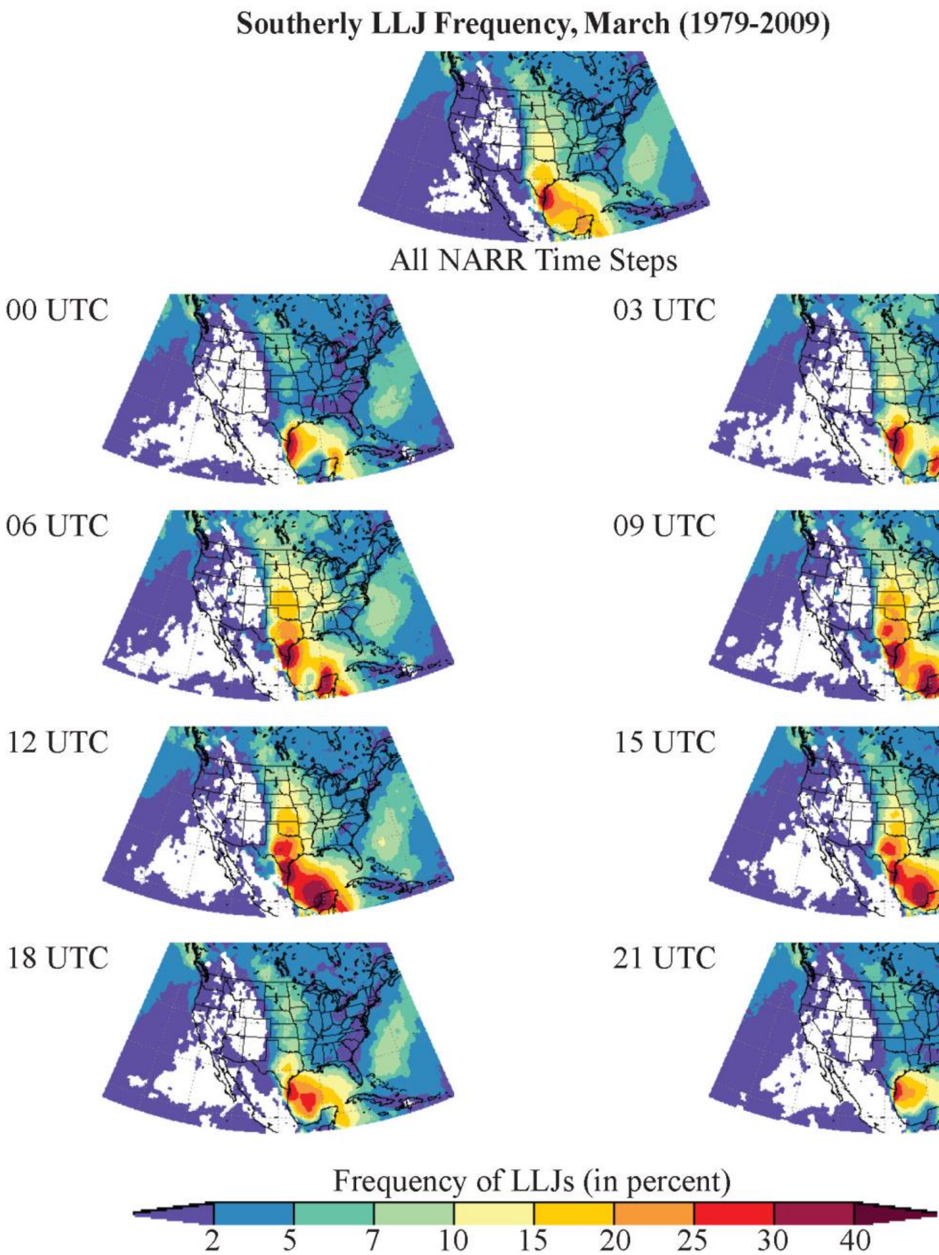

Figure 51. March frequency of S-LLJs from 1979 to 2009 expressed as a percentage of the total number of time steps, summed over all NARR time steps (top figure) and individually for each time step (bottom figures). Gridpoints with no jet cases and/or surface elevations >2km MSL are shown in white.

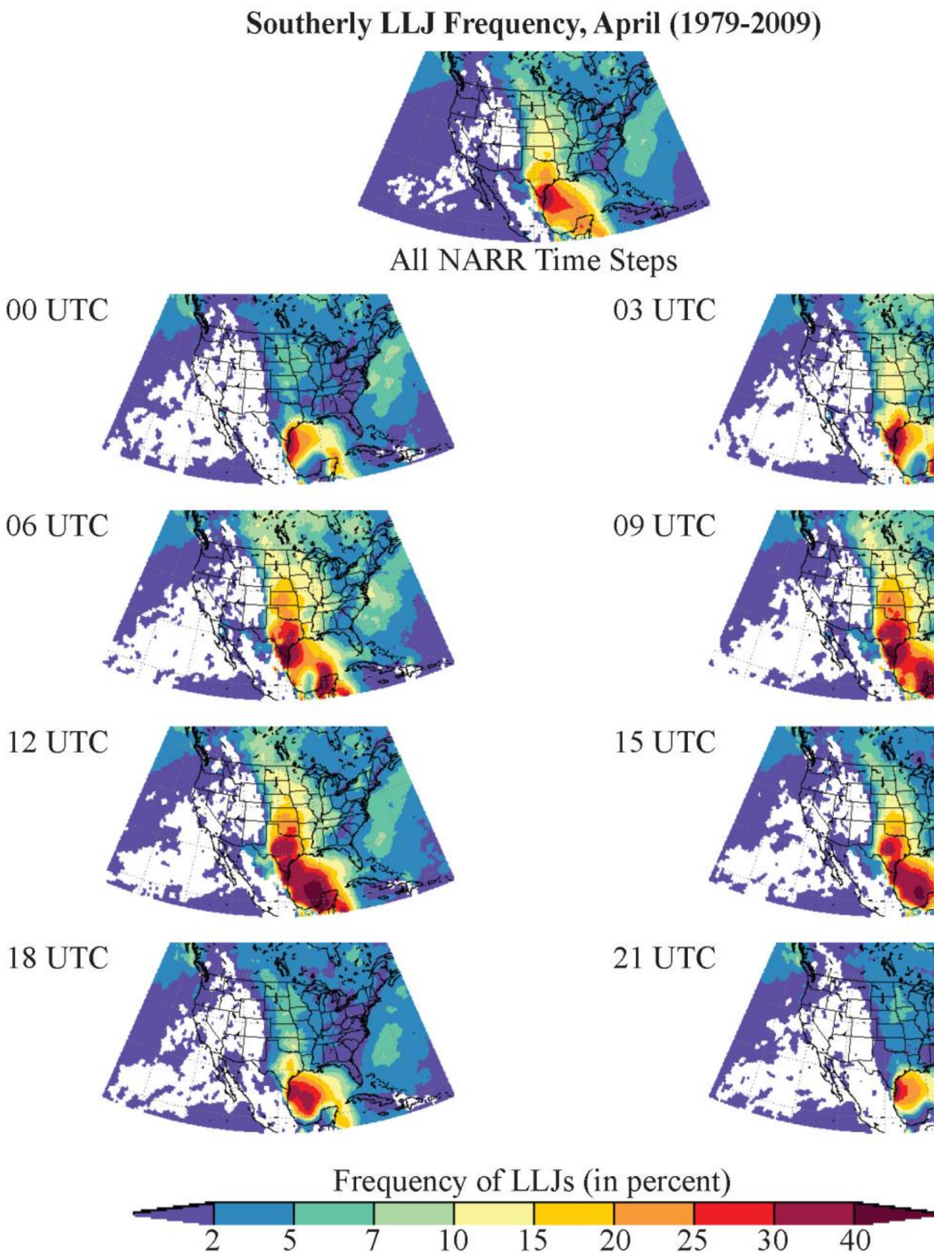

Figure 52. April frequency of S-LLJs from 1979 to 2009 expressed as a percentage of the total number of time steps, summed over all NARR time steps (top figure) and individually for each time step (bottom figures). Gridpoints with no jet cases and/or surface elevations >2km MSL are shown in white.

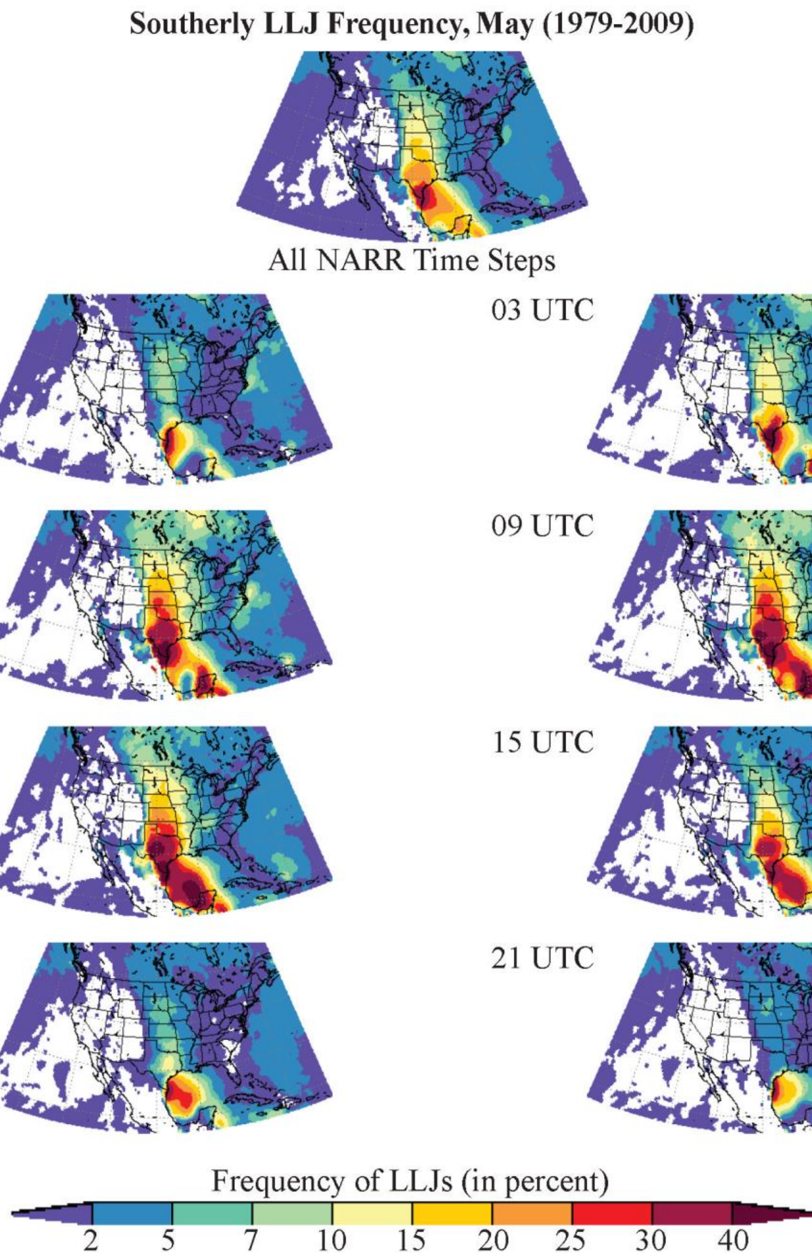

Figure 53. May frequency of S-LLJs from 1979 to 2009 expressed as a percentage of the total number of time steps, summed over all NARR time steps (top figure) and individually for each time step (bottom figures). Gridpoints with no jet cases and/or surface elevations >2km MSL are shown in white.

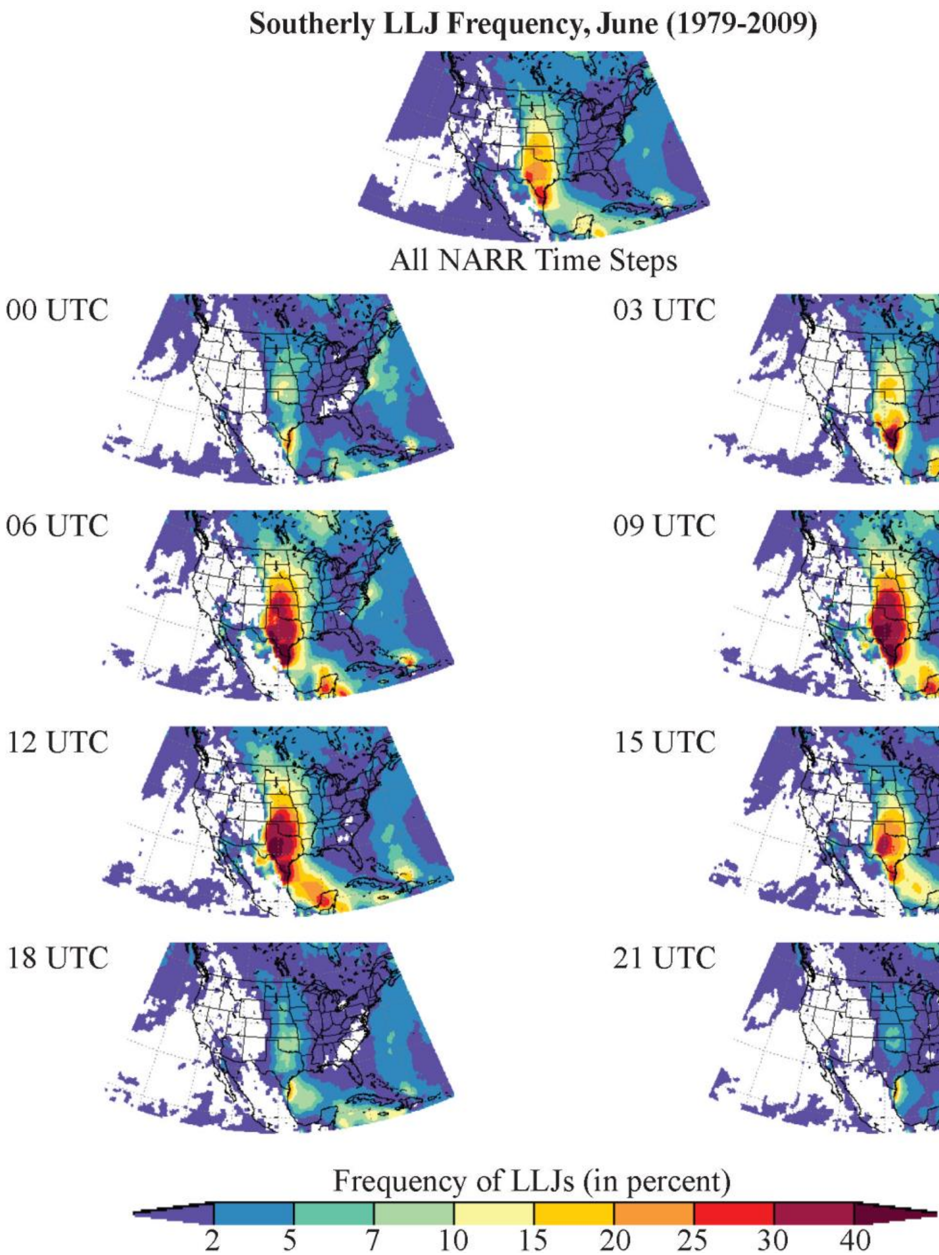

Figure 54. June frequency of S-LLJs from 1979 to 2009 expressed as a percentage of the total number of time steps, summed over all NARR time steps (top figure) and individually for each time step (bottom figures). Gridpoints with no jet cases and/or surface elevations >2km MSL are shown in white.

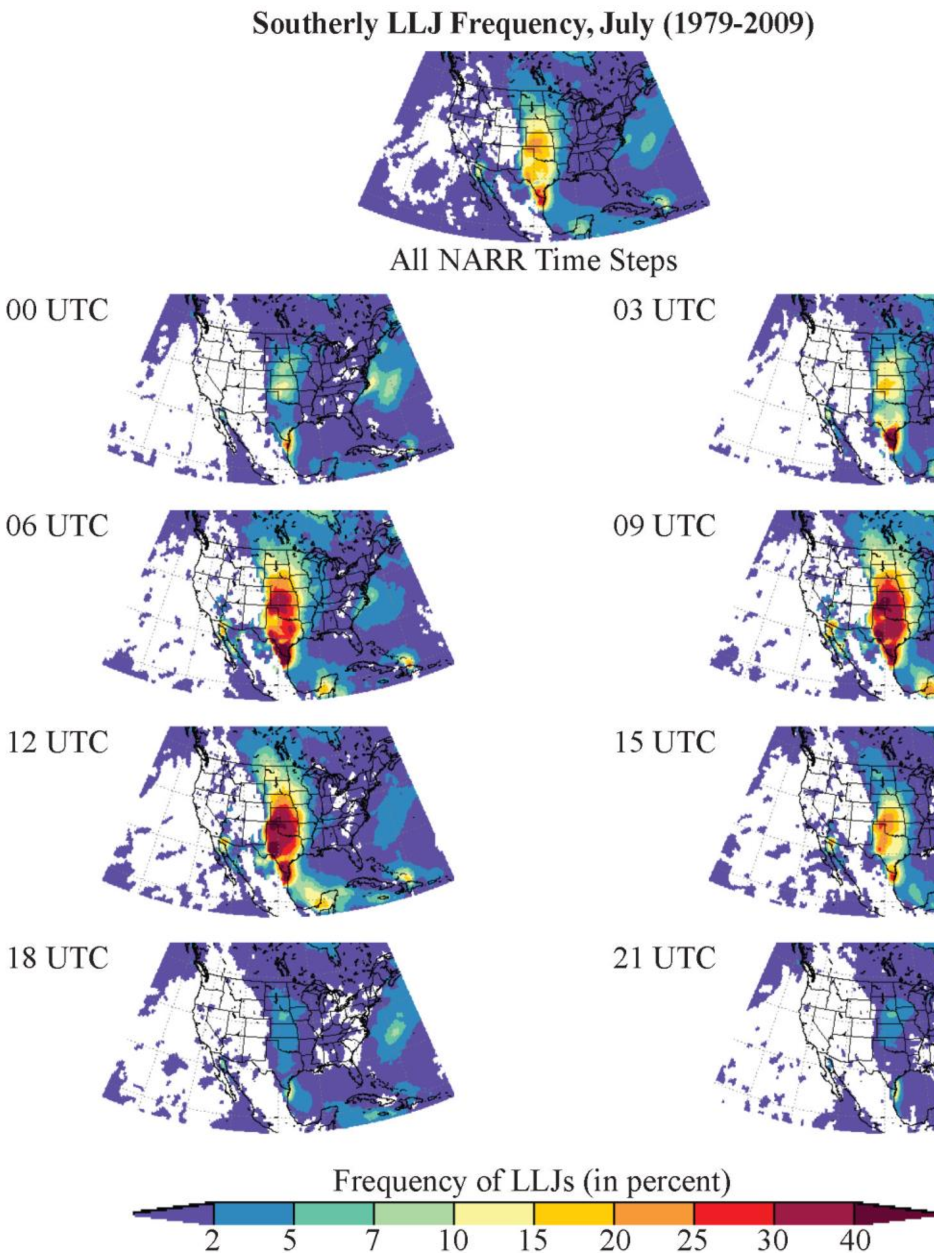

Figure 55. July frequency of S-LLJs from 1979 to 2009 expressed as a percentage of the total number of time steps, summed over all NARR time steps (top figure) and individually for each time step (bottom figures). Gridpoints with no jet cases and/or surface elevations >2km MSL are shown in white.

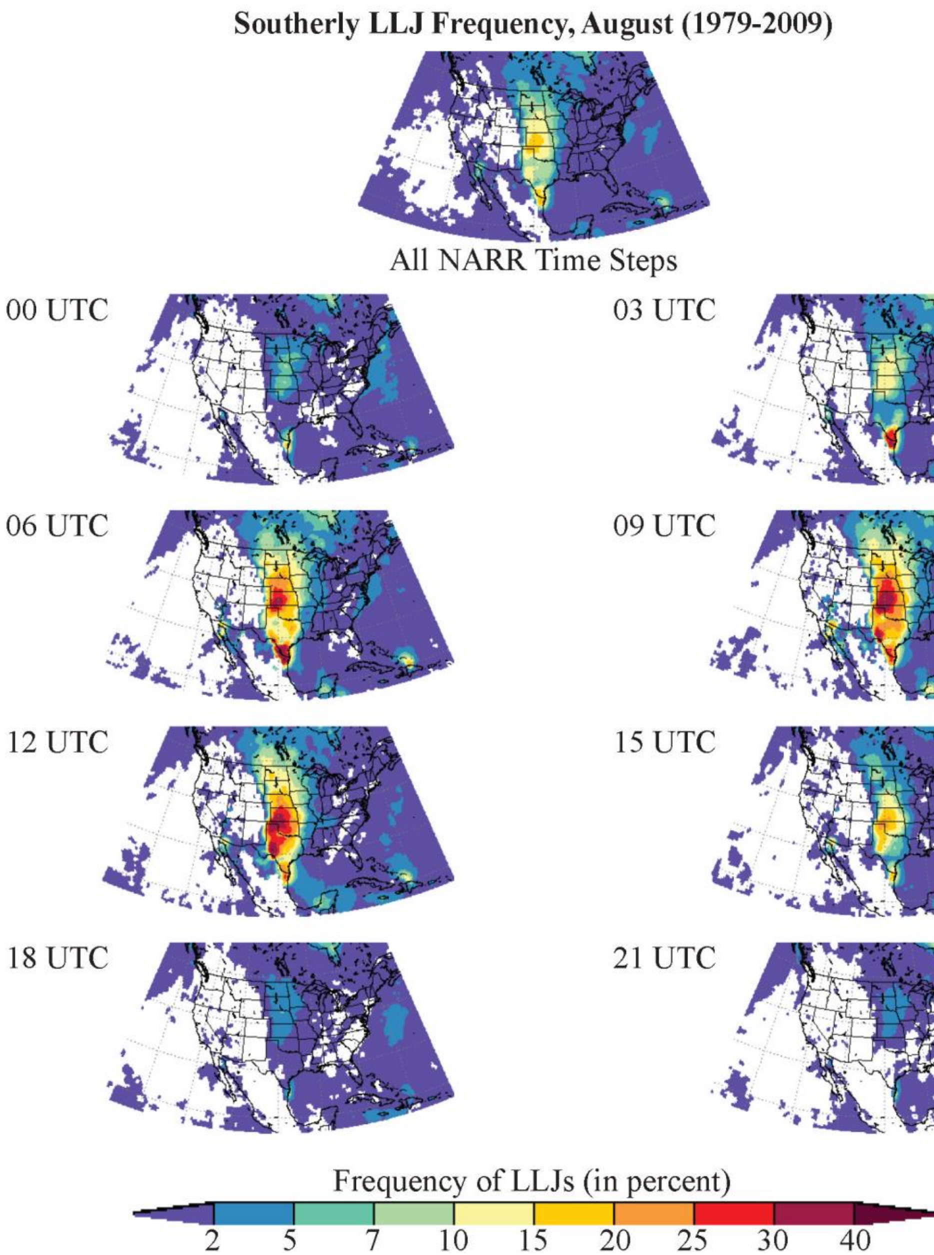

Figure 56. August frequency of S-LLJs from 1979 to 2009 expressed as a percentage of the total number of time steps, summed over all NARR time steps (top figure) and individually for each time step (bottom figures). Gridpoints with no jet cases and/or surface elevations >2km MSL are shown in white.

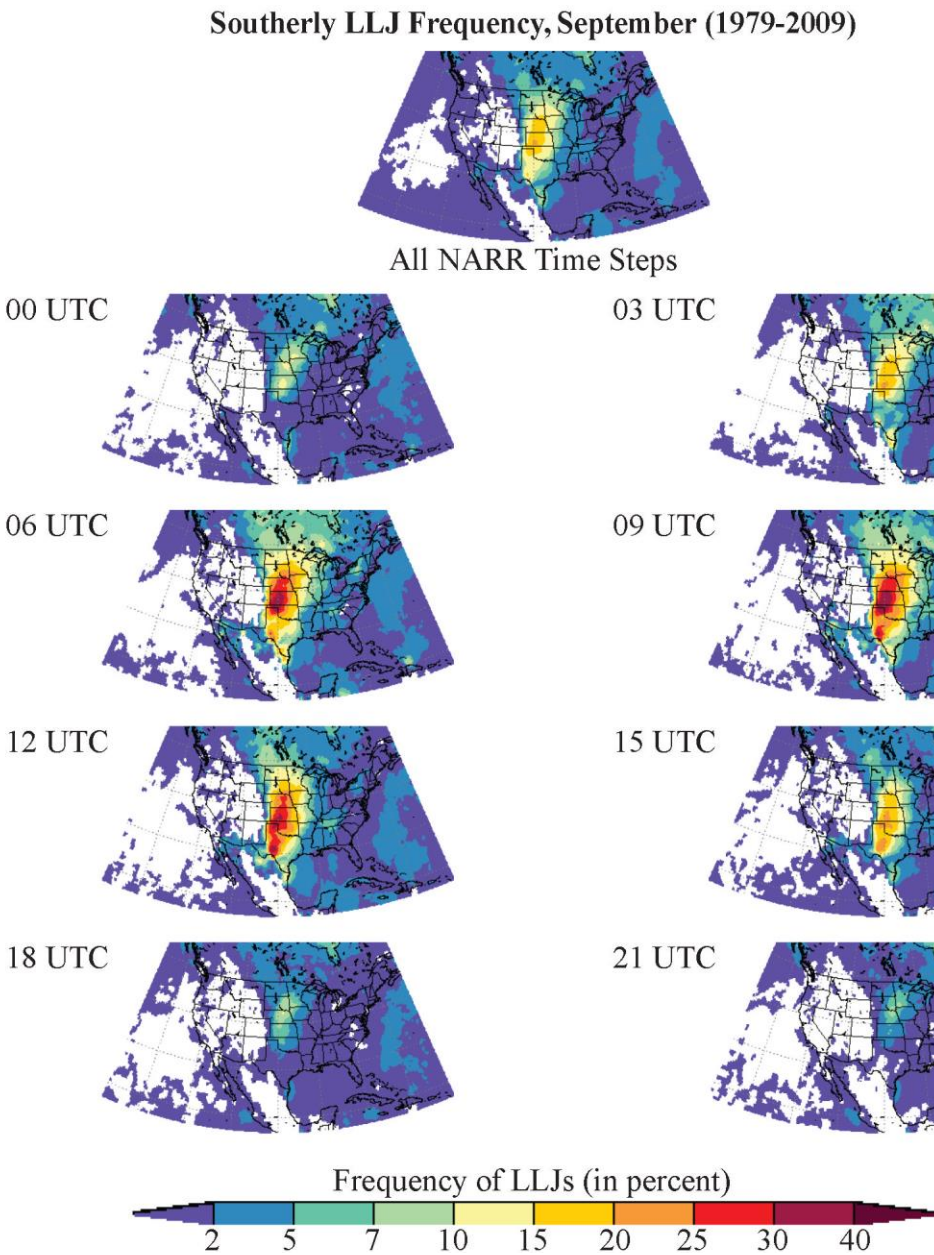

Figure 57. September frequency of S-LLJs from 1979 to 2009 expressed as a percentage of the total number of time steps, summed over all NARR time steps (top figure) and individually for each time step (bottom figures). Gridpoints with no jet cases and/or surface elevations >2km MSL are shown in white.

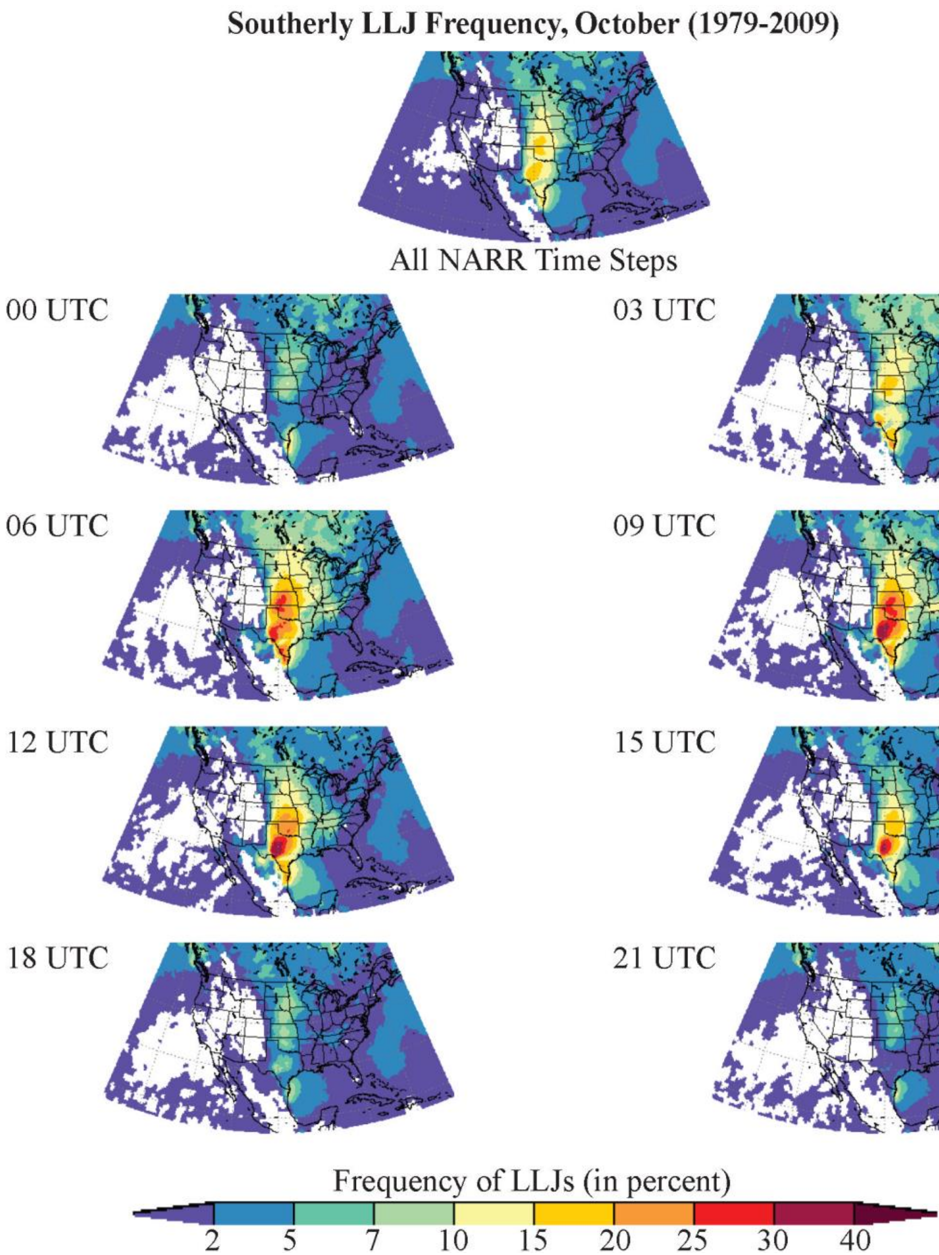

Figure 58. October frequency of S-LLJs from 1979 to 2009 expressed as a percentage of the total number of time steps, summed over all NARR time steps (top figure) and individually for each time step (bottom figures). Gridpoints with no jet cases and/or surface elevations >2km MSL are shown in white.

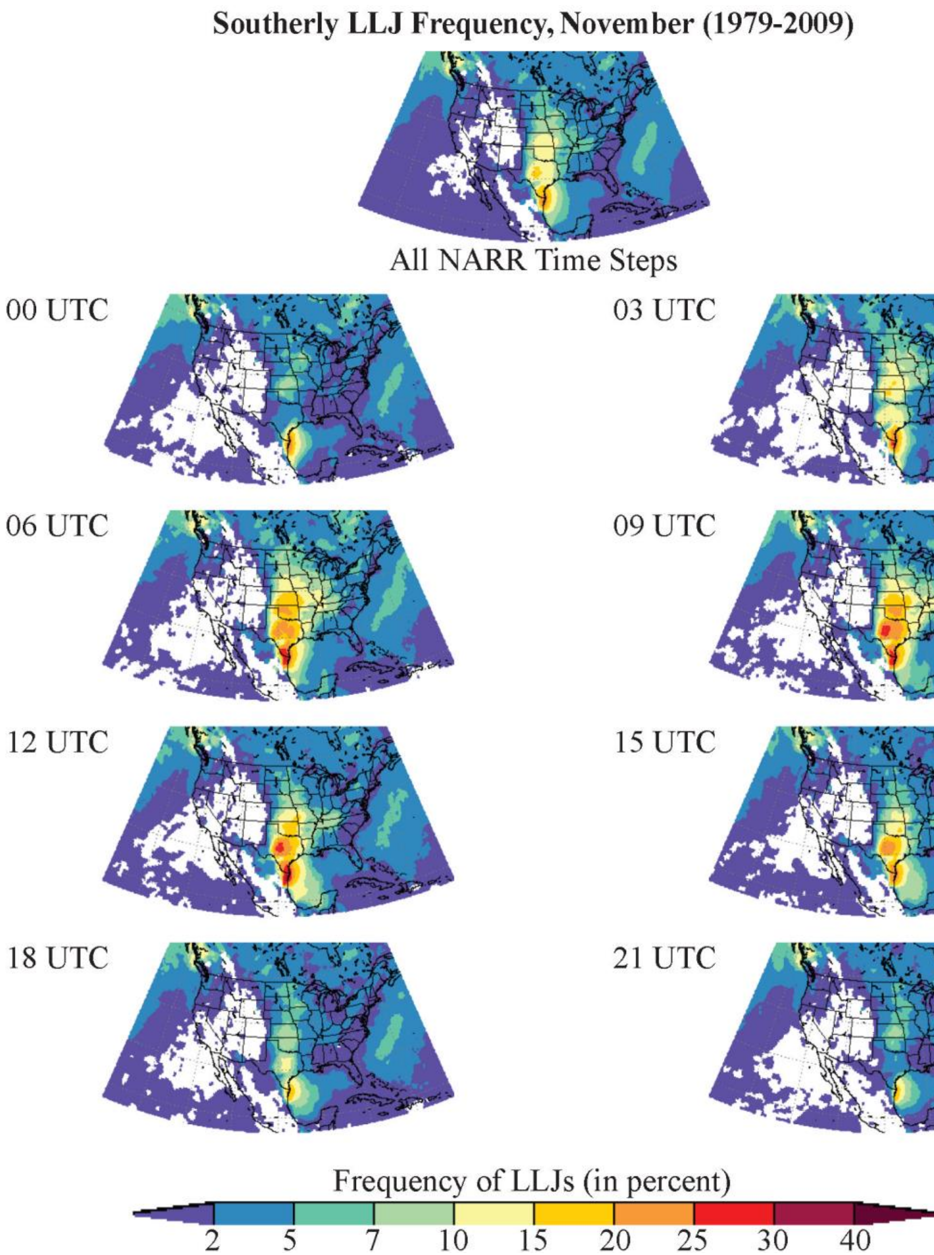

Figure 59. November frequency of S-LLJs from 1979 to 2009 expressed as a percentage of the total number of time steps, summed over all NARR time steps (top figure) and individually for each time step (bottom figures). Gridpoints with no jet cases and/or surface elevations >2km MSL are shown in white.

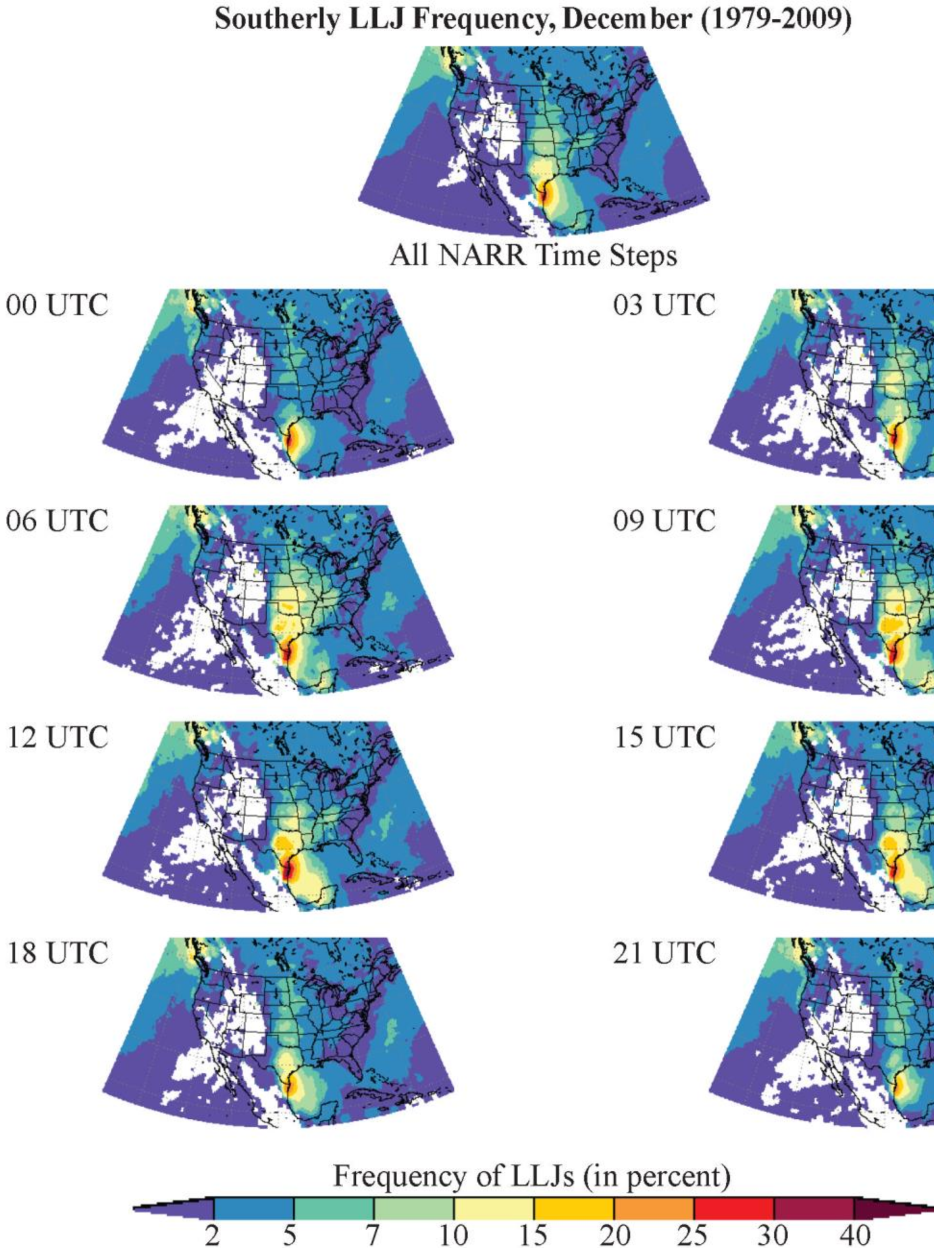

Figure 60. December frequency of S-LLJs from 1979 to 2009 expressed as a percentage of the total number of time steps, summed over all NARR time steps (top figure) and individually for each time step (bottom figures). Gridpoints with no jet cases and/or surface elevations >2km MSL are shown in white.

Appendix B: Northerly Low-Level Jet Frequency Maps

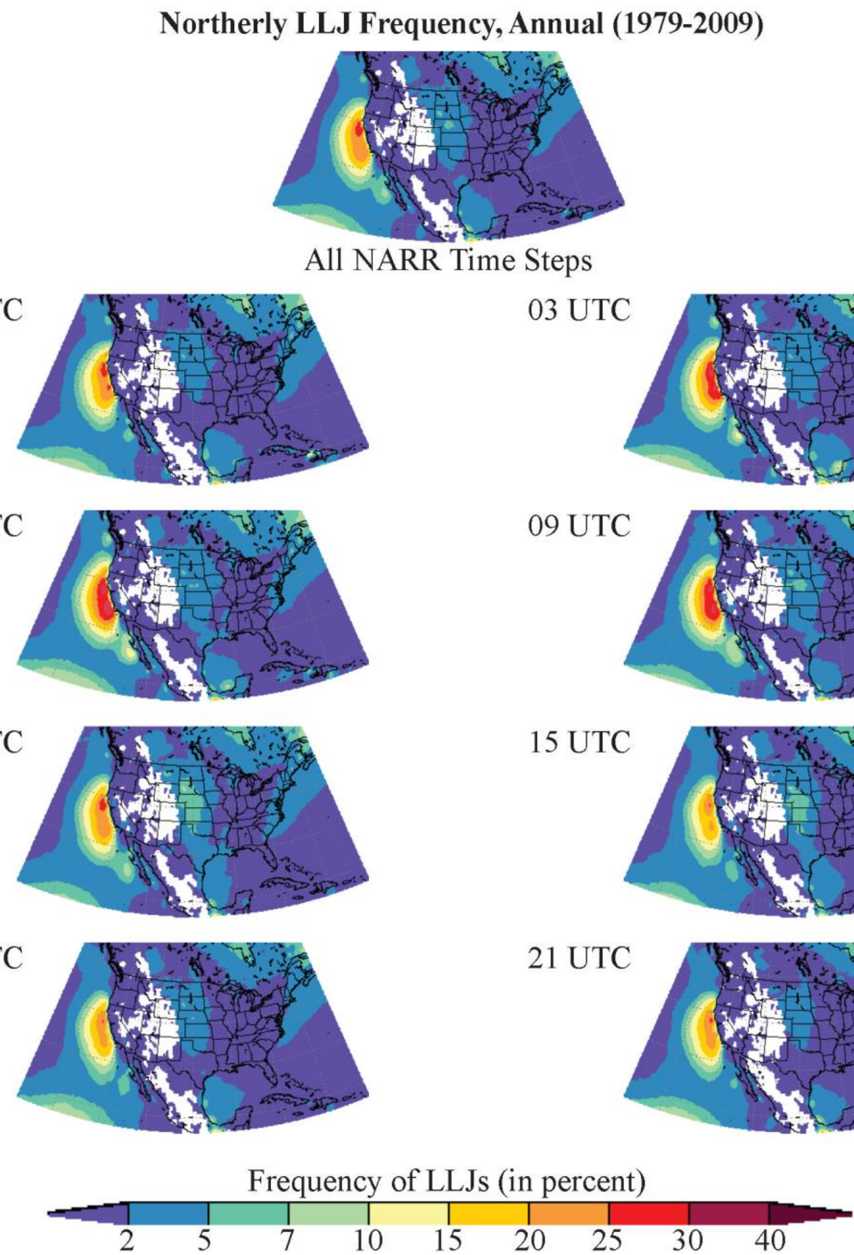

Figure 61. Annual frequency of N-LLJs from 1979 to 2009 expressed as a percentage of the total number of time steps, summed over all NARR time steps (top figure) and individually for each time step (bottom figures). Gridpoints with no jet cases and/or surface elevations >2km MSL are shown in white.

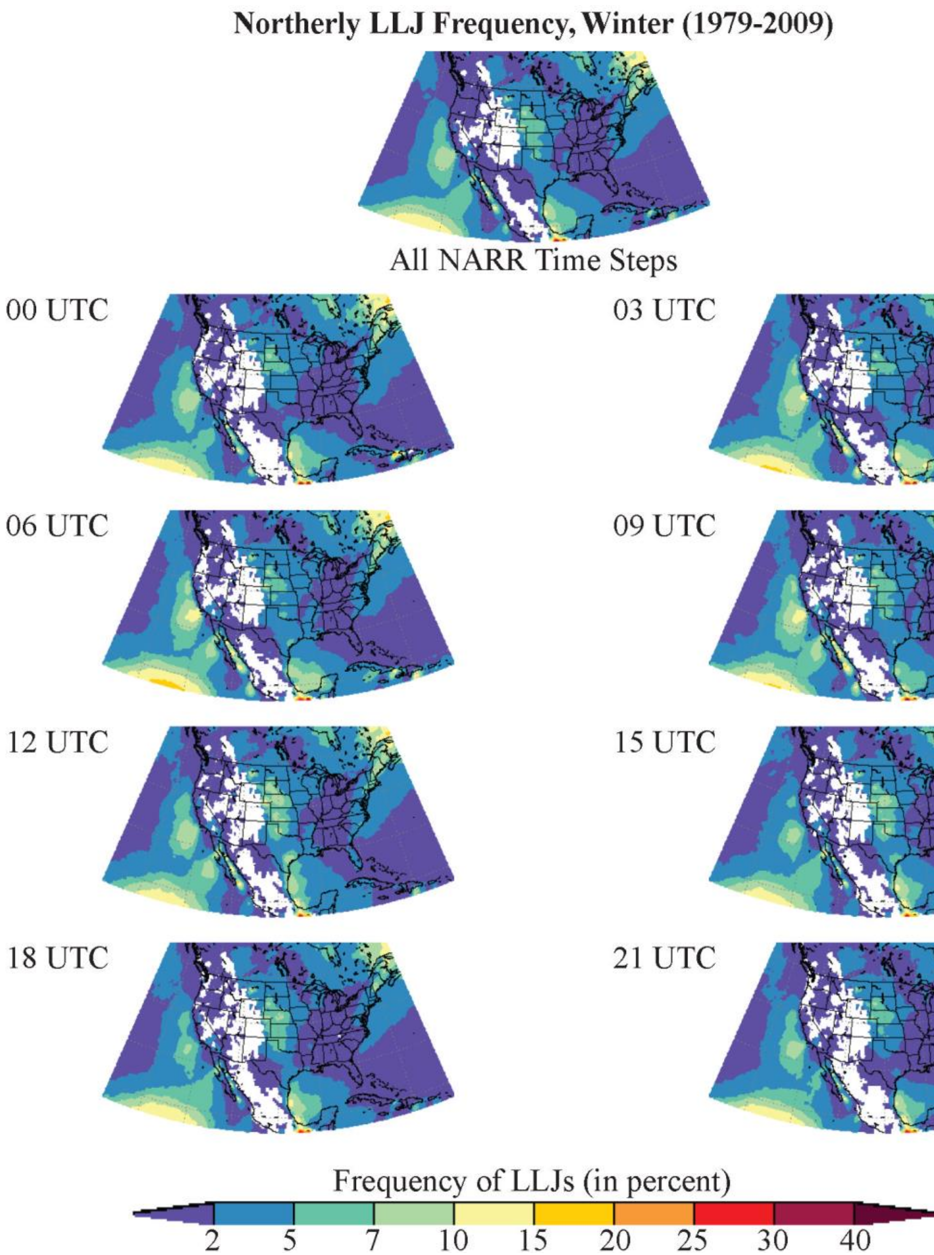

Figure 62. Winter frequency of N-LLJs from 1979 to 2009 expressed as a percentage of the total number of time steps, summed over all NARR time steps (top figure) and individually for each time step (bottom figures). Gridpoints with no jet cases and/or surface elevations >2km MSL are shown in white.

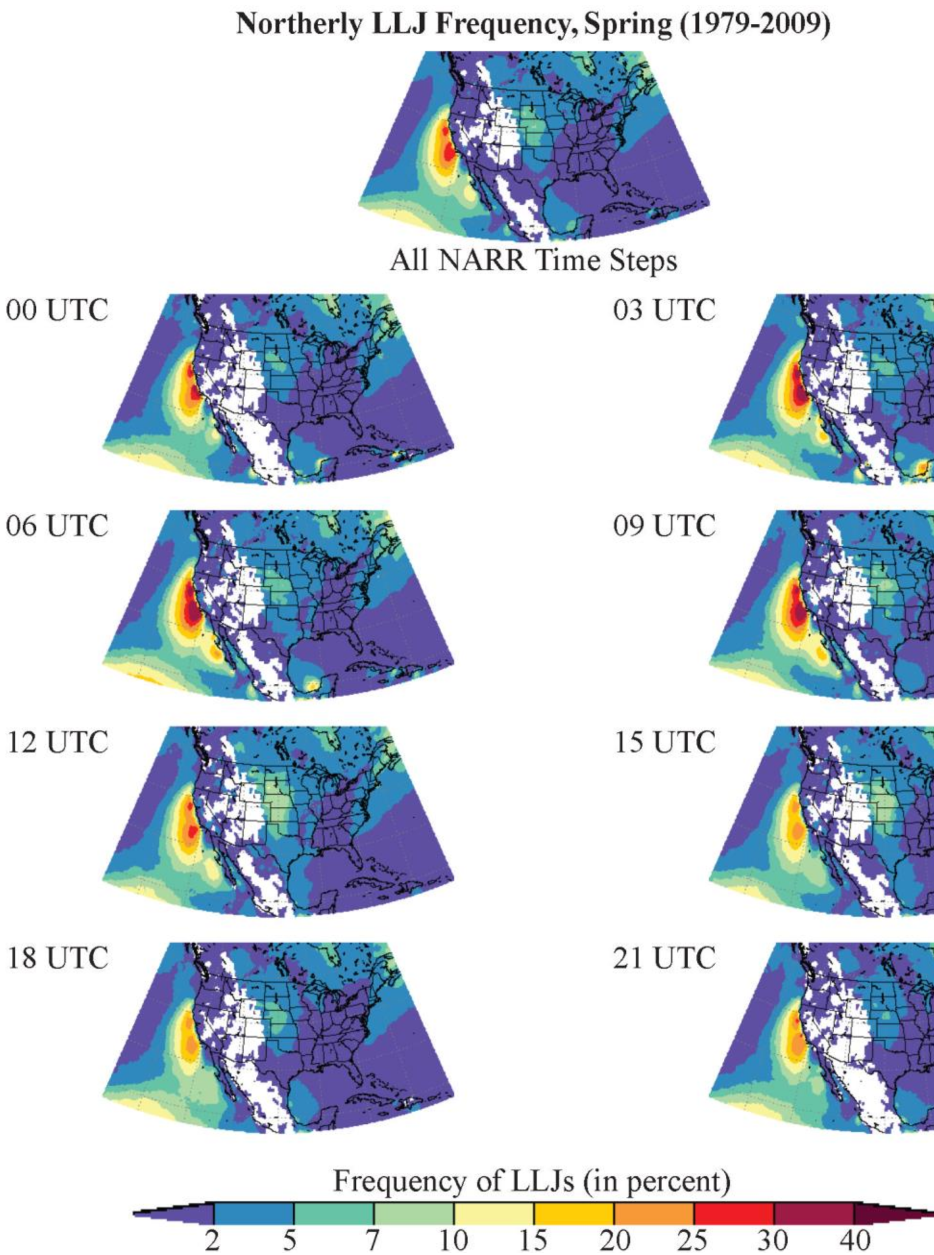

Figure 63. Spring frequency of N-LLJs from 1979 to 2009 expressed as a percentage of the total number of time steps, summed over all NARR time steps (top figure) and individually for each time step (bottom figures). Gridpoints with no jet cases and/or surface elevations >2km MSL are shown in white.

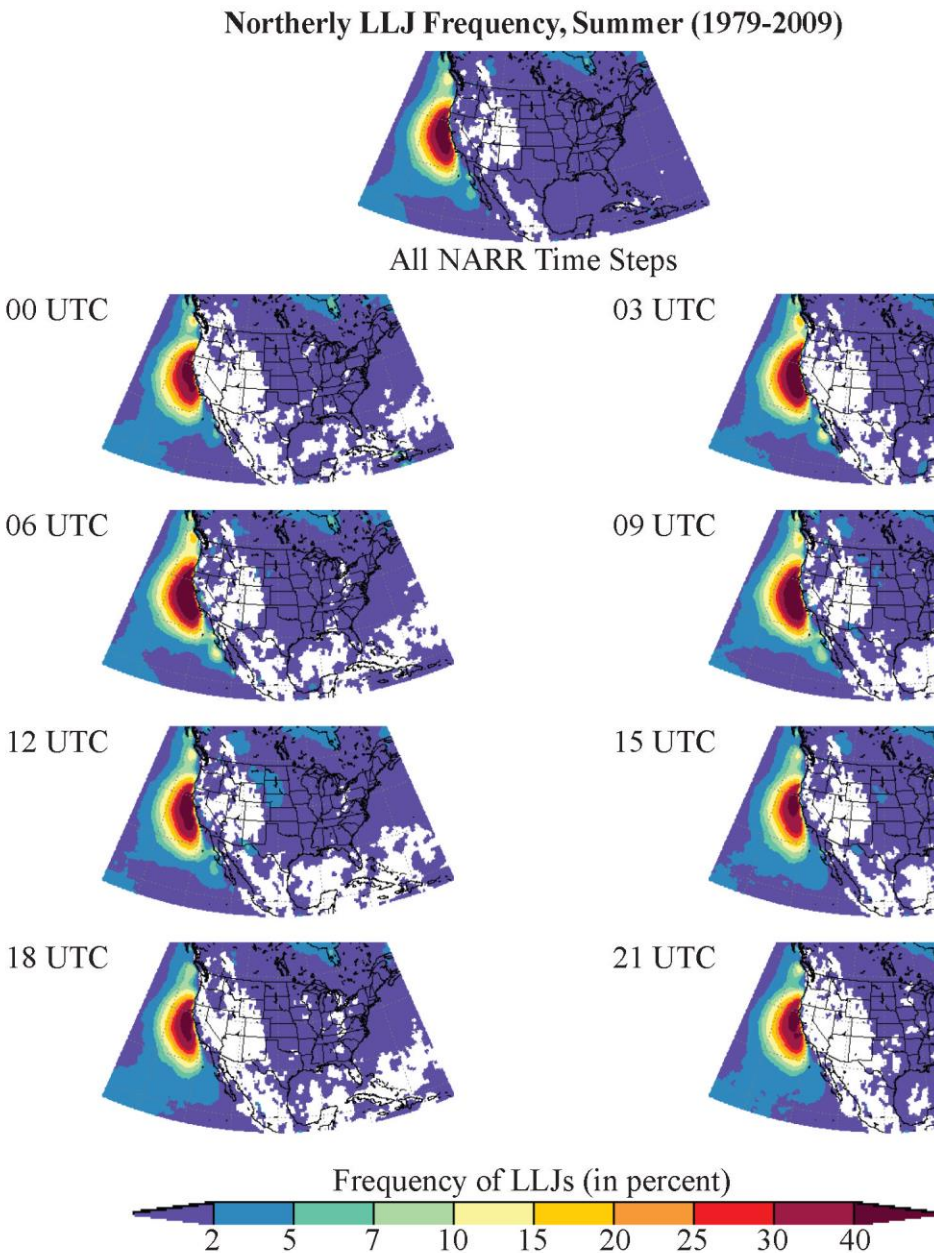

Figure 64. Summer frequency of N-LLJs from 1979 to 2009 expressed as a percentage of the total number of time steps, summed over all NARR time steps (top figure) and individually for each time step (bottom figures). Gridpoints with no jet cases and/or surface elevations >2km MSL are shown in white.

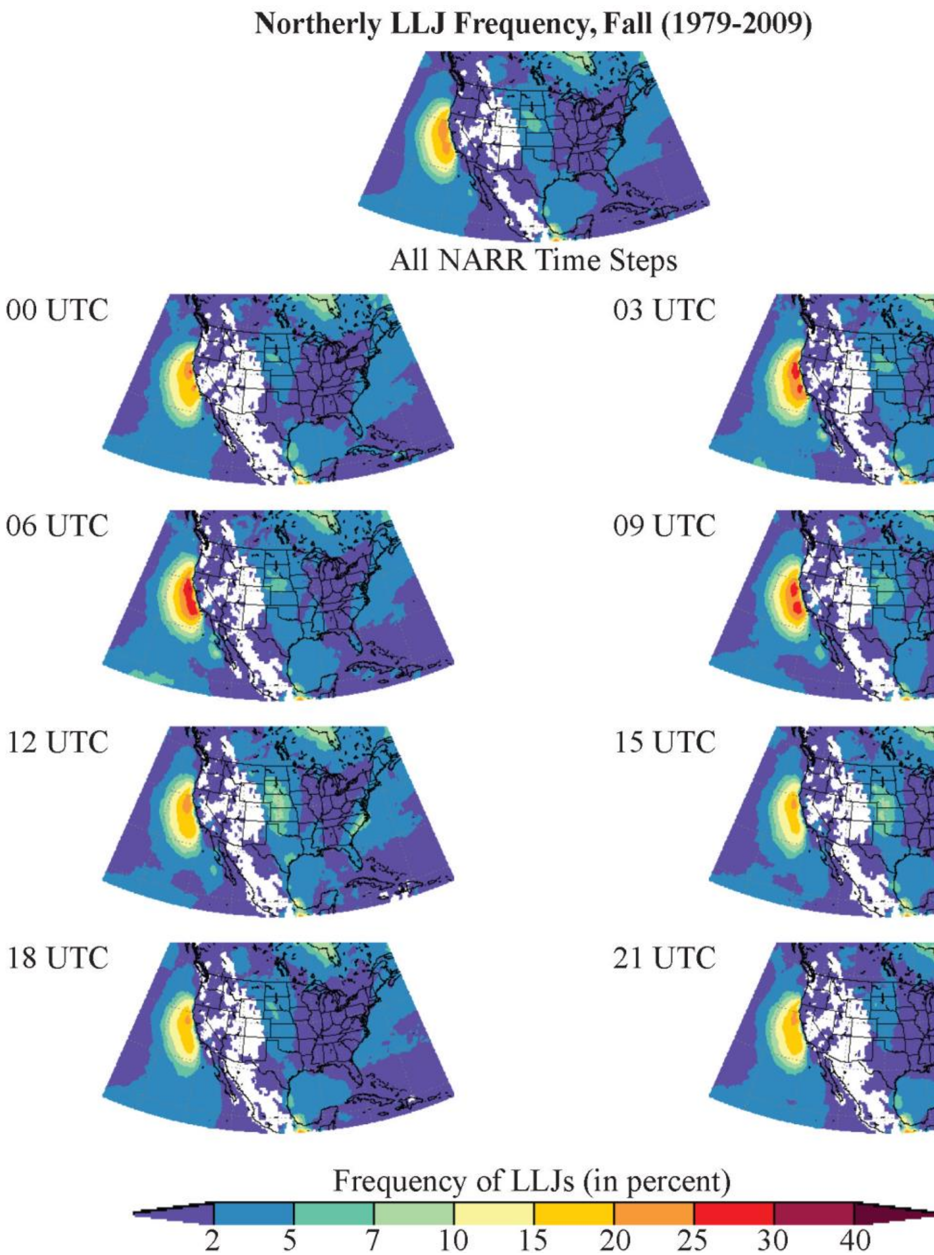

Figure 65. Fall frequency of N-LLJs from 1979 to 2009 expressed as a percentage of the total number of time steps, summed over all NARR time steps (top figure) and individually for each time step (bottom figures). Gridpoints with no jet cases and/or surface elevations >2km MSL are shown in white.

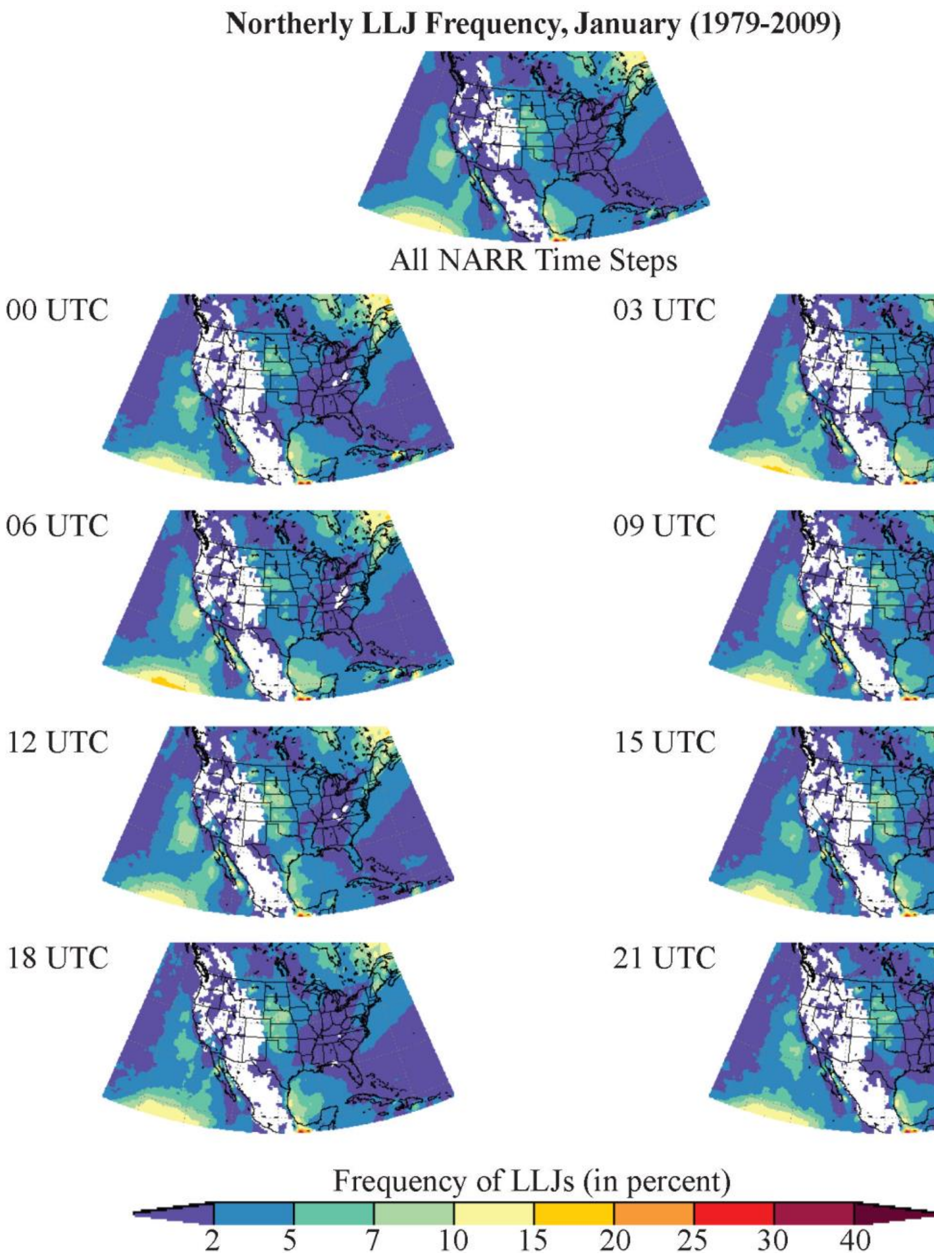

Figure 66. January frequency of N-LLJs from 1979 to 2009 expressed as a percentage of the total number of time steps, summed over all NARR time steps (top figure) and individually for each time step (bottom figures). Gridpoints with no jet cases and/or surface elevations >2km MSL are shown in white.

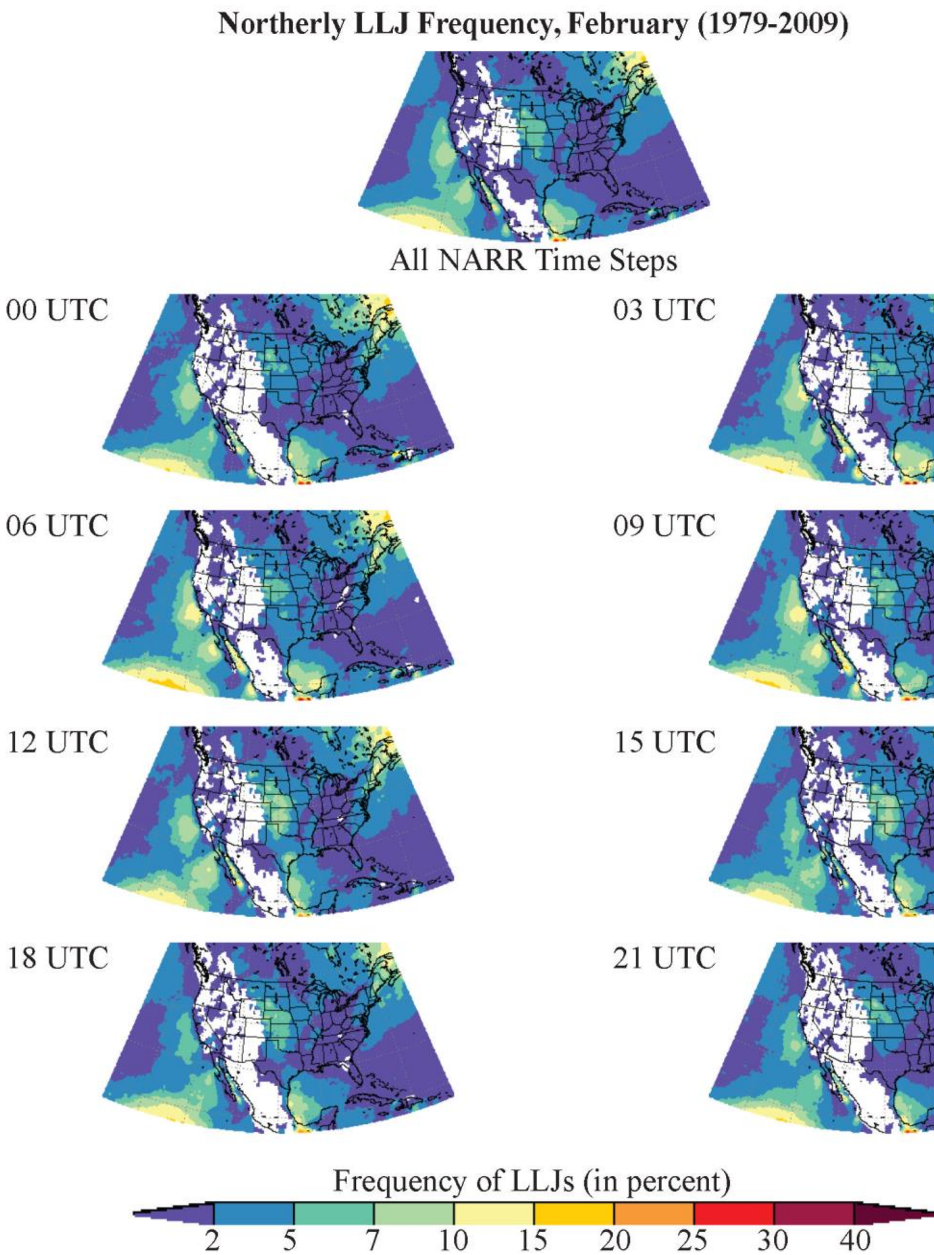

Figure 67. February frequency of N-LLJs from 1979 to 2009 expressed as a percentage of the total number of time steps, summed over all NARR time steps (top figure) and individually for each time step (bottom figures). Gridpoints with no jet cases and/or surface elevations >2km MSL are shown in white.

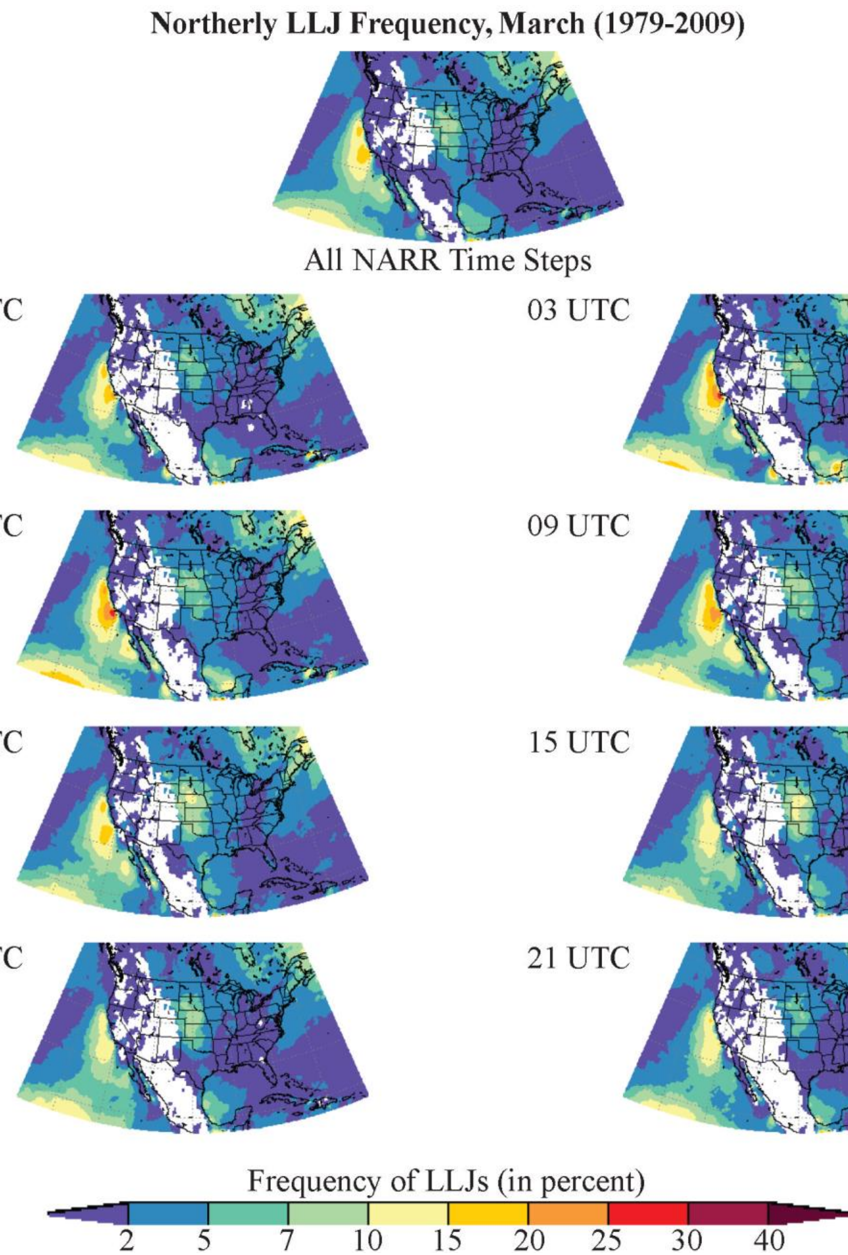

Figure 68. March frequency of N-LLJs from 1979 to 2009 expressed as a percentage of the total number of time steps, summed over all NARR time steps (top figure) and individually for each time step (bottom figures). Gridpoints with no jet cases and/or surface elevations >2km MSL are shown in white.

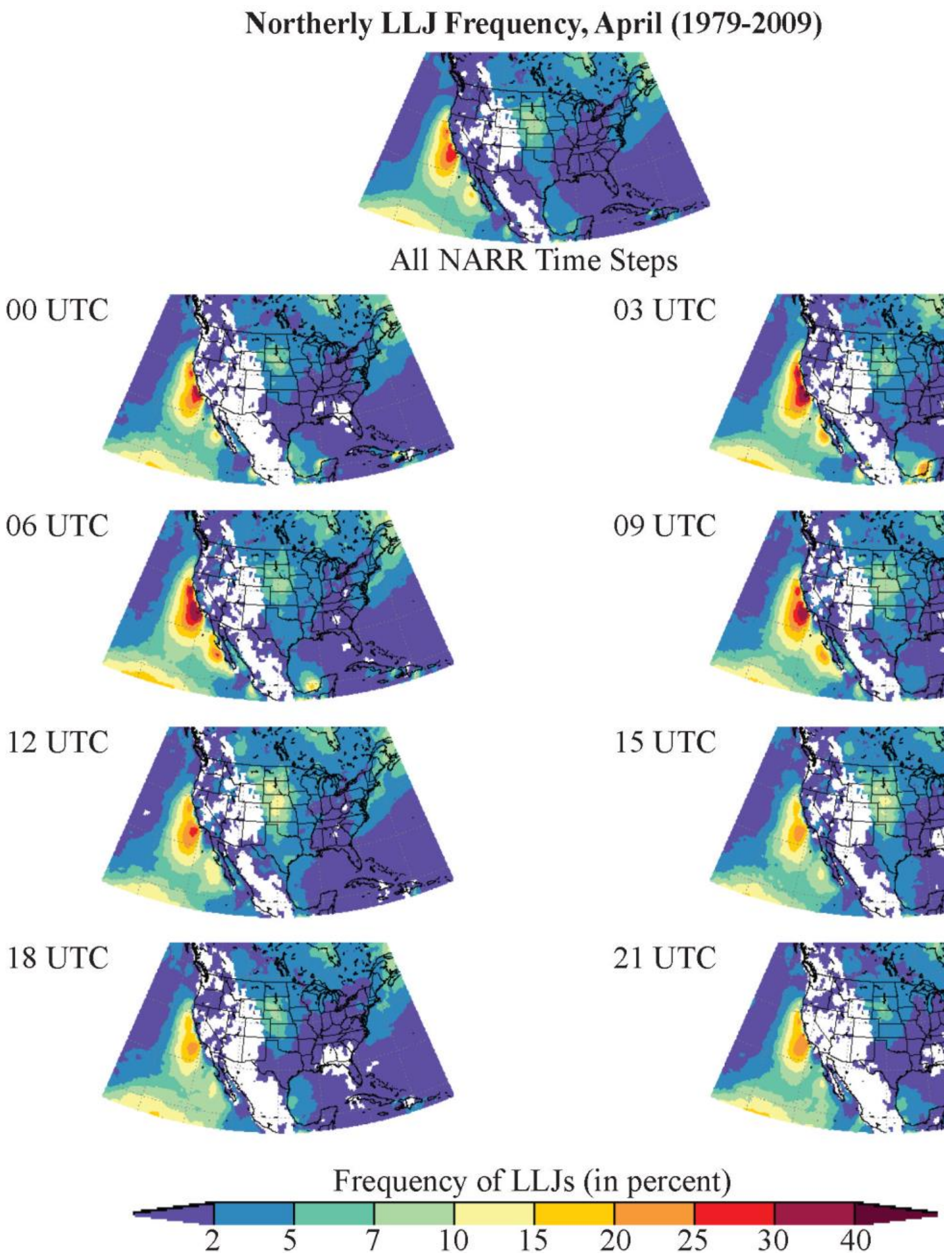

Figure 69. April frequency of N-LLJs from 1979 to 2009 expressed as a percentage of the total number of time steps, summed over all NARR time steps (top figure) and individually for each time step (bottom figures). Gridpoints with no jet cases and/or surface elevations >2km MSL are shown in white.

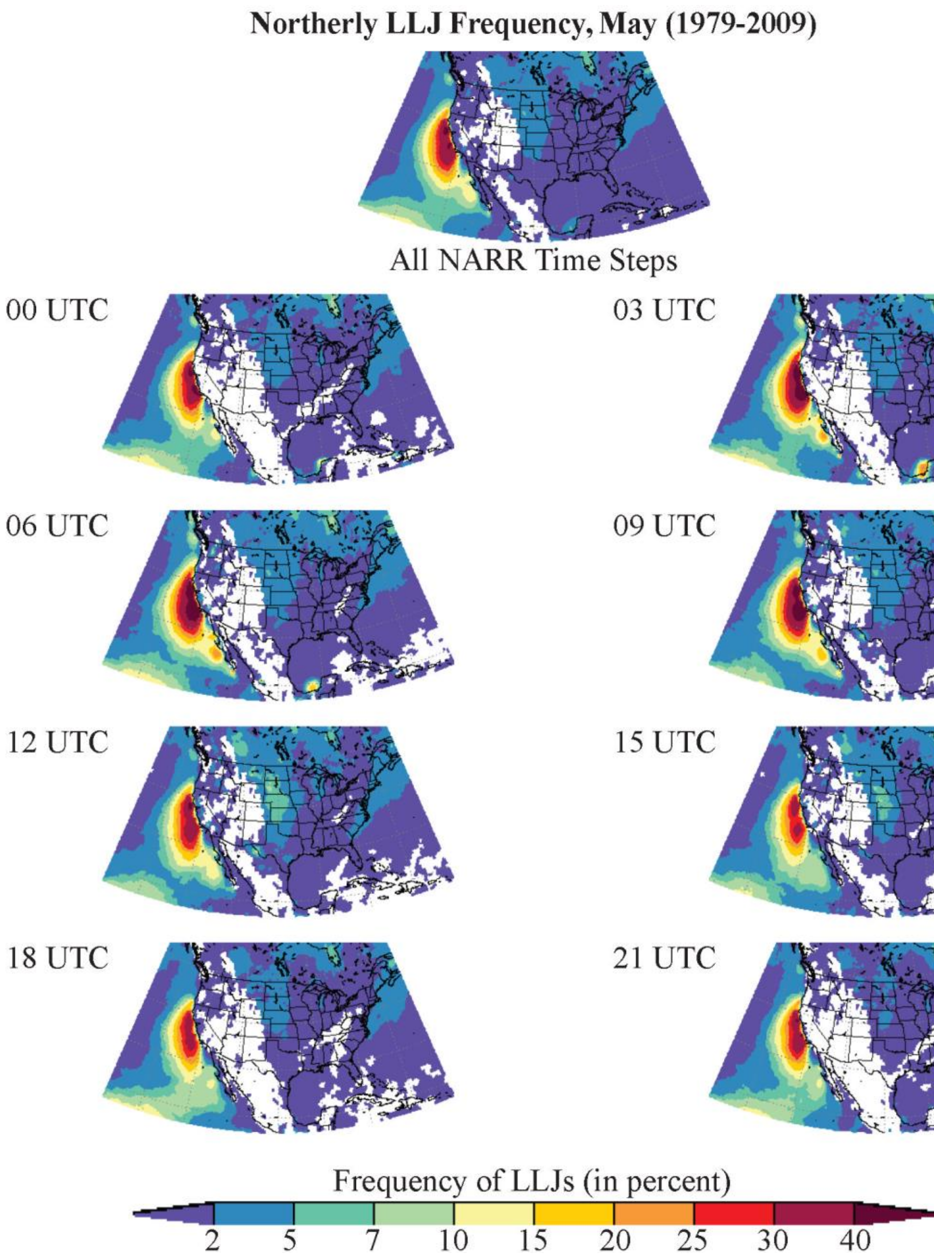

Figure 70. May frequency of N-LLJs from 1979 to 2009 expressed as a percentage of the total number of time steps, summed over all NARR time steps (top figure) and individually for each time step (bottom figures). Gridpoints with no jet cases and/or surface elevations >2km MSL are shown in white.

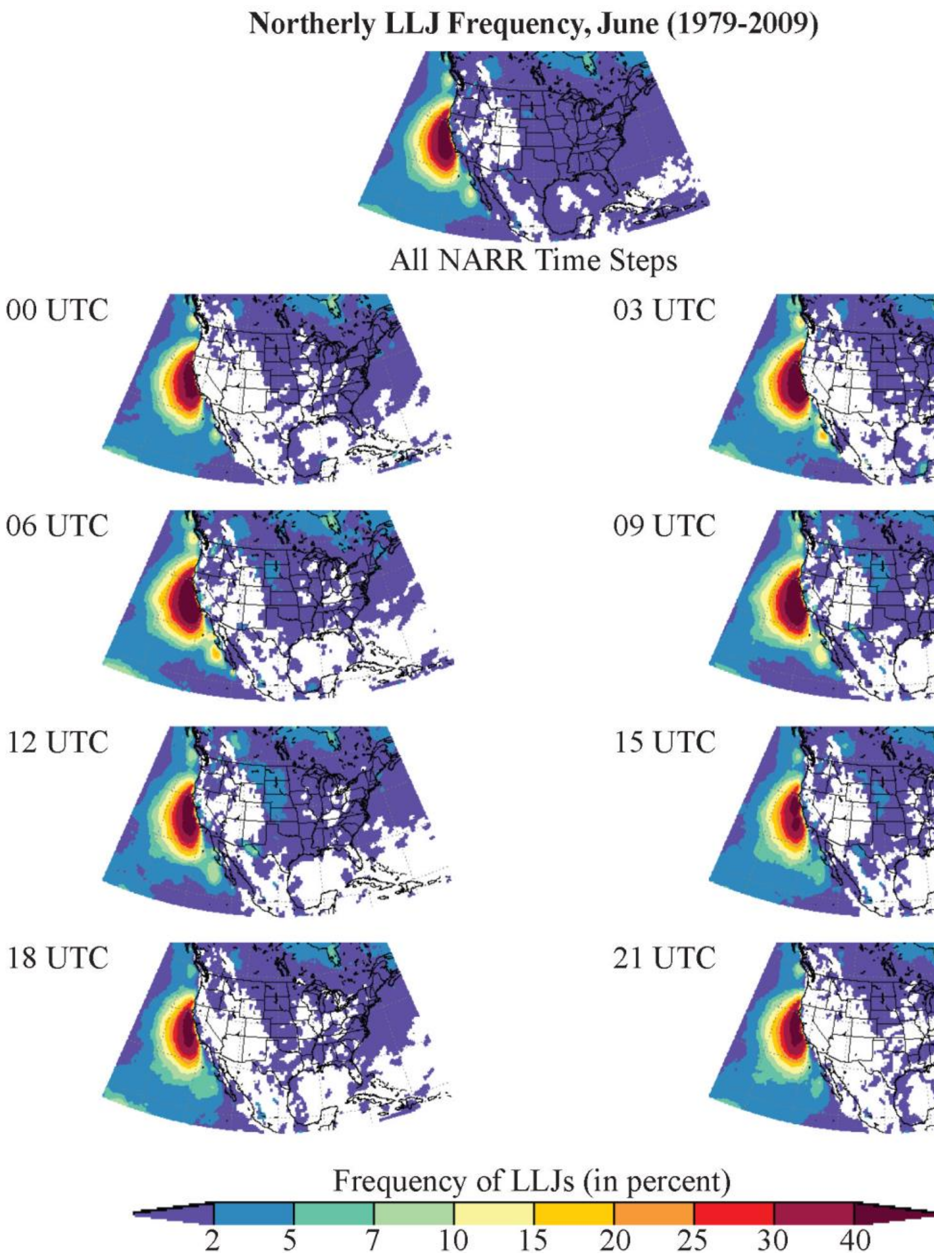

Figure 71. June frequency of N-LLJs from 1979 to 2009 expressed as a percentage of the total number of time steps, summed over all NARR time steps (top figure) and individually for each time step (bottom figures). Gridpoints with no jet cases and/or surface elevations >2km MSL are shown in white.

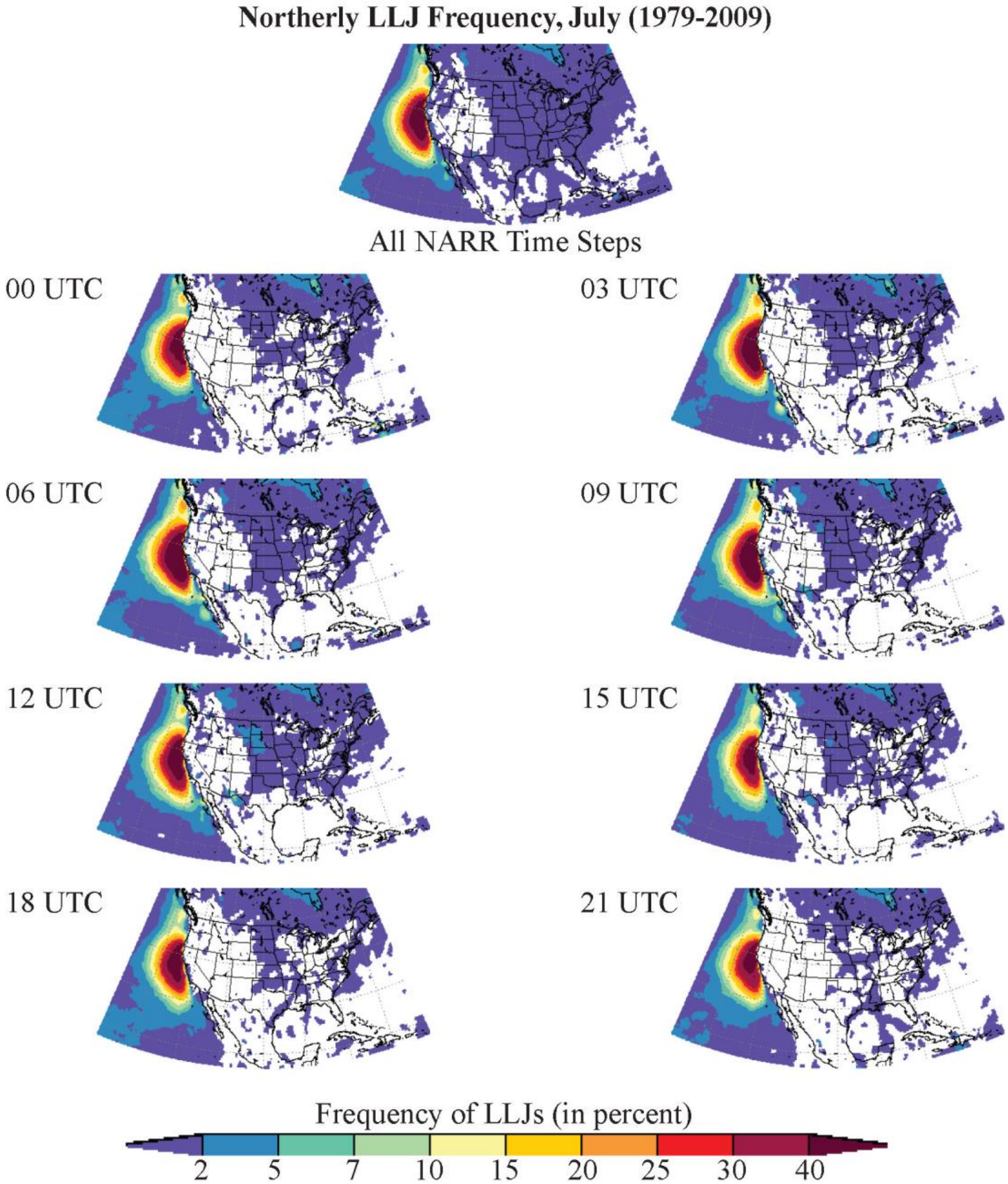

Figure 72. July frequency of N-LLJs from 1979 to 2009 expressed as a percentage of the total number of time steps, summed over all NARR time steps (top figure) and individually for each time step (bottom figures). Gridpoints with no jet cases and/or surface elevations >2km MSL are shown in white.

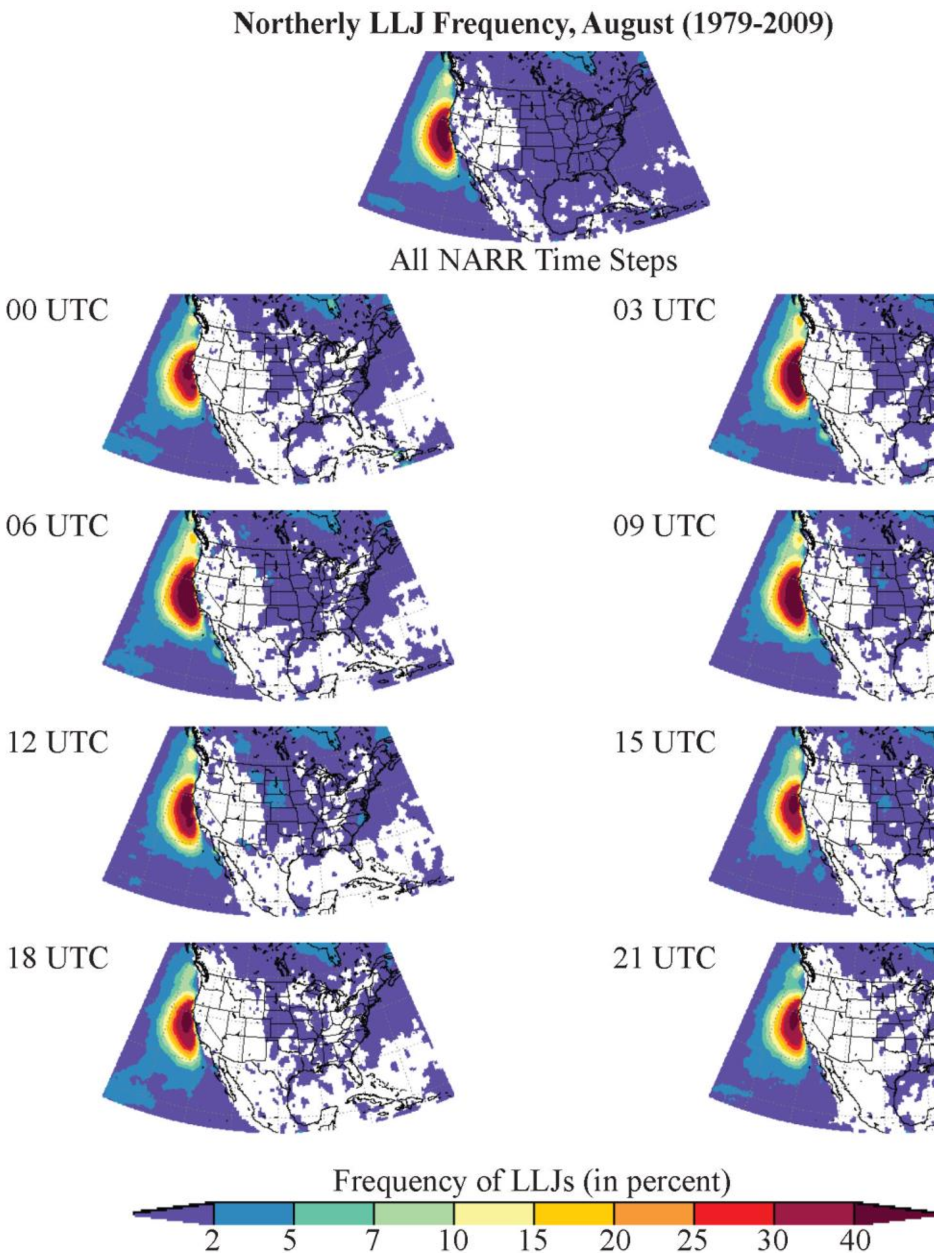

Figure 73. August frequency of N-LLJs from 1979 to 2009 expressed as a percentage of the total number of time steps, summed over all NARR time steps (top figure) and individually for each time step (bottom figures). Gridpoints with no jet cases and/or surface elevations >2km MSL are shown in white.

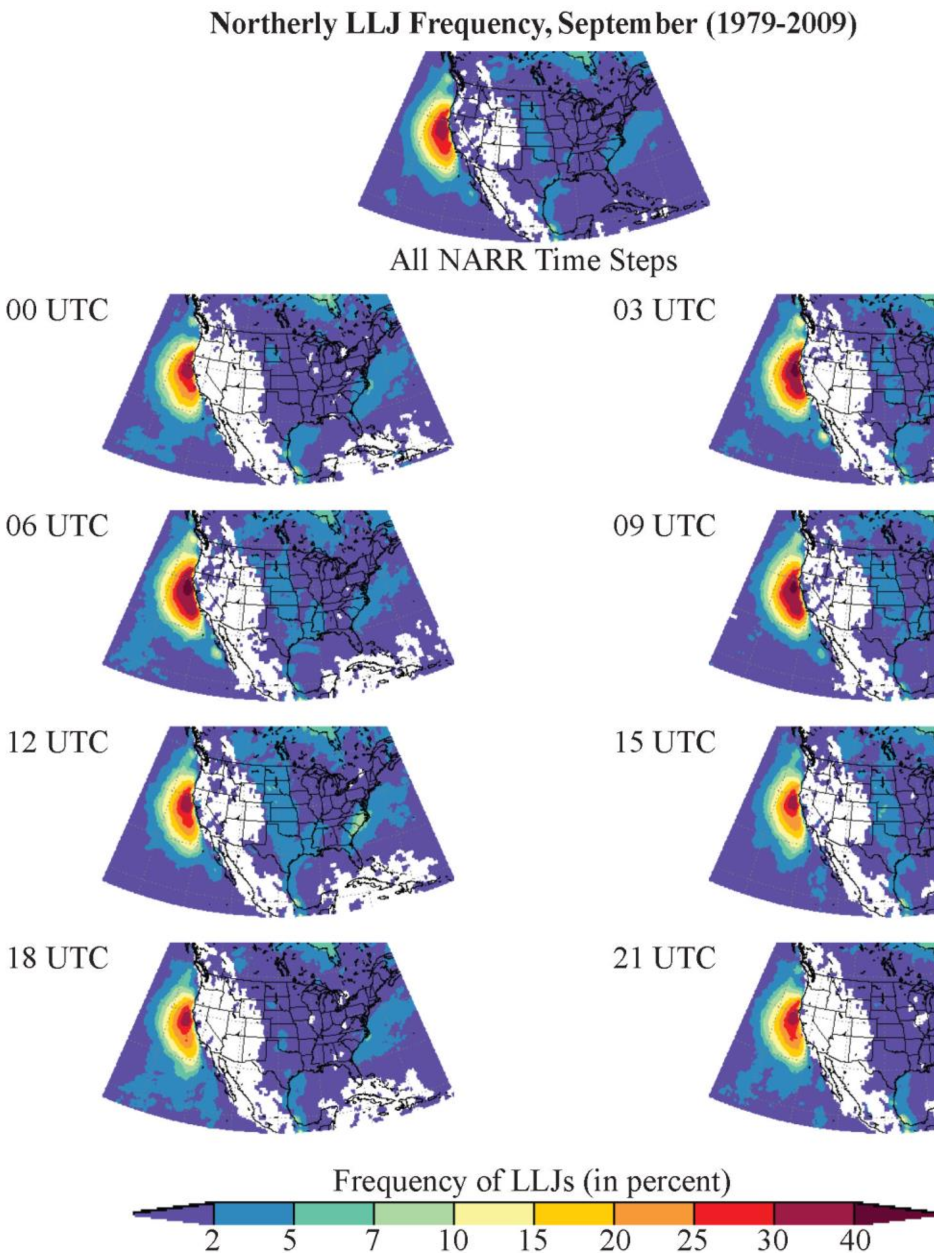

Figure 74. September frequency of N-LLJs from 1979 to 2009 expressed as a percentage of the total number of time steps, summed over all NARR time steps (top figure) and individually for each time step (bottom figures). Gridpoints with no jet cases and/or surface elevations >2km MSL are shown in white.

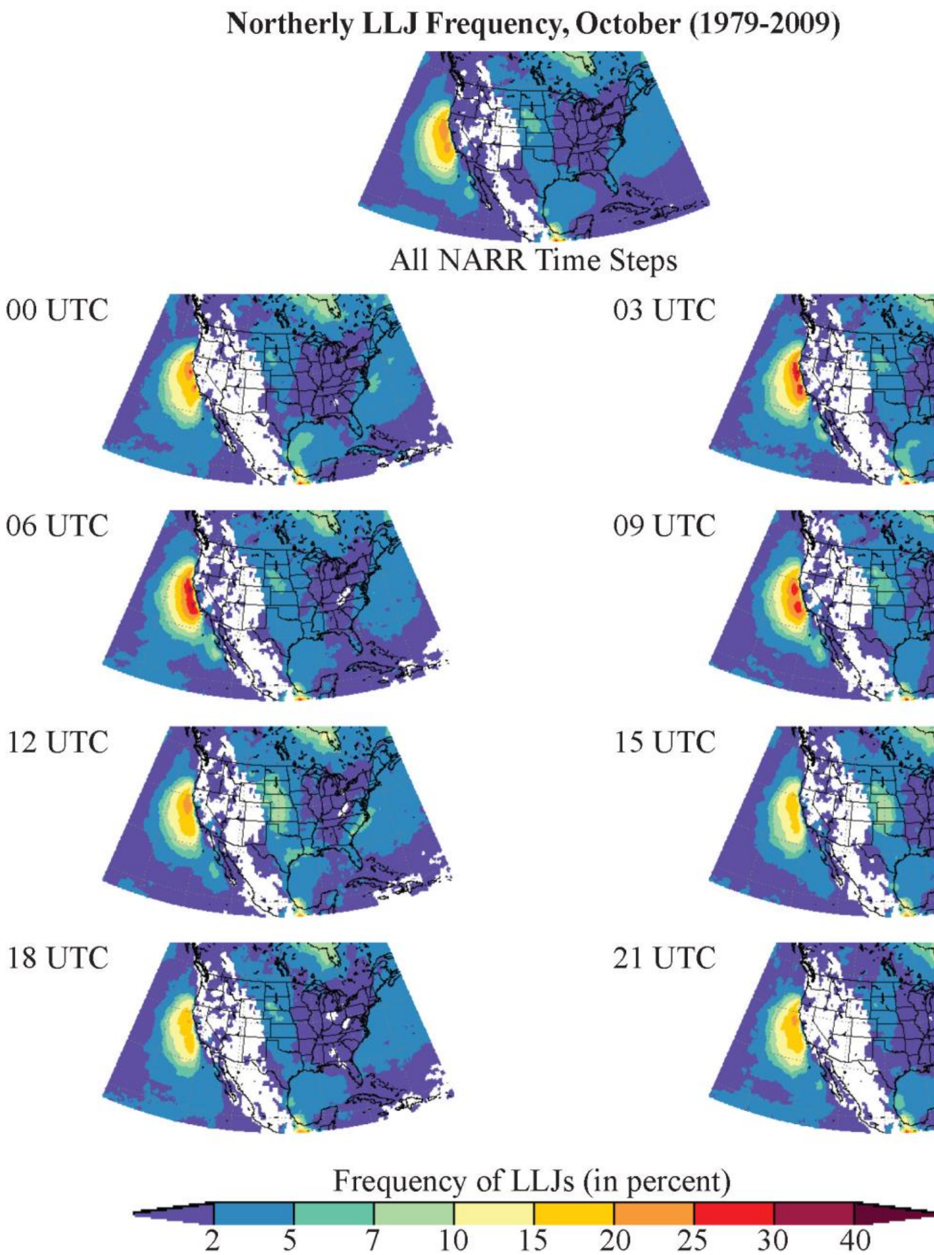

Figure 75. October frequency of N-LLJs from 1979 to 2009 expressed as a percentage of the total number of time steps, summed over all NARR time steps (top figure) and individually for each time step (bottom figures). Gridpoints with no jet cases and/or surface elevations >2km MSL are shown in white.

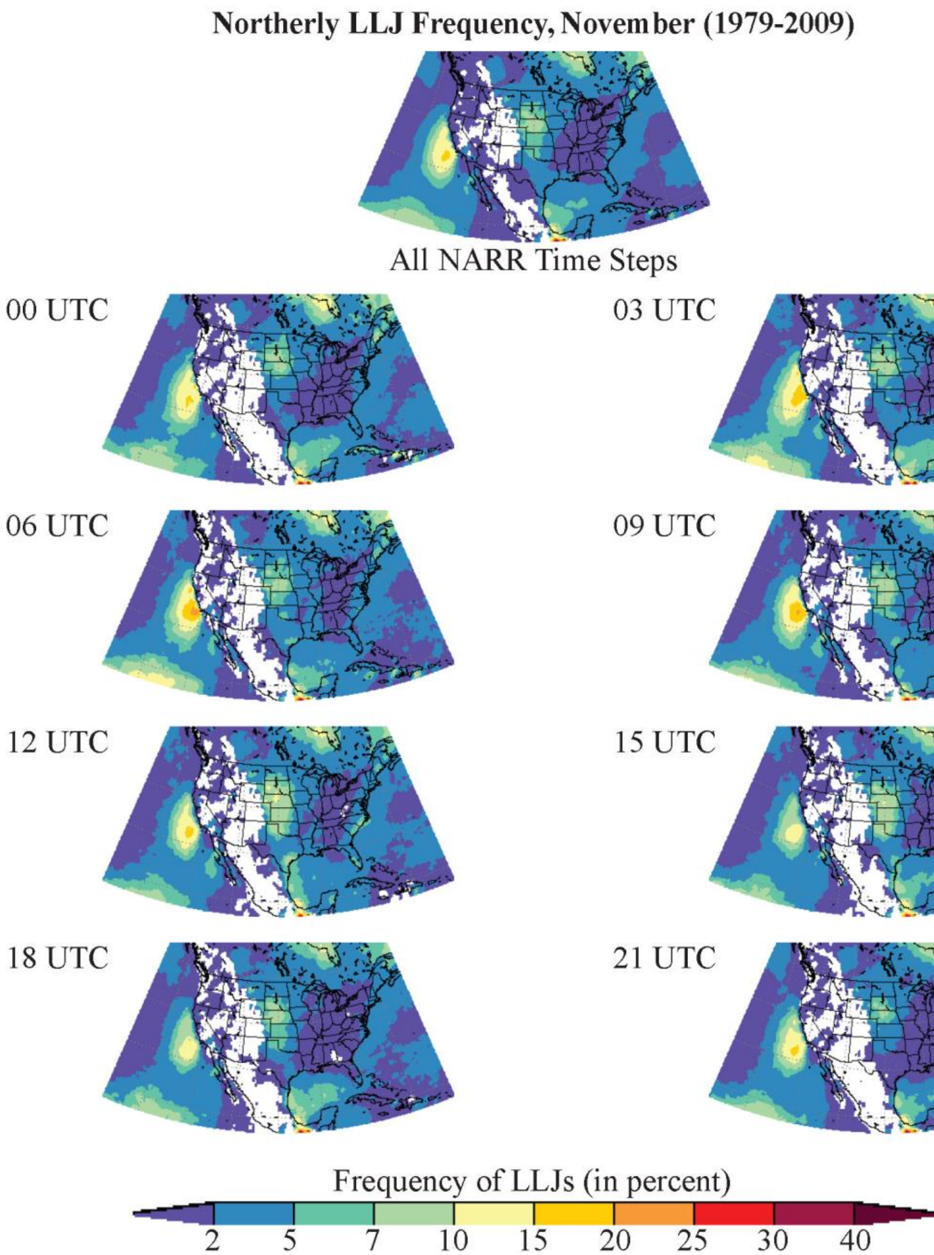

Figure 76. November frequency of N-LLJs from 1979 to 2009 expressed as a percentage of the total number of time steps, summed over all NARR time steps (top figure) and individually for each time step (bottom figures). Gridpoints with no jet cases and/or surface elevations >2km MSL are shown in white.

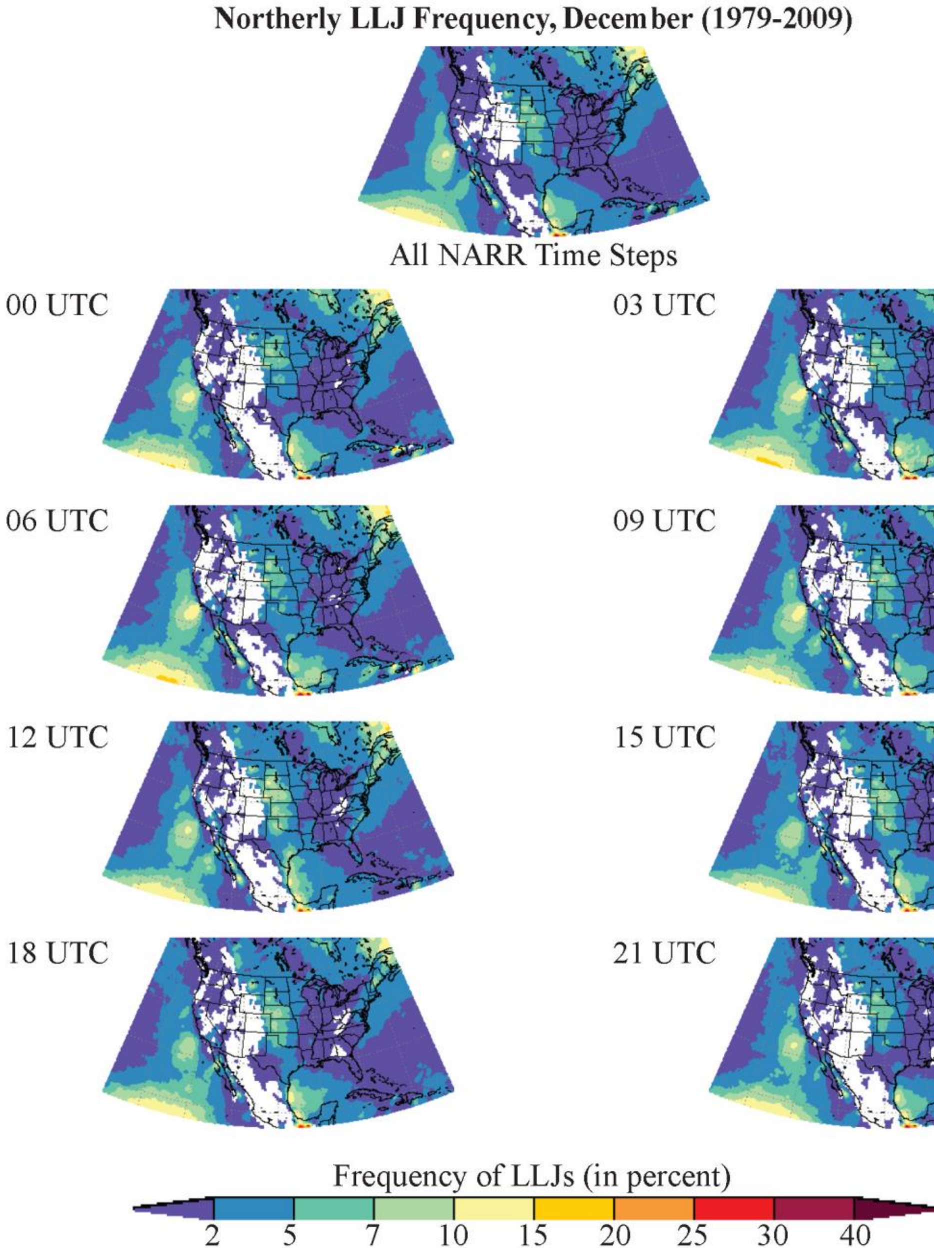

Figure 77. December frequency of N-LLJs from 1979 to 2009 expressed as a percentage of the total number of time steps, summed over all NARR time steps (top figure) and individually for each time step (bottom figures). Gridpoints with no jet cases and/or surface elevations >2km MSL are shown in white.

APPENDIX C

Average Speed of Southerly Low-Level Jets

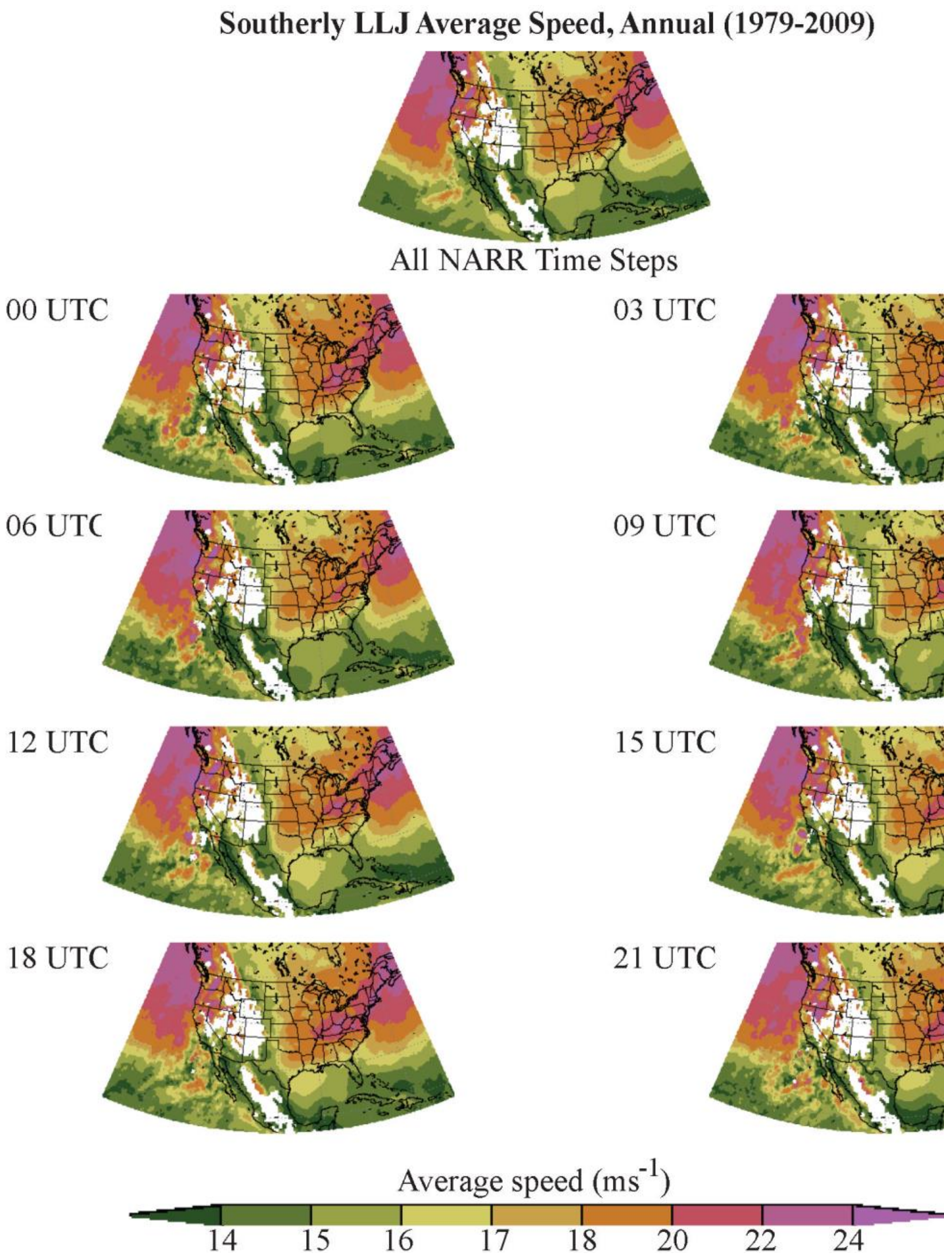

Figure 78. Annual average speed (meters per second) of S-LLJs from 1979 to 2009. Includes annual average speed across all NARR time steps and annual average speed at each individual NARR time step. Gridpoints with no jet cases and/or surface elevations >2km MSL are shown in white.

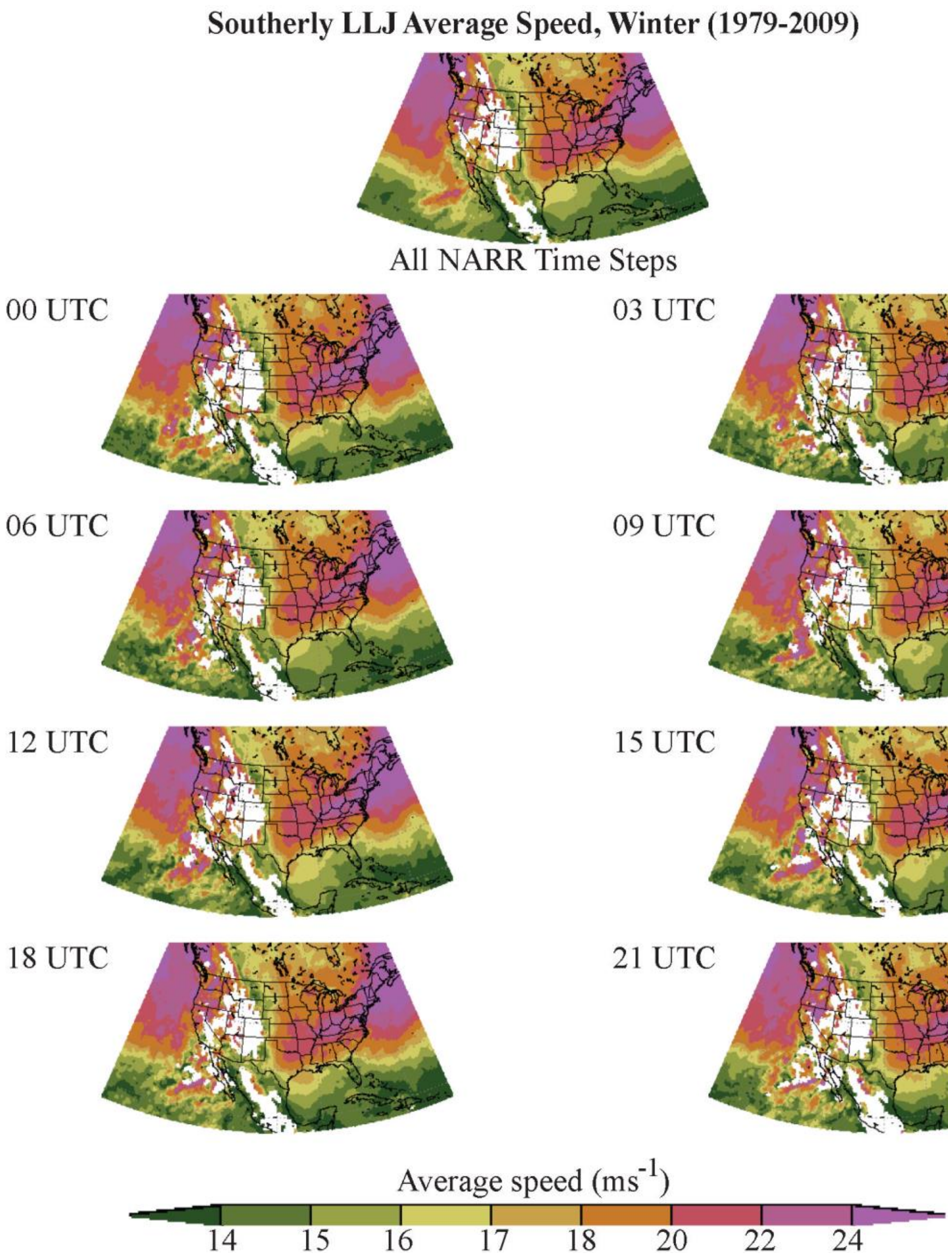

Figure 79. Average speed (meters per second) for S-LLJs that occurred during winter from 1979-2009, for all jets (top figure) and for jets at each of the NARR time steps (bottom figures). Gridpoints with no jet cases and/or surface elevations >2km MSL are shown in white.

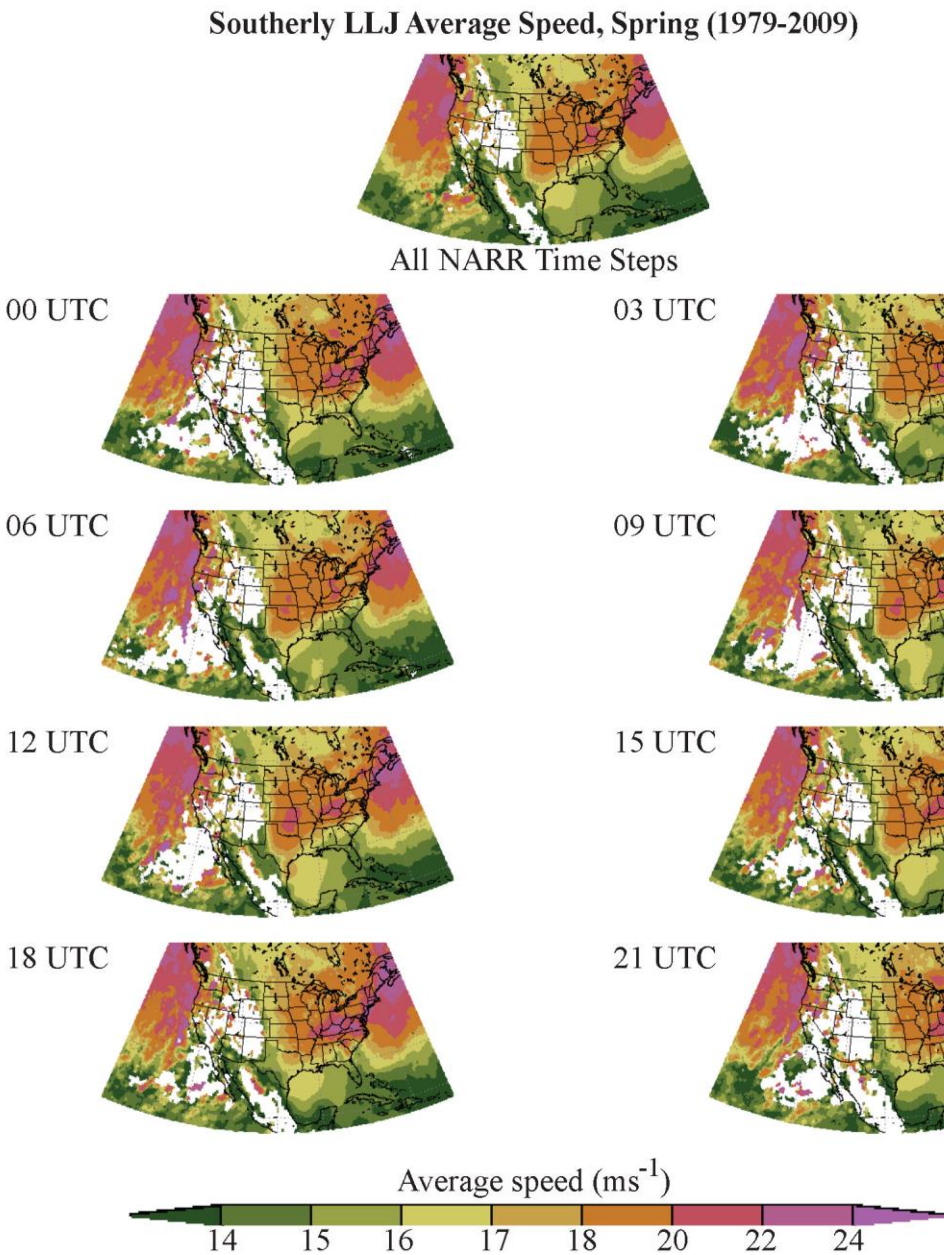

Figure 80. Average speed (meters per second) for S-LLJs that occurred during spring from 1979-2009, for all jets (top figure) and for jets at each of the NARR time steps (bottom figures). Gridpoints with no jet cases and/or surface elevations >2km MSL are shown in white.

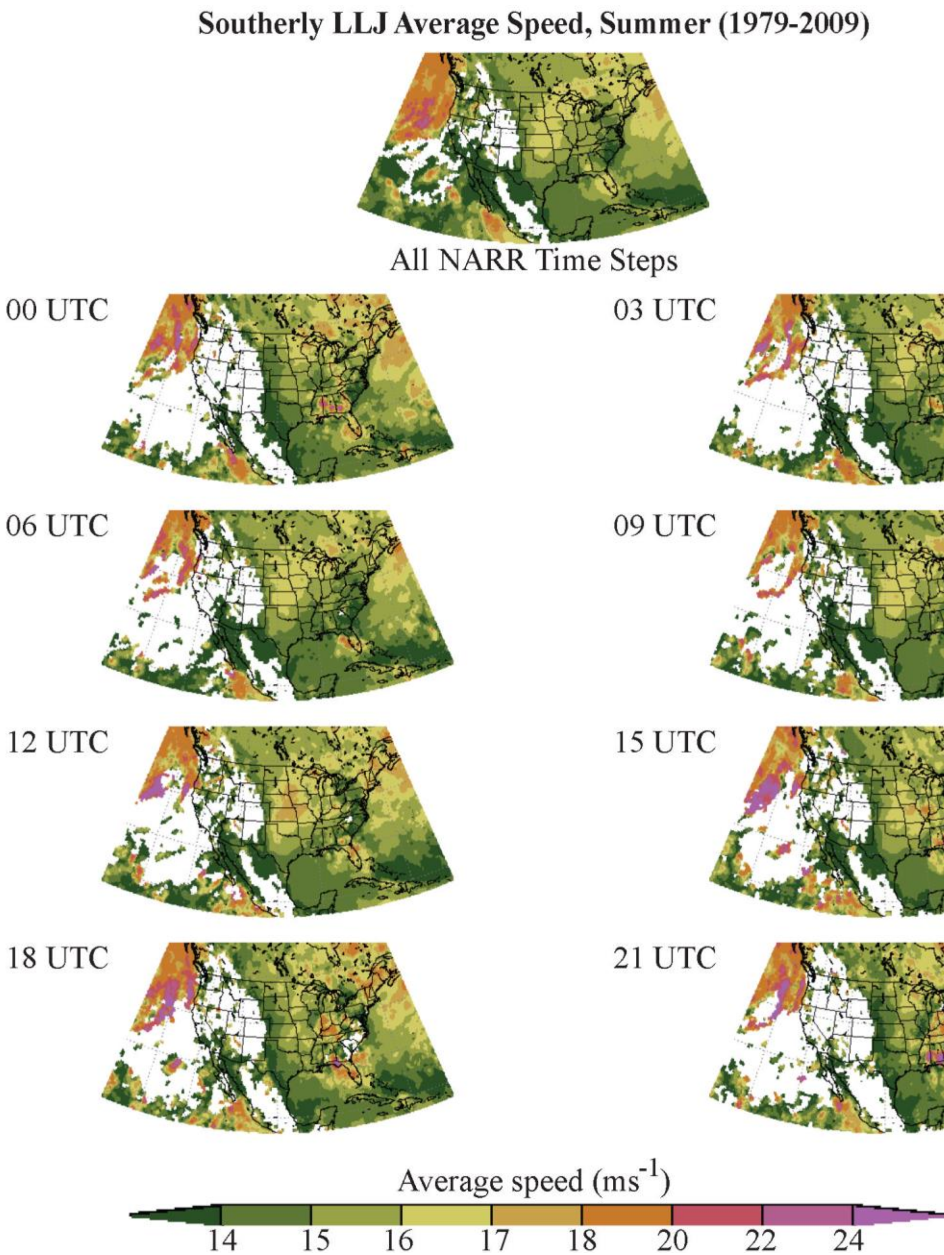

Figure 81. Average speed (meters per second) for S-LLJs that occurred during summer from 1979-2009, for all jets (top figure) and for jets at each of the NARR time steps (bottom figures). Gridpoints with no jet cases and/or surface elevations >2km MSL are shown in white.

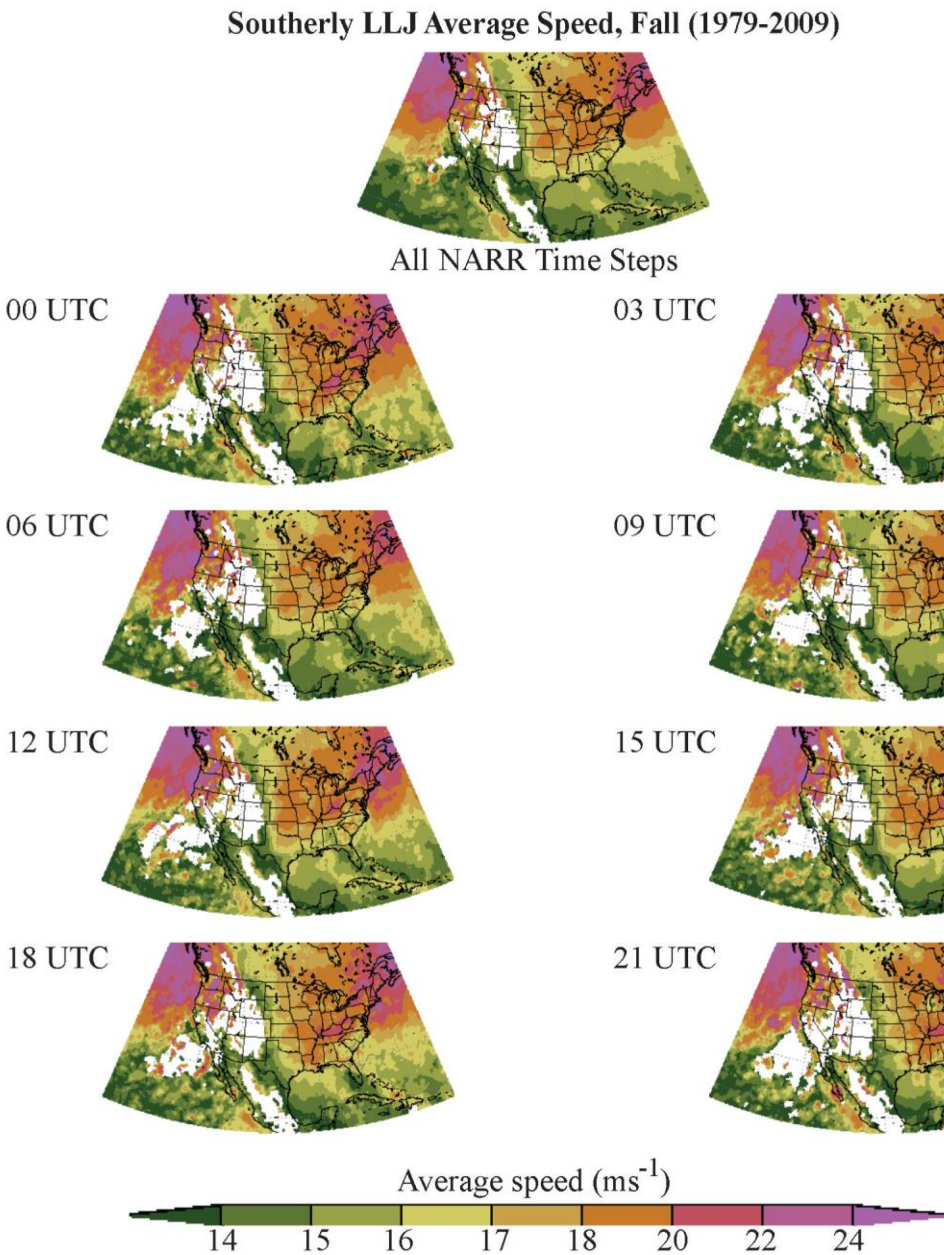

Figure 82. Average speed (meters per second) for S-LLJs that occurred during fall from 1979-2009, for all jets (top figure) and for jets at each of the NARR time steps (bottom figures). Gridpoints with no jet cases and/or surface elevations >2km MSL are shown in white.

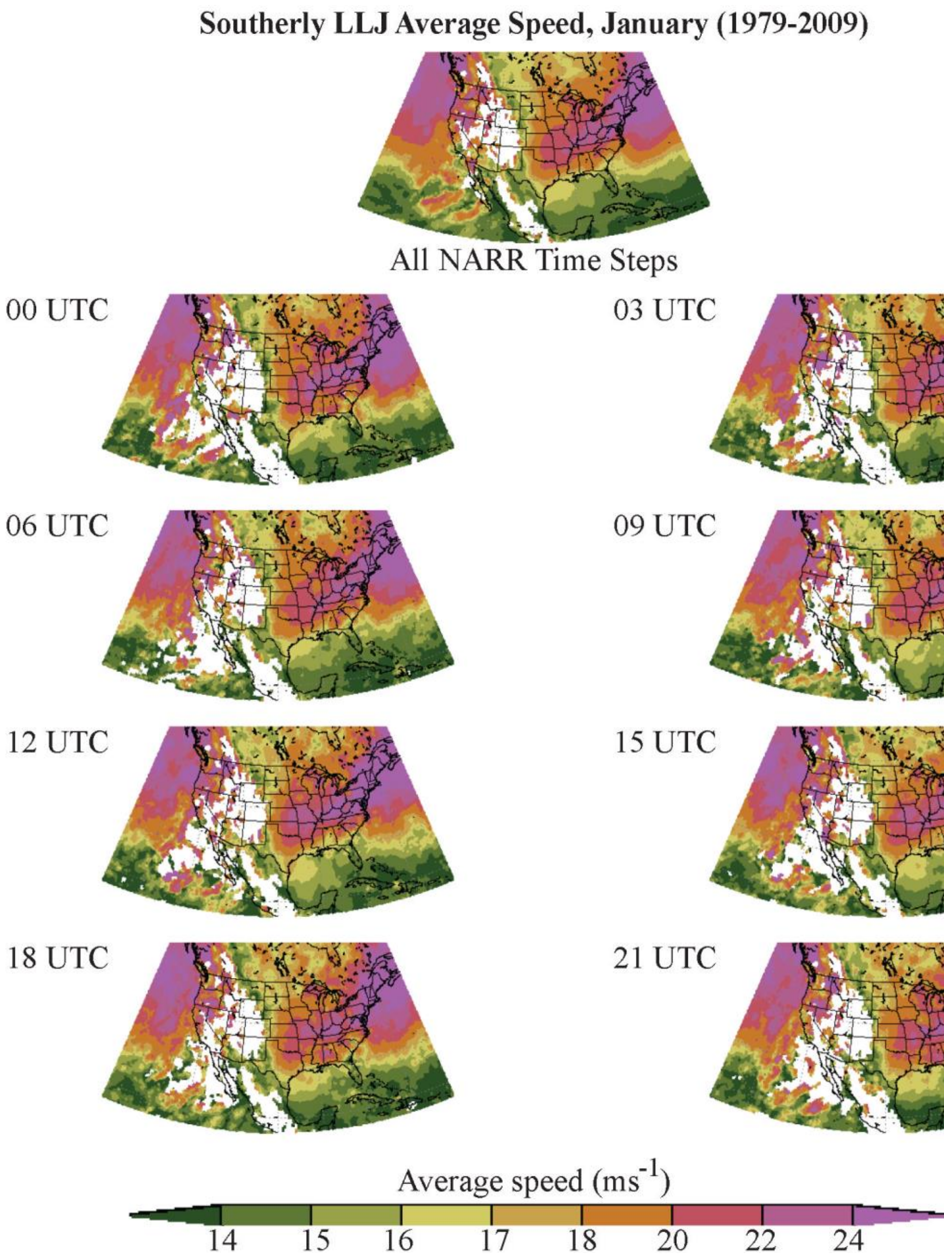

Figure 83. Average speed (meters per second) for S-LLJs that occurred during January from 1979-2009, for all jets (top figure) and for jets at each of the NARR time steps (bottom figures). Gridpoints with no jet cases and/or surface elevations >2km MSL are shown in white.

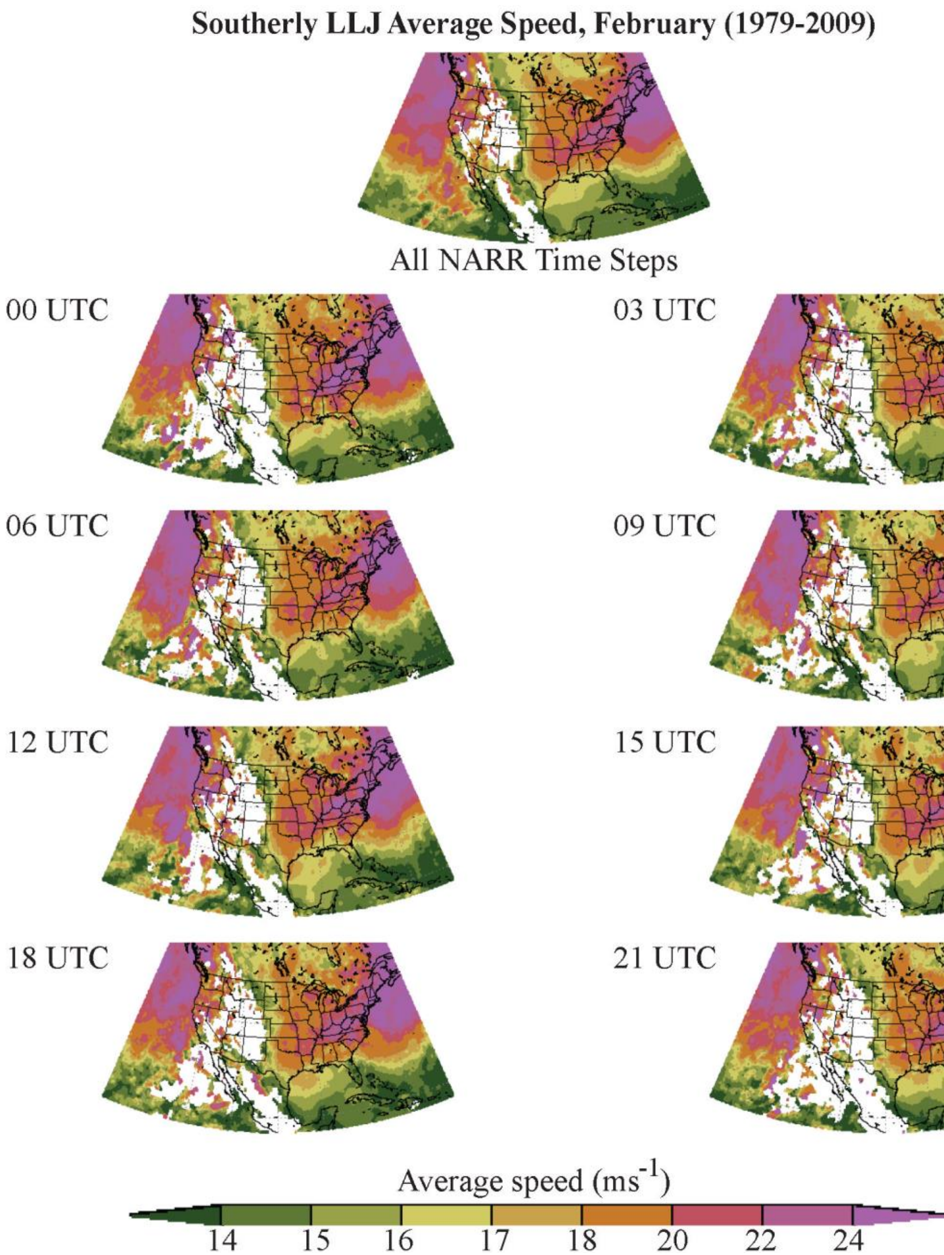

Figure 84. Average speed (meters per second) for S-LLJs that occurred during February from 1979-2009, for all jets (top figure) and for jets at each of the NARR time steps (bottom figures). Gridpoints with no jet cases and/or surface elevations >2km MSL are shown in white.

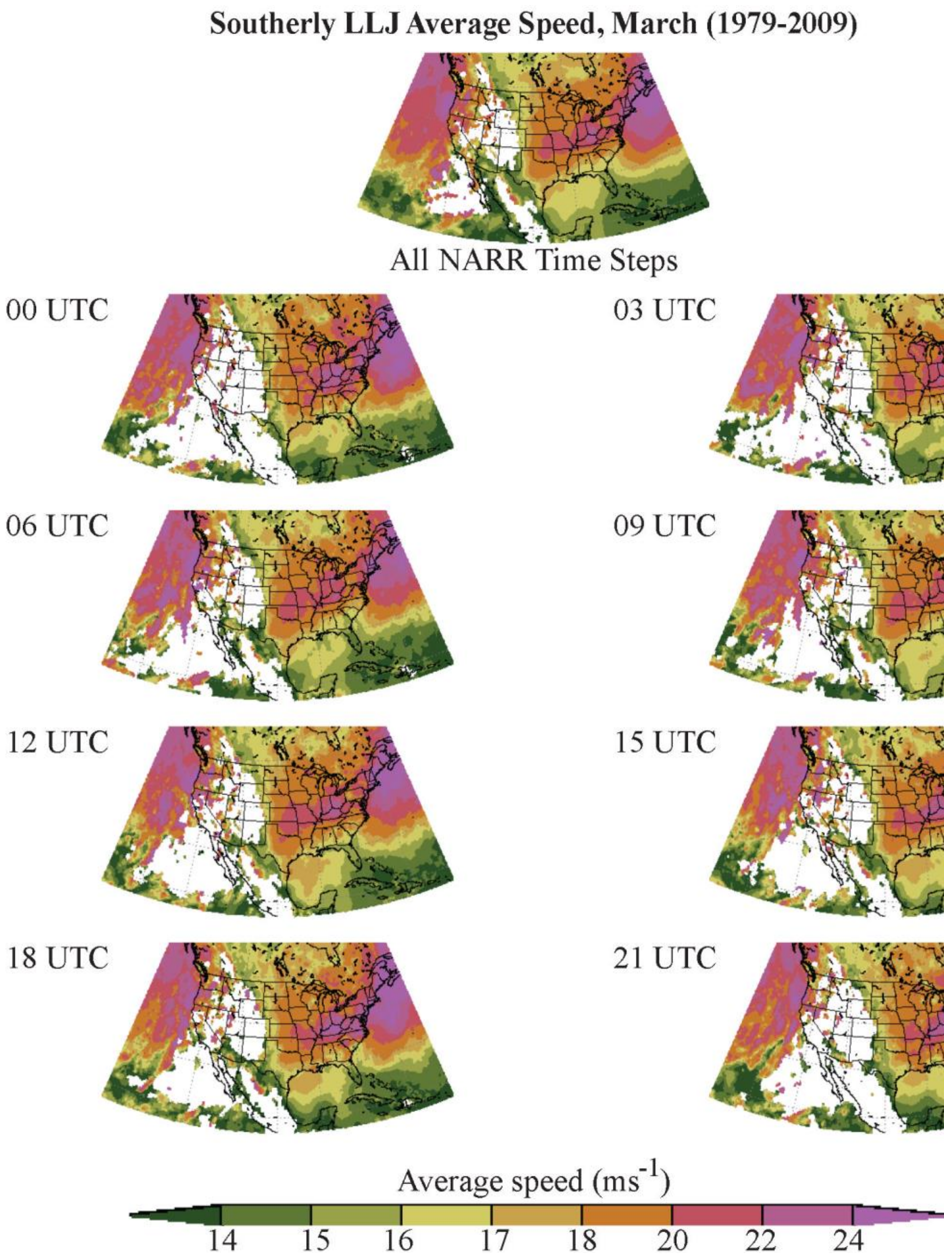

Figure 85. Average speed (meters per second) for S-LLJs that occurred during March from 1979-2009, for all jets (top figure) and for jets at each of the NARR time steps (bottom figures). Gridpoints with no jet cases and/or surface elevations >2km MSL are shown in white.

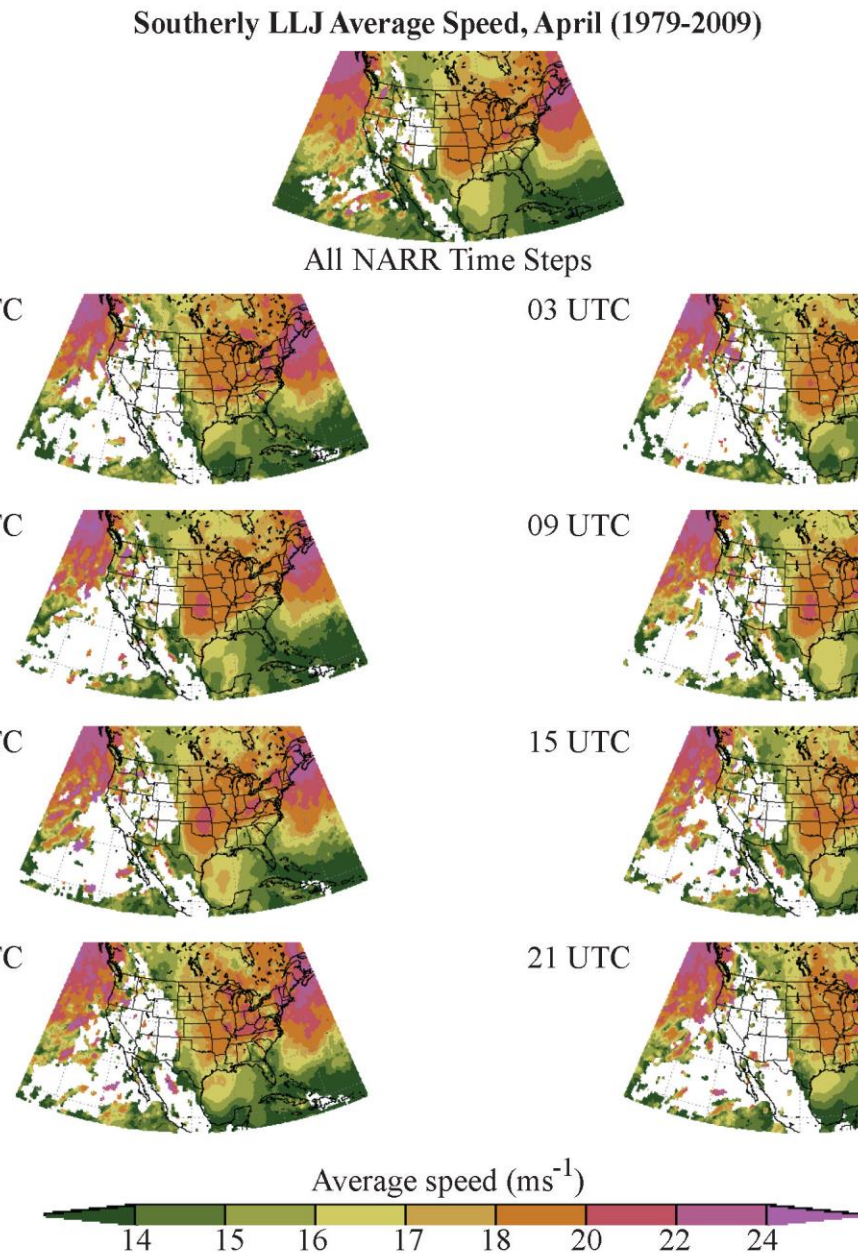

Figure 86. Average speed (meters per second) for S-LLJs that occurred during April from 1979-2009, for all jets (top figure) and for jets at each of the NARR time steps (bottom figures). Gridpoints with no jet cases and/or surface elevations >2km MSL are shown in white.

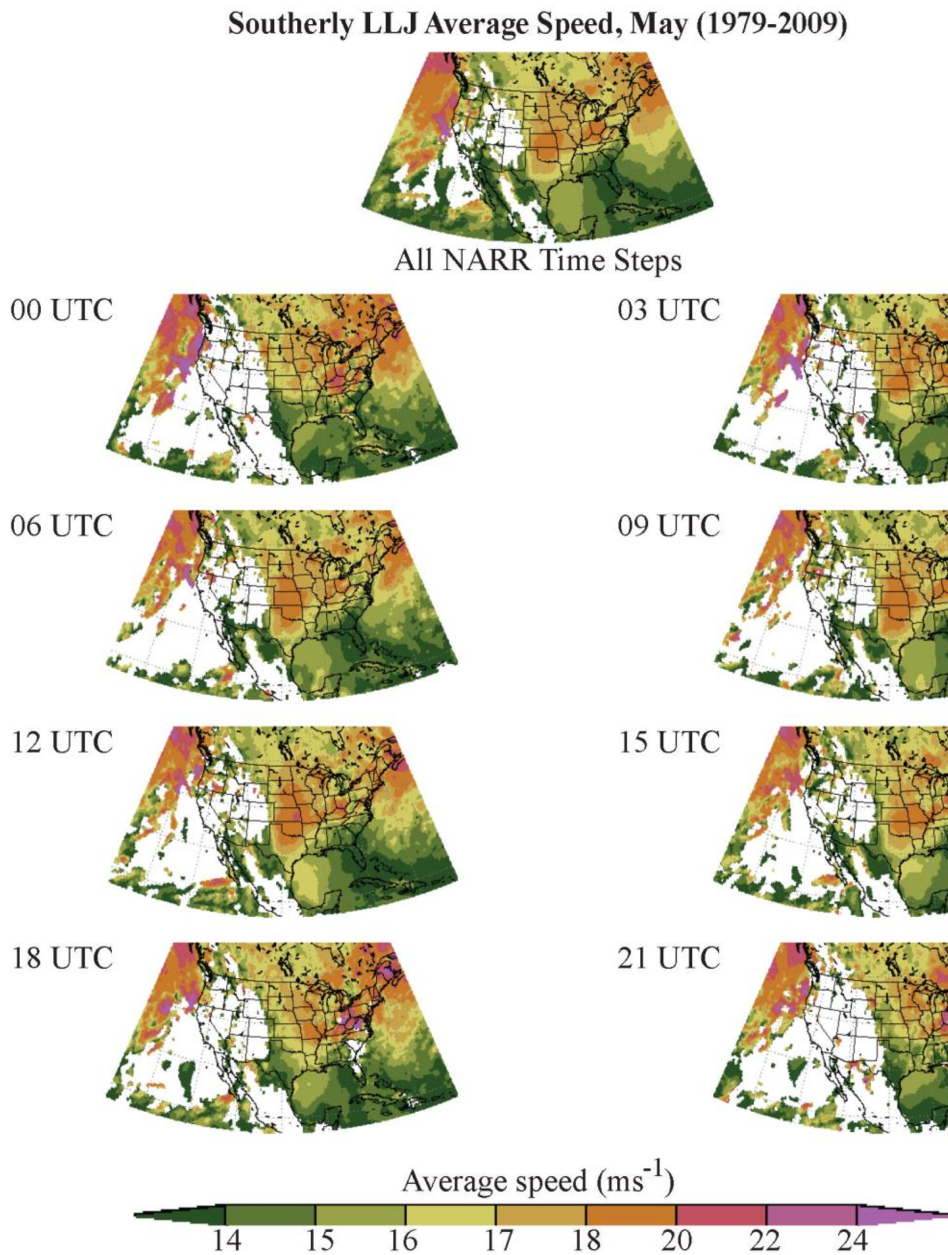

Figure 87. Average speed (meters per second) for S-LLJs that occurred during May from 1979-2009, for all jets (top figure) and for jets at each of the NARR time steps (bottom figures). Gridpoints with no jet cases and/or surface elevations >2km MSL are shown in white.

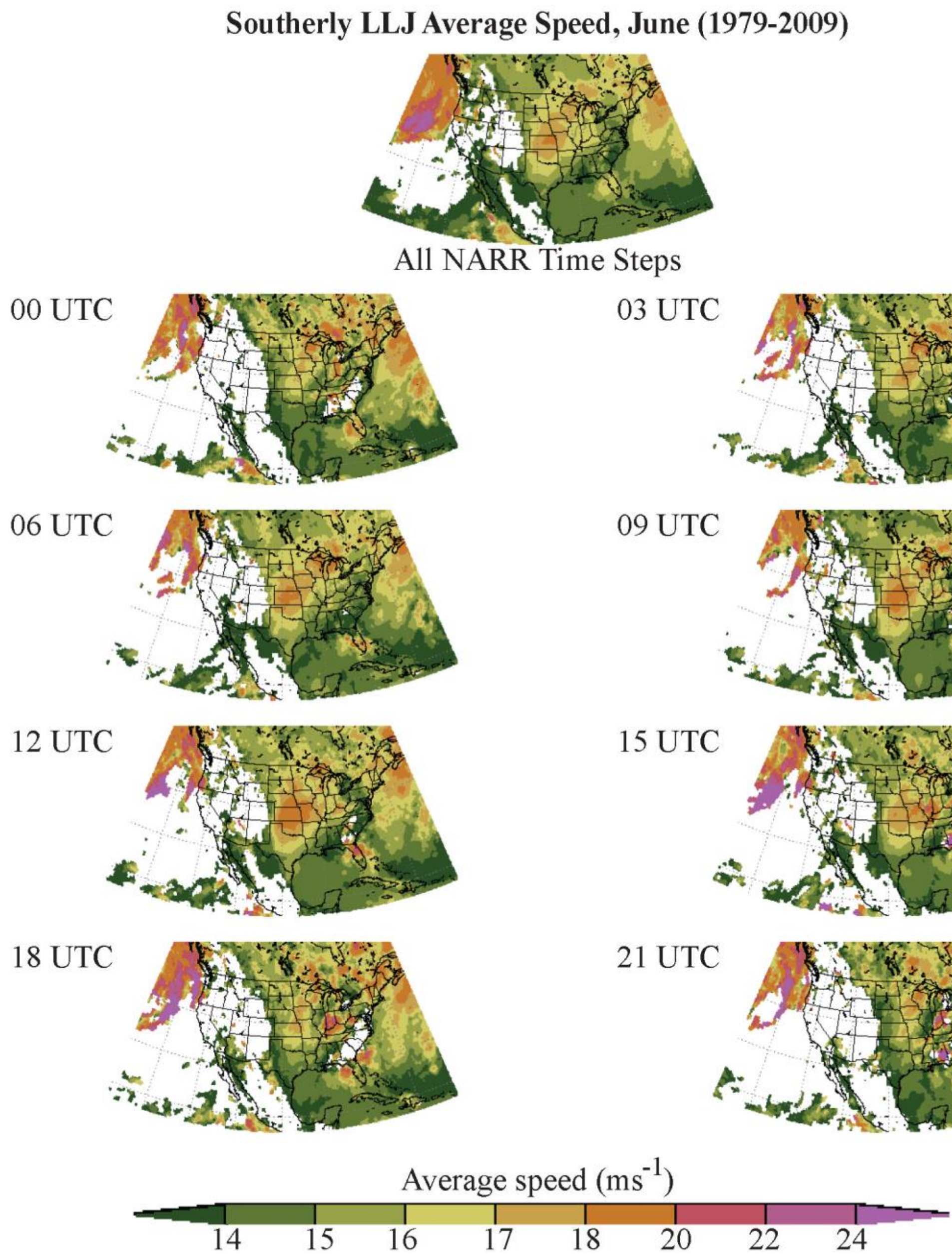

Figure 88. Average speed (meters per second) for S-LLJs that occurred during June from 1979-2009, for all jets (top figure) and for jets at each of the NARR time steps (bottom figures). Gridpoints with no jet cases and/or surface elevations >2km MSL are shown in white.

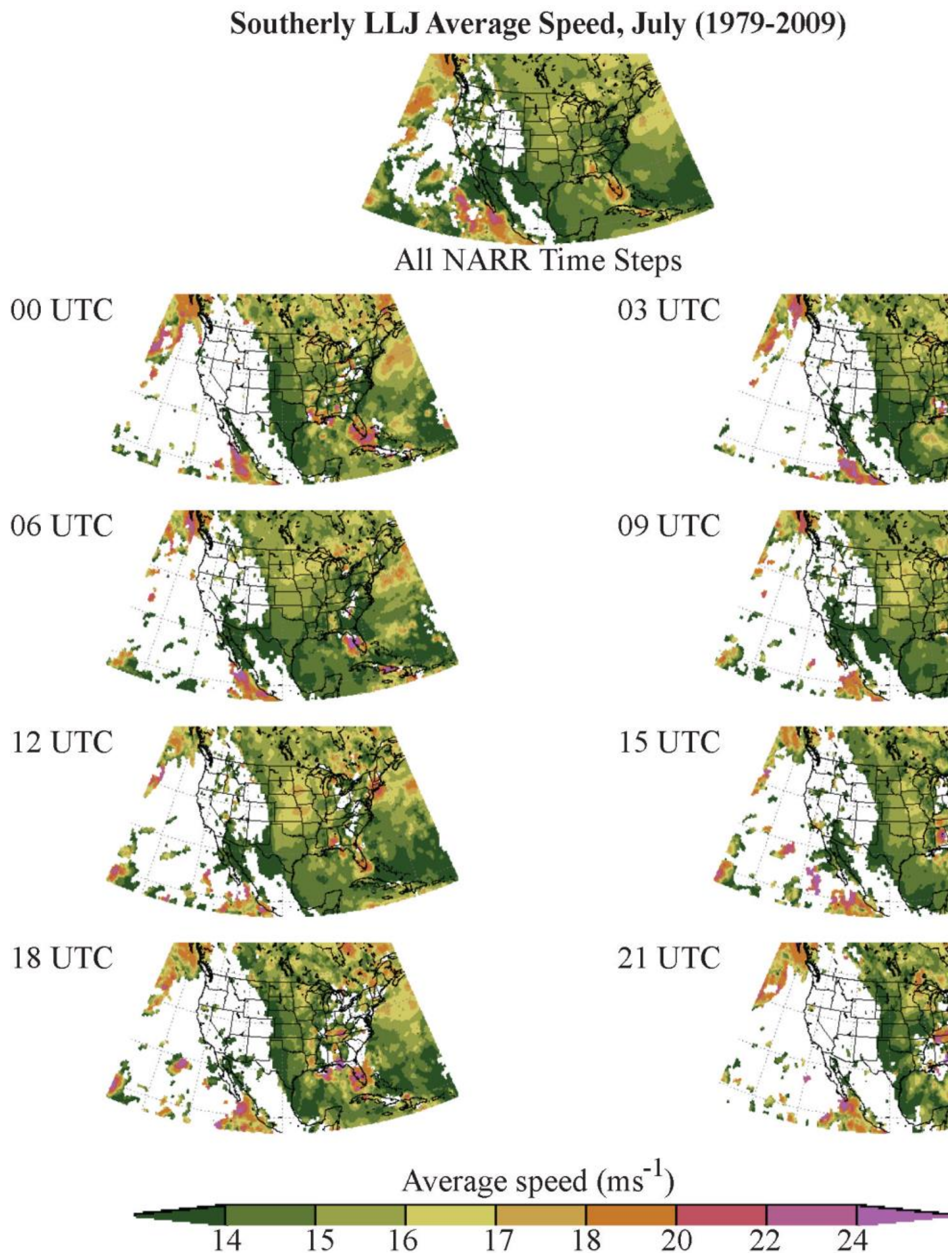

Figure 89. Average speed (meters per second) for S-LLJs that occurred during July from 1979-2009, for all jets (top figure) and for jets at each of the NARR time steps (bottom figures). Gridpoints with no jet cases and/or surface elevations >2km MSL are shown in white.

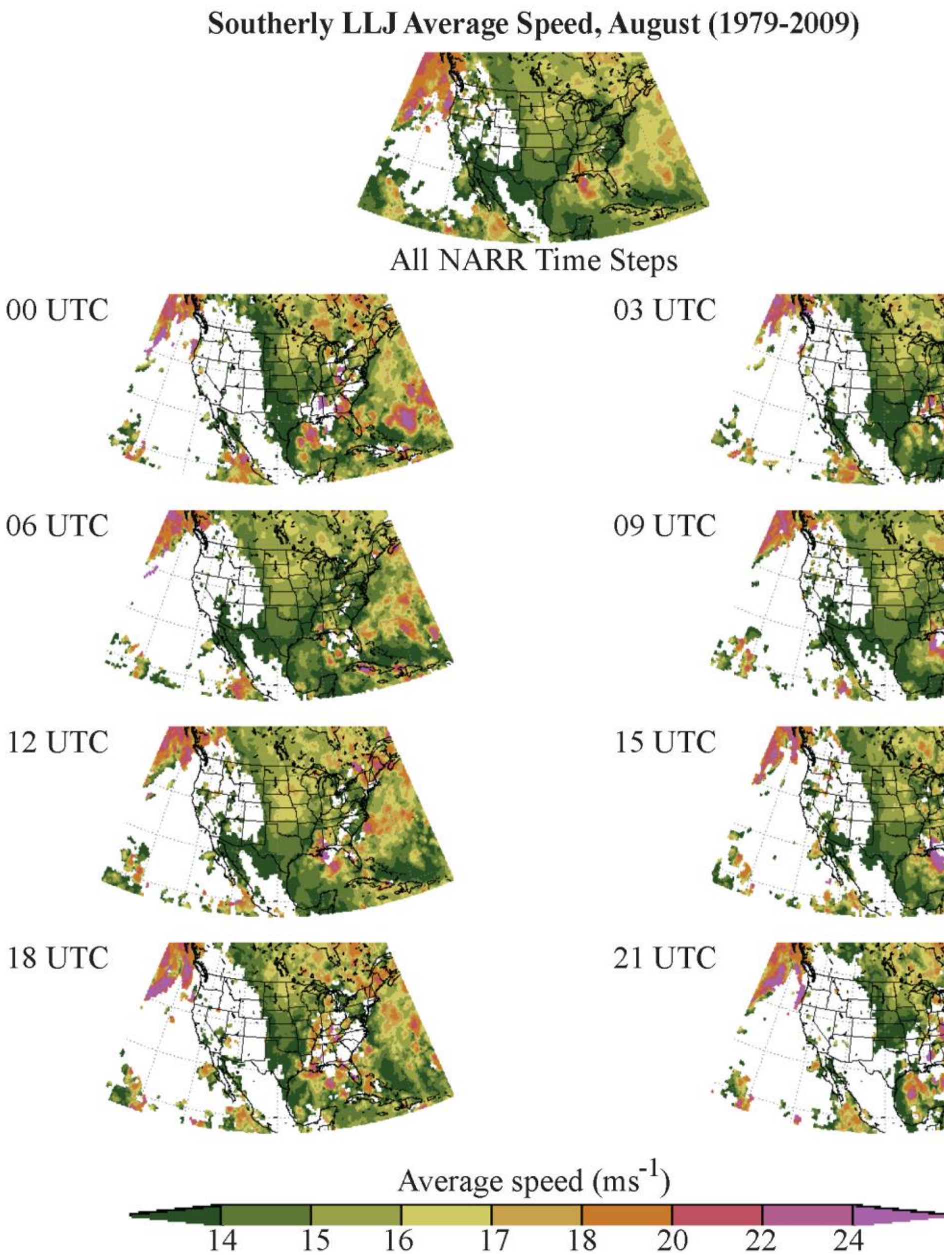

Figure 90. Average speed (meters per second) for S-LLJs that occurred during August from 1979-2009, for all jets (top figure) and for jets at each of the NARR time steps (bottom figures). Gridpoints with no jet cases and/or surface elevations >2km MSL are shown in white.

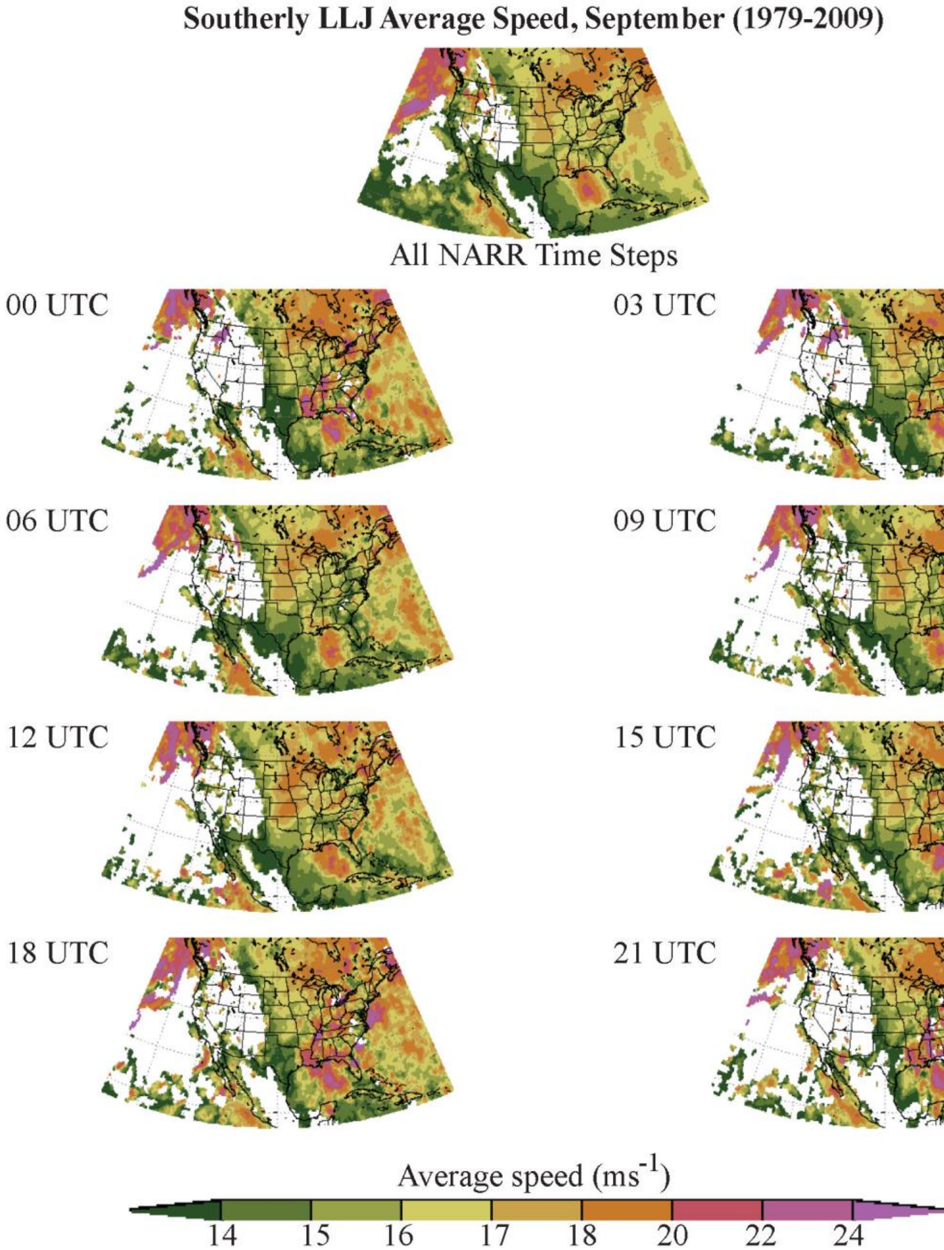

Figure 91. Average speed (meters per second) for S-LLJs that occurred during September from 1979-2009, for all jets (top figure) and for jets at each of the NARR time steps (bottom figures). Gridpoints with no jet cases and/or surface elevations >2km MSL are shown in white.

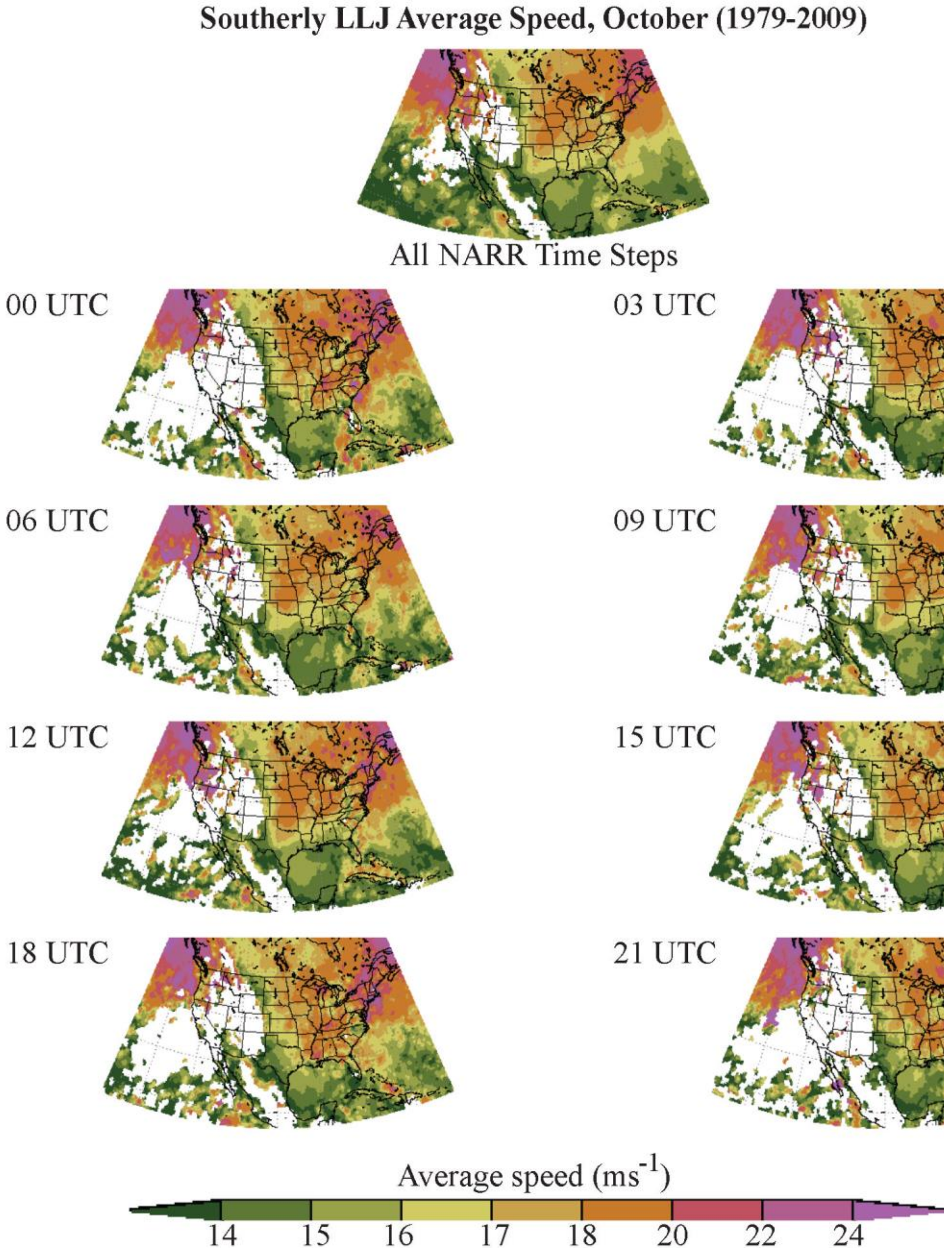

Figure 92. Average speed (meters per second) for S-LLJs that occurred during October from 1979-2009, for all jets (top figure) and for jets at each of the NARR time steps (bottom figures). Gridpoints with no jet cases and/or surface elevations >2km MSL are shown in white.

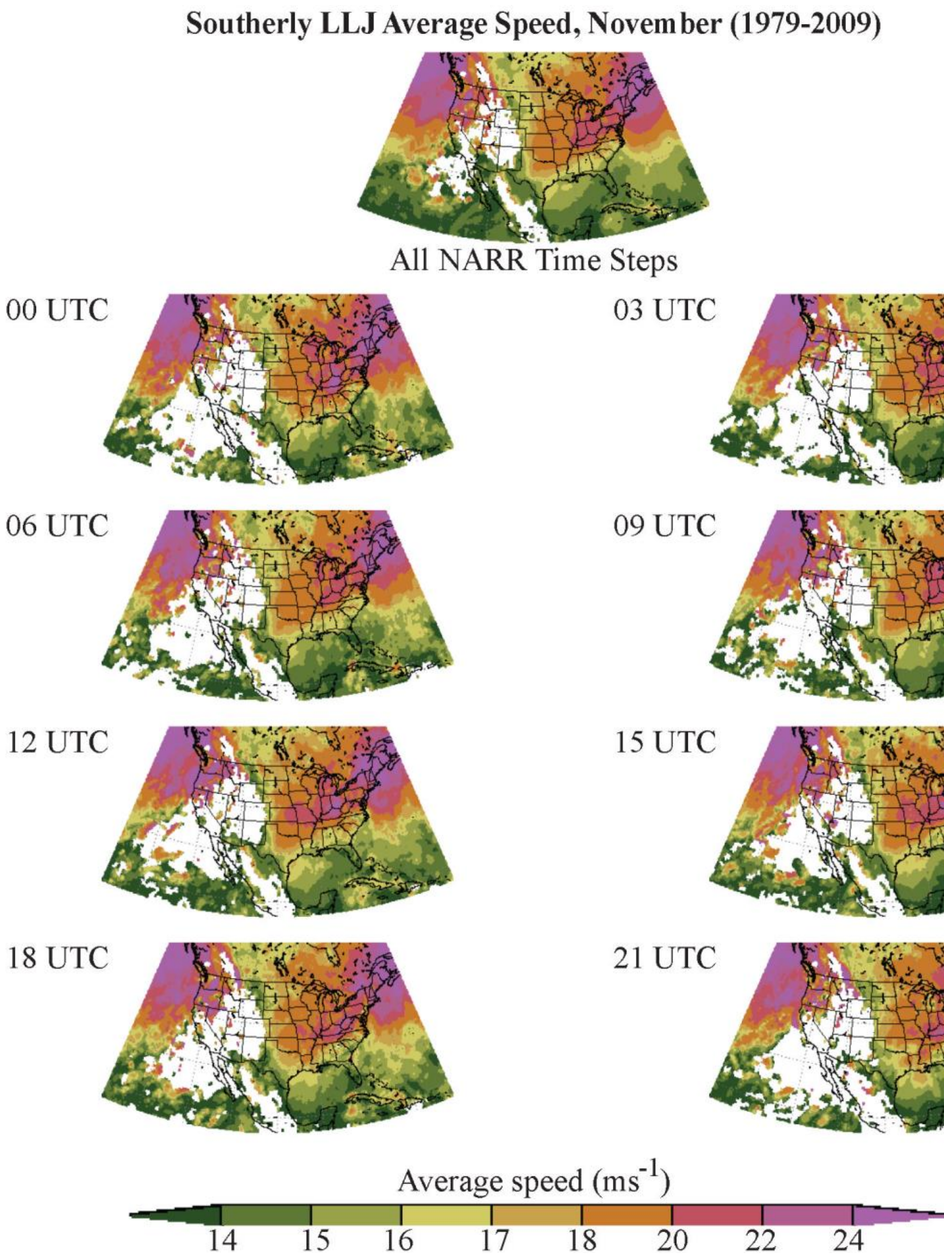

Figure 93. Average speed (meters per second) for S-LLJs that occurred during November from 1979-2009, for all jets (top figure) and for jets at each of the NARR time steps (bottom figures). Gridpoints with no jet cases and/or surface elevations >2km MSL are shown in white.

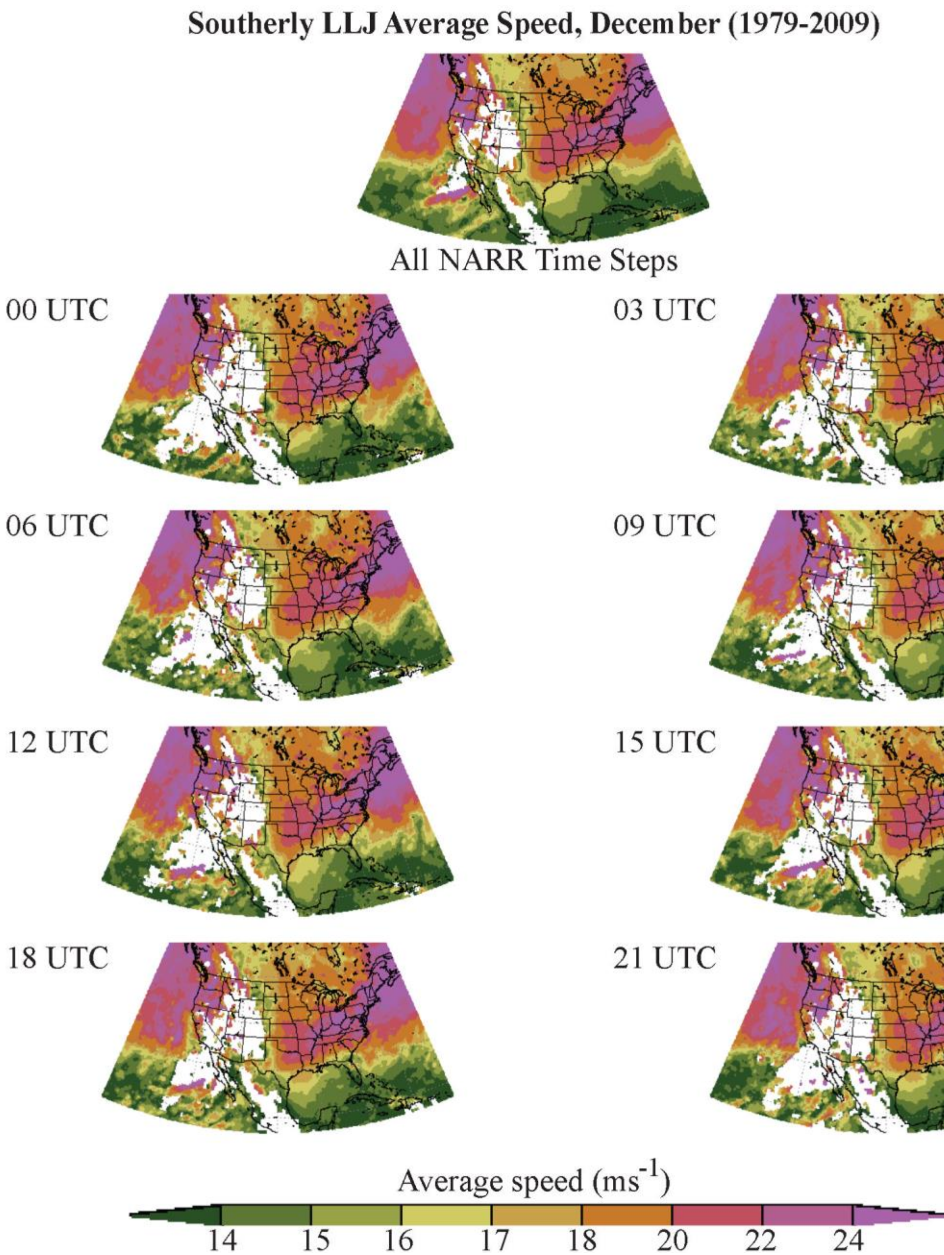

Figure 94. Average speed (meters per second) for S-LLJs that occurred during December from 1979-2009, for all jets (top figure) and for jets at each of the NARR time steps (bottom figures). Gridpoints with no jet cases and/or surface elevations >2km MSL are shown in white.

APPENDIX D

Average Speed of Northerly Low-Level Jets

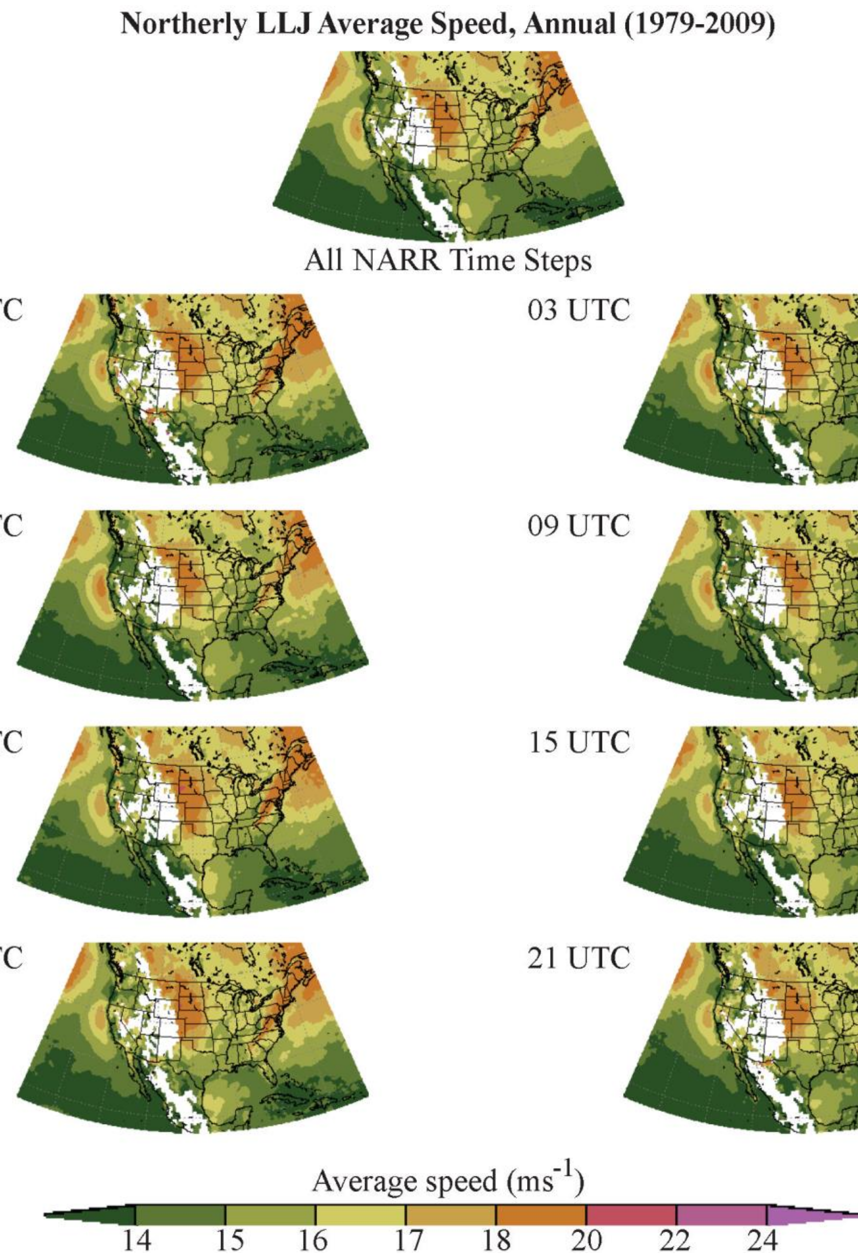

Figure 95. Annual average speed (meters per second) of N-LLJs from 1979 to 2009. Includes annual average speed across all NARR time steps and annual average speed at each individual NARR time step. Gridpoints with no jet cases and/or surface elevations >2km MSL are shown in white.

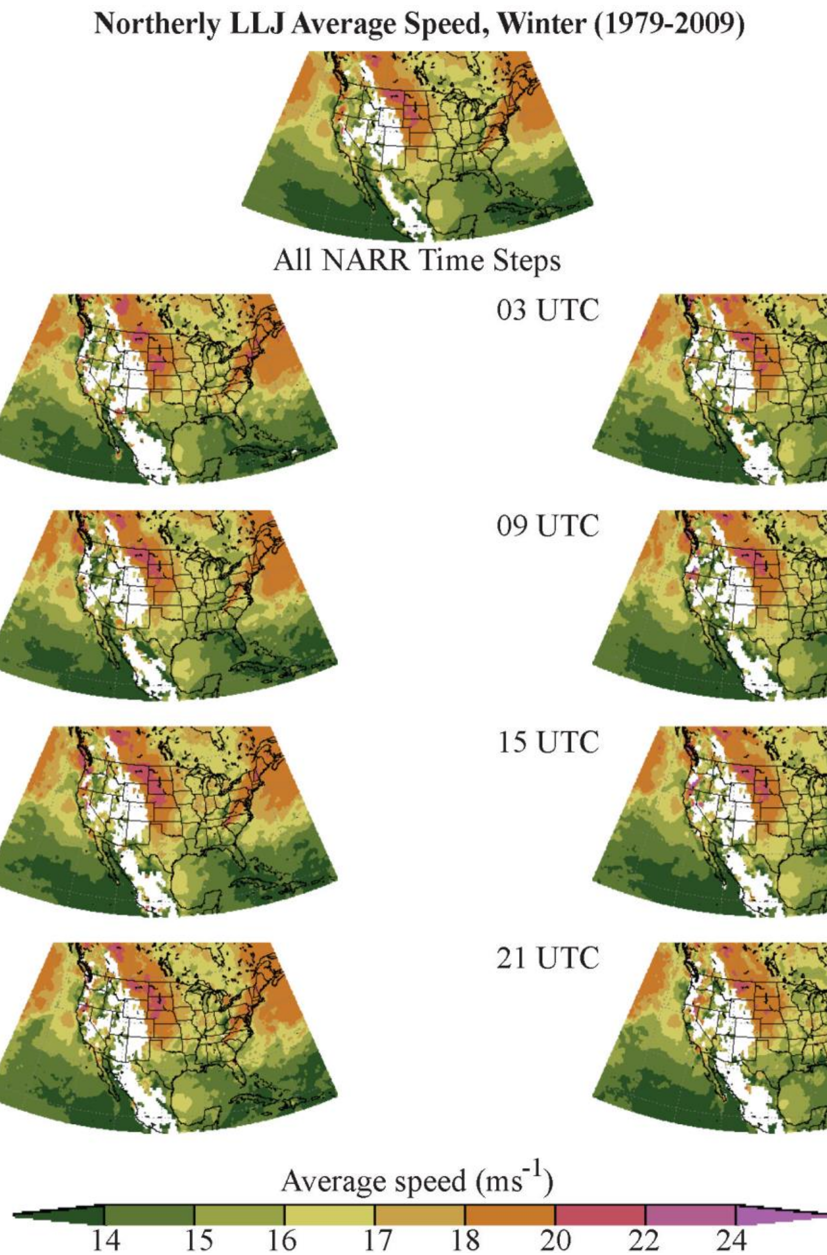

Figure 96. Average speed (meters per second) for N-LLJs that occurred during winter from 1979-2009, for all jets (top figure) and for jets at each of the NARR time steps (bottom figures). Gridpoints with no jet cases and/or surface elevations >2km MSL are shown in white.

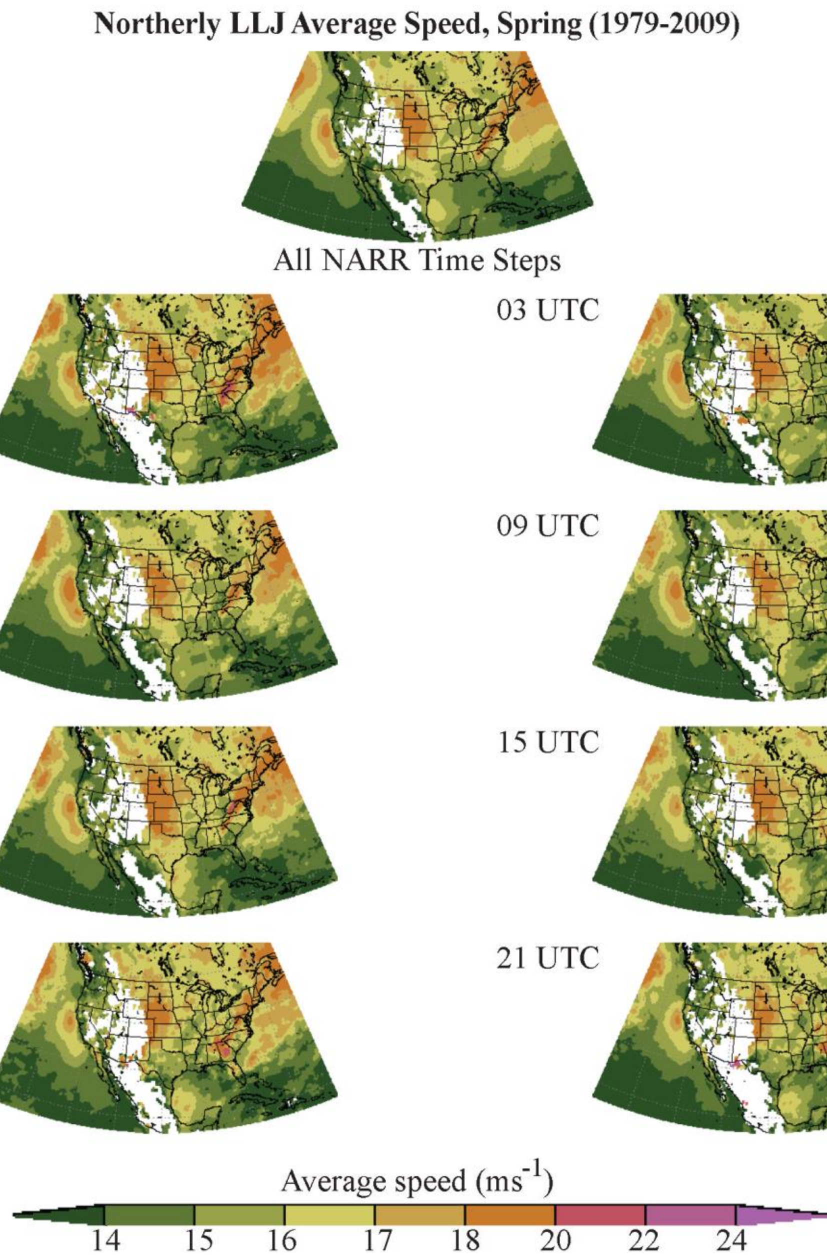

Figure 97. Average speed (meters per second) for N-LLJs that occurred during spring from 1979-2009, for all jets (top figure) and for jets at each of the NARR time steps (bottom figures). Gridpoints with no jet cases and/or surface elevations >2km MSL are shown in white.

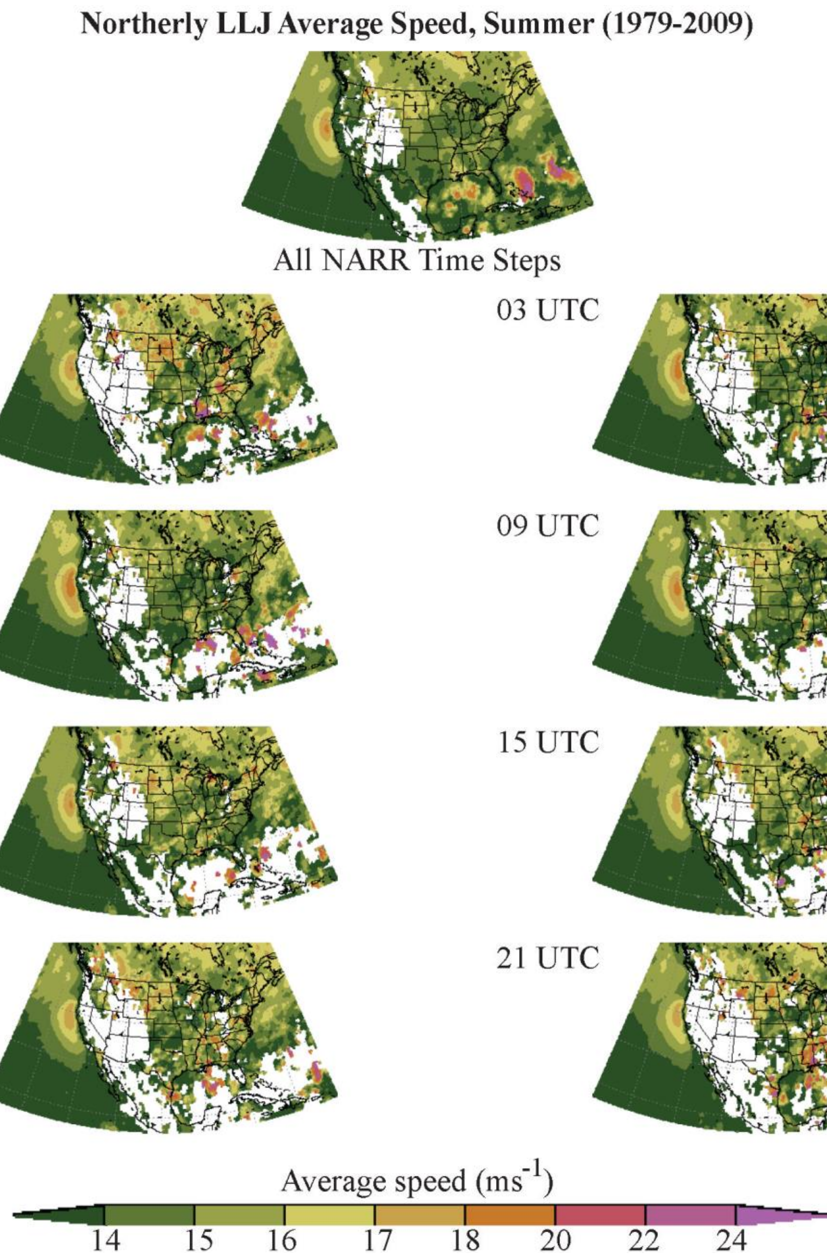

Figure 98. Average speed (meters per second) for N-LLJs that occurred during summer from 1979-2009, for all jets (top figure) and for jets at each of the NARR time steps (bottom figures). Gridpoints with no jet cases and/or surface elevations >2km MSL are shown in white.

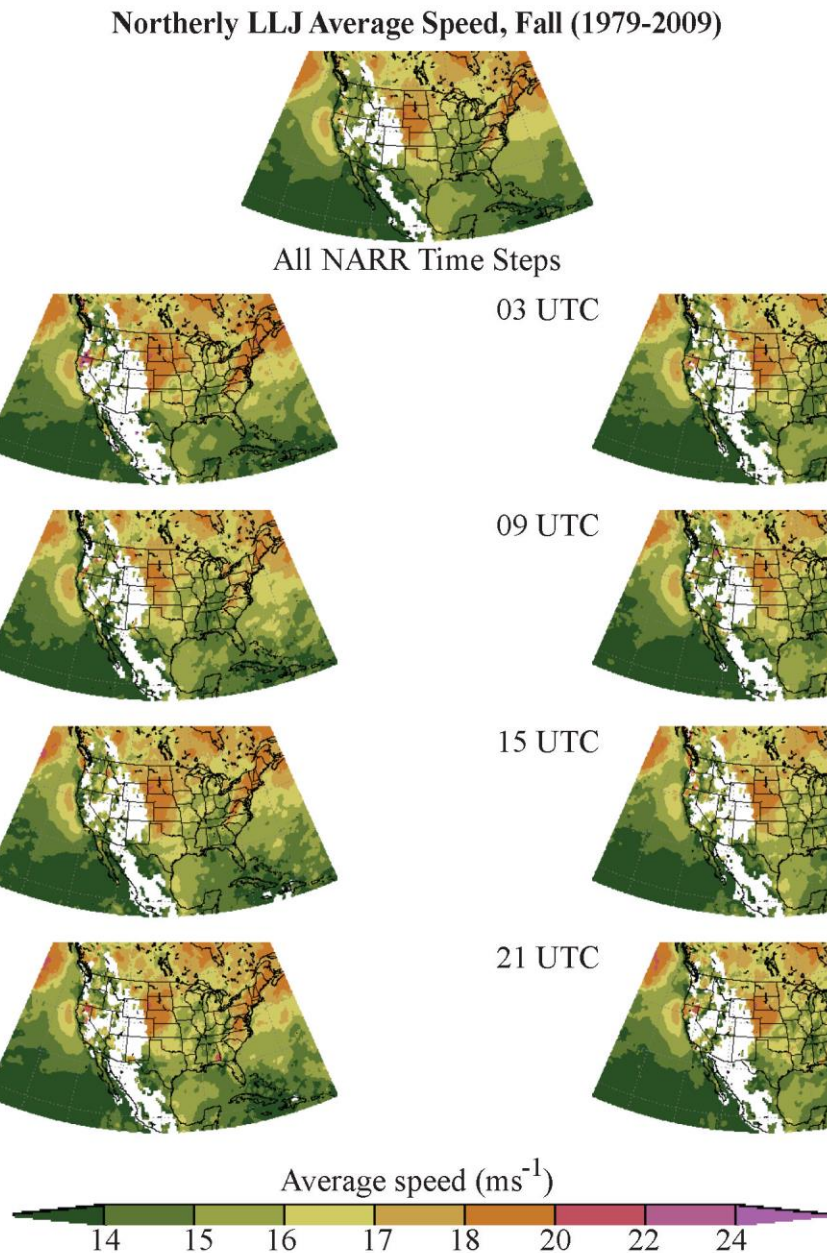

Figure 99. Average speed (meters per second) for N-LLJs that occurred during fall from 1979-2009, for all jets (top figure) and for jets at each of the NARR time steps (bottom figures). Gridpoints with no jet cases and/or surface elevations >2km MSL are shown in white.

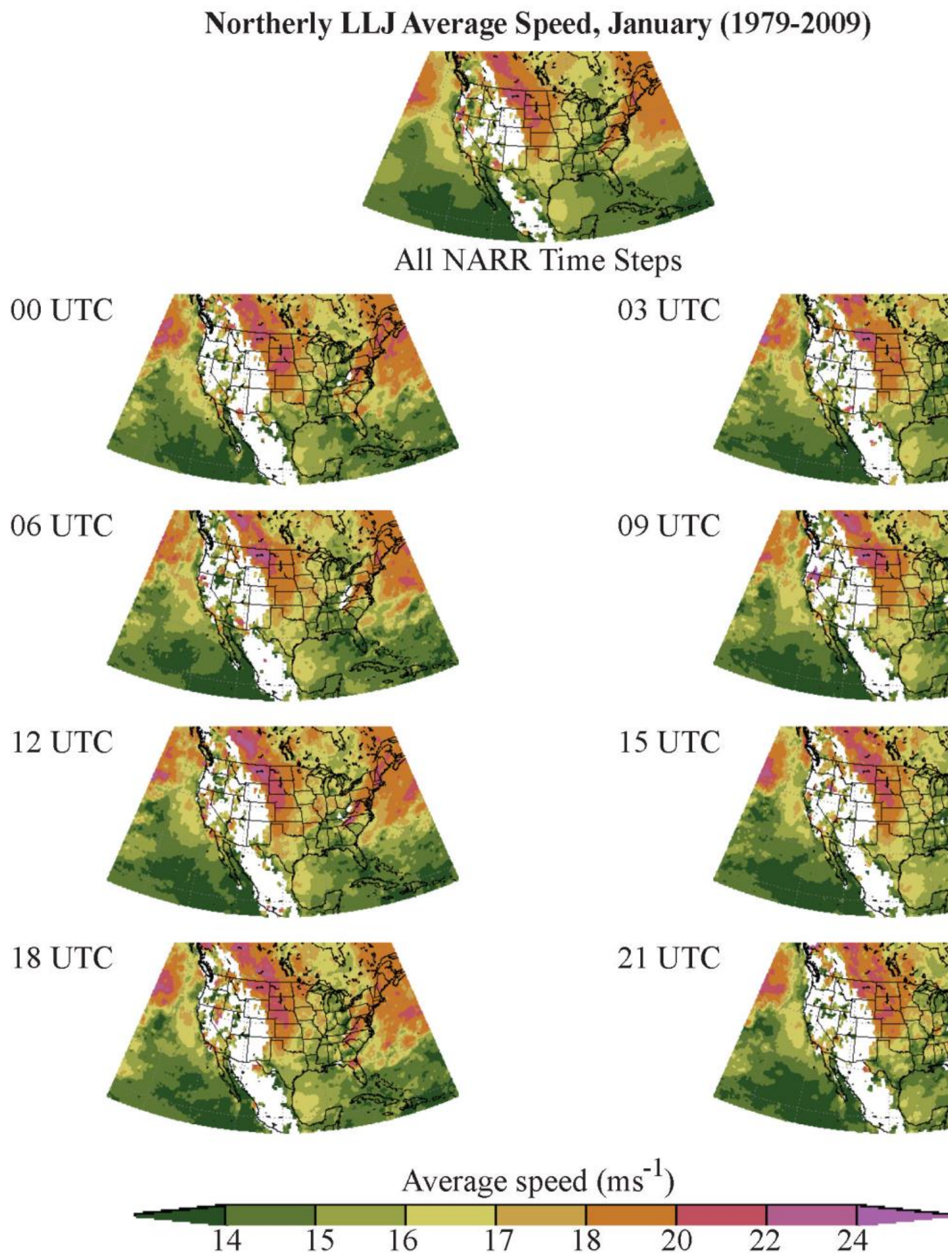

Figure 100. Average speed (meters per second) for N-LLJs that occurred during January from 1979-2009, for all jets (top figure) and for jets at each of the NARR time steps (bottom figures). Gridpoints with no jet cases and/or surface elevations >2km MSL are shown in white.

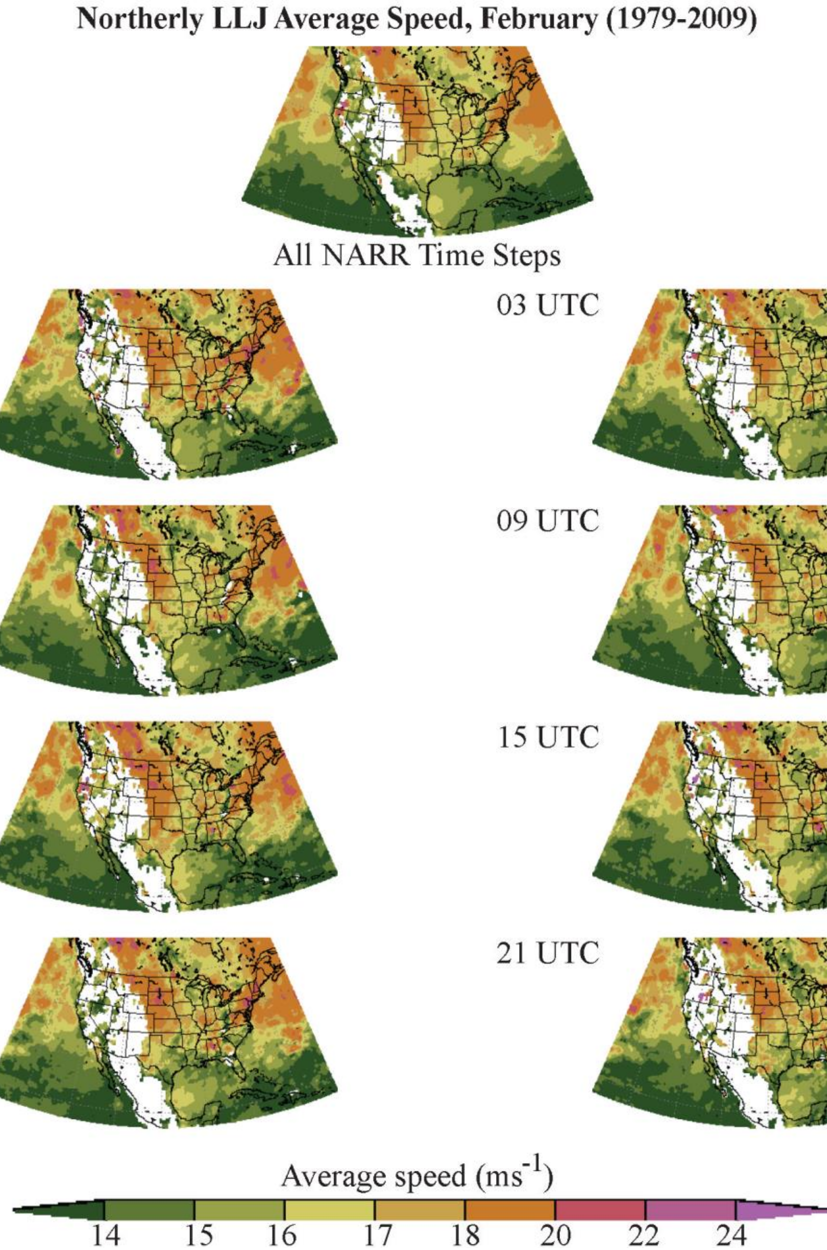

Figure 101. Average speed (meters per second) for N-LLJs that occurred during February from 1979-2009, for all jets (top figure) and for jets at each of the NARR time steps (bottom figures). Gridpoints with no jet cases and/or surface elevations >2km MSL are shown in white.

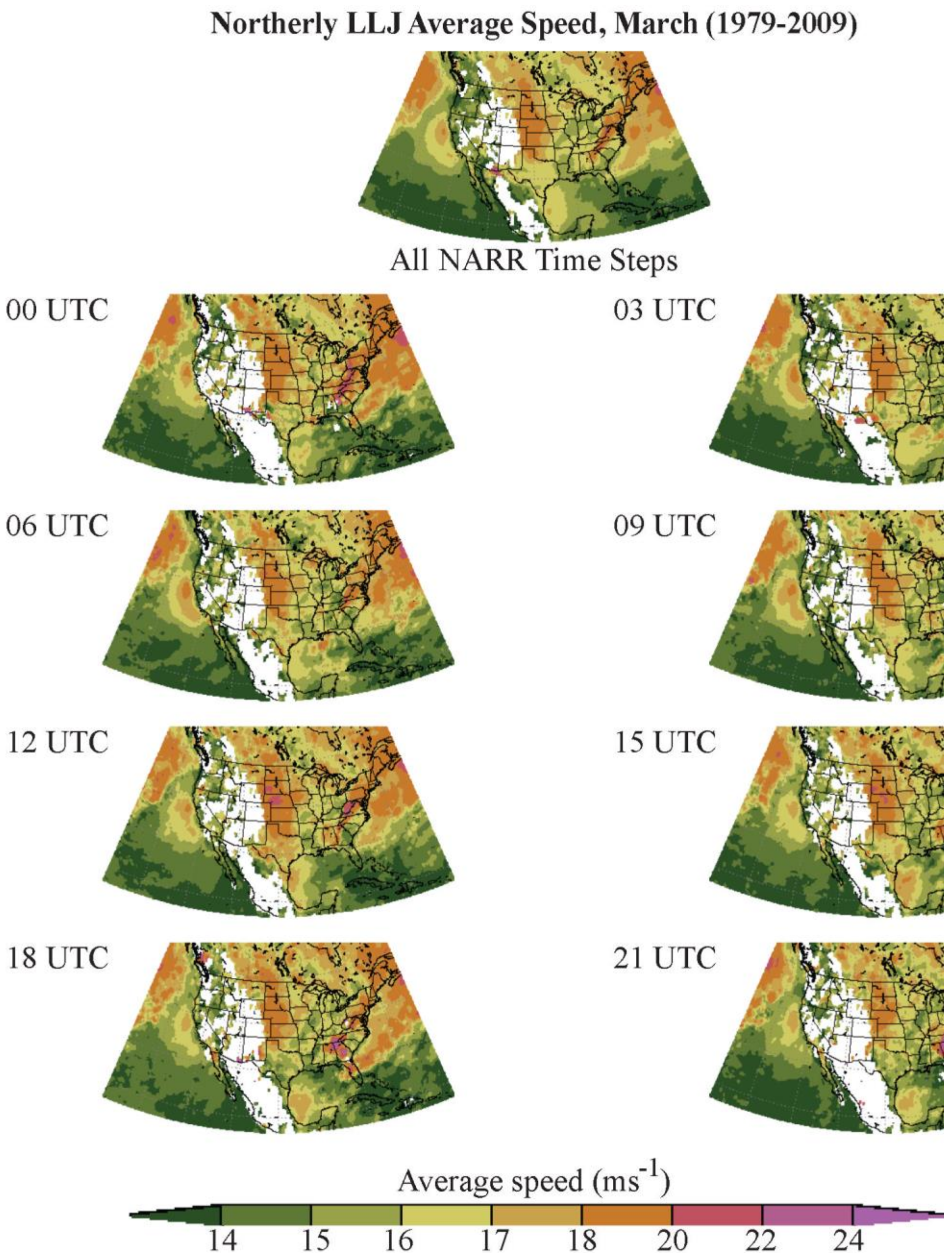

Figure 102. Average speed (meters per second) for N-LLJs that occurred during March from 1979-2009, for all jets (top figure) and for jets at each of the NARR time steps (bottom figures). Gridpoints with no jet cases and/or surface elevations >2km MSL are shown in white.

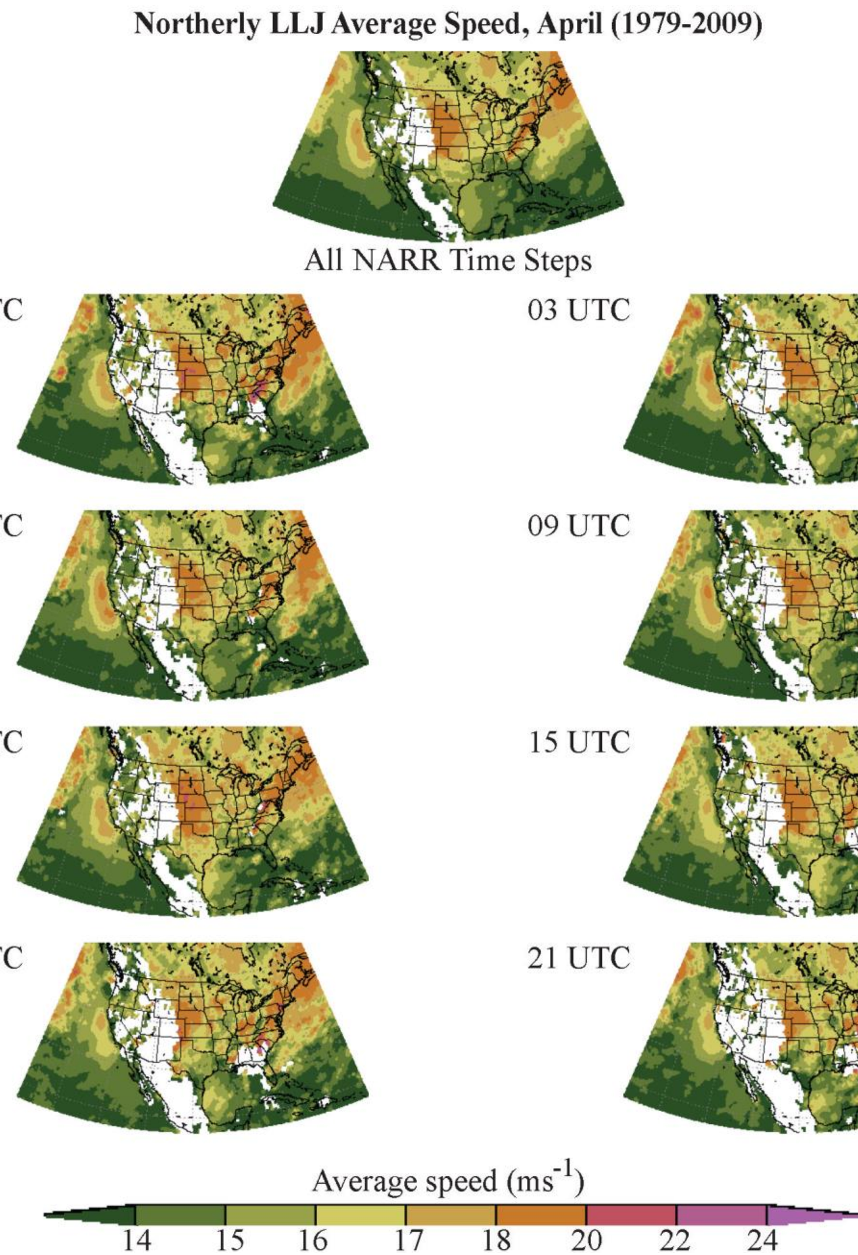

Figure 103. Average speed (meters per second) for N-LLJs that occurred during April from 1979-2009, for all jets (top figure) and for jets at each of the NARR time steps (bottom figures). Gridpoints with no jet cases and/or surface elevations >2km MSL are shown in white.

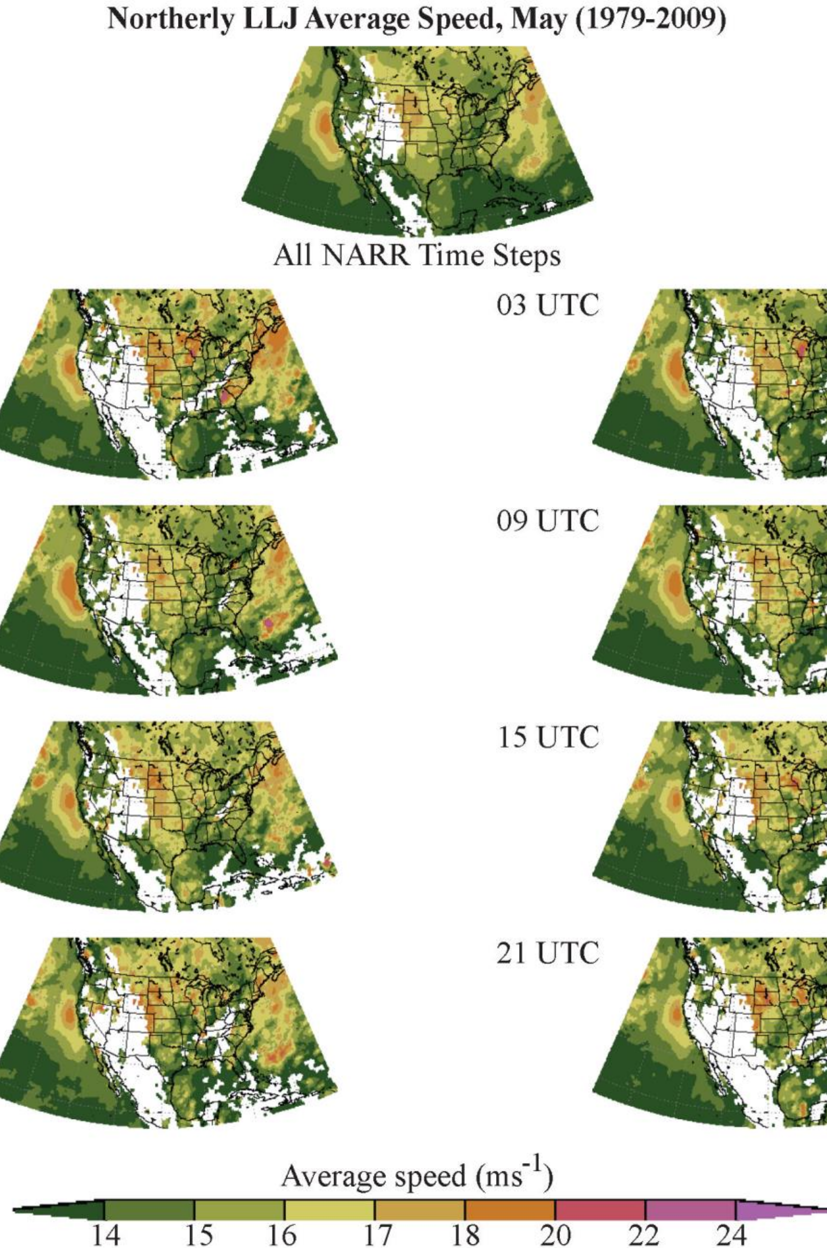

Figure 104. Average speed (meters per second) for N-LLJs that occurred during May from 1979-2009, for all jets (top figure) and for jets at each of the NARR time steps (bottom figures). Gridpoints with no jet cases and/or surface elevations >2km MSL are shown in white.

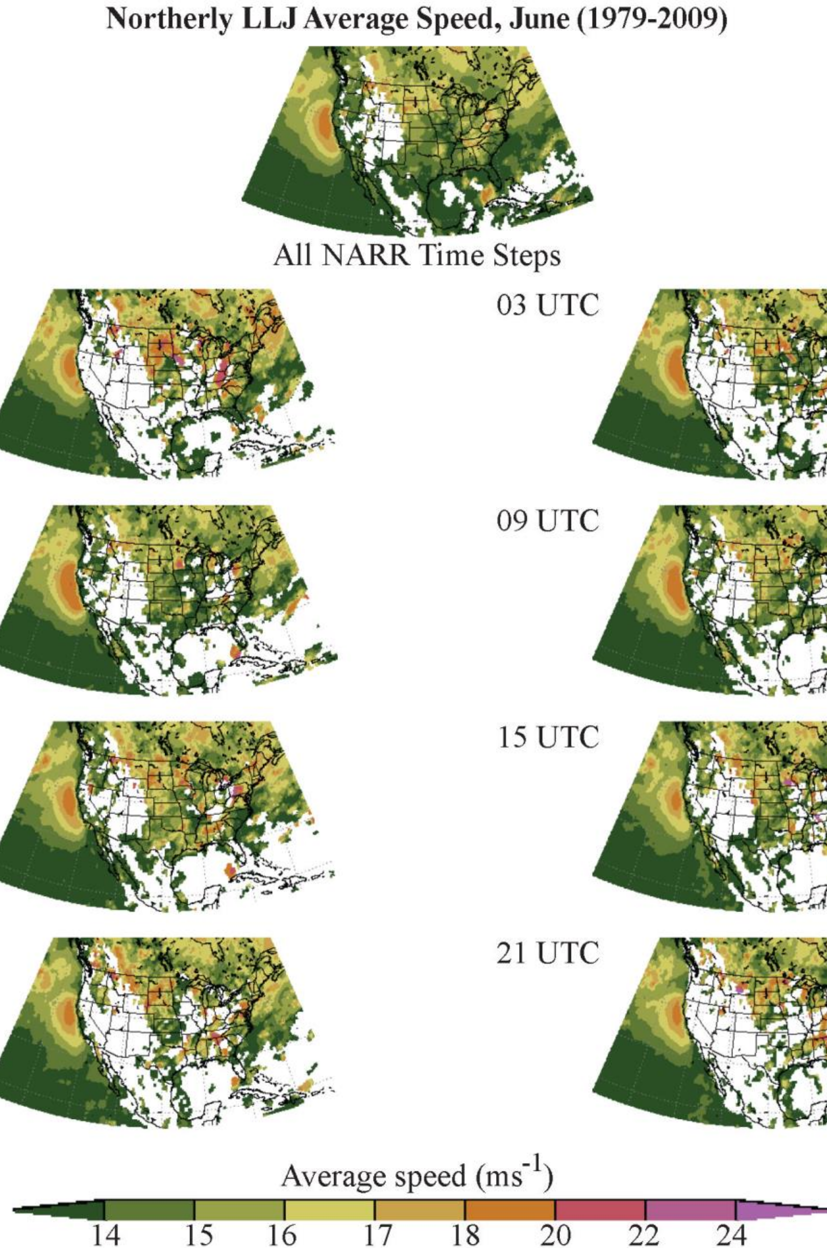

Figure 105. Average speed (meters per second) for N-LLJs that occurred during June from 1979-2009, for all jets (top figure) and for jets at each of the NARR time steps (bottom figures). Gridpoints with no jet cases and/or surface elevations >2km MSL are shown in white.

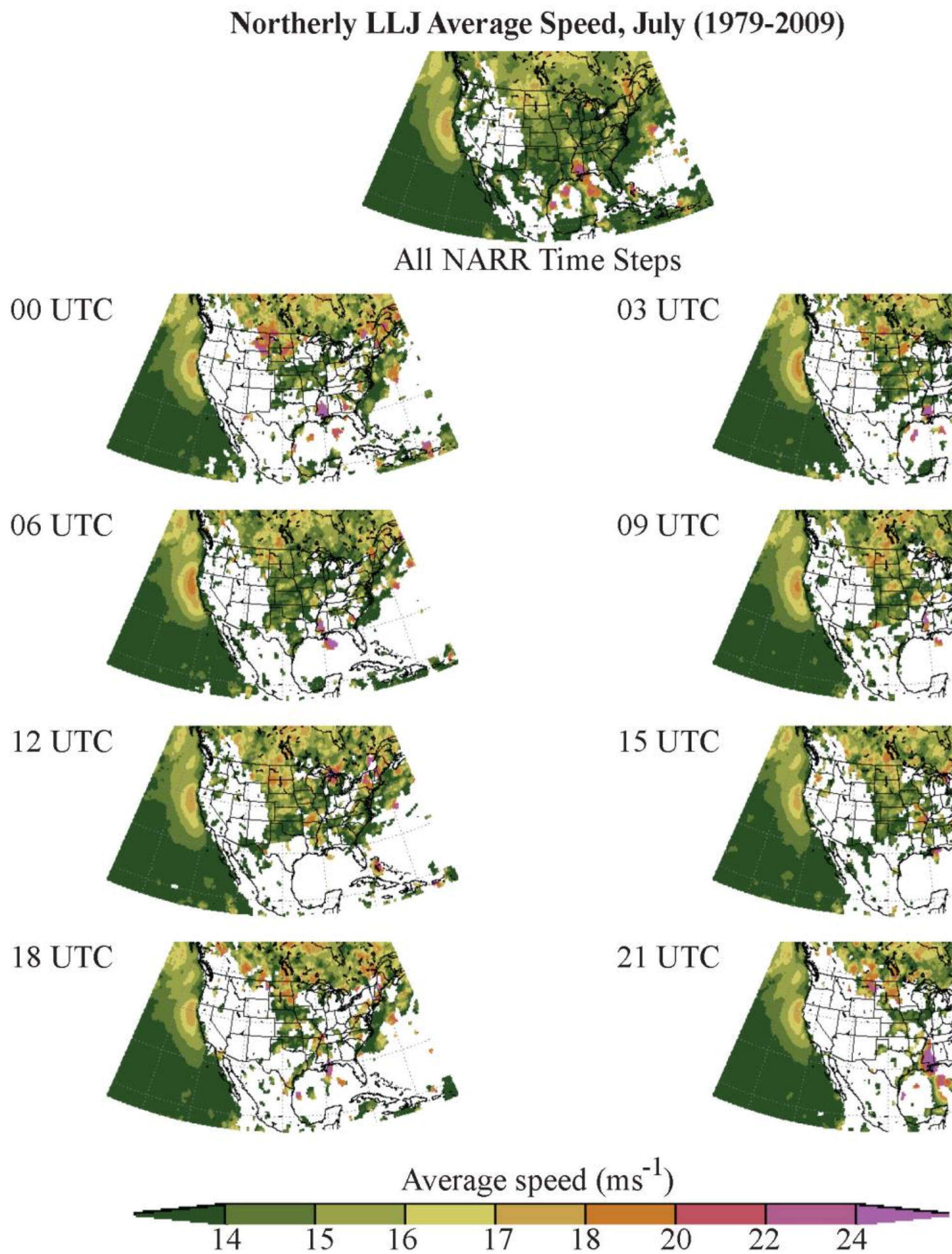

Figure 106. Average speed (meters per second) for N-LLJs that occurred during July from 1979-2009, for all jets (top figure) and for jets at each of the NARR time steps (bottom figures). Gridpoints with no jet cases and/or surface elevations >2km MSL are shown in white.

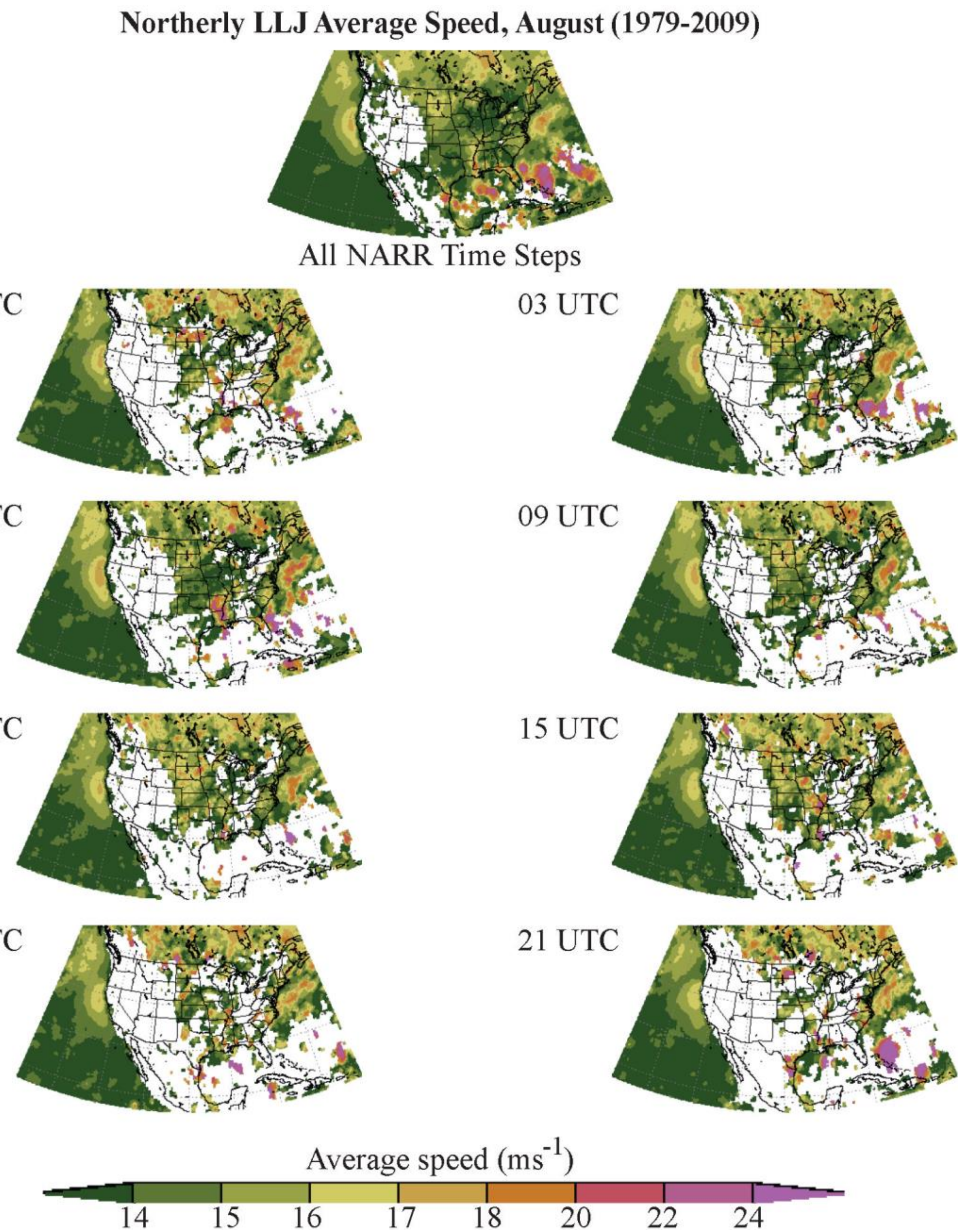

Figure 107. Average speed (meters per second) for N-LLJs that occurred during August from 1979-2009, for all jets (top figure) and for jets at each of the NARR time steps (bottom figures). Gridpoints with no jet cases and/or surface elevations >2km MSL are shown in white.

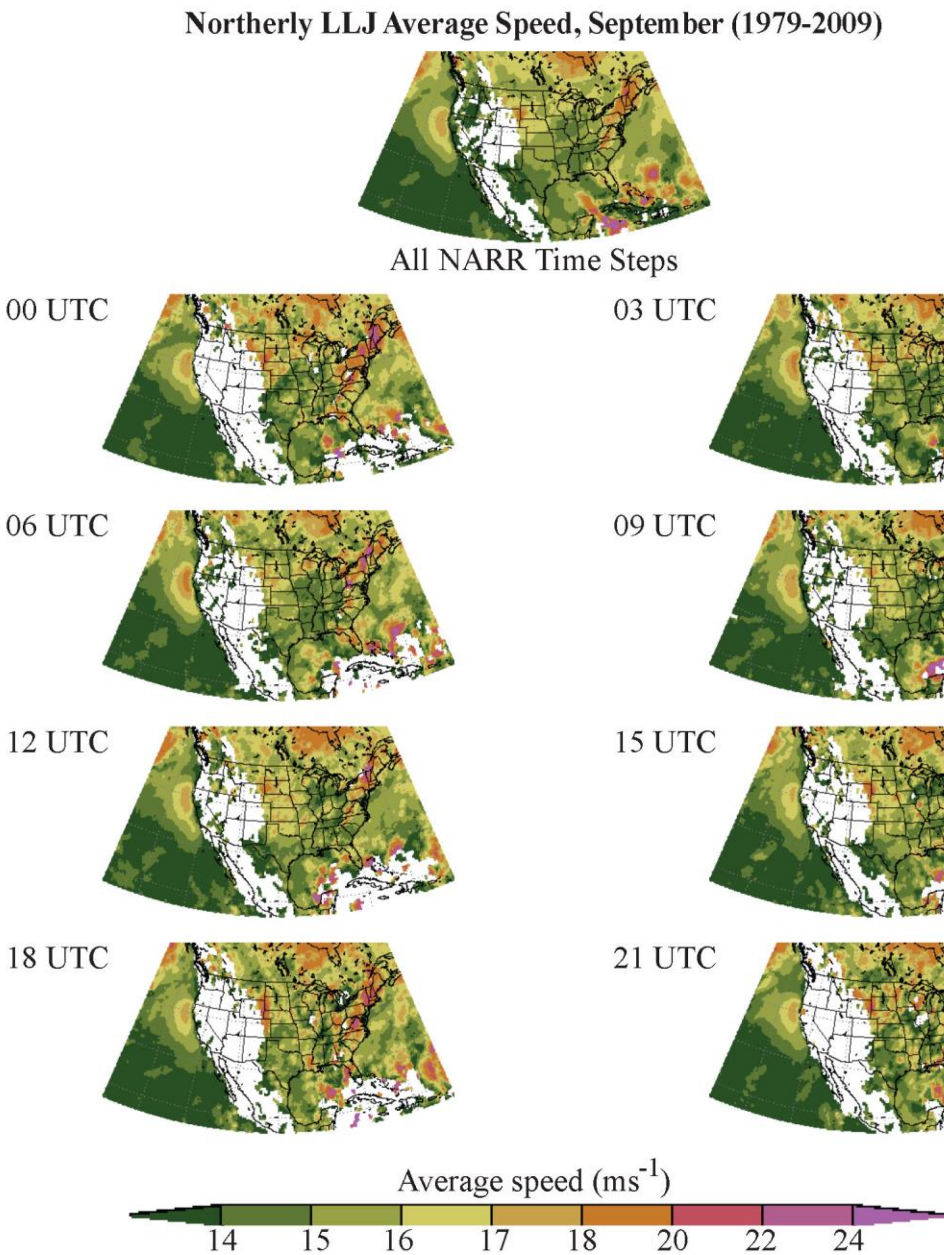

Figure 108. Average speed (meters per second) for N-LLJs that occurred during September from 1979-2009, for all jets (top figure) and for jets at each of the NARR time steps (bottom figures). Gridpoints with no jet cases and/or surface elevations >2km MSL are shown in white.

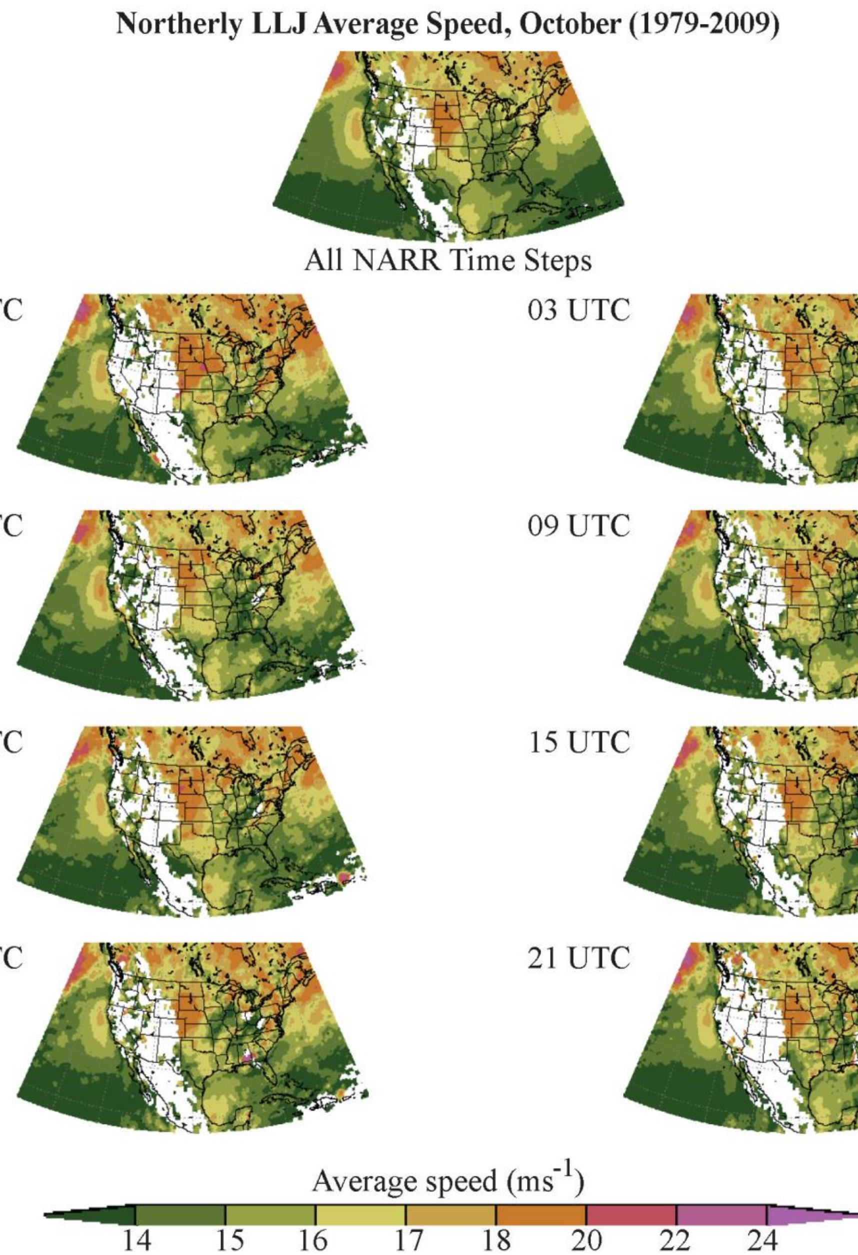

Figure 109. Average speed (meters per second) for N-LLJs that occurred during October from 1979-2009, for all jets (top figure) and for jets at each of the NARR time steps (bottom figures). Gridpoints with no jet cases and/or surface elevations >2km MSL are shown in white.

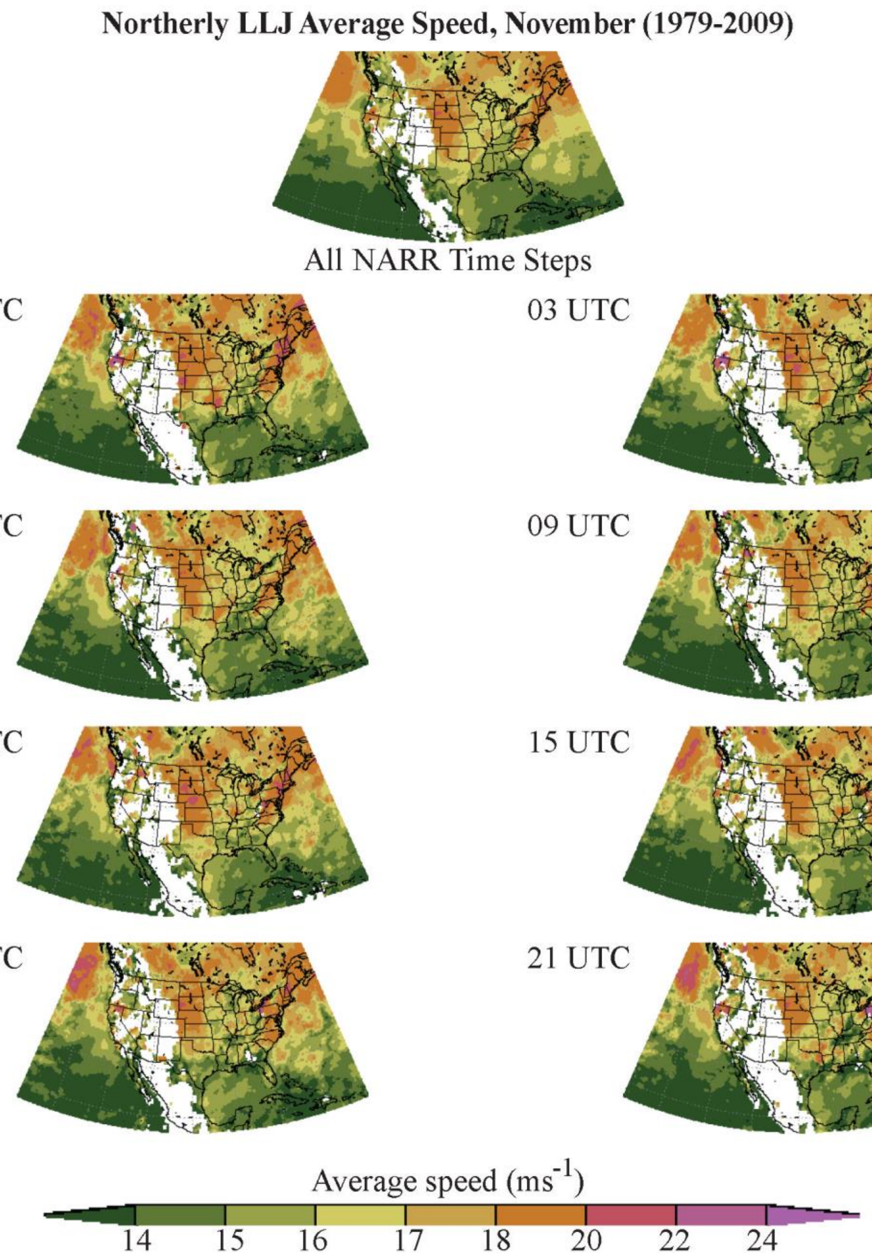

Figure 110. Average speed (meters per second) for N-LLJs that occurred during November from 1979-2009, for all jets (top figure) and for jets at each of the NARR time steps (bottom figures). Gridpoints with no jet cases and/or surface elevations >2km MSL are shown in white.

Figure 111. Average speed (meters per second) for N-LLJs that occurred during December from 1979-2009, for all jets (top figure) and for jets at each of the NARR time steps (bottom figures). Gridpoints with no jet cases and/or surface elevations >2km MSL are shown in white.

APPENDIX E

Average Elevation of Southerly Low-Level Jets

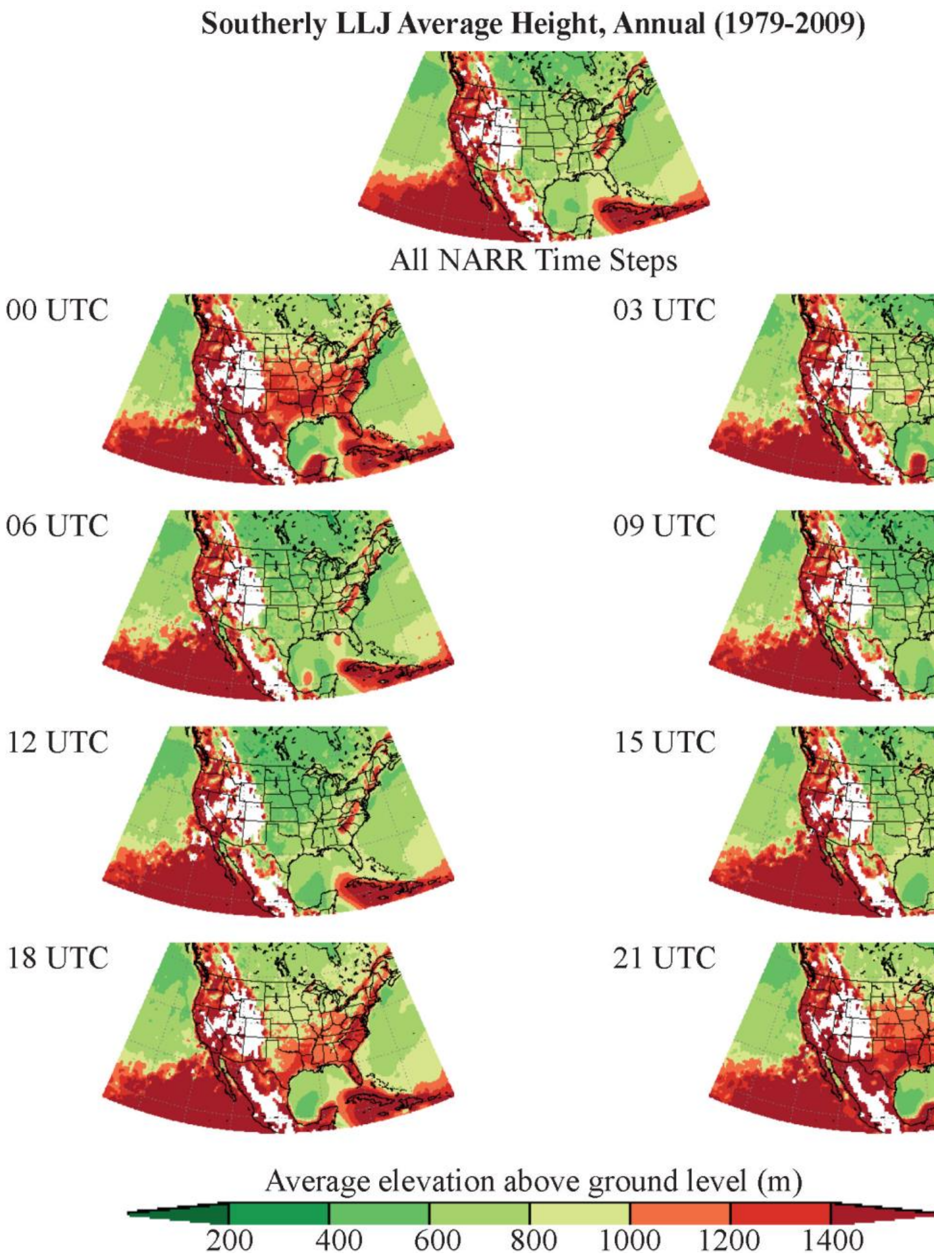

Figure 112. Annual average elevation (meters of above ground level) for S-LLJs that from 1979 to 2009, for all jets (top figure) and for jets at each of the NARR time steps (bottom figures). Gridpoints with no jet cases and/or surface elevations >2km MSL are shown in white.

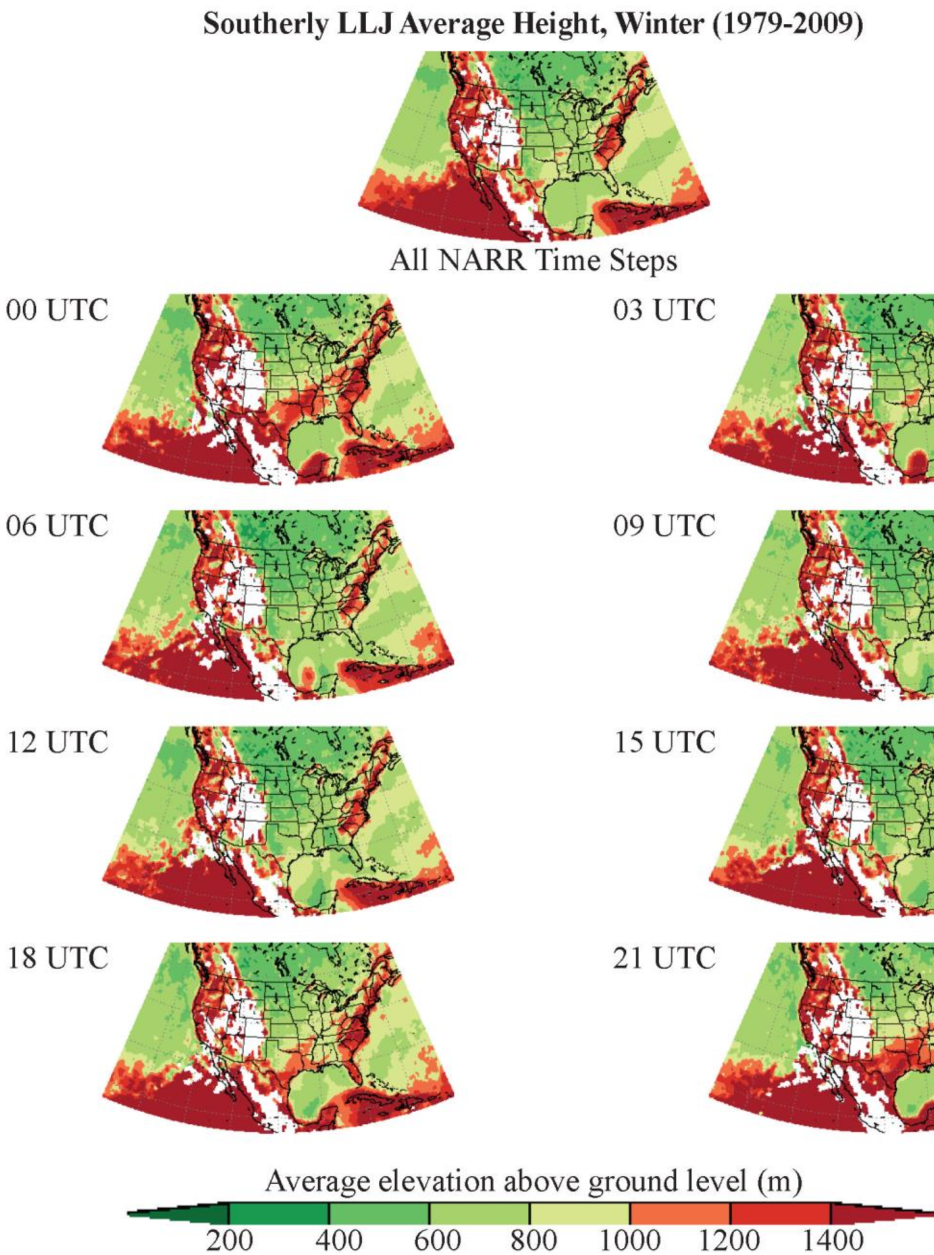

Figure 113. Average elevation (meters of above ground level) for S-LLJs that occurred during winter from 1979 to 2009, for all jets (top figure) and for jets at each of the NARR time steps (bottom figures). Gridpoints with no jet cases and/or surface elevations >2km MSL are shown in white.

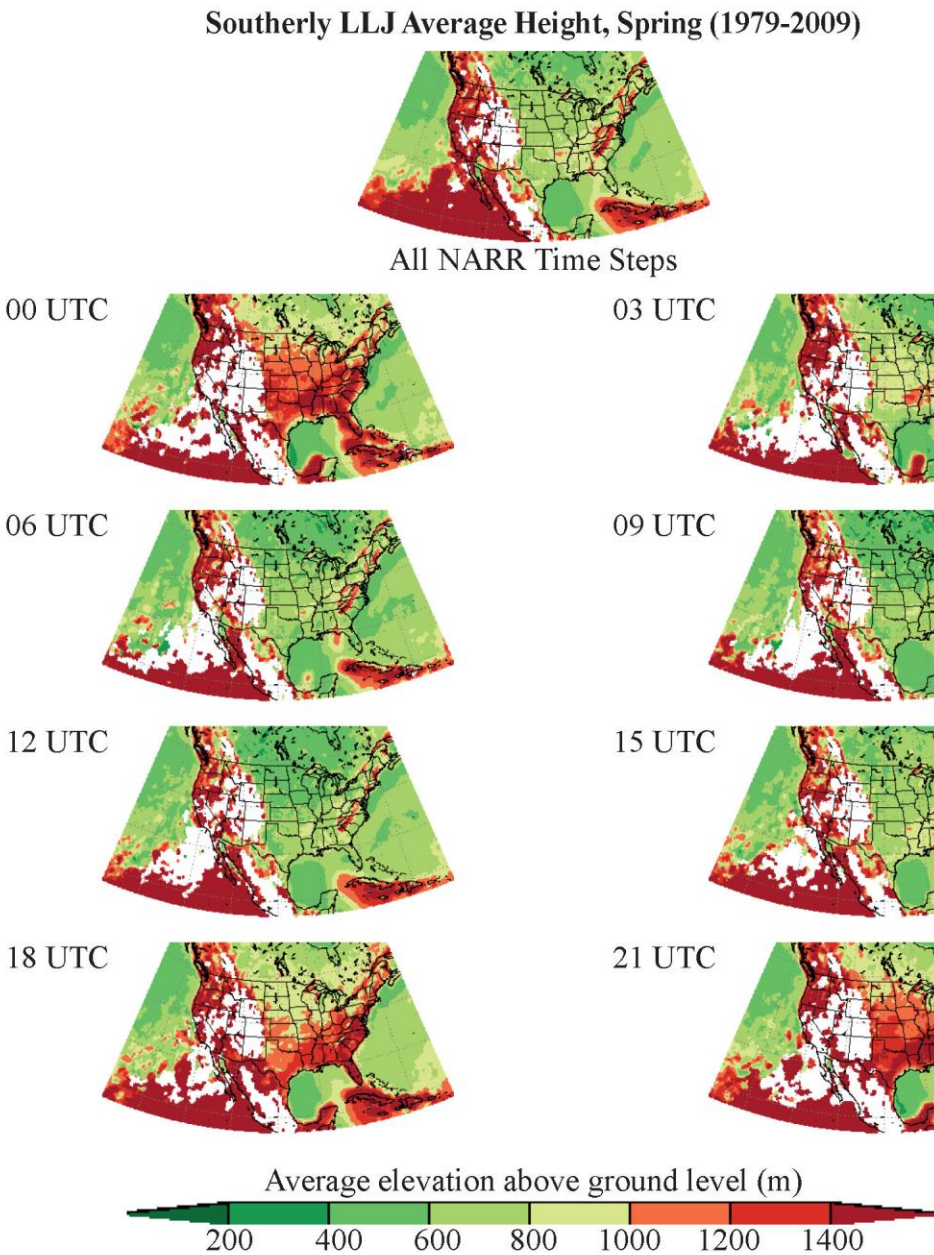

Figure 114. Average elevation (meters of above ground level) for S-LLJs that occurred during spring from 1979 to 2009, for all jets (top figure) and for jets at each of the NARR time steps (bottom figures). Gridpoints with no jet cases and/or surface elevations >2km MSL are shown in white.

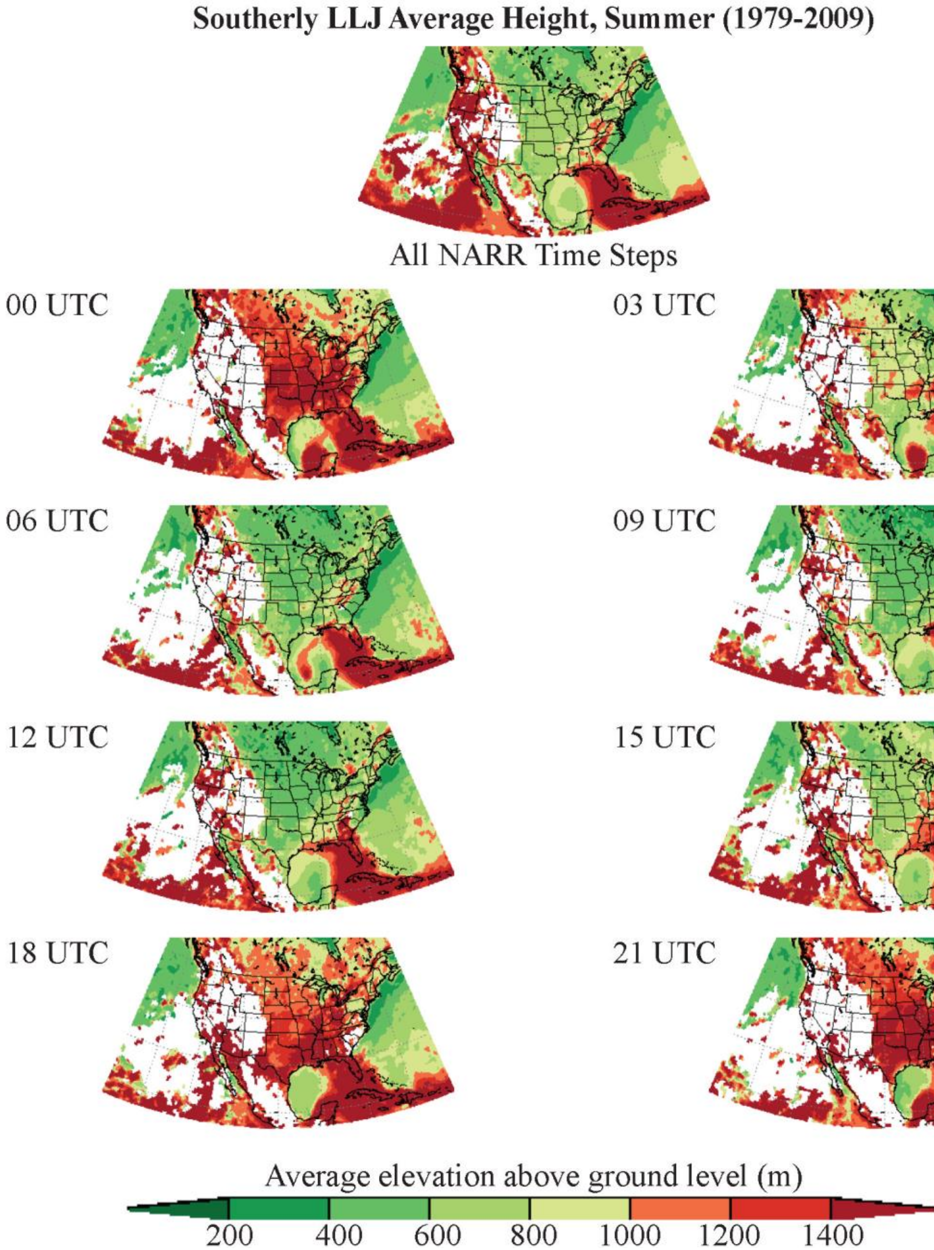

Figure 115. Average elevation (meters of above ground level) for S-LLJs that occurred during summer from 1979 to 2009, for all jets (top figure) and for jets at each of the NARR time steps (bottom figures). Gridpoints with no jet cases and/or surface elevations >2km MSL are shown in white.

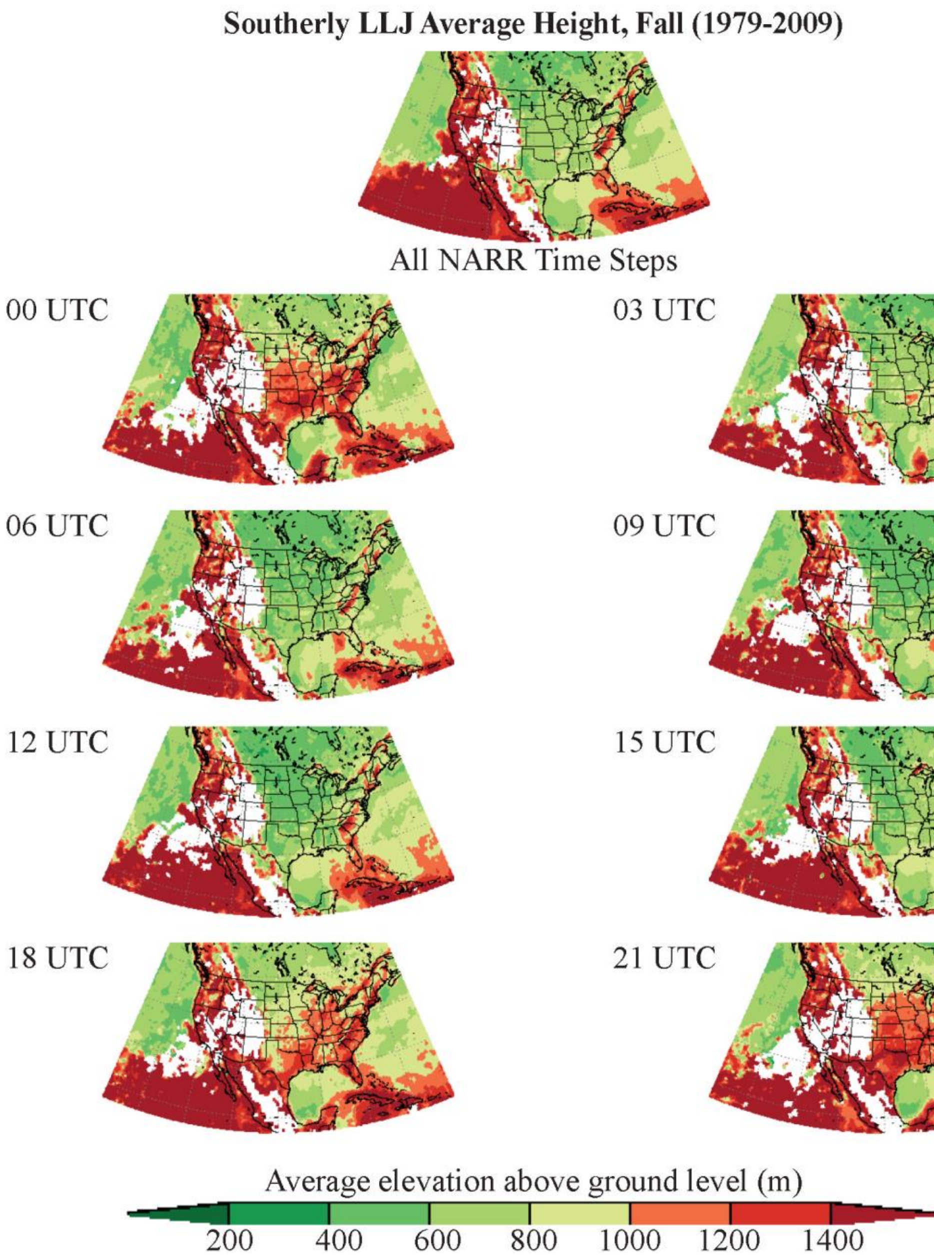

Figure 116. Average elevation (meters of above ground level) for S-LLJs that occurred during fall from 1979 to 2009, for all jets (top figure) and for jets at each of the NARR time steps (bottom figures). Gridpoints with no jet cases and/or surface elevations >2km MSL are shown in white.

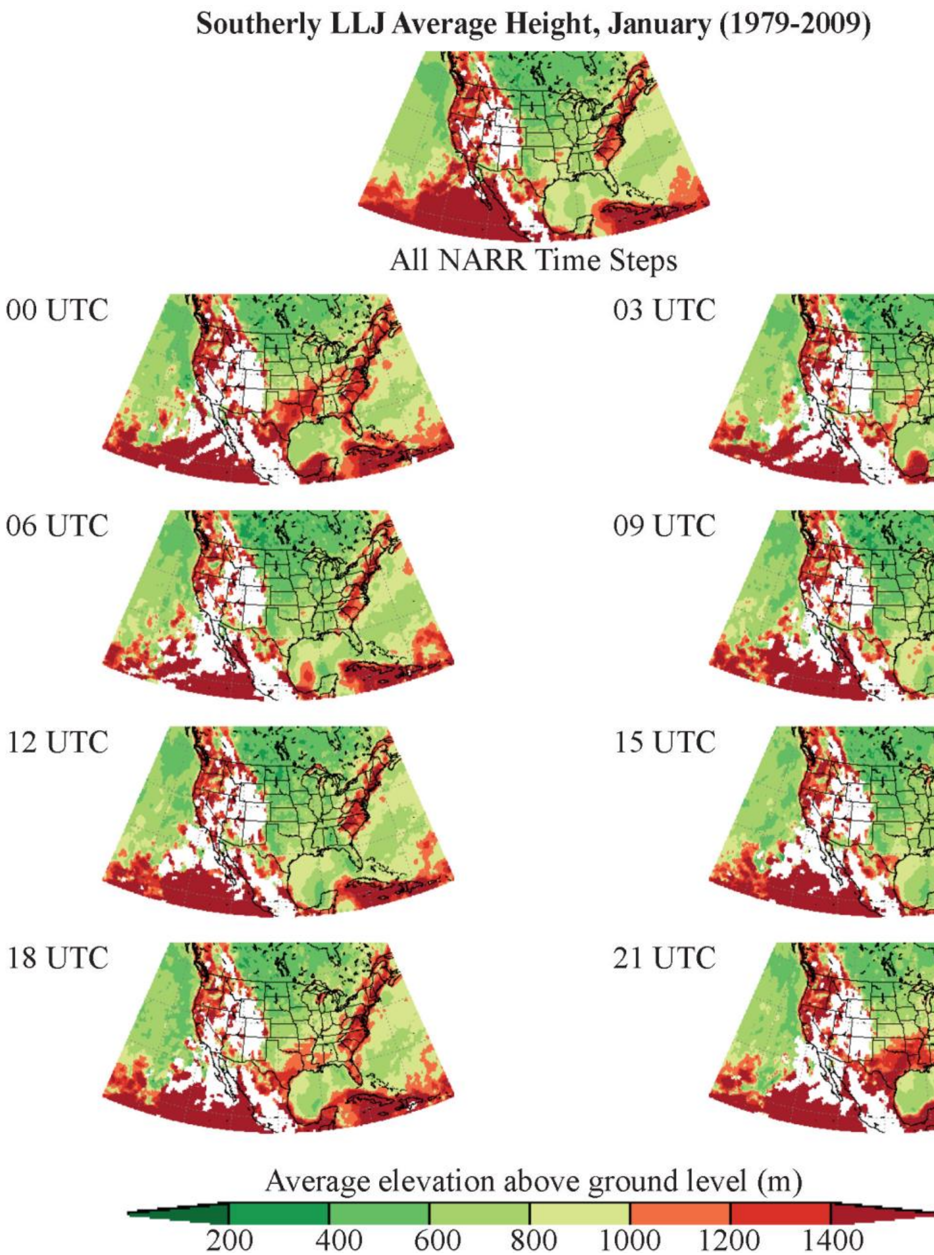

Figure 117. Average elevation (meters of above ground level) for S-LLJs that occurred during January from 1979 to 2009, for all jets (top figure) and for jets at each of the NARR time steps (bottom figures). Gridpoints with no jet cases and/or surface elevations >2km MSL are shown in white.

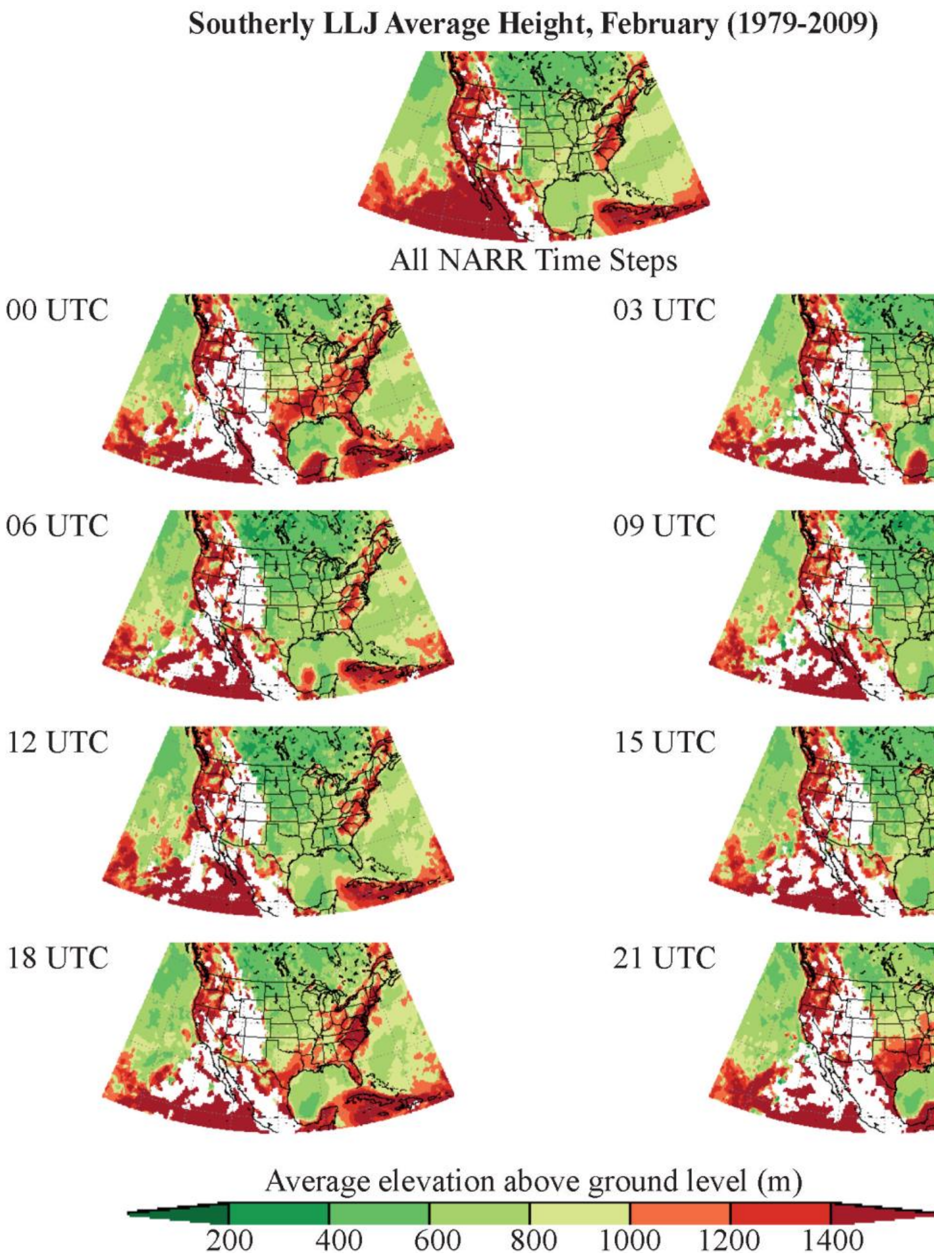

Figure 118. Average elevation (meters of above ground level) for S-LLJs that occurred during February from 1979 to 2009, for all jets (top figure) and for jets at each of the NARR time steps (bottom figures). Gridpoints with no jet cases and/or surface elevations >2km MSL are shown in white.

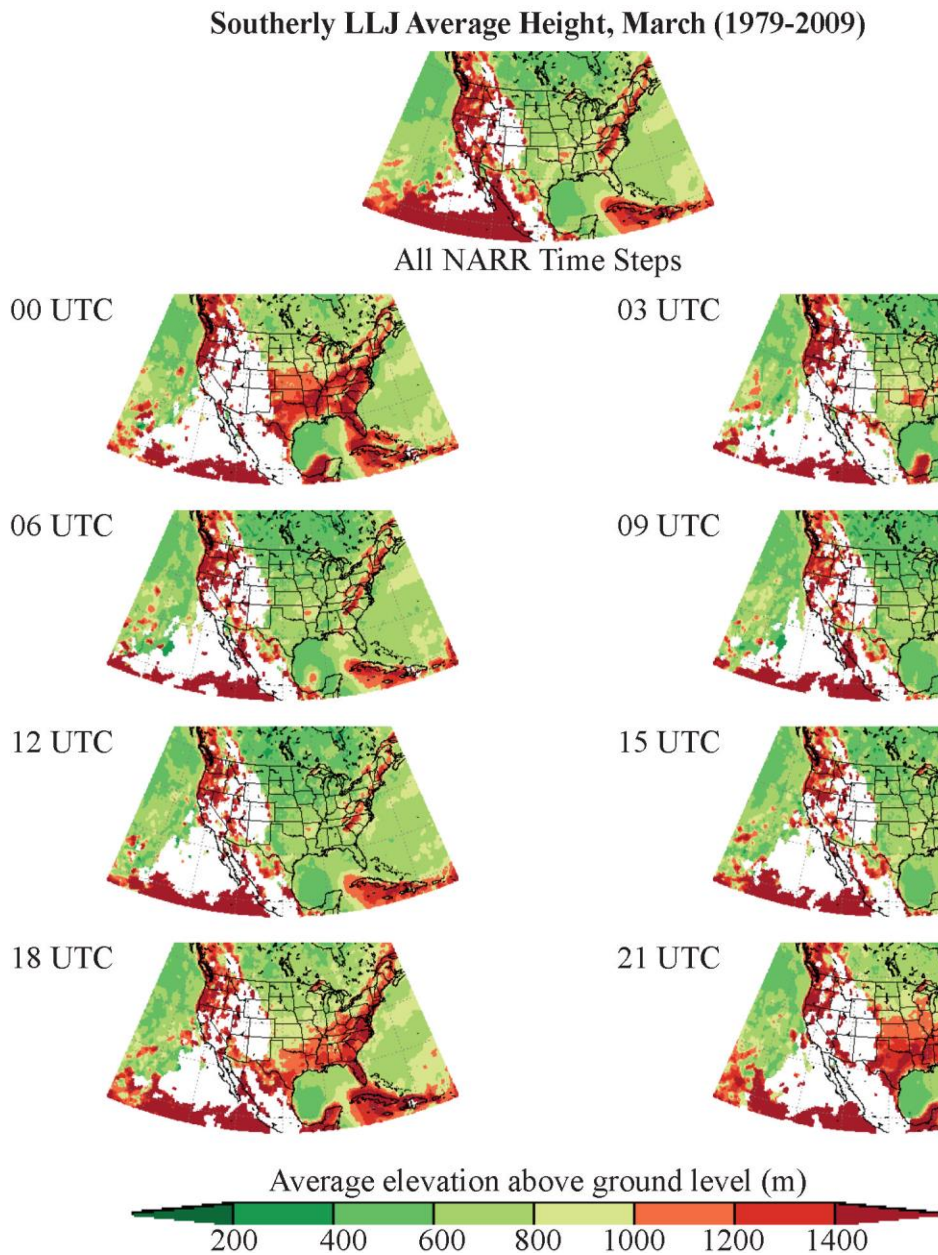

Figure 119. Average elevation (meters of above ground level) for S-LLJs that occurred during March from 1979 to 2009, for all jets (top figure) and for jets at each of the NARR time steps (bottom figures). Gridpoints with no jet cases and/or surface elevations >2km MSL are shown in white.

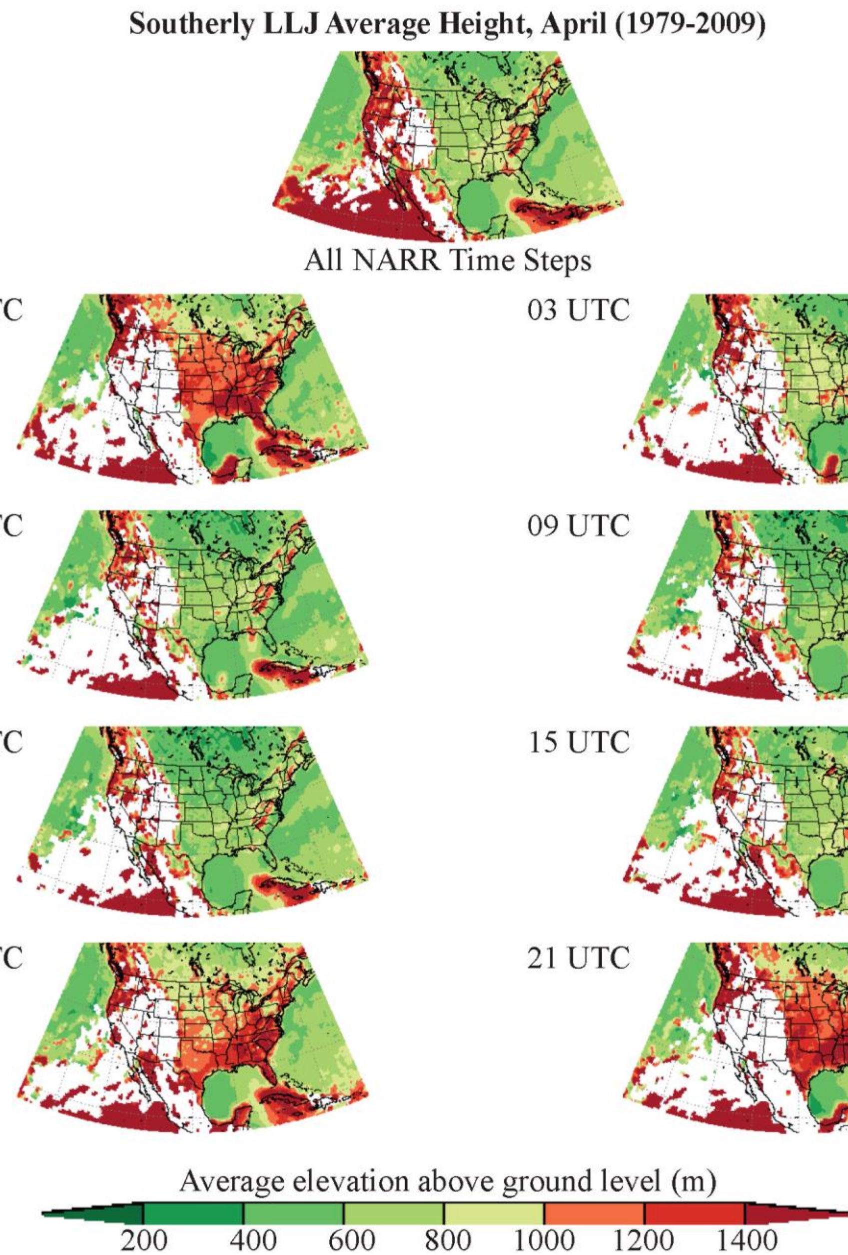

Figure 120. Average elevation (meters of above ground level) for S-LLJs that occurred during April from 1979 to 2009, for all jets (top figure) and for jets at each of the NARR time steps (bottom figures). Gridpoints with no jet cases and/or surface elevations >2km MSL are shown in white.

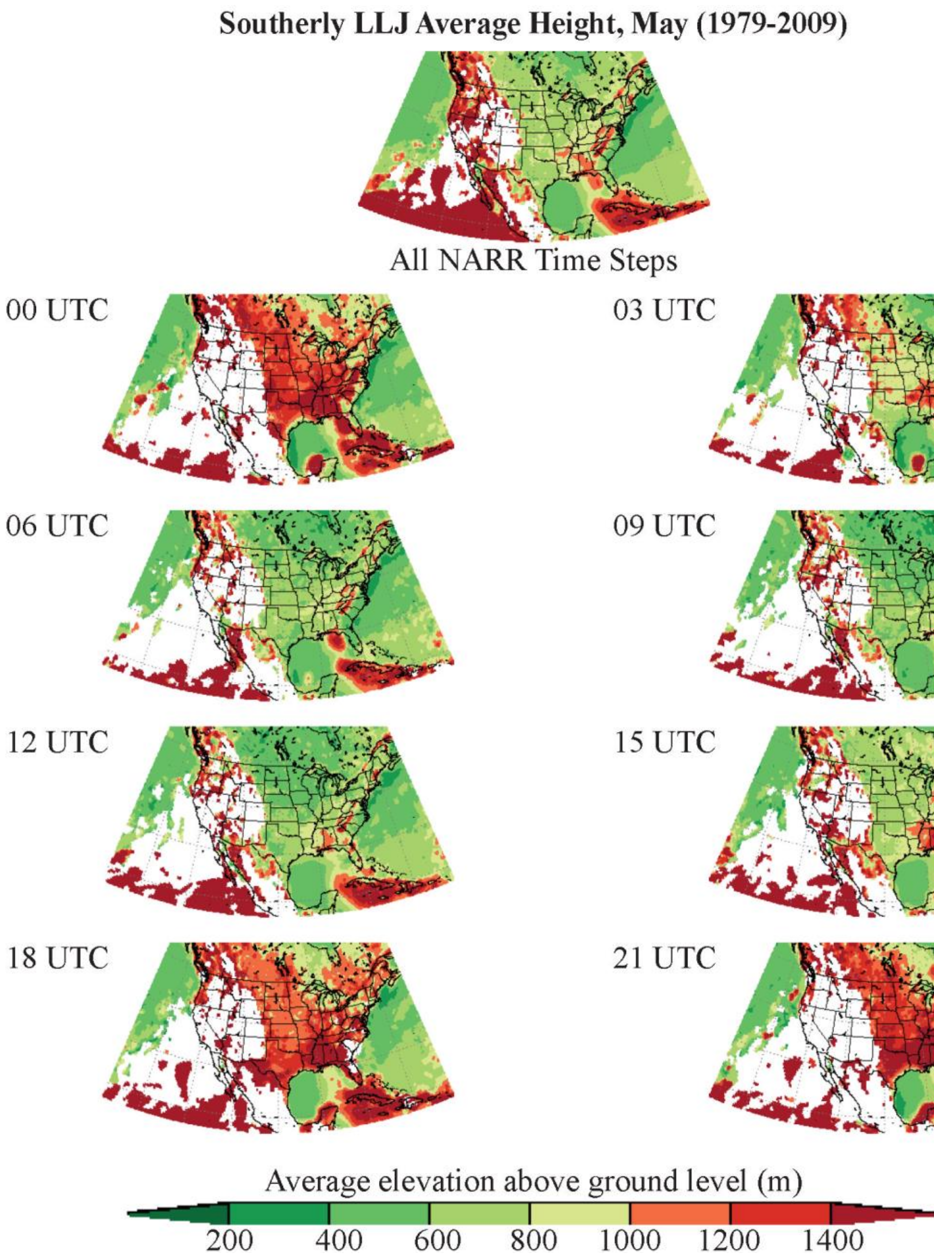

Figure 121. Average elevation (meters of above ground level) for S-LLJs that occurred during May from 1979 to 2009, for all jets (top figure) and for jets at each of the NARR time steps (bottom figures). Gridpoints with no jet cases and/or surface elevations >2km MSL are shown in white.

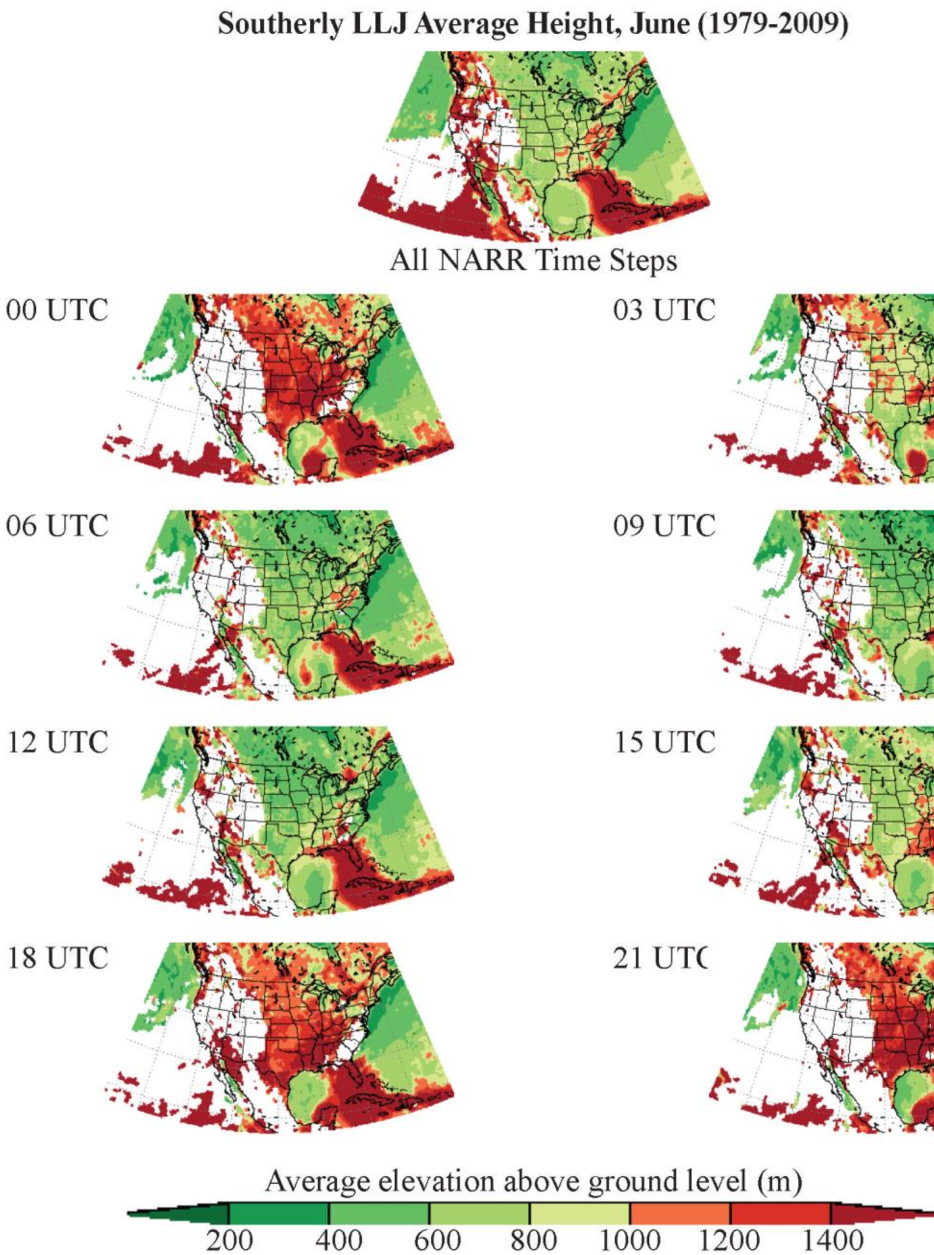

Figure 122. Average elevation (meters of above ground level) for S-LLJs that occurred during June from 1979 to 2009, for all jets (top figure) and for jets at each of the NARR time steps (bottom figures). Gridpoints with no jet cases and/or surface elevations >2km MSL are shown in white.

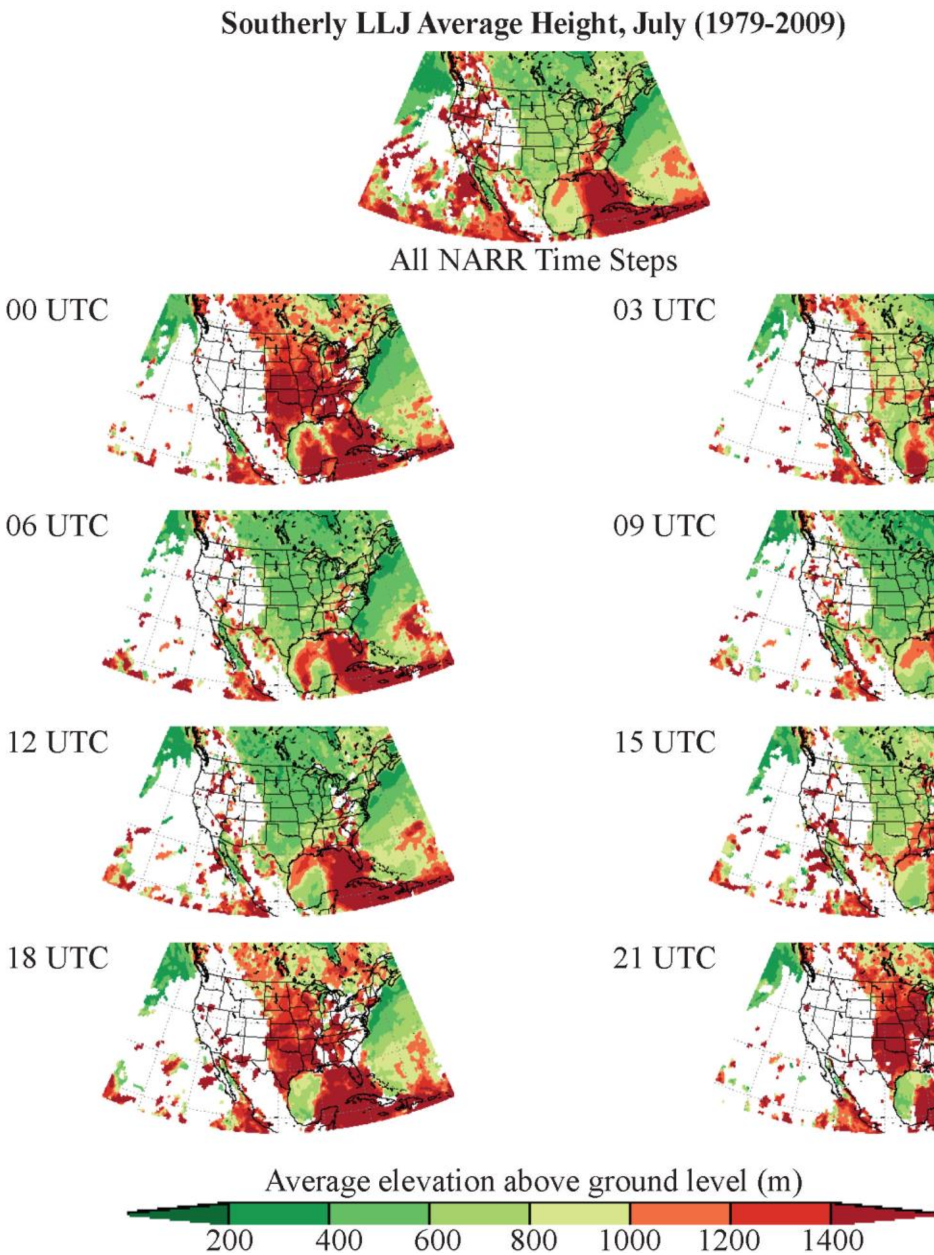

Figure 123. Average elevation (meters of above ground level) for S-LLJs that occurred during July from 1979 to 2009, for all jets (top figure) and for jets at each of the NARR time steps (bottom figures). Gridpoints with no jet cases and/or surface elevations >2km MSL are shown in white.

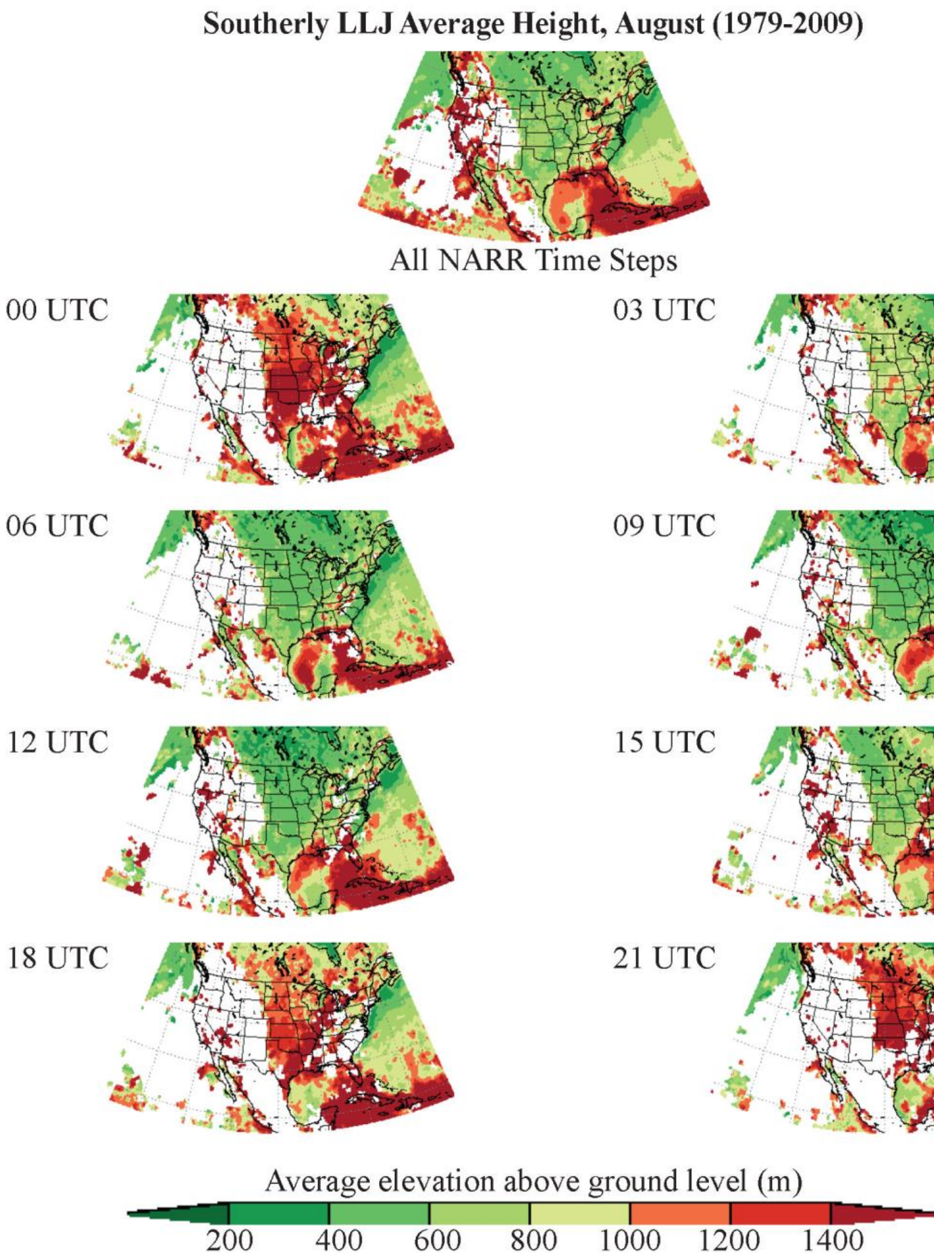

Figure 124. Average elevation (meters of above ground level) for S-LLJs that occurred during August from 1979 to 2009, for all jets (top figure) and for jets at each of the NARR time steps (bottom figures). Gridpoints with no jet cases and/or surface elevations >2km MSL are shown in white.

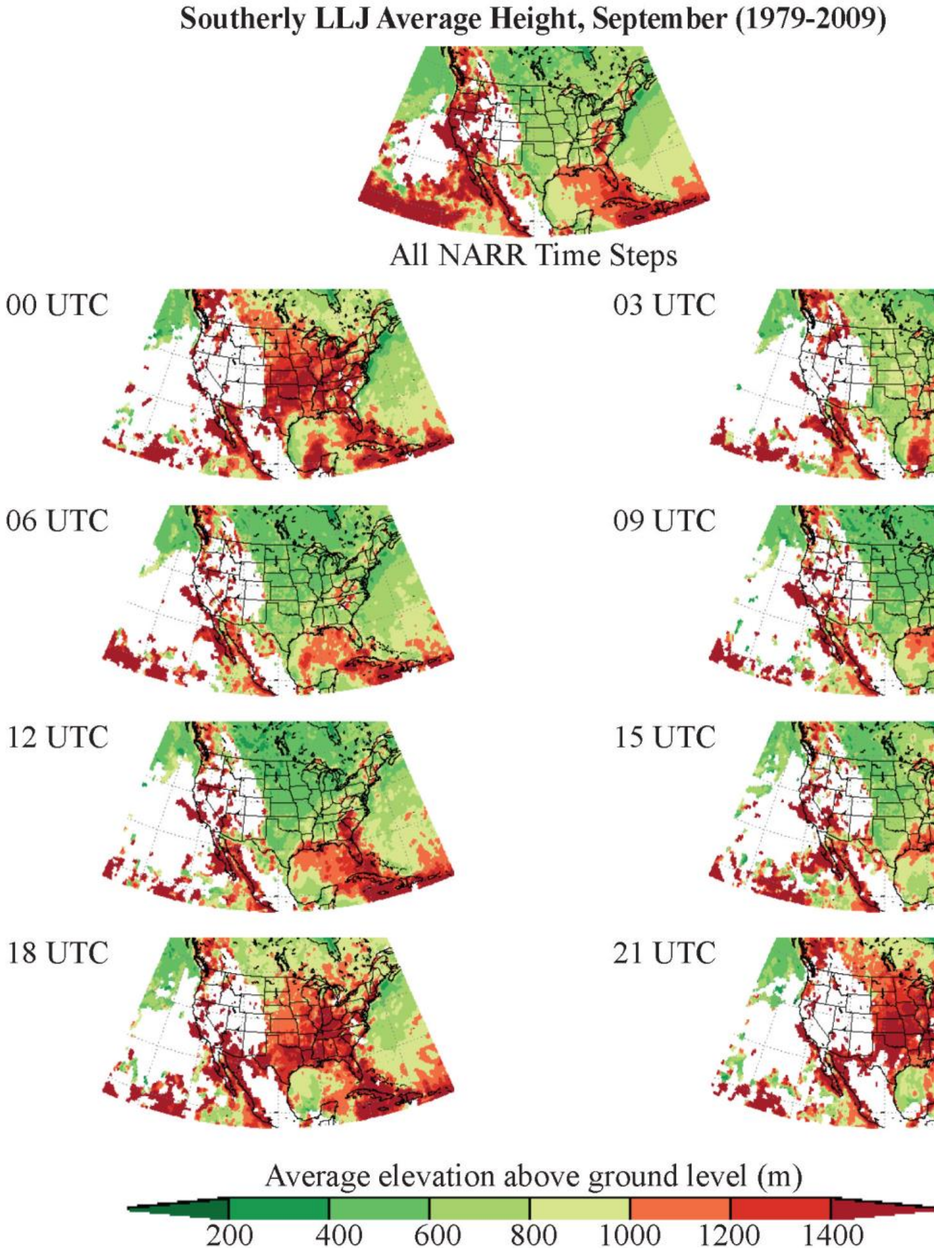

Figure 125. Average elevation (meters of above ground level) for S-LLJs that occurred during September from 1979 to 2009, for all jets (top figure) and for jets at each of the NARR time steps (bottom figures). Gridpoints with no jet cases and/or surface elevations >2km MSL are shown in white.

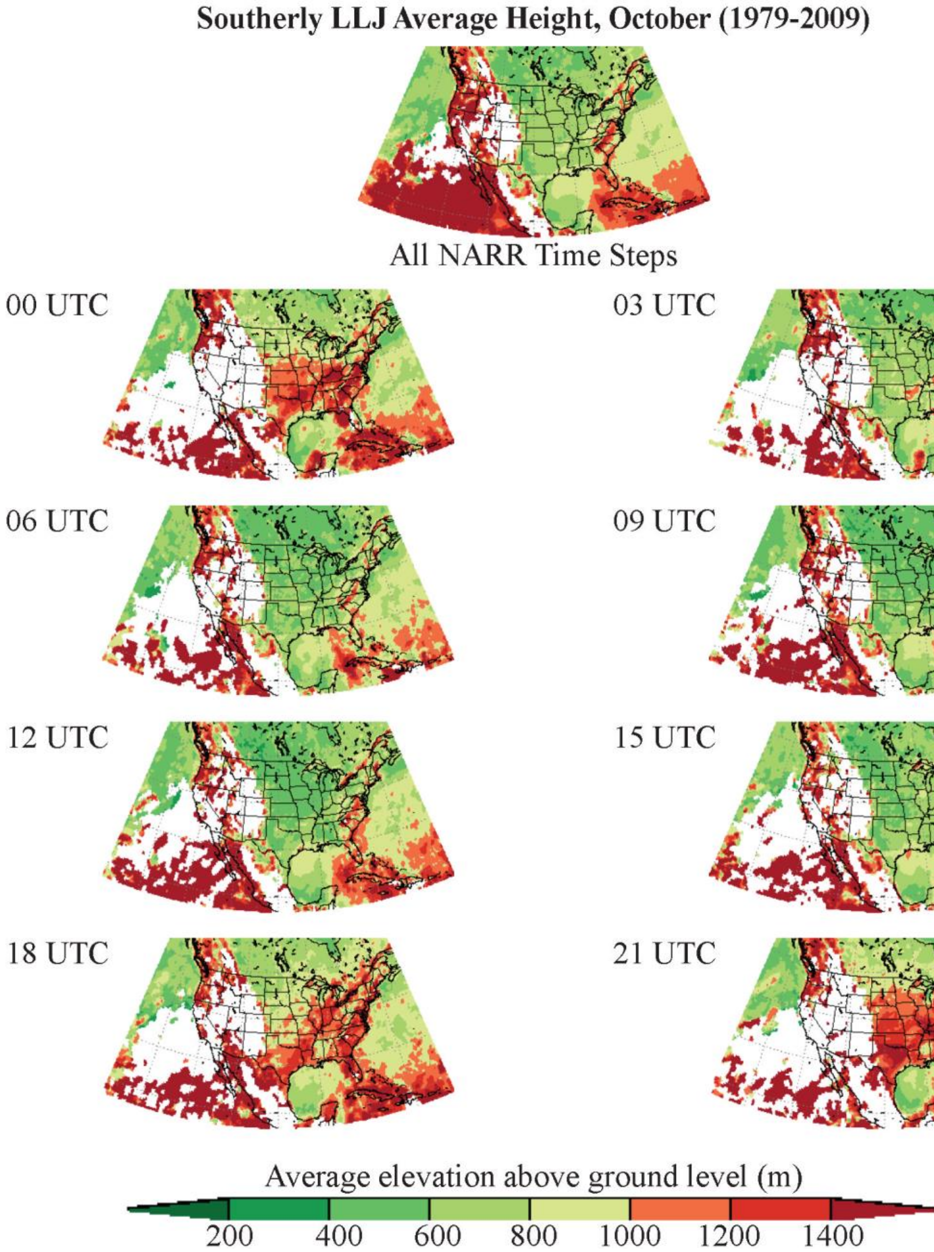

Figure 126. Average elevation (meters of above ground level) for S-LLJs that occurred during October from 1979 to 2009, for all jets (top figure) and for jets at each of the NARR time steps (bottom figures). Gridpoints with no jet cases and/or surface elevations >2km MSL are shown in white.

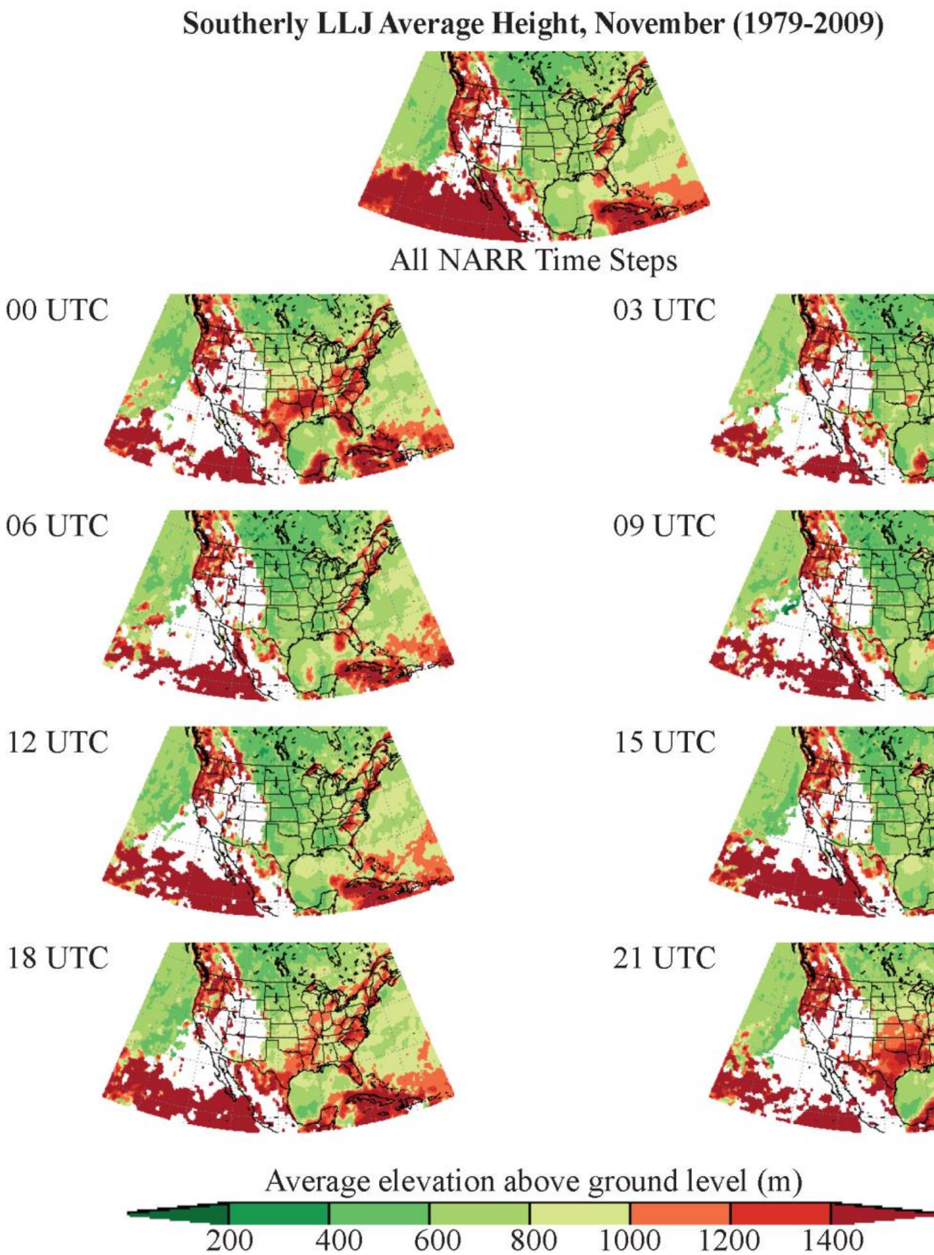

Figure 127. Average elevation (meters of above ground level) for S-LLJs that occurred during November from 1979 to 2009, for all jets (top figure) and for jets at each of the NARR time steps (bottom figures). Gridpoints with no jet cases and/or surface elevations >2km MSL are shown in white.

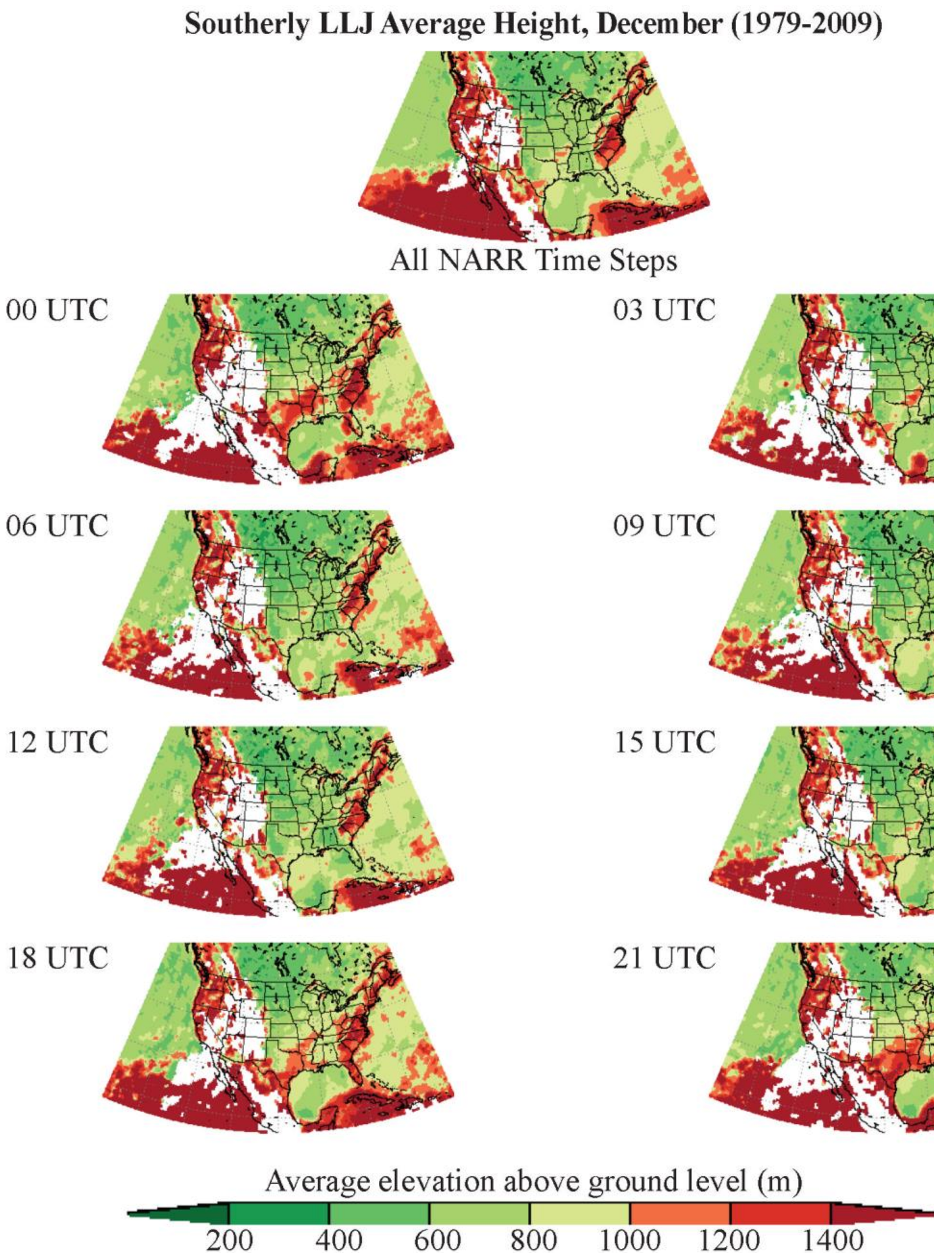

Figure 128. Average elevation (meters of above ground level) for S-LLJs that occurred during December from 1979 to 2009, for all jets (top figure) and for jets at each of the NARR time steps (bottom figures). Gridpoints with no jet cases and/or surface elevations >2km MSL are shown in white.

APPENDIX F

Average Elevation of Northerly Low-Level Jets

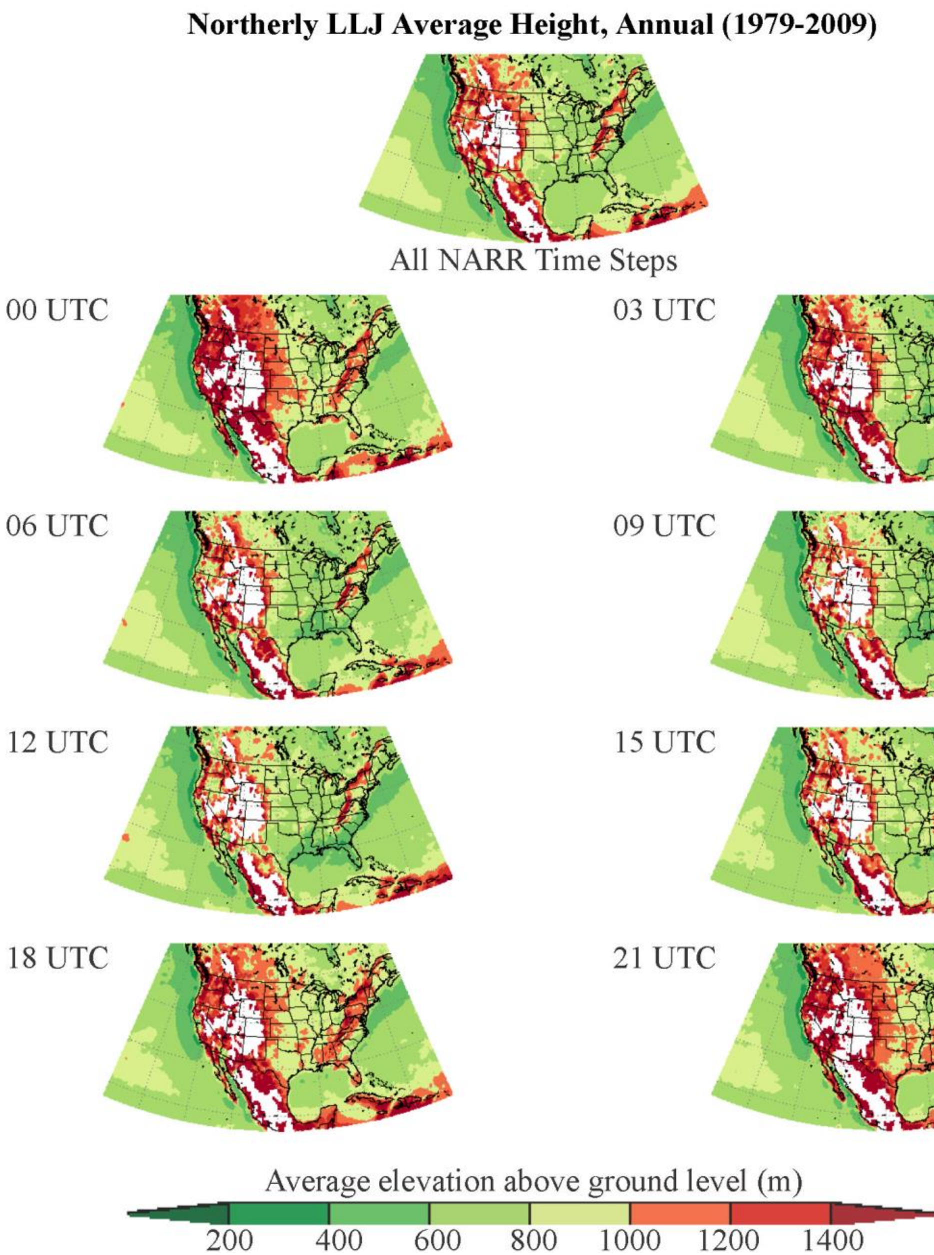

Figure 129. Annual average elevation (meters of above ground level) for N-LLJs that from 1979 to 2009, for all jets (top figure) and for jets at each of the NARR time steps (bottom figures). Gridpoints with no jet cases and/or surface elevations >2km MSL are shown in white.

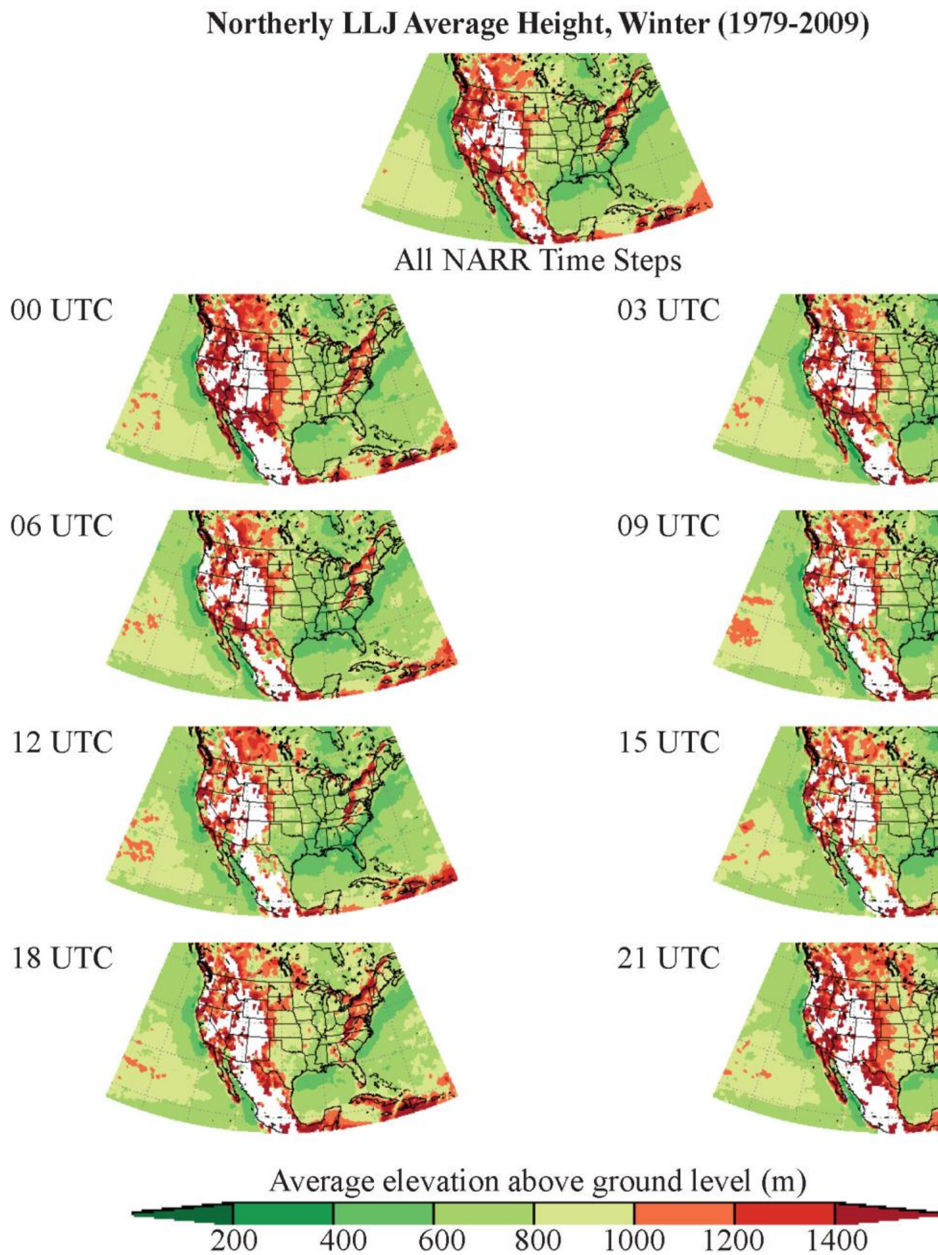

Figure 130. Average elevation (meters of above ground level) for N-LLJs that occurred during winter from 1979 to 2009, for all jets (top figure) and for jets at each of the NARR time steps (bottom figures). Gridpoints with no jet cases and/or surface elevations >2km MSL are shown in white.

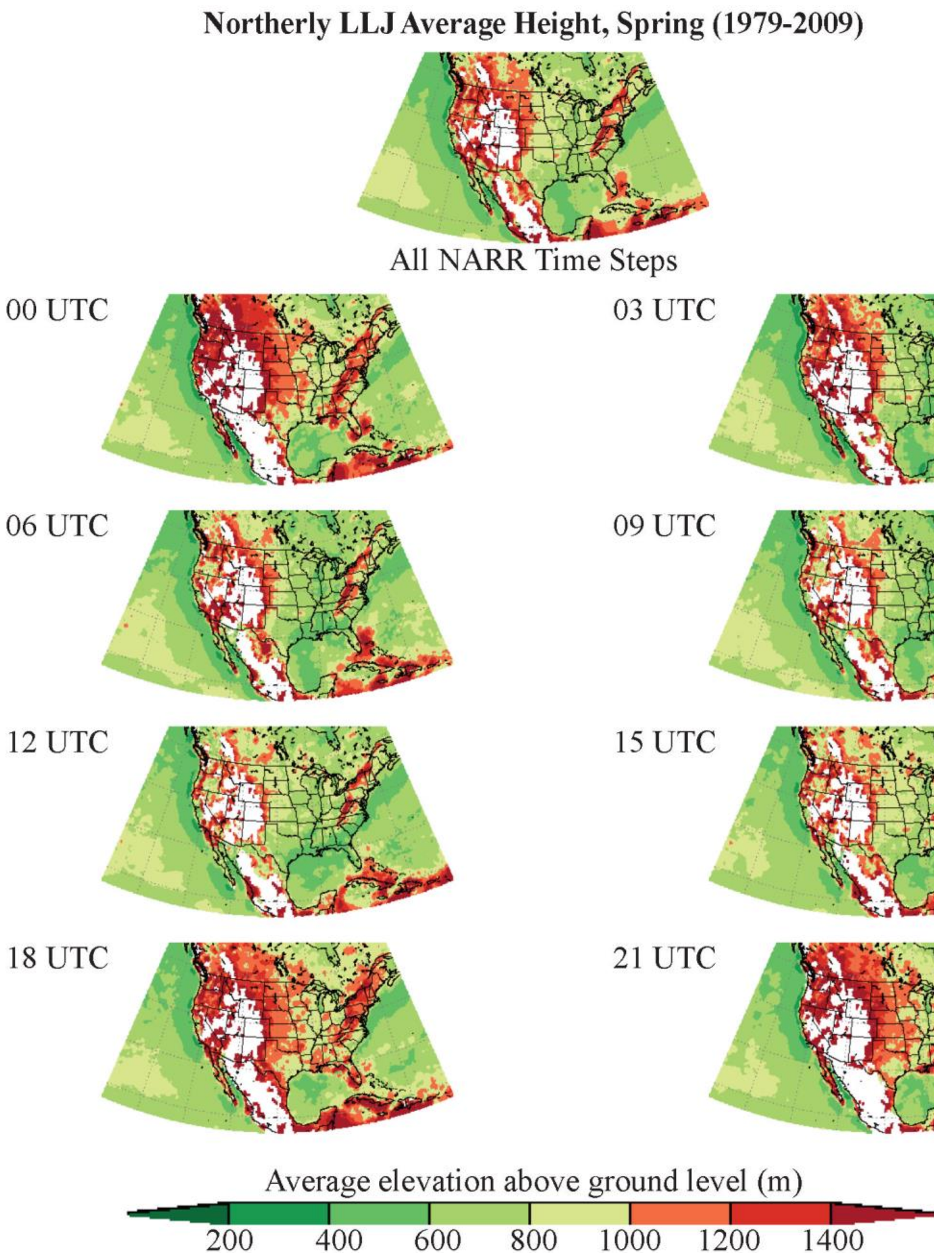

Figure 131. Average elevation (meters of above ground level) for N-LLJs that occurred during spring from 1979 to 2009, for all jets (top figure) and for jets at each of the NARR time steps (bottom figures). Gridpoints with no jet cases and/or surface elevations >2km MSL are shown in white.

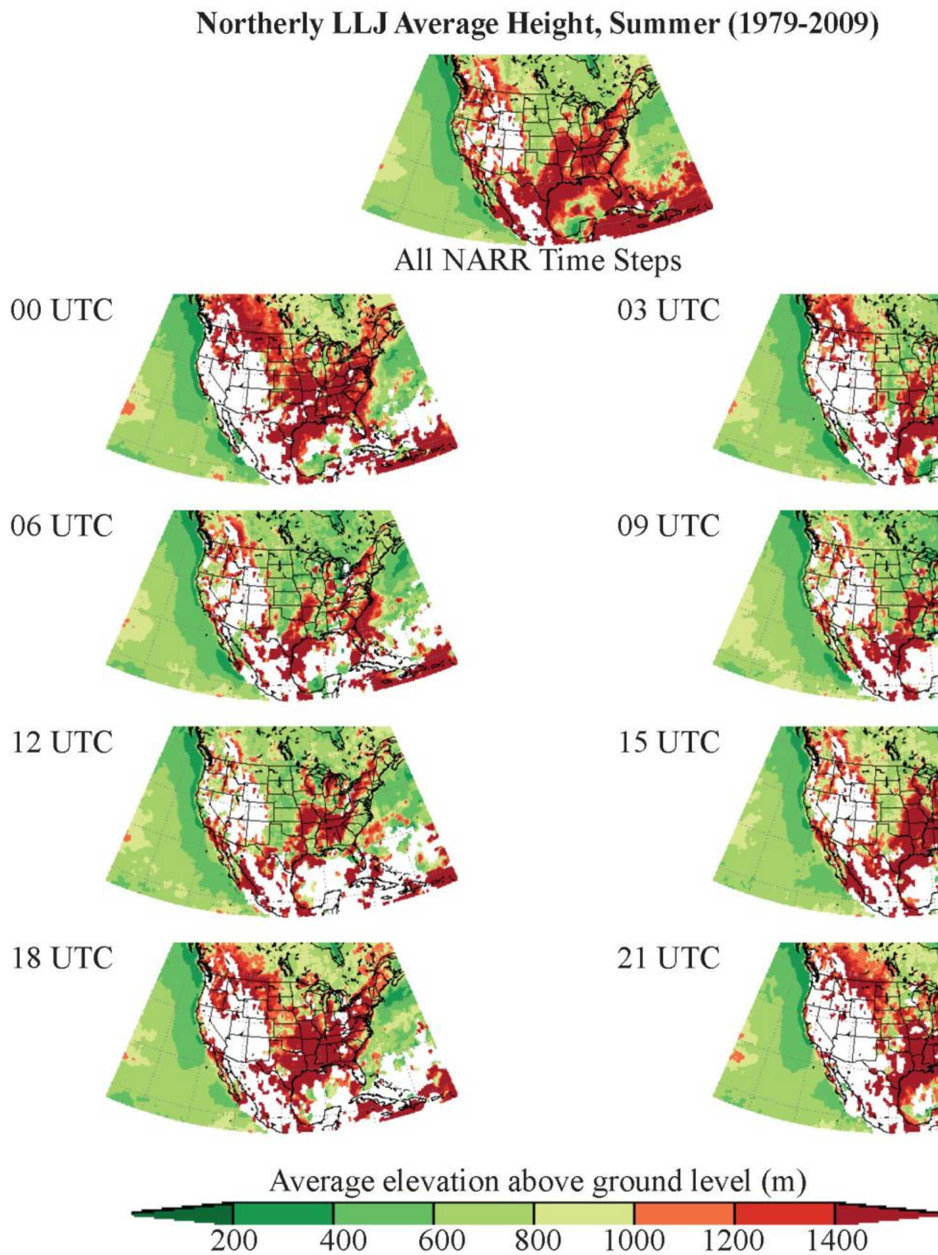

Figure 132. Average elevation (meters of above ground level) for N-LLJs that occurred during summer from 1979 to 2009, for all jets (top figure) and for jets at each of the NARR time steps (bottom figures). Gridpoints with no jet cases and/or surface elevations >2km MSL are shown in white.

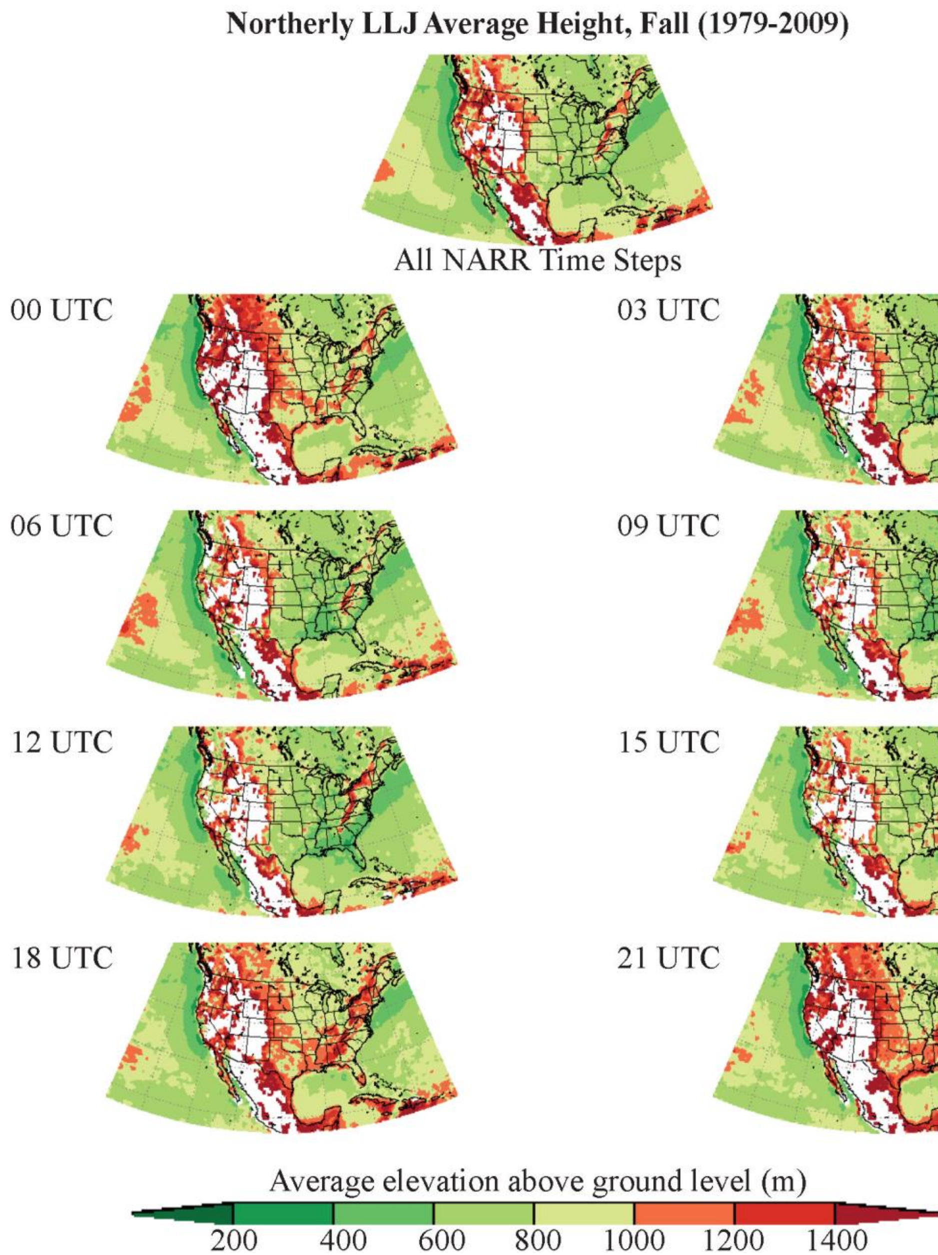

Figure 133. Average elevation (meters of above ground level) for N-LLJs that occurred during fall from 1979 to 2009, for all jets (top figure) and for jets at each of the NARR time steps (bottom figures). Gridpoints with no jet cases and/or surface elevations >2km MSL are shown in white.

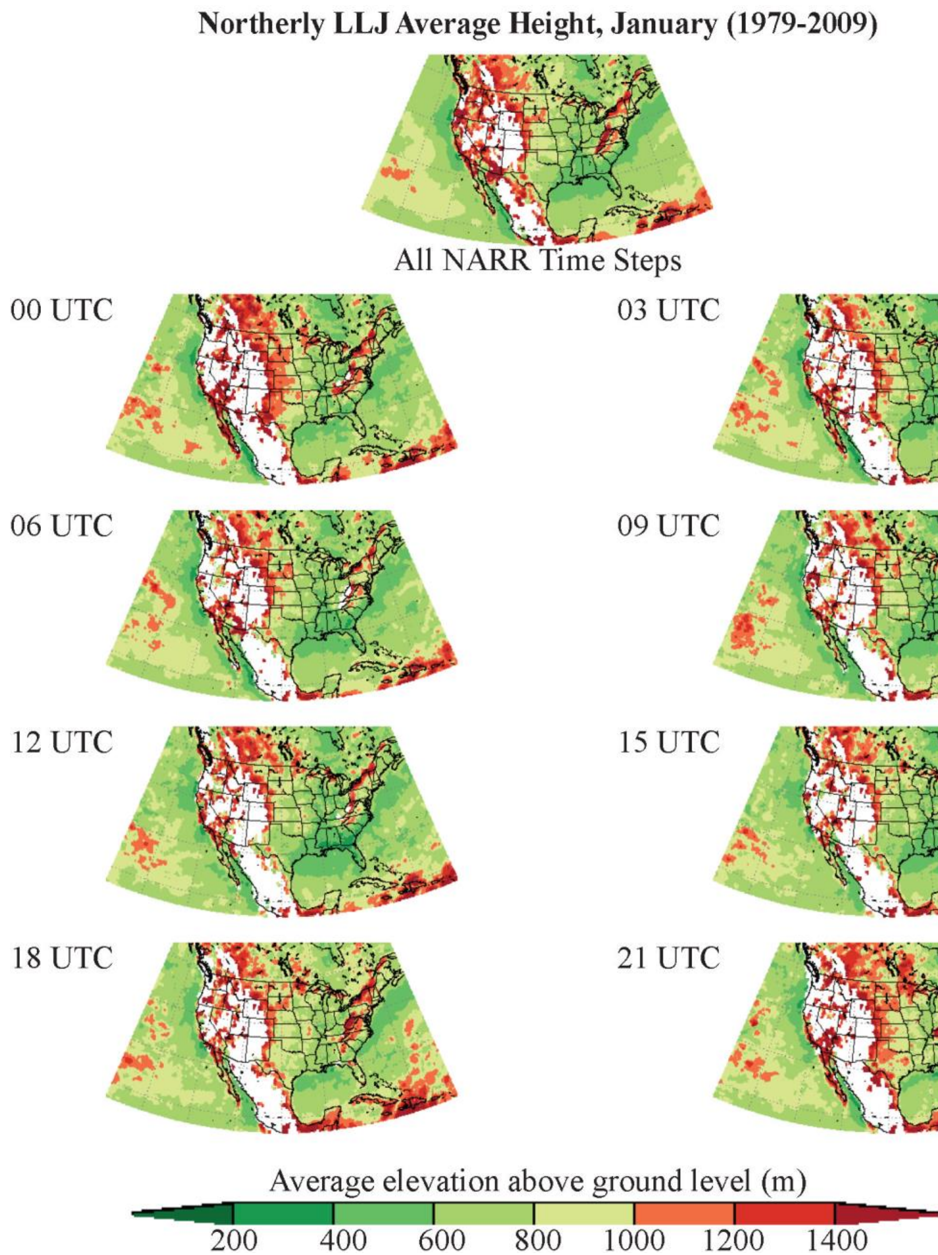

Figure 134. Average elevation (meters of above ground level) for N-LLJs that occurred during January from 1979 to 2009, for all jets (top figure) and for jets at each of the NARR time steps (bottom figures). Gridpoints with no jet cases and/or surface elevations >2km MSL are shown in white.

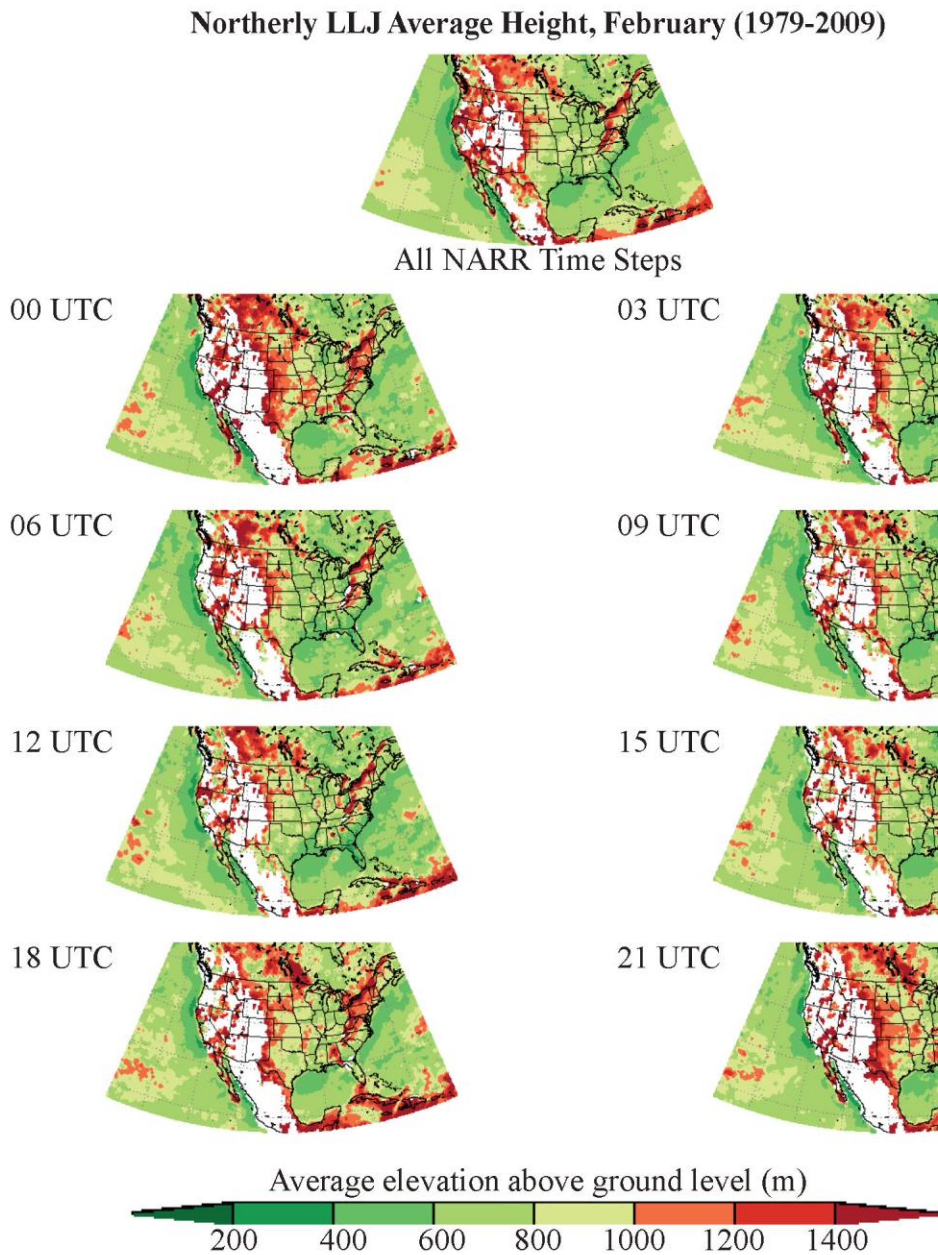

Figure 135. Average elevation (meters of above ground level) for N-LLJs that occurred during February from 1979 to 2009, for all jets (top figure) and for jets at each of the NARR time steps (bottom figures). Gridpoints with no jet cases and/or surface elevations >2km MSL are shown in white.

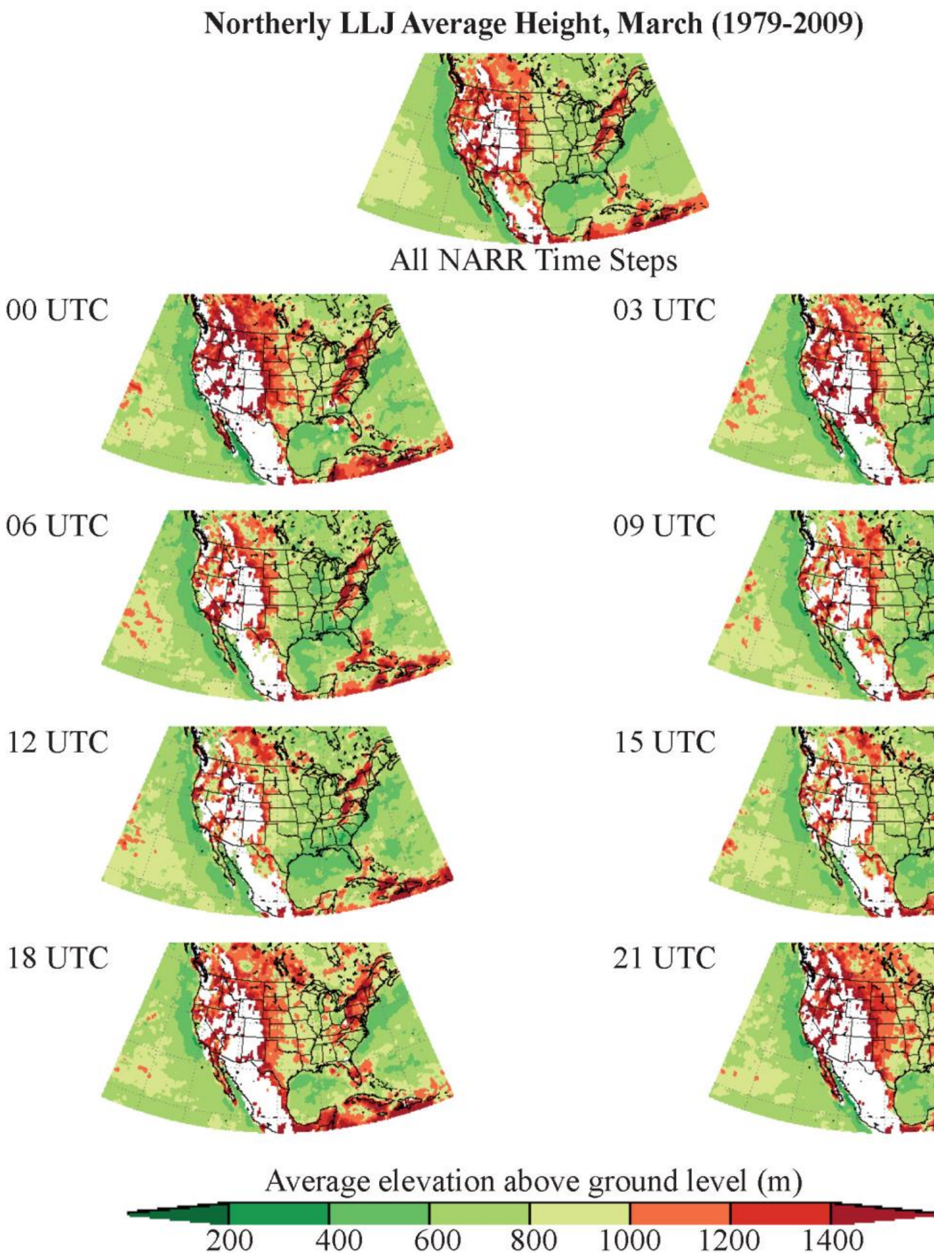

Figure 136. Average elevation (meters of above ground level) for N-LLJs that occurred during March from 1979 to 2009, for all jets (top figure) and for jets at each of the NARR time steps (bottom figures). Gridpoints with no jet cases and/or surface elevations >2km MSL are shown in white.

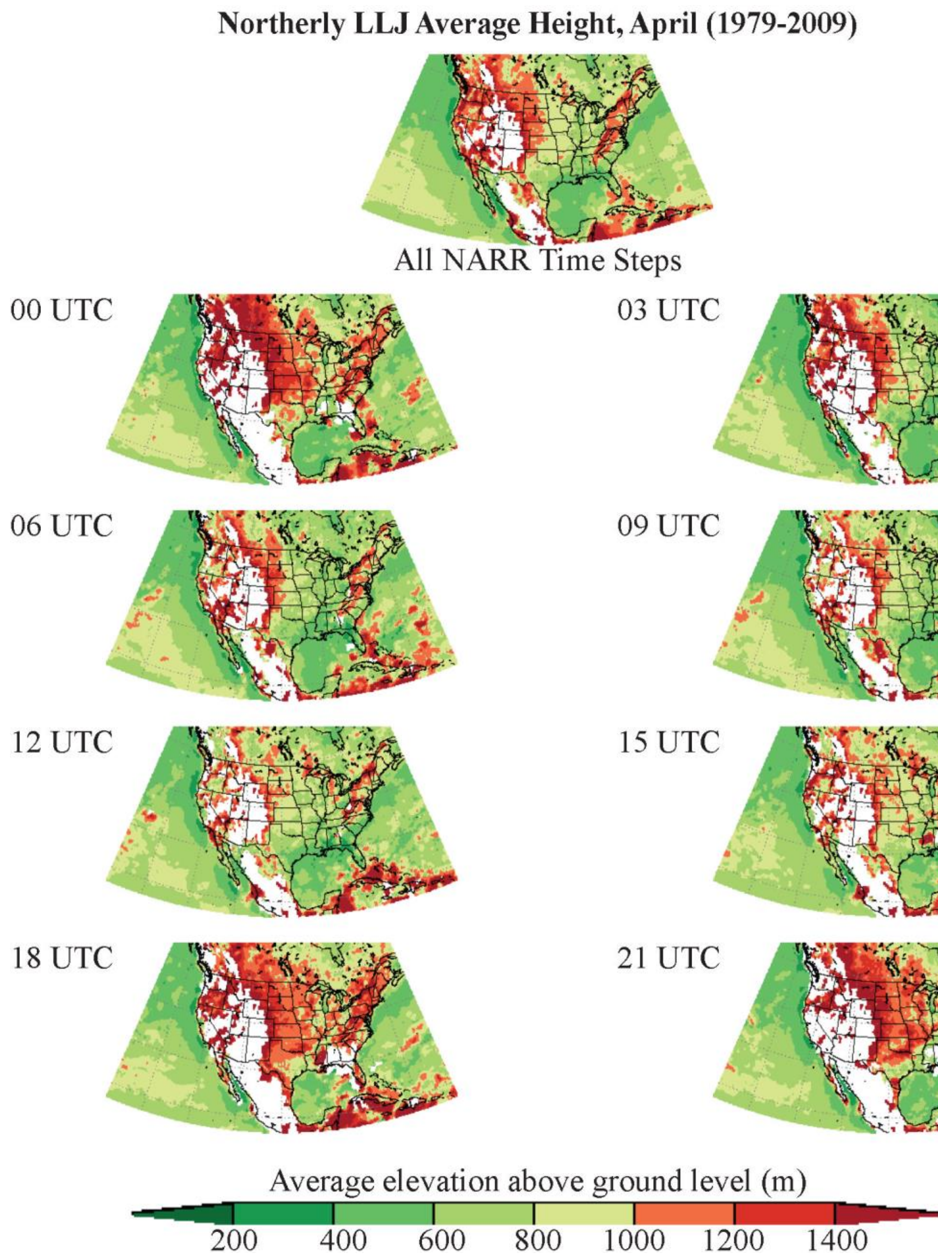

Figure 137. Average elevation (meters of above ground level) for N-LLJs that occurred during April from 1979 to 2009, for all jets (top figure) and for jets at each of the NARR time steps (bottom figures). Gridpoints with no jet cases and/or surface elevations >2km MSL are shown in white.

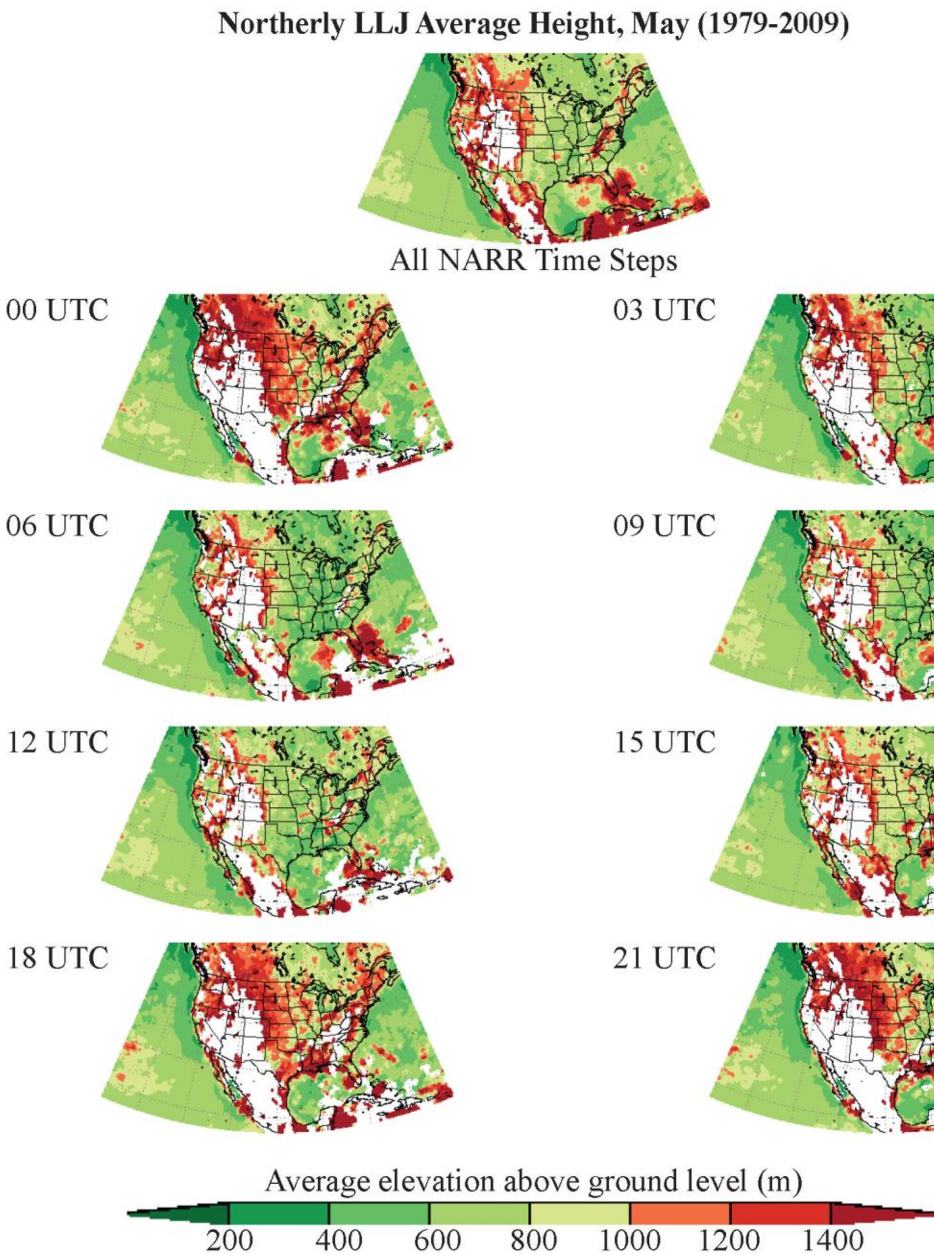

Figure 138. Average elevation (meters of above ground level) for N-LLJs that occurred during May from 1979 to 2009, for all jets (top figure) and for jets at each of the NARR time steps (bottom figures). Gridpoints with no jet cases and/or surface elevations >2km MSL are shown in white.

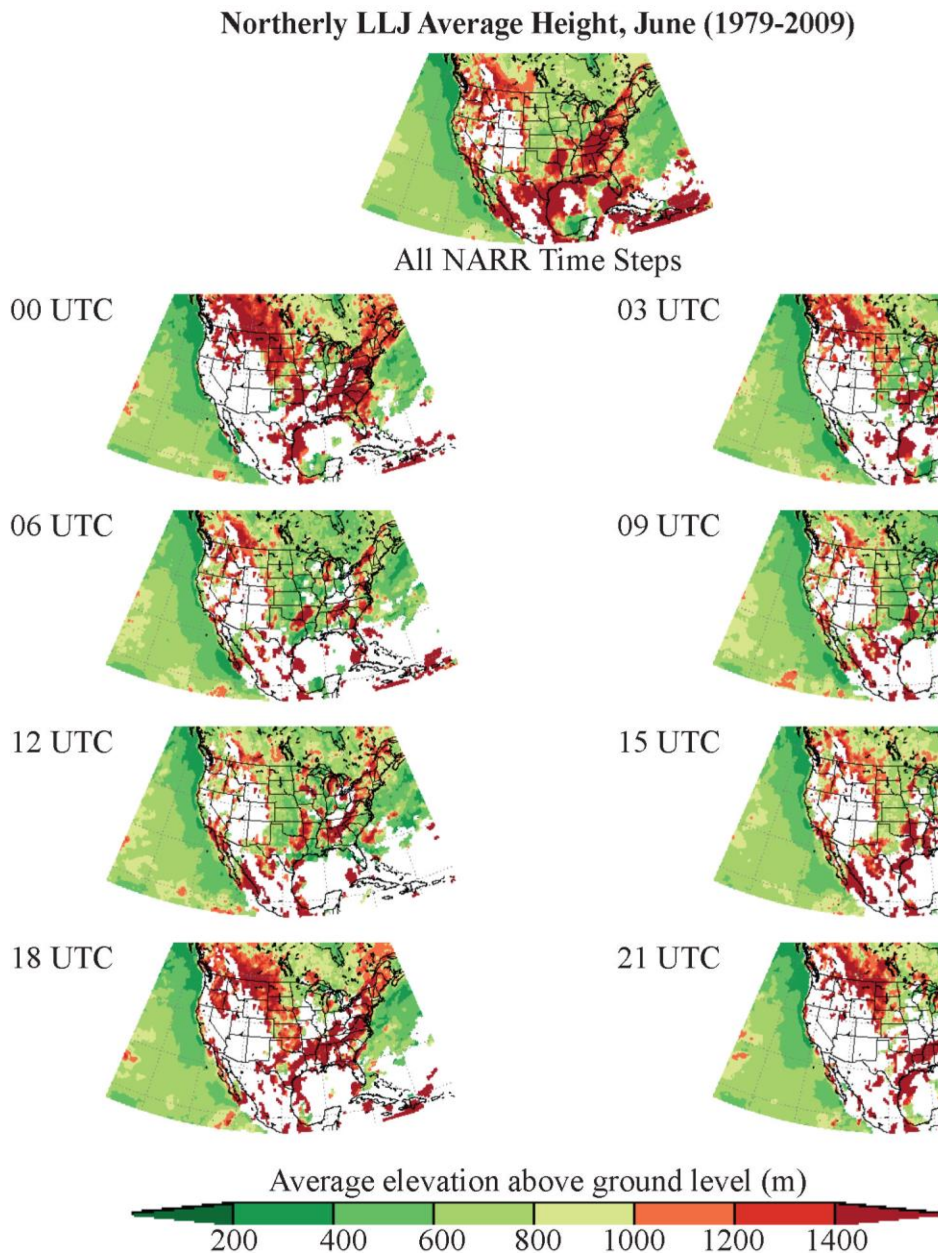

Figure 139. Average elevation (meters of above ground level) for N-LLJs that occurred during June from 1979 to 2009, for all jets (top figure) and for jets at each of the NARR time steps (bottom figures). Gridpoints with no jet cases and/or surface elevations >2km MSL are shown in white.

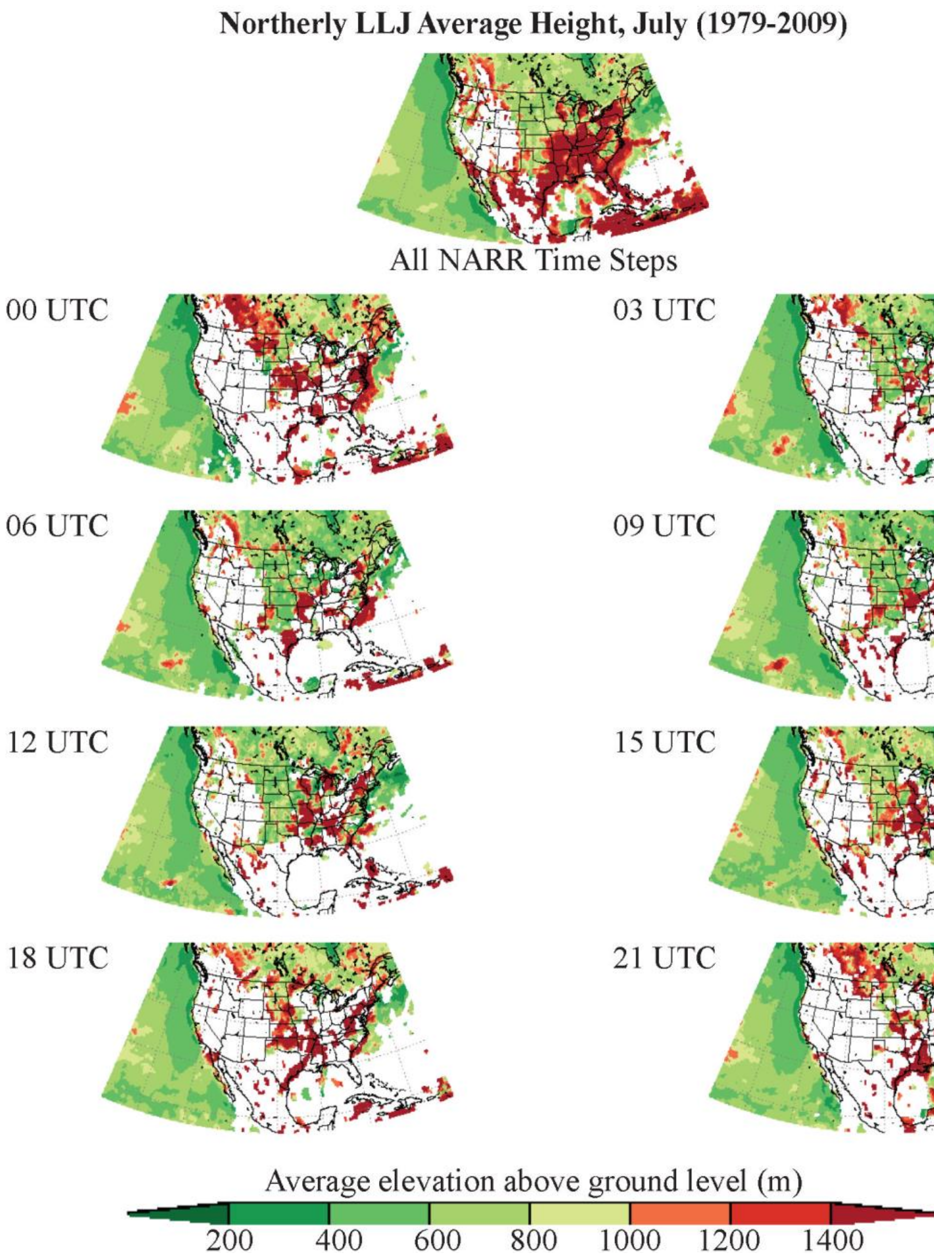

Figure 140. Average elevation (meters of above ground level) for N-LLJs that occurred during July from 1979 to 2009, for all jets (top figure) and for jets at each of the NARR time steps (bottom figures). Gridpoints with no jet cases and/or surface elevations >2km MSL are shown in white.

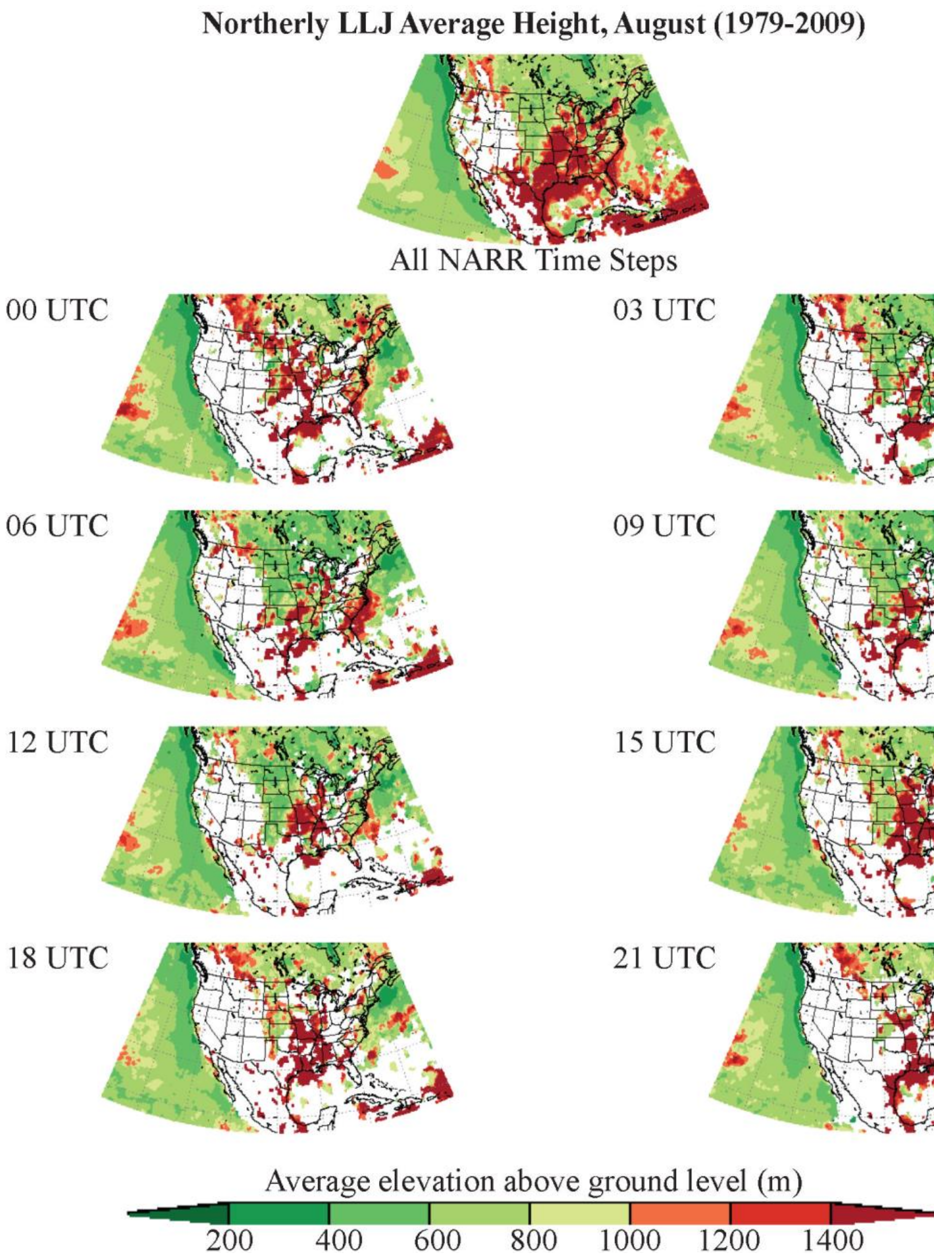

Figure 141. Average elevation (meters of above ground level) for N-LLJs that occurred during August from 1979 to 2009, for all jets (top figure) and for jets at each of the NARR time steps (bottom figures). Gridpoints with no jet cases and/or surface elevations >2km MSL are shown in white.

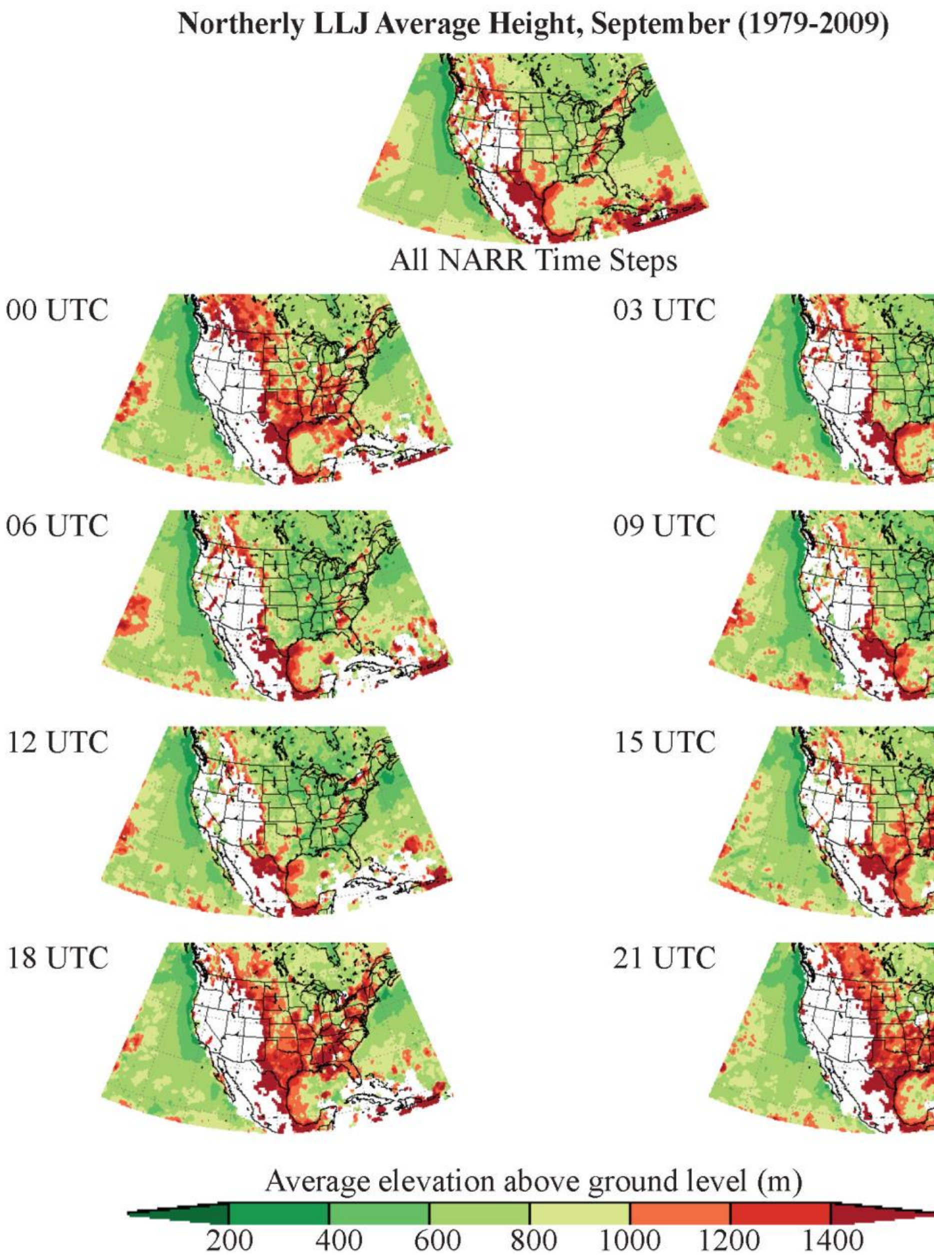

Figure 142. Average elevation (meters of above ground level) for N-LLJs that occurred during September from 1979 to 2009, for all jets (top figure) and for jets at each of the NARR time steps (bottom figures). Gridpoints with no jet cases and/or surface elevations >2km MSL are shown in white.

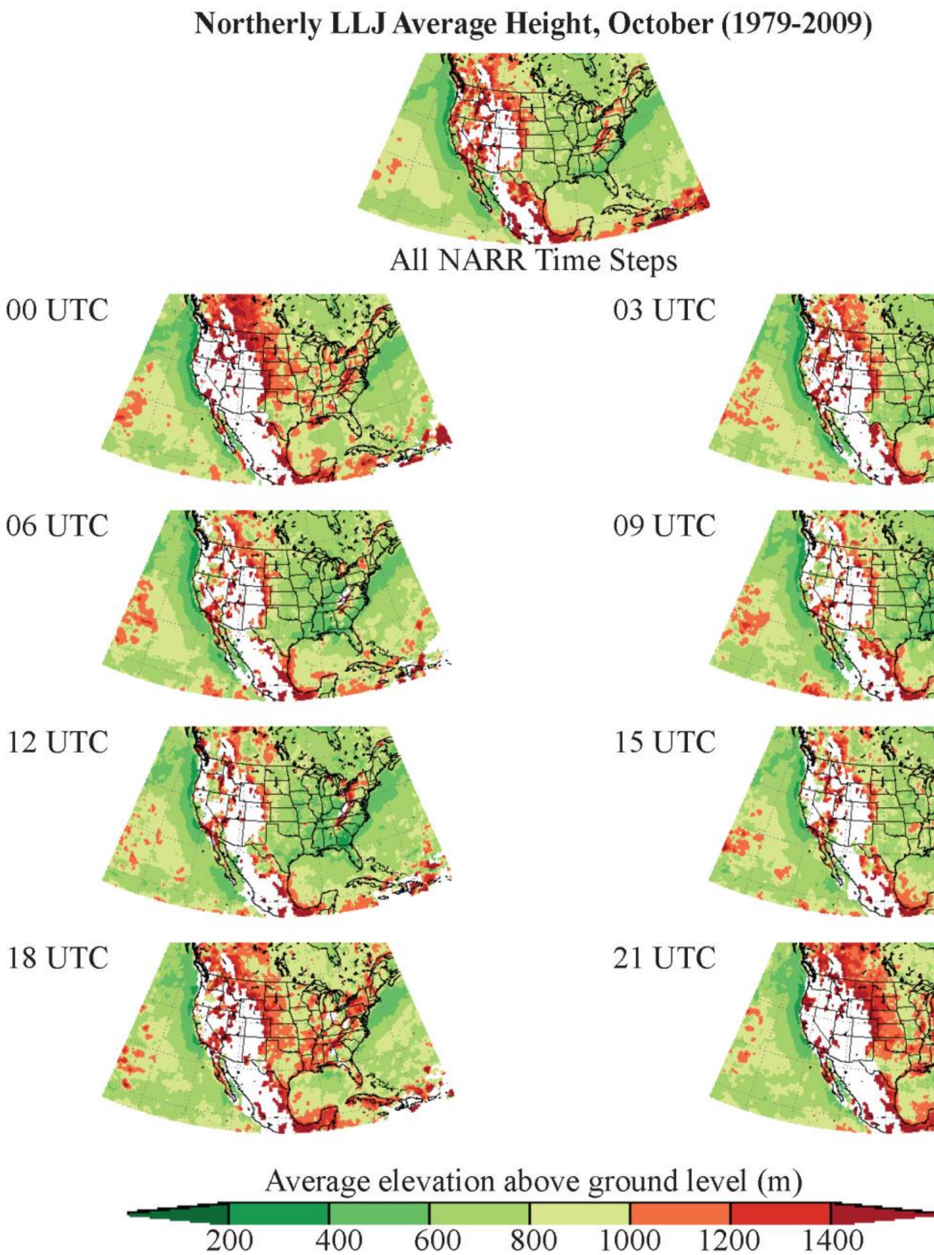

Figure 143. Average elevation (meters of above ground level) for N-LLJs that occurred during October from 1979 to 2009, for all jets (top figure) and for jets at each of the NARR time steps (bottom figures). Gridpoints with no jet cases and/or surface elevations >2km MSL are shown in white.

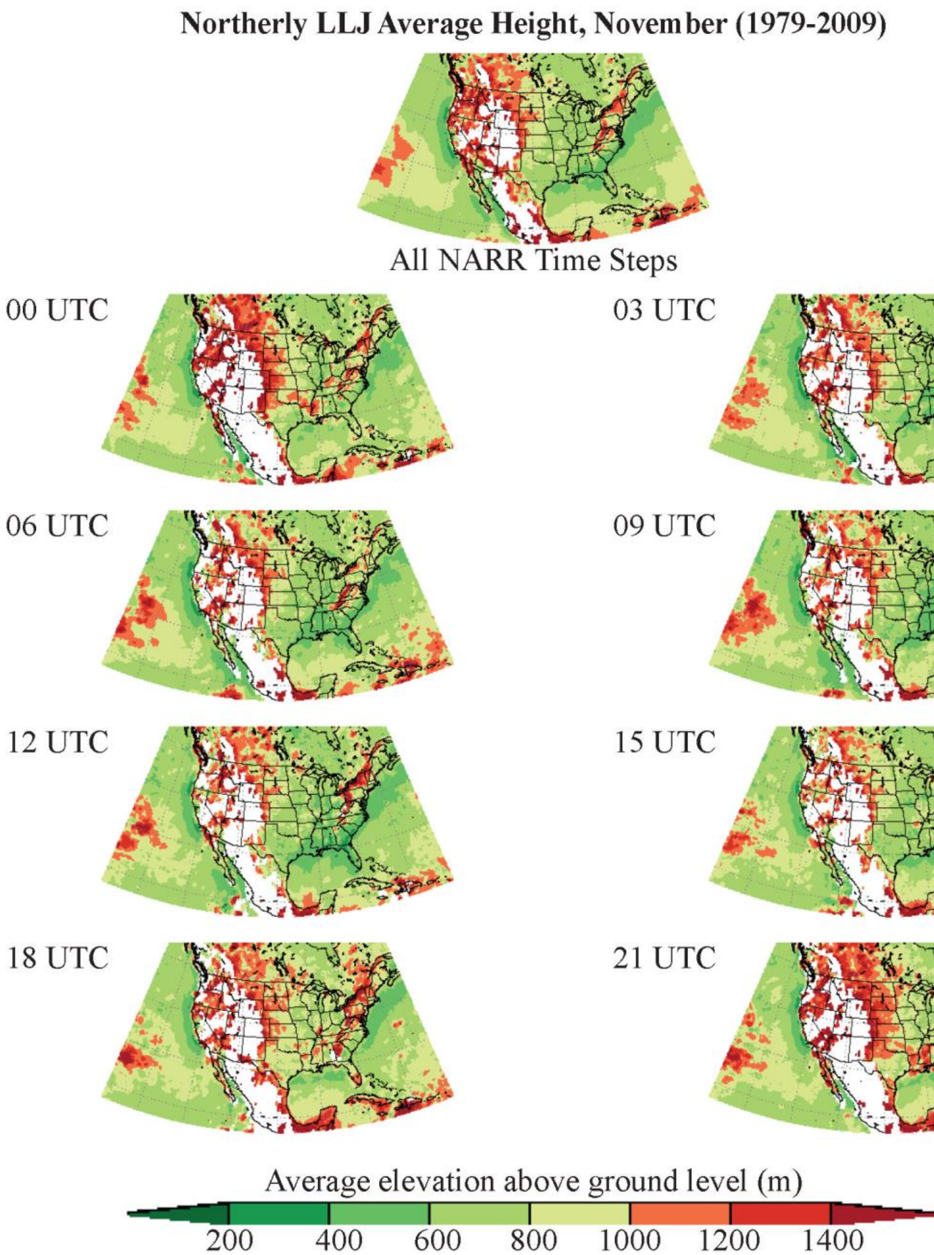

Figure 144. Average elevation (meters of above ground level) for N-LLJs that occurred during November from 1979 to 2009, for all jets (top figure) and for jets at each of the NARR time steps (bottom figures). Gridpoints with no jet cases and/or surface elevations >2km MSL are shown in white.

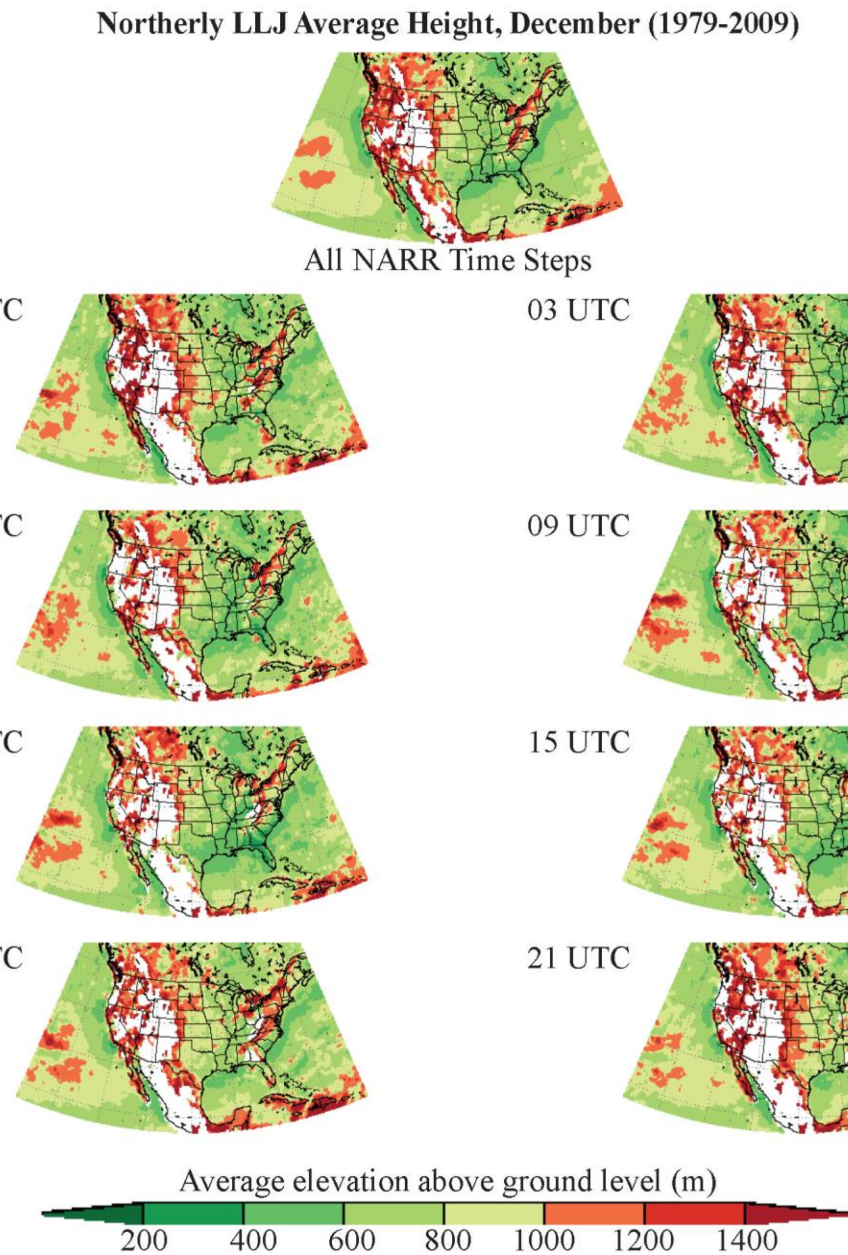

Figure 145. Average elevation (meters of above ground level) for N-LLJs that occurred during December from 1979 to 2009, for all jets (top figure) and for jets at each of the NARR time steps (bottom figures). Gridpoints with no jet cases and/or surface elevations >2km MSL are shown in white.

BIBLIOGRAPHY

BIBLIOGRAPHY

Amador, J. A., 2008: The Intra-Americas Sea low-level jet. *Ann. N. Y. Acad. Sci.*, **1146,** 153-188.

Andreas, E.L., K.J. Claffy, and A.P. Makshtas, 2000: Low-level atmospheric jets and inversions over the western Weddell Sea. *Boundary-Layer Meteor.*, **97,** 459-486.

Arritt, R.W., T.D. Rink, M. Segal, and D.P. Todey, 1997: The Great Plains low-level jet during the warm season of 1993. *Mon. Wea. Rev.*, **125,** 2176-2193.

Banta, R.M., R.K. Newsom, J.K. Lundquist, Y.L. Pichugina, R.L. Coulter, and L. Mahrt, 2002: Nocturnal low-level jet characteristics over Kansas during CASES-99. *Boundary-Layer Meteor.*, **105,** 221-252.

Bielli, S., P. Barbour, R. Samelson, E. Skyllingstad, and J. Wilczak, 2002: Numerical study of the diurnal cycle along the central Oregon coast during summertime northerly flow. *Mon. Wea. Rev.*, **130,** 992-1008.

Bierly, G. D., and J. A. Winkler, 2001: A composite analysis of airstreams within cold-season Colorado cyclones. *Wea. Forecasting*, **16,** 57-80.

Blackadar, A.K., 1957: Boundary layer wind maxima and their significance for the growth of nocturnal inversions. *Bull. Amer. Meteor. Soc.*, **38,** 282-290.

Bonner, W.D., 1966: Case study of thunderstorm activity in relation to the low-level jet. *Mon. Wea. Rev.*, **94,** 167-178.

Bonner, W.D., 1968: Climatology of the low-level jet. *Mon. Wea. Rev.*, **96,** 833-850.

Bonner, W. D. and J. Paegle, 1970: Diurnal variations in boundary layer winds over the south-central U.S. in summer. *Mon. Wea. Rev.*, **98,** 735-744.

Bosart, L. F., 1990: Degradation of the North American radiosonde network. *Wea. Forecasting*, **5,** 527-532.

Browning, K. A., and C.W. Pardoe, 1973: Structure of low-level jet streams ahead of mid-latitude cold fronts. *Q. J. R. Meteorol. Soc.*, **99,** 619-638.

Buajitti, K. and A. K. Blackadar, A. K., 1957: Theoretical studies of diurnal wind-structure variations in the planetary boundary layer. *Q.J.R. Meteorol. Soc.*, **83,** 486–500.

Burk, S. D. and W. T. Thompson, 1996: The summertime low-level jet and marine boundary layer structure along the California coast. *Mon. Wea. Rev.*, **124,** 668-686.

Carlson, T.N., 1980: Airflow through midlatitude cyclones and the comma cloud pattern. *Mon. Wea. Rev.*, **108**, 1498-1509.

Chao, S. Y., 1985: Coastal jets in the lower atmosphere. *J. Phys. Oceanogr.*, **15,** 361-371.

Charney, J. J., X. Bian, B. E. Potter, and W. E. Heilman, 2003: Low level jet impacts on fire evolution in the Mack Lake and other severe wildfires. Proc., 2nd International Wildland Fire Ecology and Fire Management Congress and 5th Symposium on Fire and Forest Meteorology, November 16-20, Orlando, FL. American Meteorological Society. 1.5.

Chen, S., 1986: Simulation of the stratiform region of a mesoscale convective system. M.S. thesis, Dept. of Atmospheric Science, Colorado State University, 107 pp. [Available from Colorado State University, Fort Collins, CO 80523, U.S.A.]

Chen, Y., X. A. Chen, Y. Zhang, 1994: A Diagnostic Study of the Low-Level Jet during TAMEX IOP 5. *Mon. Wea. Rev.*, **122**, 2257–2284.

Cook, K.H., E.K. Vizy, Z.S. Launer, and C.M. Patricola, 2008: Springtime intensification of the Great Plains low-level jet and Midwest precipitation in GCM simulations of the twenty-first century. *J. Climate,* **21,** 6321-6340.

Cook, K. H., and E. K. Vizy, 2010: Hydrodynamics of the Caribbean low-level jet and its relationship to precipitation. *J. Climate*, **23,** 1477-1494.

Davis, R.E., B.P. Hayden, D.A. Gay, W.L. Phillips, and G.V. Jones, 1997: The North Atlantic subtropical anticyclone. *J. Climate,* **10,** 728-744.

Davis, C., S. Low-Nam, and C. Mass, 2000: Dynamics of a Catalina Eddy revealed by numerical simulation. *Mon. Wea. Rev.*, **128,** 2885–2904.

Doyle, J. D., and T. T. Warner, 1991: A Carolina coastal low-level jet during GALE IOP 2. *Mon. Wea. Rev.*, **119,** 2414-2428.

Fast, J. D., and M. D. McCorcle, 1990: A Two-Dimensional Numerical Sensitivity Study of the Great Plains Low-Level Jet. *Mon. Wea. Rev.*, **118**, 151–164.

Guentchev, G. S., 2007: Changes in atmospheric circulation over Europe and the relationship to temperature extremes in Bulgaria. Ph.D. dissertation, Michigan State University, 439 pp. [Available from Michigan State University, East Lansing, MI 48824, U.S.A.]

Harman, J. R., 1987: Mean monthly North American anticyclone frequencies, 1950-79. *Mon. Wea. Rev.*, **115,** 2840-2848.

Hefland, H.M. and S.D. Schubert, 1995: Climatology of the simulated Great Plains low-level jet and its contributions to the continental moisture budget of the United States. *J. Climate,* **8,** 784-806.

Higgins, R.W., Y. Yao, E.S. Yarosh, J.E. Janowiak, and K.C. Mo, 1997: Influence of the Great Plains low-level jet on summertime precipitation and moisture transport over the central United States. *J. Climate*, **10,** 481-507.

Hoecker, W. H., 1965: Comparative physical behavior of southerly boundary-layer wind jets. *Mon. Wea. Rev.*, **93**, 133–144.

Holt, T. R., 1996: Mesoscale forcing of a boundary layer jet along the California coast. *J. Geophys. Res.*, **101,** 4235-4254.

Holton, J.R., 1967: The diurnal boundary layer wind oscillation above sloping terrain. *Tellus*, **19,** 199-205.

Hoxit, L. R., 1975: Diurnal variations in planetary boundary-layer winds over land. *Boundary-Layer Meteor.*, **8,** 21-38.

Izumi, Y., 1964: The evolution of temperature and velocity profiles during breakdown of a nocturnal inversion and a low-level jet. *J. Appl. Meteor. Climatol.,* **3,** 70-82.

Kapela, A.F., P.W. Leftwich, and R. Van Ess, 1995: Forecasting the impacts of strong wintertime post-cold front winds in the northern plains. *Wea. Forecasting*, **10,** 229-244.

Mesinger, F., G. DiMego, E. Kalnay, K. Mitchell, P.C. Shafran, W. Ebisuzaki, D. Jovic, J. Woollen, E. Rogers, E. H. Berbery, M. B. Ek, Y. Fan, R. Grumbine, W. Higgins, H. Li, Y. Lin, G. Manikin, D. Parrish, and W. Shi, 2006: North American regional reanalysis. *Bull. Amer. Meteor. Soc.*, **87,** 343-360.

Mitchell, M. J., R. W. Arritt, and K. Labas, 1995: A climatology of the warm season Great Plains low-level jet using wind profiler observations. *Wea. Forecasting*, **10,** 576-591.

Muñoz, E., A. J. Busalacchi, S. Nigam, and A. Ruiz-Barradas, 2008: Winter and summer structure of the Caribbean low-level jet. *J. Climate*, **21,** 1260-1276.

Muñoz, E. and D. Enfield, 2011: The boreal spring variability of the Intra-Americas low-level jet and its relation with precipitation and tornadoes in the eastern United States. *Climate Dyn.*, **36,** 247-259.

Paegle, J., and G. E. Rasch, 1973: Three-Dimensional Characteristics of Diurnally Varying Boundary-Layer Flows. *Mon. Wea. Rev.*, **101**, 746–756.

Parish, T. R., A. R. Rodi, and R. D. Clark, 1988: A case study of the summertime Great Plains low level jet. *Mon. Wea. Rev.*, **116**, 94–105.

Parish, T. R., 2000: Forcing of the summertime low-level jet along the California coast. *J. App. Meteor. Climatol.,* **39,** 2421-2433.

Pitchford, K. L., and J. London, 1962: The low-level jet as related to nocturnal thunderstorms over Midwest United States. *J. Appl. Meteor.*, **1,** 43-47.

Ralph, F. M., P. J. Neiman, and R. Rotunno, 2005: Dropsonde observations in low-level jets over the northeastern Pacific Ocean from CALJET-1998 and PACJET-2001: Mean vertical-profile and atmospheric-river characteristics. *Mon. Wea. Rev.*, **133,** 889-910.

Rife, D.L., J.O. Pinto, A.J. Monaghan, C.A. Davis, and J.R. Hannan, 2010: Global distribution and characteristics of diurnally varying low-level jets. *J. Climate,* **23,** 5041-5064.

Schwartz, B. E., and C.A. Doswell, 1991: North American rawinsonde observations: problems, concerns, and a call to action. *Bull. Amer. Meteor. Soc.*, **72,** 1885-1886.

Shadbolt, R. P., E. A. Waller, J. P. Messina, and J. A. Winkler, 2006: Source regions of lower-tropospheric airflow trajectories for the lower peninsula of Michigan: A 40-year air mass climatology. *J. Geophys. Res.,* **111,** D21117, doi: *10.1029/2005JD006657.*

Shafran, Perry, J. Woollen, W. Ebisuzaki, W. Shi, Y. Fan, R. Grumbine, and M. Fennessy, 2004: Observational data used for assimilation in the NCEP North American Regional Reanalysis. 14th Conf. on Applied Climatology, paper 1.4, Combined Preprints CD-ROM, 84th AMS Annual Meeting, Seattle, WA.

Sjostedt, D.W., J.T. Sigmon, and S.J. Colucci, 1990: The Carolina nocturnal low-level jet: synoptic climatology and a case study. *Wea. Forecasting*, **5,** 404-415.

Stensrud, D.J., 1996: Importance of low-level jets to climate: a review. *J. Climate,* **9,** 1698-1711.

Storm, B., J. Dudhia, S. Basu, A. Swift, and I. Giammanco, 2009: Evaluation of the weather research and forecasting model on forecasting low-level jets: implications for wind energy. *Wind Energ.*, **12,** 81-90.

Ting, M., and H. Wang, 2006: The role of the North American topography on the maintenance of the Great Plains summer low-level jet. *J. Atmos. Sci.*, **63**, 1056–1068.

Uccellini, L. W. and D. R. Johnson, 1979: Coupling of upper and lower tropospheric jet streaks and implications for the development of severe convective storms. *Mon. Wea. Rev.*, **107,** 682-703.

Uccellini, L. W., 1980: On the role of upper tropospheric jet streaks and leeside cyclogenesis in the development of low-level jet in the Great Plains. *Mon. Wea. Rev.*, **108,** 1689-1696.

Wagner, A., 1939: Concerning the daily wind in the free atmosphere. *Beitrage Zur Physik der freien Atmosphare* **25,** 145-170.

Walters, C.K., 2001: Airflow configurations of warm season southerly low-level wind maxima in the Great Plains. Part II: the synoptic and subsynoptic-scale environment. *Wea. Forecasting*, **16,** 531-551.

Walters, C.K. and J.A. Winkler, 2001: Airflow configurations of warm season southerly low-level wind maxima in the Great Plains. Part I: spatial and temporal characteristics and relationship to convection. *Wea. Forecasting*, **16,** 513-530.

Walters, C.K., J.A. Winkler, R. P. Shadbolt, J. van Ravensway, and G. D. Bierly, 2008: A long-term climatology of southerly and northerly low-level jets for the central United States. *Ann. Assoc. Amer. Geogr*. **98,** 521-552.

Walters, C.K., J.A. Winkler, S. Husseini, R. Keeling, J. Nicolic, and S. Zhong, 2013: Detection of low-level jets in the North American Regional Reanalysis (NARR): a comparison with rawinsonde observations. Submitted to Journal of Applied Meteorology and Climatology.

Weaver, S. J., and S. Nigam, 2008: Variability of the Great Plains low-level jet: Large-scale circulation context and hydroclimate impacts. *J. Climate*, **21,** 1532–1551.

Wexler H., 1961: A boundary layer interpretation of the low-level jet. *Tellus,* **13,** 368-378.

Whittaker, L.M., and L.H. Horn, 1981: Geographical and seasonal distribution of North American cyclogenesis, 1958-1977. *Mon. Wea. Rev.*, **109,** 2312-2322.

Winkler, J. A., 2004: The impact of technology upon in situ atmospheric observations and climate science. *Geography and Technology*, S. D. Brunn, S. L. Cutter, and J. W. Harrington Jr., Eds. Springer Netherlands, 461-490.

Winkler, J. A., G. S. Guentchev, Perdinan, P. N. Tan, S. Zhong, M. Liszewska, Z. Abraham, T. Niedzwiedz, and Z. Ustrnul, 2011: Climate scenario development and applications for local/regional climate change impact assessment: an overview for the non-climate scientist. *Geogr. Compass*. **5,** 275-300.

Whiteman, C.D., X. Bian, and S. Zhong, 1997: Low-level jet climatology from enhanced rawinsonde observations at a site in the southern Great Plains. *J. Appl. Meteor. Climatol.,* **36,** 1363-1376.

Wu, Y. and S. Raman, 1998: The summertime Great Plains low level jet and the effect of its origin on moisture transport. *Boundary-Layer Meteor.*, **88,** 445-466.

Zhang, D. L., S. Zhang S. J. Weaver, 2006: Low-level jets over the mid-Atlantic states: warm-season climatology and a case study. *J. Appl. Meteor. Climatol.*, **45,** 194-209.

Zhong, S., J. D. Fast, and X. Bian, 1996: A case study of the Great Plains low-level jet using wind profiler network data and a high-resolution mesoscale model. *Mon. Wea. Rev.,* **124,** 785-806.

Zishka, K. M. and P.J. Smith, 1980: The climatology of cyclones and anticyclones over North America and surrounding ocean environs for January and July, 1950-77. *Mon. Wea. Rev.*, **108,** 387-401.